UNIVERSIDAD COMPLUTENSE DE MADRID

FACULTAD DE CIENCIAS QUÍMICAS
DEPARTAMENTO DE INGENIERÍA QUÍMICA

TESIS DOCTORAL

Fraccionamiento del extracto de la separación de aromáticos de gasolinas y naftas con líquidos iónicos

MEMORIA PARA OPTAR AL GRADO DE DOCTOR

PRESENTADA POR

Pablo Navarro Tejedor

DIRECTORES

Francisco Rodríguez Somolinos
Julián García González

Madrid, 2017

Universidad Complutense de Madrid

Facultad de Ciencias Químicas

Departamento de Ingeniería Química

Tesis Doctoral

Fraccionamiento del extracto de la separación de aromáticos de gasolinas y naftas con líquidos iónicos

Memoria que para optar al Título de Doctor por la Universidad Complutense de Madrid en el Programa de Doctorado de Ingeniería Química presenta:

Pablo Navarro Tejedor

Dirigida por:

Prof. Dr. Francisco Rodríguez Somolinos

Prof. Dr. Julián García González

Fraccionamiento del extracto de la separación de aromáticos de gasolinas y naftas con líquidos iónicos

Pablo Navarro Tejedor

Tesis Doctoral, Universidad Complutense de Madrid, España

ISBN 978-84-608-6226-0

D. Francisco Rodríguez Somolinos y D. Julián García González, Catedrático y Profesor Titular en el Departamento de Ingeniería Química de la Universidad Complutense de Madrid,

Certifican que este trabajo de investigación titulado: “Fraccionamiento del extracto de la separación de aromáticos de gasolinas y naftas con líquidos iónicos” constituye la memoria que presenta D. Pablo Navarro Tejedor para optar al grado de Doctor y que ha sido realizada en los laboratorios del Departamento de Ingeniería Química de la Universidad Complutense de Madrid bajo su dirección.

Y para que conste a los efectos oportunos, firman el presente certificado en Madrid a 9 de Febrero de 2016

Prof. Dr. Francisco Rodríguez Somolinos Prof. Dr. Julián García González

Agradecimientos

“Para obrar, el que da debe olvidar pronto, y el que recibe, nunca.” Séneca.

Agradecer a mis directores de tesis la oportunidad brindada de realizar la tesis doctoral en el programa de doctorado en Ingeniería Química. A Francisco Rodríguez Somolinos, por su papel motivador y responsable de todas las oportunidades disfrutadas a lo largo de mi experiencia predoctoral. A Julián García González, por la libertad y exigencia con la que entiende el mundo de la investigación y la docencia, porque gracias a ello he podido crecer personal y profesionalmente.

Agradecer a todos los profesores del grupo de investigación: Mercedes Oliet Palá, Fernando Mirada Coronel, Virginia Alonso Rubio y Juan Carlos Domínguez Toribio, todas las ayudas en los campos de la docencia e investigación, así como la cercanía mostrada estos años.

Agradecer a Marcos todas las lecciones disfrutadas desde que empezamos a compartir la Ingeniería Química como amigos, motivándome a ser siempre un poco mejor cada día. Extenderle todos los éxitos obtenidos en el marco de esta tesis doctoral. Agradecer a Silvia y a Emilio todos los buenos consejos que en el campo de la extracción de aromáticos me han dado; y a Ester y a Belén por facilitarme los primeros pasos en el uso de la TGA y el DSC.

A Jean–Baptiste por enseñarme que una planificación experimental nunca es lo suficientemente intensa (y que los crisoles de alúmina pueden levitar). A Tamara, por los momentos de desconexión y los consejos, que son casi tan importantes como los momentos de trabajo. A todos los demás compañeros de viaje: Ana, María, Victoria, María del Mar y Noemí, por hacerlo mucho más ameno.

Agradecer a Paco Solís y a Jesús Plaza toda su ayuda y lo ameno de su compañía; un cromatógrafo de gases sin helio, hidrógeno y aire, no es un cromatógrafo de gases.

Agradecer a Raquel todos los sacrificios personales y profesionales que ha realizado y realizará para permitirme crecer en el mundo de la investigación; pero más te debo por compartir tu vida conmigo.

A mis padres, Rosa y Manuel, porque gracias a su educación y esfuerzo he podido disfrutar de una vida que posiblemente no merezca.

A Rubén, porque siempre ha estado ahí, enseñándome que además de años cumplimos experiencias, de las cuales tenemos que aprender para seguir.

A Emilio, Raquel, Emilio y Carlos, por parecer que llevo toda la vida con dos familias y por animarme a crecer profesionalmente, aguantando mis aburridas historias de trabajo.

A mis abuelos, tíos y primos, porque siempre han mostrado un gran interés en mi futuro. Y al resto de mi familia de acogida, por acortar las distancias entre Madrid y Valladolid, Santander o Ginebra, y por su apoyo e interés.

A todos los profesores, compañeros y amigos que he tenido durante todas las etapas formativas, porque todas las experiencias, buenas y malas, te enseñan.

A mi abuelo José Manuel, con quien ojalá hubiera podido compartir un capítulo más. Cerrar contigo estos agradecimientos, mas nunca olvidarte.

“Bien acierta quien sospecha que siempre yerra”

Francisco de Quevedo

Índice

Resumen

Título

Fraccionamiento del extracto de la separación de aromáticos de gasolinas y naftas con líquidos iónicos.

Marco y financiación

La tesis doctoral se ha llevado a cabo en los laboratorios del Departamento de Ingeniería Química, situados en la Facultad de Ciencias Químicas de la Universidad Complutense de Madrid, dentro del Grupo de Investigación UCM 910717 “Desarrollo de Procesos y Productos de Bajo Impacto Ambiental”. Los directores de la misma han sido los doctores D. Francisco Rodríguez Somolinos y D. Julián García González.

Las labores de investigación y formación se han financiado a través del Ministerio de Economía y Competitividad (MINECO) al amparo de los proyectos CTQ2011–23533 “Extracción líquido–líquido de aromáticos de gasolinas de reformado y de pirólisis con mezclas binarias de líquidos iónicos y regeneración del disolvente” y CTQ2014–53655–R “Diseño de un proceso de extracción de hidrocarburos aromáticos de gasolina de pirólisis empleando una mezcla binaria de líquidos iónicos”, así como por la Comunidad de Madrid a partir de los proyectos S2009/PPQ–1546 “Empleo de líquidos iónicos como alternativa a los disolventes orgánicos en procesos avanzados de separación” y S2013/MAE–2800 “Los líquidos iónicos como alternativa a los disolventes orgánicos en procesos y productos”.

Además, el doctorando ha disfrutado de una beca de Formación de Personal Investigador (FPI) del MINECO con referencia BES–2012–052312 desde diciembre de 2012.

Introducción y objetivos

Los hidrocarburos aromáticos, principalmente benceno, tolueno, etilbenceno y xilenos, identificados comúnmente bajo el acrónimo BTEX, son compuestos de relevancia en la industria petroquímica al ser materia prima para la síntesis de numerosos compuestos intermedios y en la fabricación de diversos productos finales.

Las principales fuentes de obtención de aromáticos son la gasolina de reformado proveniente del reformado catalítico de la nafta alimentada al *pool* de gasolinas y la gasolina de pirólisis obtenida en el craqueo térmico de naftas en la producción de olefinas. En ambos casos, los aromáticos se encuentran combinados con otros hidrocarburos (principalmente naftenos, parafinas y olefinas) formando mezclas complejas, caracterizadas por la proximidad de sus puntos de ebullición y la formación de mezclas azeotrópicas entre sus componentes. Esto hace que una rectificación simple no se pueda utilizar como operación de separación de estas mezclas. Por ello, se hace necesario recurrir a otras técnicas de separación como es el caso de la extracción líquido–líquido.

En este sentido, una de las líneas de investigación que en los últimos años ha cobrado más importancia es la sustitución de los compuestos orgánicos volátiles utilizados como disolvente en las operaciones de extracción líquido–líquido de mezclas de hidrocarburos aromáticos y alifáticos por otros más respetuosos con el medio ambiente. Por sus características únicas, los líquidos iónicos (sales líquidas a temperaturas inferiores a los 373 K) se encuentran en una posición privilegiada y son considerados como los posibles sustitutos de los disolventes orgánicos.

Las principales ventajas ofrecidas por los líquidos iónicos para su empleo en procesos de separación son su despreciable volatilidad y el elevado número de especies, lo cual permite encontrar líquidos iónicos con propiedades adecuadas para cada separación específica. Concretamente, ciertos líquidos iónicos puros con cationes piridinio o imidazolio y la mayoría de sus mezclas binarias han mostrado buenas propiedades en la extracción de aromáticos.

La investigación de los procesos de extracción de hidrocarburos aromáticos de sus mezclas con compuestos alifáticos empleando líquidos iónicos se ha centrado principalmente en la determinación experimental y el modelado del equilibrio líquido–líquido de mezclas formadas por *n*–heptano, tolueno y líquidos iónicos puros, en los que se ha evaluado la capacidad de los líquidos iónicos como disolventes en términos de selectividad y coeficiente de reparto.

Estas mezclas de hidrocarburos se han formulado atendiendo tanto a las composiciones típicas de gasolinas de reformado y pirólisis, principales fuentes de obtención a día de hoy de hidrocarburos aromáticos, como a aquellas otras de baja concentración de BTEX para las cuales no se cuenta en la actualidad con tecnología disponible, como es el caso de la nafta alimentada al *cracker* de etileno. También han sido numerosos los estudios de las propiedades físicas de los líquidos iónicos empleados como disolventes de extracción, destacando la extensa colección de datos publicados hasta la fecha de densidad y viscosidad dinámica.

Sin embargo, el fraccionamiento de las mezclas características de la corriente de extracto obtenida en la separación de aromáticos de gasolinas y naftas con líquidos iónicos no se ha estudiado hasta la fecha; por ello, no ha sido posible establecer de forma rigurosa la viabilidad de un proceso alternativo de extracción de aromáticos con líquidos iónicos.

En consecuencia, el objetivo de esta tesis doctoral ha sido establecer un proceso general de fraccionamiento de la corriente de extracto de la separación de aromáticos de gasolinas y naftas con líquidos iónicos. Así pues, se pretende formular un esquema de separación de la corriente de extracto en tres corrientes: una primera de aromáticos con pureza suficiente para garantizar su ulterior aplicación, otra en la que se recuperen los compuestos no aromáticos y, por último, una corriente de líquidos iónicos regenerados que pueda ser recirculada a la columna de extracción.

Objetivos específicos

El fraccionamiento de la corriente de extracto de la separación de aromáticos de las gasolinas de reformado y pirólisis y de la nafta alimentada al *cracker* de etileno con líquidos iónicos requiere de la realización, principalmente, de tres estudios experimentales, los cuales definen los objetivos específicos de esta tesis doctoral:

- Evaluación de la estabilidad térmica de los líquidos iónicos puros y sus mezclas binarias con el objetivo de establecer el intervalo de temperaturas de aplicación de este tipo de compuestos.
- Medición de los calores específicos de los líquidos iónicos puros y sus mezclas binarias con el fin de conocer, llegado el caso, las necesidades energéticas del proceso de fraccionamiento de la corriente de extracto.
- Determinación experimental y modelado del equilibrio líquido–vapor de mezclas representativas de corrientes de extracto, {alifáticos + aromáticos + líquidos iónicos}, con la idea de proponer una secuencia de separación por destilación súbita de los componentes que integran dicha corriente.

Resultados y conclusiones

En primer lugar se ha abordado el estudio de la estabilidad térmica de los líquidos iónicos. Para ello, se ha realizado una evaluación de las curvas de descomposición térmica obtenidas tanto por análisis termogravimétrico dinámico como isotermo. Si bien, por un lado se han obtenido buenos resultados cualitativos con los ensayos dinámicos, también se ha demostrado la necesidad de realizar ensayos isotermos para obtener los intervalos térmicos de aplicación de los líquidos iónicos. Ahora bien, dado que los ensayos isotermos requieren de mucho tiempo de experimentación, se han realizado predicciones de estabilidad térmica para ciclos de 8000 horas a partir de datos dinámicos, obteniendo así los límites térmicos de estabilidad para el empleo de los líquidos iónicos a escala industrial.

Por otro lado, en el caso de las mezclas binarias de líquidos iónicos se ha propuesto una regla de mezcla que ha permitido predecir su proceso de descomposición térmica a partir de las correspondientes a los líquidos iónicos puros implicados en la mezcla.

La segunda parte del trabajo, la medición de los calores específicos de los líquidos iónicos puros y de sus mezclas binarias, se ha realizado con éxito, obteniendo una relación polinómica de segundo orden de los calores específicos con respecto a la temperatura dentro del intervalo de estabilidad térmica previamente definido para todos los líquidos iónicos y sus mezclas.

En las dos etapas de caracterización térmica de los líquidos iónicos cabe destacar el gran impacto de las tres publicaciones en las que se recogen los resultados obtenidos, ya que a 9 de febrero de 2016 se han citado en su conjunto en 48 ocasiones.

Además, en esta tesis doctoral se ha realizado de forma pionera tanto la evaluación de la estabilidad térmica como la medición de los calores específicos de mezclas binarias de líquidos iónicos.

Finalmente, se ha abordado también por primera vez en esta tesis doctoral el estudio del equilibrio líquido–vapor de mezclas representativas de corrientes de extracto de la separación de aromáticos de gasolinas y naftas con líquidos iónicos. Para ello, se ha desarrollado un método de determinación del equilibrio líquido–vapor para mezclas formadas por hidrocarburos y líquidos iónicos, éstos últimos en elevada concentración.

La técnica experimental desarrollada se ha basado en el empleo de un inyector de espacio de cabeza acoplado a un cromatógrafo de gases, de manera que el equilibrio líquido–vapor se reproduce en el inyector a la temperatura de equilibrio, determinándose a partir del análisis de la fase vapor tanto la composición de la fase líquida como la presión parcial de cada hidrocarburo en el equilibrio.

A partir de los datos de equilibrio líquido–vapor de mezclas {*n*–heptano + tolueno + líquidos iónicos} se ha concluido que:

- La volatilidad relativa *n*–heptano/tolueno en las mezclas {*n*–heptano + tolueno + líquidos iónicos} se ve fuertemente incrementada cuando se compara con la correspondiente a la mezcla {*n*–heptano + tolueno}.
- Existe una relación directa entre la selectividad tolueno/*n*–heptano observada en el equilibrio líquido–líquido y la volatilidad relativa *n*–heptano/tolueno.
- Se observa un incremento de la volatilidad relativa *n*–heptano/tolueno en todas las mezclas al disminuir el valor de la temperatura.

Ampliando este estudio a otras mezclas {alifático + aromático + líquidos iónicos}, se ha confirmado que las conclusiones anteriores se pueden extender a la recuperación del compuesto alifático de cualquier mezcla {alifático + aromático} presente en la corriente extracto. Además, se ha empleado con éxito la regla de mezcla de Yalkowsky–Roseman para la predicción de los equilibrios líquido–vapor de las mezclas {alifático + aromático + líquidos iónicos}.

Por último, se ha abordado el estudio del equilibrio líquido–vapor del extracto de la separación de aromáticos de modelos de gasolinas y naftas con la mezcla de líquidos iónicos {[4empy][Tf_2N] (0,3) + [emim][DCA] (0,7)}. Estos datos de equilibrio líquido–vapor han sido la base para el desarrollo de un proceso de fraccionamiento de la corriente de extracto basado en tres unidades de destilación súbita adiabáticas que permiten obtener unas corrientes de aromáticos con una pureza del 99,8 % para las corrientes modelo de gasolinas y del 98,5 % para la de la nafta alimentada al *cracker* de etileno.

Abstract

Title

Hydrocarbon recovery from the extract stream obtained in the aromatic separation from gasolines and naphthas using ionic liquids

Frame and funding

This PhD Thesis was carried out in the Chemical Engineering Departament laboratories, situated into the Chemical Sciences Faculty from the Complutense University of Madrid, collaborating with the UCM research group 910717 “Desarrollo de Procesos y Productos de Bajo Impacto Ambiental”. The Thesis was leaded by Prof. Dr. Francisco Rodríguez Somolinos and Prof. Dr. Julián García González.

The researches and academic issues related to this PhD Thesis were funded by the *Ministerio de Economía y Competitividad* (MINECO), under the CTQ2011–23533 and CTQ2014–53655–R projects, and by the *Comunidad de Madrid* under the S2009/PPQ–1546 and S2013/MAE–2800 proyects.

In addition to this, the PhD student was also funded by the MINECO with a FPI grant (Reference BES–2012–052312).

Introduction and aim of the work

The aromatic hydrocarbons, mainly benzene, toluene, ethylbenzene, and xylenes (BTEX), are important compounds in the Petrochemical Industry, being used as manufactures in the synthesis of intermediate products as phenol, cyclohexane, and styrene and also as final products in the cases of rubbers, lubricants, pesticides, plastics, or paints.

The main sources for aromatics are reformer and pyrolysis gasolines. In both cases, the aromatic fraction is combined with several naphthenes, alkanes, or olefins; all these compounds have similar boiling points than those of the aromatics and several mixtures form azeotropic points. Therefore, the distillation of gasolines in order to separate the aromatics is not technically possible and thus the liquid–liquid extraction is used.

The study of ionic liquids as solvents in the aromatic extraction process to replace conventional volatile organic compounds has been quite relevant in the last decade, because of their lower impact as a result of their negligible vapor pressures.

In addition to this point, the high number of ionic liquids nowadays is another important advantage of these compounds, because it is easy to find competitive ionic liquids for a high variety of applications. Specifically, pure ionic liquids containing pyridinium and imidazolium cations and their mixtures have shown good properties in the aromatic extraction.

Until now, the goals in the aromatic extraction with ionic liquids have been the experimental determinations and modelling of the liquid–liquid equilibrium for {*n*–heptane + toluene + ionic liquid} mixtures. In addition to this, the physical characterization of the ionic liquid solvents, mainly through their density and viscosity, has been extensively done.

However, the recovery of the aromatic and aliphatic hydrocarbons from the extract stream has not been experimentally evaluated before and, because of that, the feasibility of a whole aromatic extraction process involving ionic liquids has not been stablished.

As a result, the aim of this work was the proposal of a conceptual design for the separation of the extract stream in three streams: the aromatics, the aliphatics, and the ionic liquid-based solvent regenerated.

Specific goals

To achieve the aim of this work is necessary to complete the following three studies:

- The evaluation of the thermal stability for pure and mixed ionic liquids in the aromatic extraction in order to set a temperature range of use.
- The measurement of the specific heats for pure and mixed ionic liquids to know the energy consumptions in the separation processes of the extract.
- The experimental determination and modelling of the vapor–liquid equilibria for representative systems of extract streams to propose the hydrocarbon recovery section based on flash distillation units.

Results and conclusions

Firstly, the thermal stability evaluation has been studied for several ionic liquids. Both dynamic and isothermal thermogravimetric analysis have been used to understand the thermal decomposition of ionic liquids. The dynamic experiments have been used to set the thermal stability order, whereas isothermal runs have been employed to calculate decomposition temperatures for long–term.

In addition to this, the dynamic runs have been employed to predict the maximum operation temperature for ionic liquids for long–term, as a result of the high cost associated to isothermal experiments.

On the other hand, a mixing rule has been proposed for the case of binary mixtures of ionic liquids in order to evaluate the ideality of mixture in the thermal decomposition process.

Secondly, the specific heats of the ionic liquids and their binary mixtures have been determined and the results have been modelled to a second order polynomial equation as a function of temperature.

In both thermal studies, it is important to highlight the 48 cites obtained in the three articles that summarized the results, since 2013. Indeed, the evaluation of the thermal stability and the determination of specific heats have been done for the first time for an ionic liquid mixture.

Finally, the vapor–liquid equilibria of the extract–type systems from the aromatic separation from their sources have been studied. For this purpose, a novel technique based on the use of a headspace injector coupled to a gas chromatograph has been developed in this PhD Thesis for systems formed by hydrocarbons and ionic liquids.

The next conclusions have been obtained from the vapor–liquid equilibria data for {*n*–heptane + toluene + ionic liquids} systems:

- The *n*–heptane/toluene relative volatility in the *{n*–heptane + toluene + ionic liquids} systems has been highly incremented in comparison with the {*n*–heptane + toluene} system.
- There is a relationship between toluene/*n*–heptane selectivity in liquid–liquid equilibria and the *n*–heptane/toluene relative volatility.
- An increase in the *n*–heptane/toluene relative volatility has been always observed with a decrease in the temperature value.

These conclusions have been confirmed by determining the vapor–liquid equilibria for other {aliphatic + aromatic + ionic liquid} systems. Also the Yalkowsky and Roseman mixing rule has been properly used to predict the vapor–liquid equilibria for {aliphatic + aromatic + ionic liquid mixtures}.

Finally, the vapor–liquid equilibria for the extract streams of the aromatic separation from gasoline and naphtha models using the {[4empy][Tf_2N] (0.3) + [emim][DCA] (0.7)} binary ionic liquid mixture has been determined. The use of three adiabatic flash distillation units has been proposed to obtain an aromatic stream with a mass purity of 99.8 and 98.5 % for the gasoline and naphtha cases, respectively.

Capítulo 1. Introducción

La tarea que inició el desarrollo de esta tesis doctoral consistió en la revisión del estado del arte de la industria de los compuestos aromáticos, la cual estuvo centrada en la identificación de sus fuentes de obtención y, fundamentalmente, en las dificultades que presenta su separación de otros compuestos de naturaleza hidrocarbonada. Asimismo, también se evaluaron las características únicas de los líquidos iónicos como disolventes de extracción líquido–líquido para su potencial aplicación en la separación de aromáticos. Finalmente, y con las conclusiones extraídas de esta revisión y las oportunidades relacionadas con la aplicación de los líquidos iónicos que se identificaron, se definieron los objetivos del trabajo.

1.1. Aplicaciones de los hidrocarburos aromáticos

Los hidrocarburos aromáticos, principalmente benceno, tolueno, etilbenceno y xilenos (*o*–xileno, *m*–xileno y *p*–xileno), identificados comúnmente bajo el acrónimo BTEX, son compuestos de gran relevancia en la industria petroquímica. Su demanda mundial ronda actualmente los 110 millones de toneladas anuales, con una tendencia al alza en la última década. Este dato revela tanto el gran volumen de mercado asociado a los hidrocarburos aromáticos como el crecimiento constante de su industria (Thyssen Krupp, 2014).

La Figura 1.1 resume algunas de las numerosas aplicaciones de los BTEX (Kirk y Othmer, 1998; Ramos Carpio, 1997; Wauquier, 2000; Fahim y col., 2010). El benceno destaca tanto por sus numerosas aplicaciones como por su demanda anual, la cual asciende a unos 50 millones de toneladas en 2013 (Thyssen Krupp, 2014). Entre los productos más importantes obtenidos a partir del benceno se encuentra el etilbenceno. Bien es cierto que el etilbenceno se puede obtener directamente en procesos de separación de aromáticos, pero su punto de ebullición es muy próximo a los de los xilenos por lo que su síntesis a partir de la alquilación de benceno es la opción más frecuente a escala industrial para su obtención (Franck y Staldelhofer, 1988).

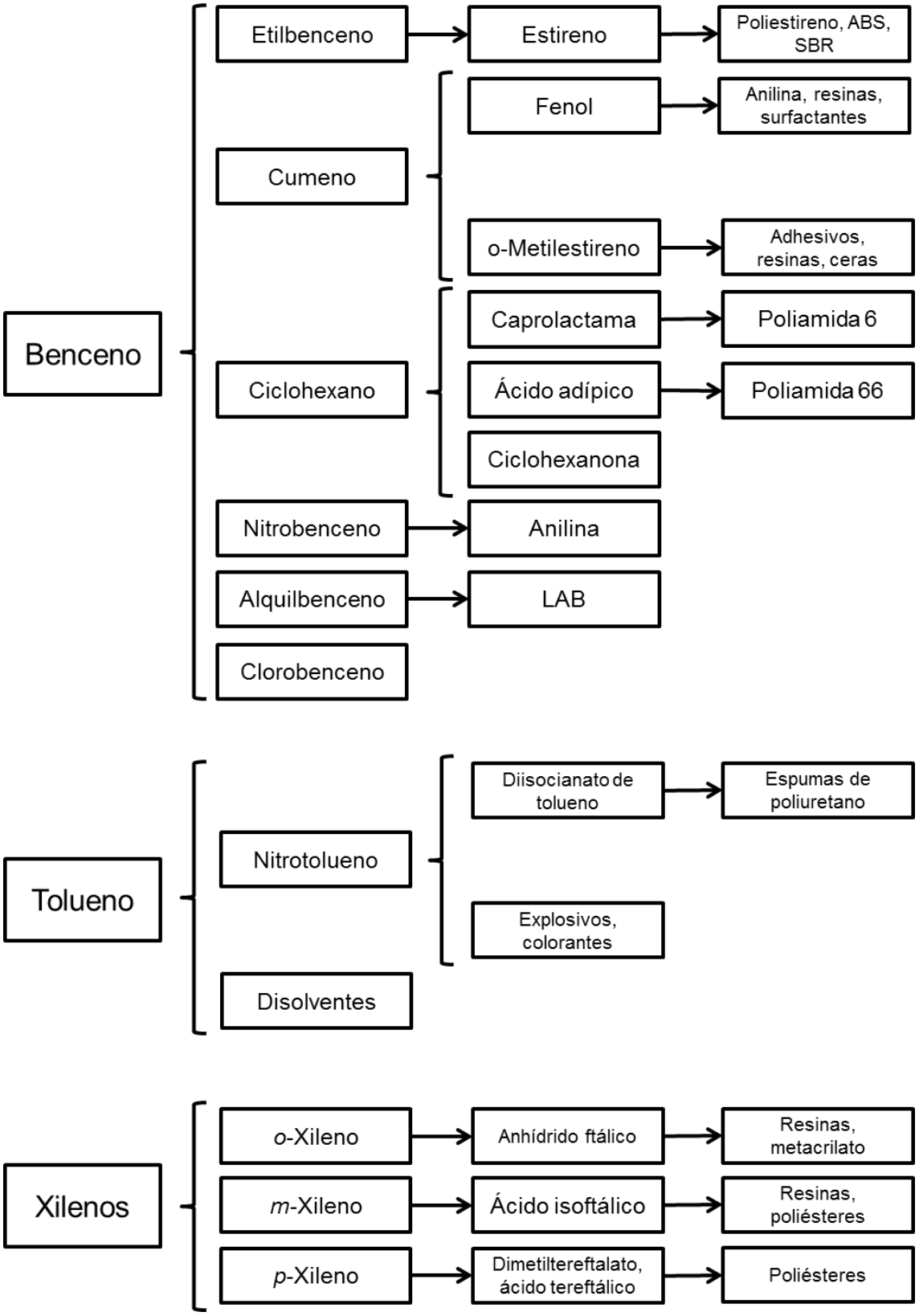

Figura 1.1. Principales aplicaciones de los BTEX: productos intermedios y finales. Fuente: Thyssen Krupp, 2014.

Las síntesis de cumeno y ciclohexano son también de gran importancia en la industria del benceno, ya que estos dos compuestos y el etilbenceno dan lugar a derivados tales como el estireno, el fenol, la caprolactama o la anilina (Figura 1.1). La industria del benceno tiene como principales productos finales, además de diversos disolventes, resinas, adhesivos y nylon (Thyssen Krupp, 2014).

El tolueno se emplea mayoritariamente en la síntesis de espumas de poliuretano y como disolvente de cubrientes, si bien también tiene una aplicación importante en las industrias de explosivos y colorantes (Kirk y Othmer, 1998).

Los xilenos, aun mostrando rutas de aprovechamiento diferenciadas, se emplean mayoritariamente en la obtención de resinas y poliésteres a partir de la síntesis de compuestos intermedios como el anhídrido ftálico y los ácidos isoftálico y tereftálico (Thyssen Krupp, 2014).

1.2. Fuentes de obtención de hidrocarburos aromáticos

Las principales fuentes de obtención de hidrocarburos aromáticos son las gasolinas de reformado y de pirólisis (Franck y Staldelhofer, 1988; Gary y col., 2007; Meyers, 2004). En Estados Unidos, el 75 % de los aromáticos se obtiene a partir de gasolinas de reformado. Este hecho se explica por la utilización de gas natural como materia prima en la síntesis de olefinas, tal y como se puede ver por la correlación entre la producción de etileno/etano y el consumo de gas natural en la última década recogida en la Figura 1.2 (EIA, 2015).

Como consecuencia, Estados Unidos destina mayoritariamente tanto la nafta como otros cortes ligeros de la destilación atmosférica del crudo a un proceso de reformado, obteniendo como principal producto la gasolina de reformado.

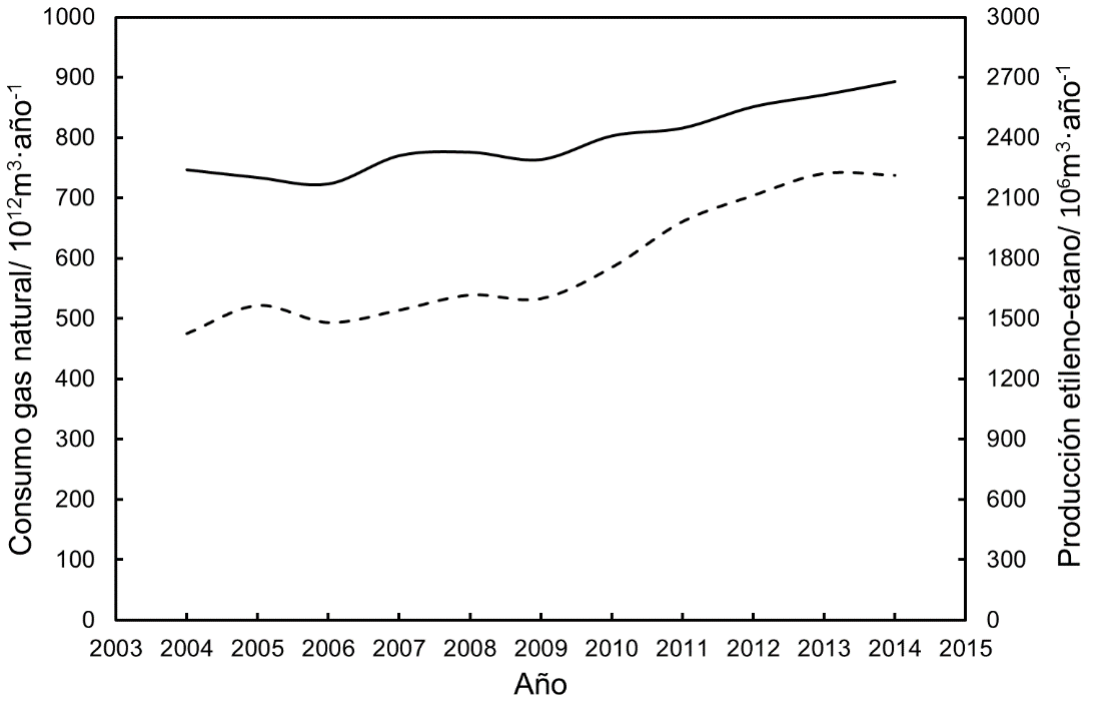

Figura 1.2. Consumo de gas natural (línea sólida) y producción de etileno–etano (línea de trazos) en Estados Unidos en la última década. Fuente: EIA, 2015.

En contraposición, Europa Occidental y Japón obtienen aromáticos fundamentalmente a partir de gasolina de pirólisis. En estas regiones los procesos de refino asociados a la nafta se enfocan hacia la obtención de olefinas debido a la menor disponibilidad de gas natural. Es decir, la nafta se somete a un proceso de craqueo térmico para obtener etileno siendo la gasolina de pirólisis un subproducto.

En función de la severidad de este proceso de craqueo, se obtienen gasolinas de pirólisis de craqueo suave o severo. Un craqueo en condiciones severas aumenta la concentración de aromáticos, en especial la de benceno seguida de la de tolueno.

En la Tabla 1.1 se recogen las composiciones típicas de las gasolinas de reformado y pirólisis. Se puede ver cómo la concentración en masa de aromáticos oscila entre un 51 % y un 66 %. El tolueno presenta siempre una concentración muy cercana al 20 %, mientras que la del benceno aumenta enormemente en los procesos de craqueo de la nafta, especialmente en condiciones severas.

Tabla 1.1. Composición másica típica de gasolina de reformado y de gasolina de pirólisis. Fuente: Franck y Staldelhofer, 1988

Compuesto	*Gasolina de reformado*	*Gasolina de pirólisis*	
		Craqueo suave	Craqueo severo
Aromáticos/ %	**55**	**51,0**	**66,2**
Benceno/ %	5	22,0	33,8
Tolueno/ %	24	17,5	19,4
o-Xileno / %	5	2,3	1,1
Etilbenceno / %	4		
m-Xileno/ %	9	6,0	6,6
p-Xileno/ %	4		
Otros aromáticos	4	3,2	5,3
No aromáticos/ %	**45**	**41,0**	**27,4**
Otros	–	8,0	6,4

1.3. Procesos convencionales de separación de aromáticos

Los hidrocarburos aromáticos se obtienen fundamentalmente a partir de gasolinas de reformado y pirólisis, en las que los aromáticos están combinados con hidrocarburos C_5 – C_{10} de naturaleza parafínica y nafténica. La separación de estas mezclas de hidrocarburos no se puede abordar mediante una destilación convencional por la proximidad de los puntos de ebullición de los compuestos que las integran, como se puede ver en la Tabla 1.2 (Henley y Seader, 1981; Fahim y col., 2010).

Tabla 1.2. Puntos de ebullición de los principales hidrocarburos presentes en gasolinas y naftas (Perry y col., 1999)

Hidrocarburo	T_{eb}/ *K*
n–hexano	342,2
n–heptano	371,6
n–octano	398,7
n–nonano	424,0
2,3–dimetilpentano	363,0
ciclohexano	353,8
benceno	353,3
tolueno	383, 8
p–xileno	411,6
m–xileno	412,3
o–xileno	417,6
etilbenceno	409,4

Para analizar más en detalle la complejidad de la separación de este tipo de mezclas se presentan a continuación las curvas de equilibrio líquido–vapor a 323,2 K para distintas mezclas alcano/aromático, tomando como referencia el *n*–heptano como compuesto no aromático y el tolueno como aromático.

En la Figura 1.3 se puede ver cómo el aumento de la longitud de cadena de los alcanos lineales dificultaría su separación del tolueno. El cambio de una estructura lineal por una cíclica, como en el caso del *n*–hexano por ciclohexano, complicaría también la separación alcano/tolueno. Sin embargo, las ramificaciones del alcano, para un mismo número de átomos de carbono, como el 2,3–dimetilpentano frente al *n*–heptano, facilitaría la separación.

En la Figura 1.4 se observa que la separación de *n*–heptano de diversos aromáticos se ve favorecida para los aromáticos más pesados, es decir etilbenceno y *p*–xileno. Además, la separación de *n*–heptano de sus mezclas con benceno muestra una dificultad adicional, ya que éste aromático es el compuesto más volátil en tal mezcla.

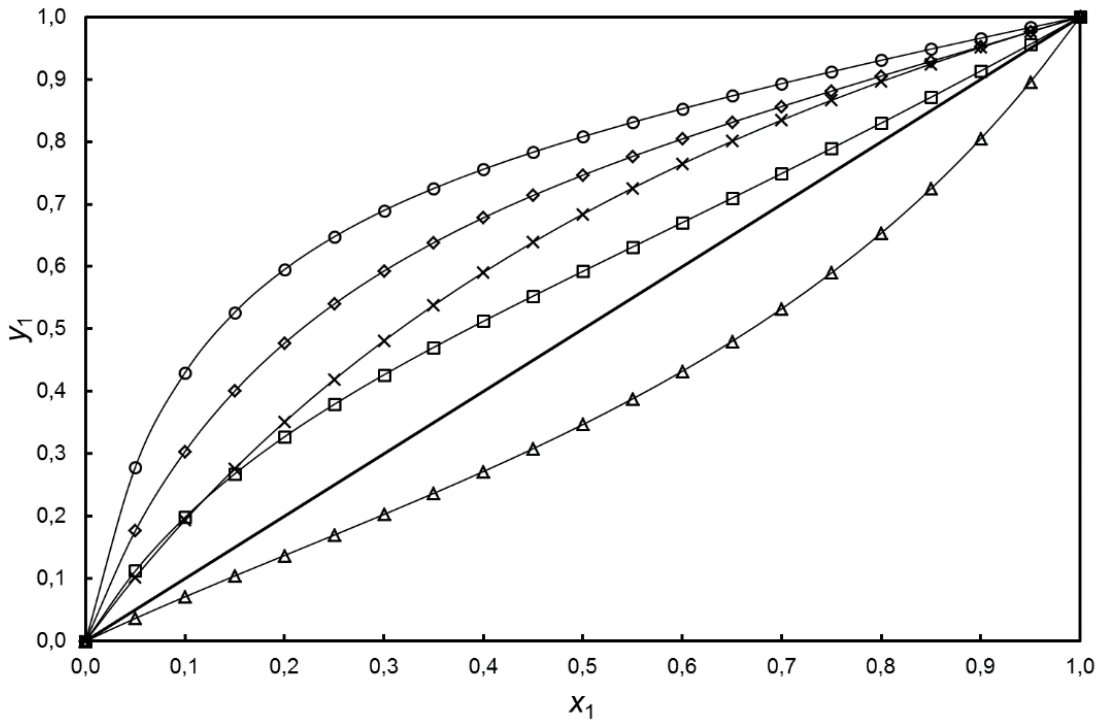

Figura 1.3. Diagramas de composición líquido (*x*) – vapor (*y*) a 323,2 K para las diversas mezclas {alifático (1) + tolueno (2)}. Compuesto alifático: *n*–hexano (○), *n*–heptano (□), *n*–octano (△), ciclohexano (◊), 2,3–dimetilpentano (×). Fuente: Aspen Plus, 2004.

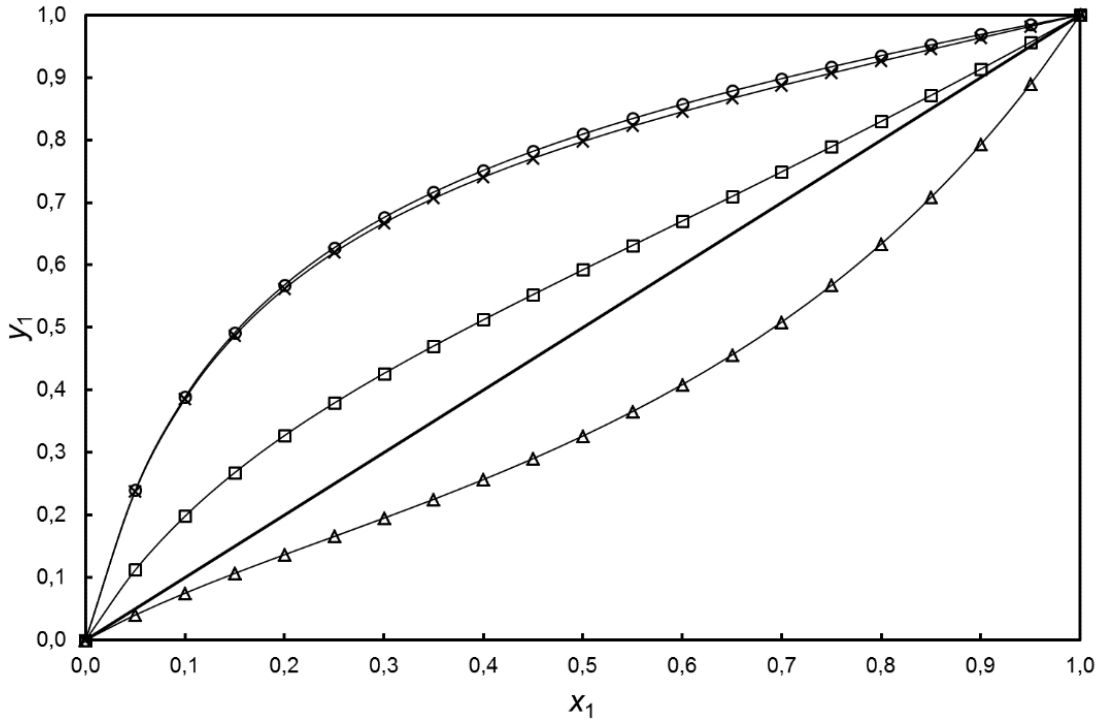

Figura 1.4. Diagramas de composición líquido (*x*) – vapor (*y*) a 323,2 K para las diversas mezclas {*n*-heptano (1) + aromático (2)}. Aromático: benceno (△), tolueno (□), etilbenceno (×), *p*–xileno (○). Fuente: Aspen Plus, 2004.

Por ello, tanto los hidrocarburos alifáticos de peso molecular elevado (> C_8) como los compuestos nafténicos y aromáticos ligeros, especialmente el benceno, dificultarían la separación de la fracción BTEX de los hidrocarburos no aromáticos. El caso del benceno merece una mención especial, ya que además de las dificultades ya comentadas, forma azeótropos con el *n*–hexano, *n*–heptano, ciclohexano y 2,3–dimetilpentano (Franck y Staldelhofer, 1988).

Los procesos existentes en la actualidad para separar los aromáticos del resto de hidrocarburos con los que están combinados se pueden clasificar en tres categorías en virtud de la operación de separación en torno a la que se diseñan: extracción líquido–líquido, destilación extractiva y destilación azeotrópica (Franck y Staldelhofer, 1988; Gary y col., 2007.

La extracción líquido–líquido es la operación más destacada de separación de aromáticos debido a que se emplea para extraer estos compuestos con una concentración comprendida entre el 20 % y el 65 % en masa, intervalo en el que se sitúan las dos fuentes de obtención mayoritarias de aromáticos (gasolinas de reformado y pirólisis).

En la Tabla 1.3 se recogen las principales características de los procesos de extracción líquido–líquido de aromáticos, ordenados en orden cronológico a su desarrollo. Como se infiere de la misma, las tecnologías han ido evolucionando hacia condiciones de operación a presión atmosférica, temperaturas bajas y menores relaciones disolvente/alimento, ya que con ello se reducen los costes de operación del proceso.

Entre todas las tecnologías empleadas a escala industrial de extracción líquido–líquido de aromáticos destaca el proceso Sulfolano (Franck y Staldelhofer, 1988). Centrando el análisis en la temperatura de operación y las condiciones de sobrepresión del proceso Sulfolano, éstas son más suaves que para el proceso Udex, el más antiguo, si bien los procesos Arosolvan e IFP presentan condiciones menos severas. Sin embargo, las propiedades extractivas del sulfolano son las que originan que actualmente el proceso Sulfolano sea el más usado a escala industrial.

Como se puede ver en la Figura 1.5, la alimentación del proceso Sulfolano, una fuente de aromáticos, y el disolvente (sulfolano) se introducen en contracorriente en una columna de extracción con contacto por pisos rotatorios que trabaja a una temperatura de 373 K y en condiciones de ligera sobrepresión. Por cabeza de la columna de extracción se recogen los compuestos no aromáticos saturados en sulfolano, el cual posteriormente se separa mediante un lavado con agua, tras el cual se purifica por destilación y se devuelve a la columna de extracción.

Tabla 1.3. Comparativa de las distintas tecnologías de extracción líquido–líquido de aromáticos a escala industrial (Franck y Staldelhofer, 1988)

Proceso	Disolvente	$T_{ebullición}$/ K	Condiciones		S/F[a]
			P/ kPa	*T*/ K	
Udex	Dietilenglicol	518	506–810	403–423	6–8
Sulfolane	Sulfolano	560	203	373	3–6
Arosolvan	N–metilpirrolidona	479	101	293–313	4–5
IFP	Dimetilsulfóxido	462	101	293–303	3–5
Morphylex	N–formilmorfilona	517	101	453–473	5–6

[a] Relación disolvente (S) / alimento (F).

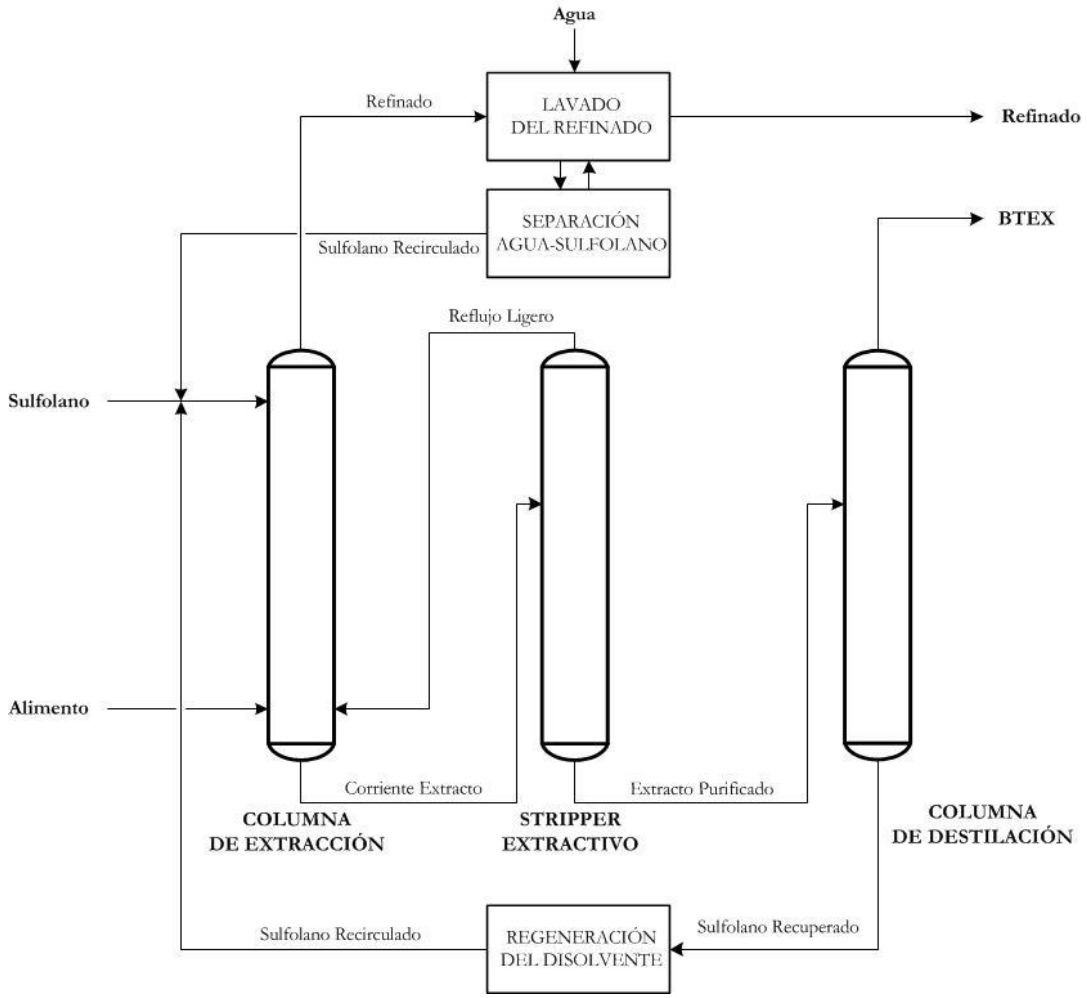

Figura 1.5. Diagrama de flujo del proceso Sulfolano.

Por el fondo de la columna se obtiene el extracto, compuesto por la mayor parte del disolvente saturado de casi la totalidad de la fracción BTEX de la alimentación y por una pequeña parte de los compuestos no aromáticos más ligeros. Las rendimientos de extracción de los aromáticos en la etapa de extracción son superiores al 99,9 % para el benceno, 99,0 % para el tolueno y 97,0 % para los xilenos (Gary y col., 2007; Wauquier, 2000).

El extracto se alimenta posteriormente a una operación de destilación extractiva, de tal manera que en esta operación de rectificación se separan los compuestos no aromáticos por cabeza para ser recirculados a la columna de extracción, mientras que la fracción BTEX y el disolvente se obtienen por el fondo, con una pureza de aromáticos con respecto a toda la fracción de hidrocarburos recuperados superior al 99,9 % en masa (Gary y col., 2007).

Finalmente, la corriente de cola de la destilación extractiva se envía a una torre de rectificación donde los aromáticos se obtienen por cabeza y por el fondo se recoge el disolvente. Antes de su recirculación a la columna de extracción, el sulfolano se somete a un proceso de regeneración en condiciones severas de temperatura y vacío.

La destilación extractiva es la segunda opción de separación de hidrocarburos aromáticos, comúnmente empleada para corrientes con una concentración de aromáticos de entre un 65 % y un 90 % en masa (Franck y Staldelhofer, 1988). Destacan los procesos de separación basados en los agentes másicos de separación: *N*–formilmorfilona, *N*–metilpirrolidona y sulfolano.

Por último, la destilación azeotrópica se emplea para corrientes de muy alto contenido de aromáticos, superiores al 90 % en masa. Es una opción de menor relevancia ya que existen pocas corrientes industriales con una concentración tan elevada de aromáticos. Estos procesos utilizan como agentes másicos disolventes como la metiletilcetona y el metanol (Gary y col., 2007).

A modo de resumen y teniendo en cuenta que las principales fuentes de obtención de aromáticos tienen un contenido en dichos compuestos de entre un 51 % y un 66 % en masa, queda justificada la importancia de los procesos de extracción líquido–líquido, así como la representatividad del proceso Sulfolano como referente en la búsqueda de nuevas tecnologías de separación de aromáticos de gasolinas de reformado y pirólisis.

1.4. Los líquidos iónicos como precursores de nuevas tecnologías de separación de hidrocarburos aromáticos

Los líquidos iónicos son sales líquidas que por definición tienen temperaturas de fusión inferiores a 373 K y están formados por un catión orgánico y un anión que puede ser tanto de naturaleza orgánica como inorgánica.

La gran mayoría de líquidos iónicos son líquidos a temperatura ambiente, lo cual permite combinar las buenas propiedades de los compuestos iónicos en los procesos de separación con la facilidad de manejo que introduce la fase líquida. Además, la prácticamente nula volatilidad de los líquidos iónicos hace que estos compuestos sean fáciles de separar por destilación de compuestos volátiles y que no produzcan emisiones a la atmósfera (De Simone, 2002; Rogers y Seddon, 2003).

Los líquidos iónicos han sido estudiados en numerosos campos de investigación de muy diversa índole, destacando sus aplicaciones como disolvente, agente másicos de separación y medio de reacción (Plechkova y Seddon, 2008).

A continuación se exponen las principales conclusiones extraídas de los estudios publicados hasta 2015 acerca del empleo de los líquidos iónicos como disolventes en la extracción de aromáticos.

En la Figura 1.6 se representan las selectividades tolueno/*n*–heptano, los coeficientes de reparto del tolueno, la densidad y la viscosidad de los líquidos iónicos puros y sus mezclas más destacados. Las propiedades extractivas y físicas del sulfolano se muestran también para conformar un marco de referencia, justificado por ser el disolvente orgánico más utilizado en la extracción líquido–líquido de aromáticos.

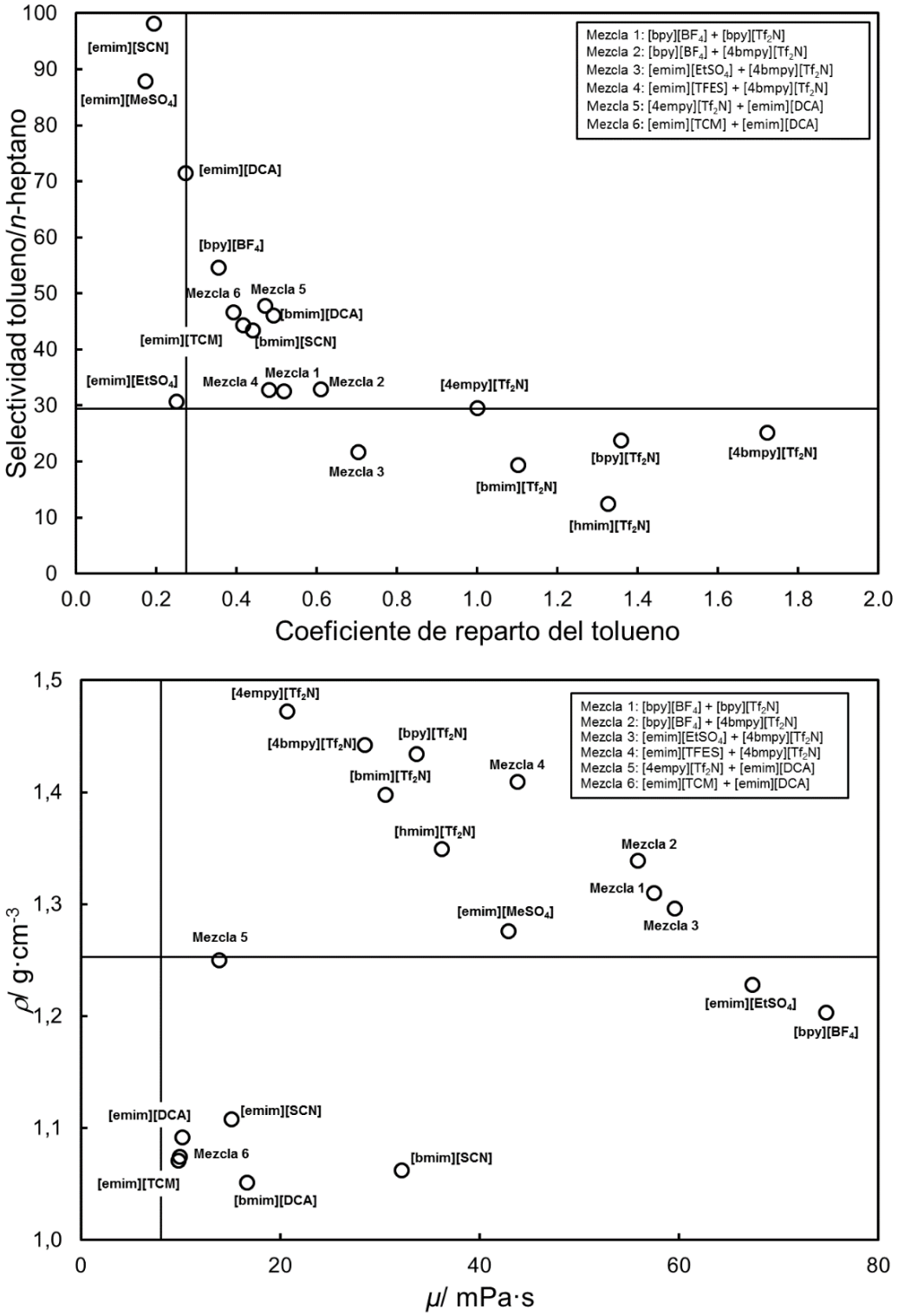

Figura 1.6. Propiedades extractivas y físicas de los líquidos iónicos como disolventes en la extracción de tolueno de sus mezclas con *n*–heptano al 10 % de tolueno y a 313,2 K. La línea sólida muestra los valores del sulfolano. Referencias: Esperança y col., 2006; Meindersma y col., 2010; García y col., 2010; Costa y col., 2011; González y col., 2011; Larriba y col., 2011; García y col., 2011a,b; Corderí y col., 2012; Larriba y col., 2012; García y col., 2012a,b,c,d; García y col., 2013; Larriba y col., 2013a; Larriba y col., 2013b; Larriba y col., 2014d; Larriba y col., 2015a; Larriba y col., 2013c; Larriba y col., 2014a,b,c.

Las propiedades extractivas se centran en la separación de tolueno de la mezcla binaria {*n*–heptano + tolueno} con un 10 % en masa del aromático, ya que ha sido el modelo más utilizado en los estudios realizados con líquidos iónicos como disolventes de extracción de aromáticos.

En este sentido, también se ha seleccionado la temperatura de 313,2 K para realizar la comparación, tanto de propiedades extractivas como físicas, por ser a la que existe una colección más extensa de datos de densidad y viscosidad de líquidos iónicos así como de datos de equilibrio líquido–líquido.

Centrando en un primer momento el análisis en los líquidos iónicos puros, la principal conclusión que se puede extraer es que difícilmente muestran de forma simultánea selectividades tolueno/*n*–heptano y coeficientes de reparto de tolueno elevados. De hecho, sólo los líquidos iónicos basados en los aniones dicianamida, tiocianato, tricianometano y tetrafluoroborato muestran coeficientes de reparto del tolueno ligeramente superiores al sulfolano junto con un incremento importante de la selectividad tolueno/*n*–heptano en comparación con dicho disolvente. En cambio, los líquidos iónicos basados en aniones bis(trifluorometilsulfonil)imida presentan elevados valores del coeficiente de reparto del tolueno, pero las selectividades tolueno/*n*–heptano apenas alcanzan las del sulfolano.

Además de las propiedades extractivas, las propiedades físicas juegan un papel fundamental en los procesos de extracción: la viscosidad en los procesos de impulsión y mezcla y en la difusión de los hidrocarburos en el disolvente, mientras que la densidad en la cinética del proceso de separación de fases (França y col., 2009).

Así pues, ampliando el análisis a las propiedades físicas, se aprecia cómo los líquidos iónicos basados en aniones dicianamida, tiocianato, tricianometano y bis(trifluorometilsulfonil)imida son los únicos que muestran viscosidades adecuadas y cercanas al sulfolano.

La densidad está inversamente relacionada con la selectividad tolueno/*n*–heptano, ya que los líquidos iónicos con bajas selectividades muestran densidades mayores que la del sulfolano, mientras que los líquidos iónicos con elevados valores de selectividad tolueno/*n*–heptano presentan densidades menores que la del sulfolano.

Analizando de forma conjunta las propiedades extractivas y físicas, los líquidos iónicos 1–etil–3–metilimidazolio tiocianato ([emim][SCN]), 1–etil–3–metilimidazolio dicianamida ([emim][DCA]) y 1–etil–3–metilimidazolio tricianometano ([emim][TCM]) muestran estructuras formadas por cationes imidazolio y cadenas alquílicas cortas, lo cual potencia su selectividad tolueno/*n*–heptano y su baja viscosidad (Arce y col., 2007; García y col., 2010; Jacquemin y col., 2007; Meindersma y de Haan, 2012). Por el contrario, el líquido iónico más destacado de elevada capacidad de extracción y altos valores de densidad es el 1–etil–4–metilpiridinio bis(trifluorometilsulfonil)imida ([4empy][Tf_2N]), ya que los cationes piridinios con dos cadenas alquílicas cortas en posición 1 y 4 potencian su capacidad de extracción y su densidad, reduciendo asimismo su viscosidad (Hansmeier y col., 2010; Meindersma y de Haan, 2012; García y col., 2011; Kim y col., 2013; Larriba y col., 2012 y 2013a).

Sin embargo, ninguno de estos líquidos iónicos puros consigue alcanzar de forma simultánea valores de las propiedades extractivas y físicas superiores a las del sulfolano. Por ello, algunos investigadores emplearon mezclas binarias de líquidos iónicos, buscando modular las propiedades extractivas y físicas a partir de la composición de la mezcla (García y col., 2012b,c,d; García y col., 2013; Larriba y col., 2013c; Larriba y col., 2014a,b,c). Con un líquido iónico de selectividades tolueno/*n*–heptano superiores a las del sulfolano y otro con coeficientes de reparto de tolueno elevados, se pueden encontrar composiciones de la mezcla en las que ambas propiedades superen al disolvente de referencia; igual ocurre con las propiedades físicas a partir de un líquido iónico de baja viscosidad y densidad y otro de elevada densidad y moderada viscosidad.

Las dos mezclas binarias de líquidos iónicos más destacadas hasta el momento han sido {[4empy][Tf_2N] (0,3) + [emim][DCA] (0,7)} y {[emim][TCM] (0,8) + [emim][DCA] (0,2)}. Ambas mostraron propiedades extractivas superiores a las del sulfolano, con viscosidades comparables con las de este disolvente orgánico. La primera mezcla, además, presenta unos valores de densidad muy similares a los del sulfolano (Larriba y col., 2013c; Larriba y col., 2014a,b,c).

El uso de la mezcla binaria {[4empy][Tf_2N] (0,3) + [emim][DCA] (0,7)} como disolvente se amplió a la extracción de aromáticos de gasolinas de reformado y pirólisis, las dos fuentes fundamentales de obtención de aromáticos, y de la nafta alimentada al *cracker* de etileno. Los resultados mostraron un aumento en la pureza de la fracción de aromáticos extraída y un ligero incremento en el número de etapas de equilibrio necesarias para alcanzar los mismos rendimientos de extracción que con el sulfolano a igualdad de relación disolvente/alimento (Larriba y col., 2014e; Larriba y col, 2015b,c).

Además de las buenas propiedades extractivas y físicas mostradas por los líquidos iónicos en su empleo como disolventes en la separación de aromáticos de sus mezclas con hidrocarburos alifáticos, hay una serie de puntos adicionales que impulsan el interés por un proceso alternativo de extracción de aromáticos con líquidos iónicos.

En primer lugar, la solubilidad de los líquidos iónicos en los hidrocarburos que conforman la corriente de refinado es muy baja, de manera que las etapas de recuperación del disolvente de la fase refinado del proceso Sulfolano no serían necesarias (Meindersma y col., 2012).

En segundo lugar, la corriente de extracto estaría formada mayoritariamente por líquido iónico y por los aromáticos extraídos; por ello, una etapa de destilación súbita sería suficiente para recuperar los hidrocarburos aromáticos del disolvente, que en este caso es de naturaleza no volátil (Anjan, 2006). Sin embargo, esta separación de los hidrocarburos aromáticos del líquido iónico tiene dos limitaciones importantes.

La pureza de los aromáticos en la fase extracto debería ser de un 99,9 % en masa para garantizar su interés comercial, para lo cual sería necesario trabajar con un líquido iónico de selectividad aromático/alifático de 440 (Gary y col., 2007; Meindersma y col., 2005; Meindersma y col., 2008). Actualmente no se ha encontrado ningún líquido iónico con selectividades aromático/alifático tan elevadas. Por ello, es necesario conocer los datos de equilibrio líquido–vapor correspondientes a las composiciones de la corriente extracto para proponer la purificación de los aromáticos extraídos antes de su separación del líquido iónico.

Por otro lado, la estabilidad térmica de los líquidos iónicos se ha determinado fundamentalmente por ensayos termogravimétricos dinámicos a una velocidad de calefacción de 10 $K \cdot min^{-1}$ (Fredlake y col., 2004; Crosthwaite y col., 2005). Este hecho, como han demostrado estudios posteriores basados en el análisis termogravimétrico isotermo para ciertos líquidos iónicos, ha sobreestimado en gran medida los intervalos de aplicación de estos compuestos (Fernández y col., 2007; Seeberger y col., 2009; Hao y col., 2010). Por tanto, se hace imprescindible obtener un intervalo de estabilidad térmica para los líquidos iónicos más destacados en la extracción de aromáticos que garantice su aplicación industrial sin que lleguen a descomponerse.

1.5. Objetivos y etapas de la tesis doctoral

El objetivo general de esta tesis doctoral es proponer un esquema de fraccionamiento del extracto de un proceso de extracción de aromáticos con líquidos iónicos. Es decir, un proceso que permita obtener una corriente de aromáticos de pureza comercial, recuperar los compuestos no aromáticos y regenerar el disolvente. Para ello, se ha planteado la realización de las tres tareas siguientes:

- Evaluar la estabilidad térmica de los líquidos iónicos puros y sus mezclas binarias en ciclos de operación industriales.
- Medir los calores específicos de los líquidos iónicos puros y sus mezclas binarias.

- Determinar los equilibrios líquido–vapor en mezclas representativas de las corrientes de extracto de la separación de aromáticos de gasolinas y naftas con líquidos iónicos.

Evaluación de la estabilidad térmica de los líquidos iónicos

Los líquidos iónicos puros [emim][SCN], [bmim][SCN], [emim][DCA], [bmim][DCA] y [emim][TCM] y las mezclas binarias {[4empy][Tf_2N] + [emim][DCA]} y {[emim][TCM] + [emim][DCA]} se han caracterizado mediante análisis termogravimétricos dinámicos e isotermos.

Los ensayos termogravimétricos dinámicos se han utilizado para evaluar comparativamente sus curvas de descomposición térmica y para predecir su estabilidad térmica en ciclos de operación industrial utilizando el modelo de Seeberger y col. (2009). Estas predicciones se han validado mediante ensayos termogravimétricos isotermos de 48 h.

En el caso de las mezclas binarias de líquidos iónicos, se ha predicho la descomposición térmica de la mezcla a partir de una regla de mezcla basada en la degradación independiente de los líquidos iónicos puros que forman tal mezcla, propuesta por vez primera en esta tesis doctoral y que ha mostrado una buena capacidad predictiva.

Medición de los calores específicos de los líquidos iónicos

Una vez establecidas las temperaturas máximas de operación, se han determinado los calores específicos de todos los líquidos iónicos puros [emim][SCN], [bmim][SCN], [emim][DCA], [bmim][DCA] y [emim][TCM] y de las mezclas binarias {[4empy][Tf_2N] + [emim][DCA]} y {[emim][TCM] + [emim][DCA]} mediante calorimetría diferencial de barrido empleando el método del zafiro. En el caso de las dos mezclas binarias de líquidos iónicos estudiadas se han calculado también por primera vez sus calores específicos de exceso y, a partir de los mismos, se ha podido evaluar la idealidad de mezcla con respecto a esta propiedad.

Estudios del equilibrio líquido–vapor en mezclas representativas de corrientes de extracto

Tras establecer las temperaturas máximas de operación de todos los líquidos iónicos y sus mezclas binarias, y una vez conocidos a partir de la bibliografía los equilibrios líquido–líquido de diversas mezclas formadas por hidrocarburos aromáticos, hidrocarburos alifáticos y líquidos iónicos, se han determinado los datos del equilibrio líquido–vapor de mezclas representativas de corrientes de extracto.

La determinación del equilibrio líquido–vapor de este tipo de mezclas no había sido realizada previamente por ningún otro grupo de investigación, por lo que inicialmente ha sido necesario el desarrollo de una nueva metodología experimental basada en el uso de un inyector de espacio de cabeza acoplado a un cromatógrafo de gases. Además, se ha definido un procedimiento experimental que minimice las incertidumbres de la técnica.

En primer lugar, la técnica se ha validado con datos de equilibrio líquido–vapor de mezclas de hidrocarburos sin líquidos iónicos, únicos datos disponibles en la bibliografía. Posteriormente, se han llevado a cabo estudios del equilibrio líquido–vapor para la mezcla {*n*–heptano + tolueno} con los líquidos iónicos puros que forman la mezcla de líquidos iónicos {[4empy][Tf_2N] + [emim][DCA]}. Además, estos datos se han ajustado al modelo termodinámico *Non–Random Two Liquids* (NRTL).

A continuación, se ha evaluado el efecto de la composición de la mezcla binaria de líquidos iónicos {[4empy][Tf_2N] + [emim][DCA]} en el equilibrio líquido–vapor de diversas mezclas {alifático + aromático}. Atendiendo a los resultados obtenidos y teniendo en cuenta también el efecto de la composición de la mezcla en la extracción de aromáticos y en las propiedades físicas de la misma se ha concluido que la composición molar más adecuada de la mezcla de líquidos iónicos es {[4empy][Tf_2N] (0,3) + [emim][DCA] (0,7)}.

Posteriormente, se han estudiado todas las mezclas pseudoternarias {alifático + aromático + {[4empy][Tf_2N] (0,3) + [emim][DCA] (0,7)}} posibles en todo el intervalo de composiciones y a varias temperaturas. Los datos de equilibrio líquido–vapor se han ajustado también al modelo NRTL.

Finalmente, se ha abordado el estudio del equilibrio líquido–vapor de corrientes de extracto obtenidas en la separación de aromáticos de modelos de gasolinas de reformado y pirólisis y de la nafta alimentada al *cracker* de etileno empleando la mezcla {[4empy][Tf_2N] (0,3) + [emim][DCA] (0,7)} como disolvente extractivo. En esta etapa, a partir de los datos del equilibrio líquido–vapor, se ha propuesto un proceso de fraccionamiento de las corrientes de extracto.

Capítulo 2. Sección experimental

El fin de este apartado consiste en exponer todos los materiales utilizados a lo largo de la investigación, así como todos los procedimientos experimentales desarrollados y empleados para poder llevar a cabo los diversos estudios demandados para alcanzar el objetivo de esta tesis doctoral. En concreto, se detallan los métodos de determinación de la estabilidad térmica, de los calores específicos y de los equilibrios líquido–vapor de mezclas de corrientes de extracto.

2.1. Materiales

En la Tabla 2.1 se recogen todos los compuestos utilizados en la parte experimental de esta tesis doctoral, detallando sus purezas. Como se puede ver, se ordenan los compuestos en tres grupos: líquidos iónicos, hidrocarburos y gases. Los líquidos iónicos se han adquirido a Iolitec GmbH, los hidrocarburos a Sigma Aldrich y los gases a Praxair.

Los líquidos iónicos se almacenaron en un desecador de humedad controlada, siempre en sus envases de origen. Asimismo, la manipulación de los líquidos iónicos se realizó bajo atmósfera seca de nitrógeno, utilizando para este propósito una cámara de guantes *Pyramid* de Erlab. Las purezas, los contenidos en agua y haluros son valores certificados por el suministrador, Iolitec, de manera que se han utilizado directamente en las condiciones en las que fueron adquiridos.

Por su parte, los hidrocarburos permanecieron en sus envases originales durante su almacenamiento. En los casos pertinentes, el tamiz molecular presente de origen garantizó unos valores bajos de humedad en el seno del hidrocarburo.

Por último, mencionar que los discos de zafiro utilizados en la determinación de los calores específicos fueron suministrados por Mettler Toledo con una pureza superior al 0,99999 en masa, garantizada por el método de fabricación *Vernuil*.

Tabla 2.1. Listado de compuestos utilizados y su pureza

Compuesto	Pureza
Líquidos iónicos	
1–etil–3–metilimidazolio dicianamida ([emim][DCA])	0,98
1–butil–3–metilimidazolio dicianamida ([bmim][DCA])	0,98
1–etil–3–metilimidazolio tiocianato ([emim][SCN])	0,98
1–etil–3–metilimidazolio tiocianato ([bmim][SCN])	0,98
1–etil–4–metilpiridinio bis(trifluorometilsulfonil)imida ([4empy][Tf_2N])	0,99
1–etil–3–metilimidazolio tricianometano ([emim][TCM])	0,98
Hidrocarburos	
n–Hexano	0,995
n–Heptano	0,997
n–Octano	0,990
2,3–Dimetilpentano	0,990
Ciclohexano	0,995
Benceno	0,995
Tolueno	0,995
p–Xileno	0,990
Etilbenceno	0,998
Gases	
Nitrógeno	S1
Helio	3X
Aire	3X
Hidrógeno	3X

2.2. Procedimientos experimentales

A continuación se describen los procedimientos experimentales desarrollados y empleados en esta tesis doctoral para la evaluación de la estabilidad térmica, la medición de los calores específicos y la determinación de los equilibrios líquido–vapor.

2.2.1. Evaluación de la estabilidad térmica

La estabilidad térmica de los líquidos iónicos se ha evaluado por análisis termogravimétrico (TGA) usando una termobalanza Mettler Toledo TGA/DSC 1 con precisiones de 0,1 K y 10^{-4} mg en las medidas de temperatura y masa, respectivamente. En la Figura 2.1 se muestra una fotografía del equipo empleado.

Figura 2.1. Termobalanza Mettler Toledo TGA/DSC 1 empleada en la evaluación de la estabilidad térmica.

Todos los experimentos se han realizado en atmósfera inerte de nitrógeno y en crisoles de alúmina de 70 µL. La masa de muestra ha sido una variable controlada en el intervalo (20 ± 1) mg, siempre cubriendo por completo la superficie del crisol. Además, el equipo previamente a su utilización se calibró con los metales In, Zn, Al y Au, en el intervalo de temperaturas comprendido entre 298,2 K y 1773,2 K.

Análisis dinámico

Los ensayos TGA dinámicos se realizaron a las velocidades de calentamiento de 5, 10 y 20 $K \cdot min^{-1}$, en el intervalo de temperaturas comprendido entre 313,2 K y 1173,2 K. La rampa de calefacción de 10 $K \cdot min^{-1}$ es la más utilizada en este tipo de análisis, de manera que su elección se fundamenta en poder comparar los resultados obtenidos con aquéllos ya publicados (Fredlake y col., 2004; Crosthwaite y col., 2005).

Se llevaron a cabo ensayos a otras dos velocidades de calefacción (5 y 20 $K \cdot min^{-1}$) buscando determinar la influencia de la rampa de calefacción en la estabilidad térmica de los líquidos iónicos.

Asimismo, también se trabajó con una velocidad de calefacción de 5 $K \cdot min^{-1}$ para poder aplicar el modelo predictivo de Seeberger y col. (2009) de estabilidad térmica para ciclos de operación industrial de larga duración.

Análisis isotermo

Los experimentos TGA isotermos se llevaron a cabo a las temperaturas de 313,2 K, 353,2 K, 393,2 K, 433,2 K y 473,2 K. En el caso del líquido iónico [4empy][Tf_2N] se amplió el estudio de TGA isotermo a 513,2 K debido a su elevada estabilidad térmica. El tiempo de análisis se fijó en 48 h, considerando suficiente este valor para obtener conclusiones representativas; en este sentido, los tiempos fijados en determinaciones similares previamente llevadas a cabo habían sido inferiores a 24 h (Fernández y col., 2007; Seeberger y col., 2009).

2.2.2. Medición de los calores específicos

La técnica de calorimetría diferencial de barrido (DSC) fue la empleada para la determinación de los calores específicos de los líquidos iónicos. En la Figura 2.2 se muestra el calorímetro Mettler Toledo DSC821e utilizado.

Para determinar los calores específicos de los líquidos iónicos se ha seleccionado el método del zafiro atendiendo a su elevada reproducibilidad, siguiendo el procedimiento detallado en la norma ASTM E 1269–01 (ASTM, 2001). Por tanto, para cada muestra se han realizado tres mediciones: el flujo de calor del blanco (crisol vacío), el flujo de calor correspondiente al zafiro (utilizado como referencia) y el flujo de calor de la muestra.

Figura 2.2. Calorímetro diferencial de barrido Mettler Toledo DSC 821e empleado en la medición de los calores específicos.

Las medidas se realizaron en crisoles de acero inoxidable de 40 µL para minimizar la resistencia a la conductividad térmica. Los crisoles se llenaron con masas controladas de líquidos iónicos puros y sus mezclas en el intervalo de (25 ± 1) mg. El equipo se calibró, previamente a su utilización, con los metales In y Al, garantizándose así su empleo en el intervalo de temperaturas comprendido entre 273,2 K y 973,2 K.

En la Figura 2.3 se recoge el perfil de temperaturas que conforma el método experimental. Previamente a la determinación del calor específico se realizó la eliminación *in situ* de la fracción de agua con un tramo isotermo a 378,2 K durante 0,5 h.

Por otro lado, el intervalo térmico en el que se determinó el calor específico de los líquidos iónicos y sus mezclas se seleccionó para garantizar la ausencia de procesos irreversibles.

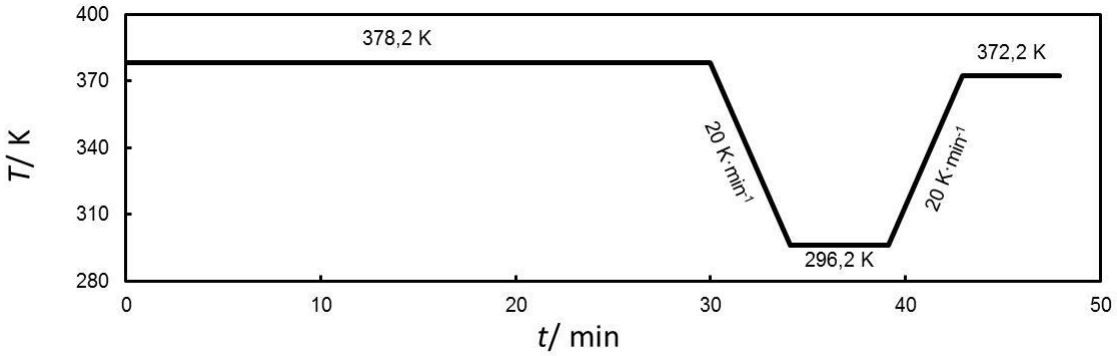

Figura 2.3. Perfil térmico del método de determinación del calor específico.

2.2.3. Determinación del equilibrio líquido–vapor

La determinación del equilibrio líquido–vapor de todas las mezclas representativas de corrientes de extracto de la separación de aromáticos de sus fuentes de obtención con líquidos iónicos se ha realizado siguiendo la misma metodología, la cual ha supuesto una de las contribuciones originales de esta tesis doctoral.

Reproducción del equilibrio líquido–vapor y análisis de las fases

El equilibrio líquido–vapor se determinó mediante una técnica estática e isoterma, empleando un inyector de espacio de cabeza Agilent 7697 A acoplado a un cromatógrafo de gases Agilent 7890 A, cuyas fotografías se recogen en la Figura 2.4.

Esta técnica permite determinar la cantidad de fase condensada que se evapora y su composición. Por tanto, conociendo la cantidad de cada compuesto en la alimentación es posible recalcular las composiciones de la fase líquida en equilibrio. Por otro lado, al ser el área de cada compuesto proporcional a su concentración en la fase vapor, esta técnica permite también determinar la presión de equilibrio (Kolb y Ettre, 1997).

En las Tablas 2.2 y 2.3 se recogen los parámetros optimizados más relevantes de los equipos implicados en el método de análisis. Salvo las temperaturas del inyector de espacio de cabeza, por ser una variable del equilibrio, los demás valores se han mantenido constantes en todas las determinaciones del equilibrio líquido–vapor.

Figura 2.4. Inyector de espacio de cabeza Agilent 7697 A (derecha) y cromatógrafo de gases Agilent 7890 A (izquierda) empleados para determinar el equilibrio líquido–vapor.

Tabla 2.2. Parámetros óptimos de operación del inyector *headspace* Agilent 7697 A

Parámetro	Valor
Parámetros generales	
Temperatura del horno/ K	323,2 – 393,2
Temperatura del *loop*/ K	378,2 – 413,2
Temperatura de la línea de transferencia/ K	443,2
Tiempo de equilibrado/ min	120
Tiempo de inyección/ min	1
Agitación/ giros·min^{-1}	100
Parámetros de la presurización del vial	
Presión final/ psi	15
Tiempo de equilibrado/ min	0,1
Parámetros del llenado del *loop*	
Presión final/ psi	10
Tiempo de equilibrado/ min	0,1

Tabla 2.3. Parámetros óptimos de operación del cromatógrafo de gases Agilent 7890 A

Parámetro	Valor
Parámetros del *inlet*	
Temperatura/ K	523,2
Flujo/ ml·min^{-1}	105
Split	50 : 1
Parámetros de la columna	
Modelo	HP – 5
Flujo/ ml·min^{-1}	2
Parámetros del horno	
Temperatura/ K	333,2– 348,2
Parámetros del detector	
Tipología	FID
Temperatura/ K	573,2
Flujo de hidrógeno/ ml·min^{-1}	30
Flujo de aire/ ml·min^{-1}	350
Flujo de helio/ ml·min^{-1}	15

El vial con la muestra y herméticamente cerrado se introduce en el horno del inyector, en el que se alcanza el equilibrio a la temperatura propia del ensayo y durante el tiempo de equilibrado preestablecido de 2 h. Tras el equilibrado y con un mecanismo de presurización/despresurización del vial se extrae una alícuota de fase vapor. Este proceso de toma de muestra se basa en el llenado de un *loop* aforado, que permite controlar con precisión el volumen de fase vapor muestreado. El contenido del *loop* se inyecta de forma automática al cromatógrafo de gases para su análisis.

El cálculo de las composiciones de la fase vapor se realiza directamente a partir de las áreas cromatográficas obtenidas en el análisis. Se utilizó el método del factor de respuesta para corregir las ligeras diferencias existentes en el ratio área/concentración de los hidrocarburos.

Por otro lado, la ecuación de los gases perfectos relaciona la concentración de un compuesto (C_i) en la fase vapor con su presión parcial (P_i):

$$P_i = C_i RT \tag{2.1}$$

donde R es la constante de los gases perfectos y T es la temperatura.

Teniendo en cuenta que la concentración de un compuesto en la fase vapor es proporcional al área desarrollada, es inmediato relacionar las áreas cromatográficas con las presiones particales de cada componente (Kolb y Ettre, 1997). Las presiones de vapor de los hidrocarburos (P_i^0) son datos muy bien definidos en bibliografía (Perry, 1999), de manera que conociendo dichos valores para un hidrocarburo, el área que desarrolla (A_i^0) y el área del mismo compuesto en una mezcla (A_i), se puede obtener la presión parcial de dicho compuesto:

$$P_i = \frac{A_i}{A_i^0} P_i^0 \tag{2.2}$$

Por último, conocidas las presiones parciales de todos los compuestos volátiles que integran la fase vapor se puede recalcular la composición de la fase líquida como:

$$x_i = \frac{z_i \cdot F - \frac{P_i \cdot V}{R \cdot T}}{\sum_{i=1}^{I} \left(z_i \cdot F - \frac{P_i \cdot V}{R \cdot T} \right)} \qquad (2.3)$$

donde *x* es la fracción molar del componente i en la fase líquida, *z* es la fracción molar de la alimentación, *F* la cantidad molar total del alimento y *V* es el volumen de espacio de cabeza correspondiente al vapor (19,0 mL).

Preparación de muestras

Las muestras de los ensayos de equilibrio se prepararon gravimétricamente mediante una balanza Mettler Toledo XS205 con una precisión de 10^{-5} g.

En primer lugar se añadió el líquido iónico o la mezcla de líquidos iónicos preparada independientemente y, posteriormente, la fracción hidrocarbonada también preparada por separado. Estas muestras se prepararon en viales cilíndricos de vidrio de 20 mL (23 x 75 mm) con tapones de aluminio y septum de teflón.

Planificación de la experimentación

Las mezclas formadas por un único hidrocarburo y uno o dos líquidos iónicos, es decir, mezclas binarias o pseudobinarias, se han preparado barriendo por completo la fracción del hidrocarburo en todo el intervalo de composiciones de la mezcla.

En el caso de mezclas ternarias y pseudoternarias, es decir, mezclas compuestas por un alifático, un aromático y uno o dos líquidos iónicos, la selección de las composiciones de las muestras es algo más compleja.

En la Figura 2.5 se muestra el equilibrio líquido–líquido de la mezcla {*n*–heptano + tolueno + [emim][DCA]} a 313,2 K para poder explicar la forma de proceder en estos casos.

La nula solubilidad del líquido iónico en la fase hidrocarbonada hace que las composiciones del refinado se sitúen en la línea de mezclas binarias {tolueno + *n*–heptano}. Por otro lado, las composiciones de la fase extracto se sitúan muy próximas a la línea de mezclas binarias {tolueno + [emim][DCA]}, por la baja solubilidad del *n*–heptano en el líquido iónico.

Para barrer por completo la zona miscible se han fijado diversas fracciones de líquido iónico, las cuales admiten como máximo las fracciones molares de *n*–heptano exenta de disolvente definidas por las composiciones de la fase extracto.

Por tanto, para cada fracción de líquido iónico fijada se han preparado mezclas de hidrocarburos de composiciones variables entre aquélla de la fase extracto y la mínima fracción molar de *n*–heptano exenta de disolvente que se pueda preparar con precisión.

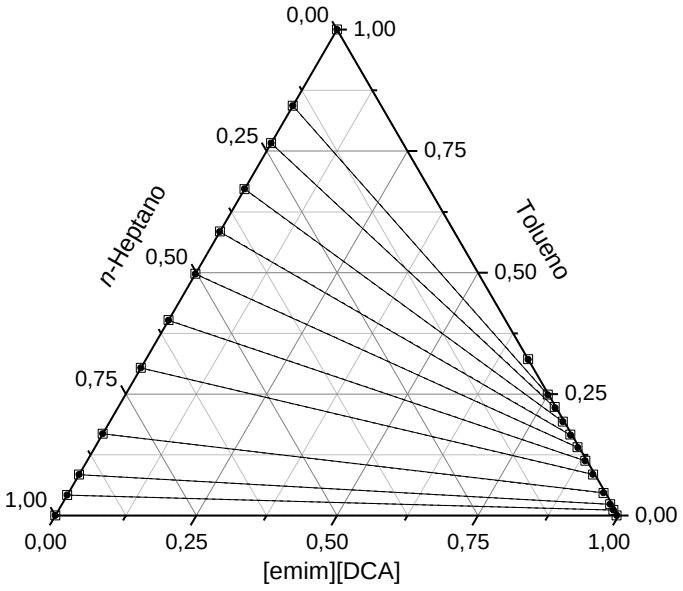

Figura 2.5. Datos del equilibrio líquido–líquido de la mezcla {*n*–heptano + tolueno + [emim][DCA]} a 313,2 K (Larriba y col., 2013b).

Por último, en las mezclas multicomponente, en las que coexisten seis o siete hidrocarburos y dos líquidos iónicos, se ha trabajado sólo en las composiciones de la corriente de extracto obtenida en la separación de aromáticos de modelos de gasolinas de reformado y pirólisis y de la nafta alimentada al *cracker* de etileno.

Capítulo 3. Resultados

En este capítulo se recogen los resultados experimentales obtenidos en el marco de la tesis doctoral. La estabilidad térmica de los líquidos iónicos puros y sus mezclas binarias se ha determinado para ciclos de operación industriales, estableciendo de este modo una temperatura máxima de operación para este tipo de compuestos. Dentro del intervalo de estabilidad térmica de los líquidos iónicos puros y sus mezclas, se han medido sus calores específicos. Por último, se han obtenido datos de equilibrio líquido–vapor de mezclas representativas de corrientes de extracto de la separación de aromáticos usando líquidos iónicos como disolvente, proponiéndose un proceso de fraccionamiento para dicha corriente.

3.1. Estabilidad térmica

El estudio de la estabilidad térmica de los líquidos iónicos puros y sus mezclas binarias se ha realizado por análisis termogravimétrico. Los resultados obtenidos se han difundido en su totalidad como parte de las publicaciones I, II y III de esta tesis doctoral.

En la Tabla 3.1 se recogen los parámetros más importantes para discutir la estabilidad térmica de los líquidos iónicos puros y sus mezclas binarias. Se han incluido las temperaturas *onset* calculadas a partir de los ensayos termogravimétricos dinámicos a la velocidad de calefacción de 5 $K \cdot min^{-1}$ y los intervalos de estabilidad térmica obtenidos a partir de experimentos termogravimétricos isotermos de 48 h.

Además, se han incluido también las temperaturas máximas de operación (MOT) para un ciclo de operación industrial de 8000 h estimadas con el modelo de Seeberger y col. (2009) a partir de los datos termogravimétricos experimentales dinámicos con una rampa de calefacción de 5 $K \cdot min^{-1}$.

Tabla 3.1. Parámetros de estabilidad térmica de los líquidos iónicos y sus mezclas

Líquidos iónicos puros			
Líquidos iónicos	T_{onset}[a]/K	T_{48h}[b]/K	*MOT*[c]/K
[emim][DCA]	557,4	393,2 – 433,2	412
[bmim][DCA]	560,2	393,2 – 433,2	428
[emim][SCN]	525,5	353,2 – 393,2	360
[bmim][SCN]	533,0	393,2 – 433,2	403
[4empy][Tf_2N]	675,7	473,2 – 513,2	480
[emim][TCM]	602,5	433,2 – 473,2	452
Mezclas binarias			
w_1	T_{onset}[a]/K	T_{48h}[b]/K	*MOT*[c]/K
{[emim][DCA] (1) + [4empy][Tf_2N] (2)}			
0,25	539,4	393,2 – 433,2	415
0,50	550,8	393,2 – 433,2	413
0,75	556,4	393,2 – 433,2	412
{[emim][DCA] (1) + [emim][TCM] (2)}			
0,25	555,5	393,2 – 433,2	414
0,50	554,1	393,2 – 433,2	412
0,75	552,0	393,2 – 433,2	412

[a] Temperatura *onset* a 5 $K \cdot min^{-1}$
[b] Intervalo de estabilidad isotermo para 48 h
[c] Temperatura máxima de operación estimada a 8000 h

Análisis dinámicos

De los resultados de la Tabla 3.1 se puede establecer que el orden de estabilidad térmica de los líquidos iónicos puros atendiendo al anión que incorporan sería: bis(trifluorometilsulfonil)imida > tricianometano > dicianamida > tiocianato. La estructura del anión determina la estabilidad térmica del líquido iónico, mientras que los sustituyentes del catión han matizado ligeramente esta propiedad del líquido iónico: [bmim] > [emim].

En la Figura 3.1 se muestra gráficamente esta tendencia para las curvas de descomposición a 10 $K \cdot min^{-1}$. La importancia del anión en la estabilidad térmica de los líquidos iónicos y la ligera mejora que presentan los sustituyentes largos en los cationes ya se observaron también en estudios previos (Fredlake y col., 2004; Crosthwaite y col., 2005; Ficke y col., 2010).

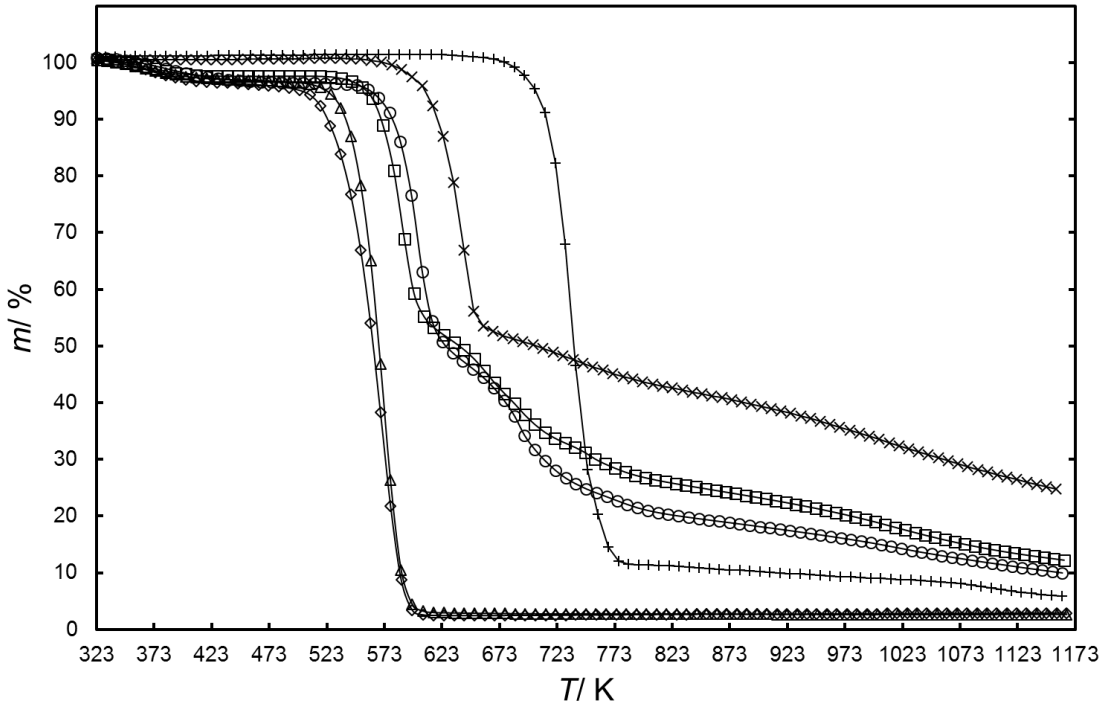

Figura 3.1. Curvas masa (*m*) – temperatura (*T*) de descomposición térmica para los líquidos iónicos puros: ◊, [emim][SCN]; △, [bmim][SCN]; □, [emim][DCA]; ○, [bmim][DCA]; ×, [emim][TCM]; +, [4empy][Tf_2N]. Rampa de calefacción: 10 K·min^{-1}.

Los resultados de los análisis termogravimétricos dinámicos de las mezclas binarias de líquidos iónicos suponen en principio una mayor dificultad de interpretación ya que en la mezcla {[emim][DCA] + [4empy][Tf_2N]} coexisten cuatro iones y en la mezcla {[emim][DCA] + [emim][TCM]} tres.

Sin embargo, se ha observado que el anión [DCA] ha condicionado la estabilidad térmica de ambas mezclas, ya que las temperaturas *onset* a 5 K·min^{-1} de todas las mezclas se acercan al del líquido iónico puro basados en dicho anión

Como se puede apreciar en la Figura 3.2, en efecto, las mezclas binarias de líquidos iónicos ofrecen temperaturas *onset* casi coincidentes con la del líquido iónico [emim][DCA] y apenas se ven afectadas por la concentración de otro líquido iónico de mayor estabilidad térmica.

.

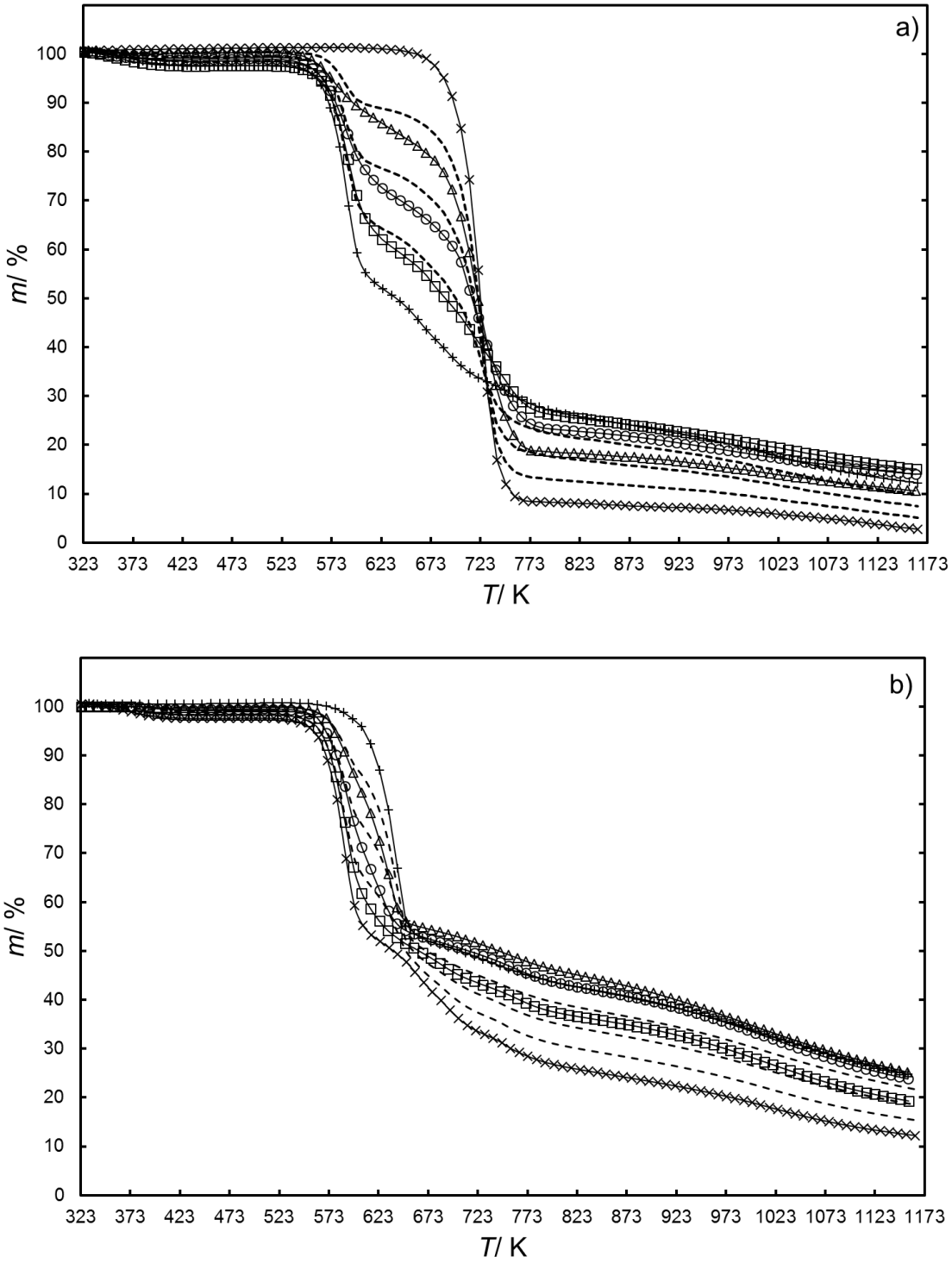

Figura 3.2. Curvas masa (*m*) – temperatura (*T*) de descomposición térmica a la rampa de calefacción de 10 K·min^{-1} para las mezclas binarias de líquidos iónicos: (a), {[4empy][Tf_2N] (*w*) + [emim][DCA] (1 - *w*)}; (b), {[emim][TCM] (*w*) + [emim][DCA] (1 - *w*)}. ×, *w* = 0; □, *w* = 0,25; ○, *w* = 0,5; △, *w* = 0,75; +, *w* = 1. Las líneas discontinuas representan los resultados predichos por la regla de mezcla propuesta en la ecuación 3.1.

Sin embargo, las curvas de descomposición térmica de las mezclas de líquidos iónicos sí que han mostrado comportamientos intermedios entre aquéllas correspondientes a los líquidos iónicos puros que la forman. Por esta razón, se ha planteado la regla de mezcla siguiente:

$$m_{\text{mezcla}} = \sum_{i=1}^{I} w_i \cdot m_i \qquad (3.1)$$

donde m_{mezcla} es la masa de la mezcla de líquidos iónicos predicha, m_i son las masas de los líquidos iónicos puros que la forman, a la misma temperatura, y w_i sus fracciones másicas en tal mezcla.

En la Figura 3.2 se observa cómo dicha regla de mezcla predice correctamente la pérdida de masa de las mezclas binarias de líquidos iónicos en los primeros procesos de descomposición térmica.

Bien es verdad que a elevadas temperaturas los productos de descomposición de los líquidos iónicos parece que interaccionan entre sí, haciendo imposible predecir el comportamiento de una mezcla binaria de líquidos iónicos a partir de los comportamientos de los líquidos iónicos puros que la integran.

Sin embargo, el cálculo de la temperatura *onset* sólo requiere de los primeros procesos de degradación; por tanto, las curvas de descomposición térmica predichas por la ecuación 3.1 para las mezclas binarias de líquidos iónicos ofrecen temperaturas *onset* totalmente coincidentes con las obtenidas experimentalmente.

Esta regla de mezcla, que ha sido aplicada por primera vez en este trabajo, se ha utilizado también con buenos resultados de predicción en las tres mezclas binarias siguientes: {[4bmpy][Tf_2N] + [bpy][BF_4]}, {[4bmpy][Tf_2N] + [emim][TFES]} y {[bpy][Tf_2N] + [bpy][BF_4]} (Larriba y col., 2015a; Navarro y col., 2015).

Análisis isotermos

En paralelo a los análisis TGA dinámicos, se realizaron experimentos TGA isotermos a las temperaturas de 313,2 K, 353,2 K, 393,2 K, 433,2 K y 473,2 K, fijando un tiempo de análisis de 48 h. Estos ensayos se realizaron tanto para líquidos iónicos puros como para sus mezclas binarias.

Comparando los valores de temperatura *onset* recogidos en la Tabla 3.1 obtenidos para una rampa de calentamiento de 5 $K \cdot min^{-1}$ y el intervalo de estabilidad térmica alcanzado a partir de los ensayos termogravimétricos isotermos, se observa que los ensayos dinámicos sobreestiman la estabilidad térmica de los líquidos iónicos.

El objetivo de estos estudios era establecer la temperatura máxima de aplicación de los líquidos iónicos y sus mezclas para ciclos de operación industrial largos. Por ello, los intervalos de estabilidad térmica obtenidos a partir de los ensayos termogravimétricos isotermos son los verdaderamente útiles para poder definir dicha temperatura.

Sin embargo, debido al elevado coste de los ensayos isotermos, se ha utilizado el modelo de predicción de comportamientos isotermos a partir de curvas de descomposición termogravimétricas dinámicas para ciclos de operación de larga duración, propuesto por Seeberger y col. (2009).

Predicción de la estabilidad térmica para ciclos de operación industriales

Seeberger y col. (2009) propusieron un modelo de primer orden con respecto a la masa para ajustar las curvas de descomposición térmica dinámicas con rampas de calefacción lentas:

$$\frac{-\mathrm{d}m}{\mathrm{d}t} = k_0 \cdot \exp\left(-\frac{E_\mathrm{A}}{\mathrm{R} \cdot T}\right) \cdot m \qquad (3.2)$$

donde m es la masa del líquido iónico, t es el tiempo transcurrido, k_0 es el factor de frecuencia de la constante de descomposición, E_A es la energía de activación, R es la constante de los gases y T es la temperatura.

A partir del factor de frecuencia y de la energía de activación es posible relacionar las temperaturas máximas de operación (MOT) de los líquidos iónicos y el tiempo máximo de estabilidad a dichas temperaturas (t_{max}):

$$\mathrm{MOT}=\frac{E_A}{R\cdot\left[4{,}6+\ln(k_0\cdot t_{max})\right]} \qquad (3.3)$$

El valor de 4,6 es el resultado de resolver el $-\ln(\ln(m_{final}/m_{inicial}))$ para una pérdida de masa inicial de un 1 %, valor considerado por varios autores como máxima pérdida de masa admisible sin que se produzca la descomposición térmica de la muestra (Seeberger y col., 2009; Crosthwaite y col., 2005).

Fijando un t_{max} de 8000 h, que se corresponde con un ciclo de operación industrial de un año, se han determinado los valores de la MOT para los líquidos iónicos puros. En la Figura 3.3 se representan los intervalos de estabilidad térmica obtenidos en los ensayos isotermos junto con los valores de la MOT para los líquidos iónicos puros. Se observa que todas las MOT se encuentran dentro del intervalo de temperaturas obtenido experimentalmente, validándose así el modelo utilizado.

En el caso de las dos mezclas binarias de líquidos iónicos, {[4empy][Tf_2N] + [emim][DCA]} y {[emim][TCM] + [emim][DCA]}, las MOT obtenidas fueron casi coincidentes con las de los líquidos iónicos basados en el anión [DCA]. Posteriores estudios de predicción de MOT para las mezclas de líquidos iónicos {[4bmpy][Tf_2N] + [bpy][BF_4]}, {[4bmpy][Tf_2N] + [emim][TFES]} y {[bpy][Tf_2N] + [bpy][BF_4]} han concluido también en que la MOT de la mezcla es casi coincidente con la del líquido iónico puro menos estable que la forma (Larriba y col., 2015a; Navarro y col., 2015).

Por tanto, la MOT de una mezcla de líquidos iónicos es prácticamente coincidente con aquélla del líquido iónico menos estable que la forma, como muestran los resultados disponibles hoy en día.

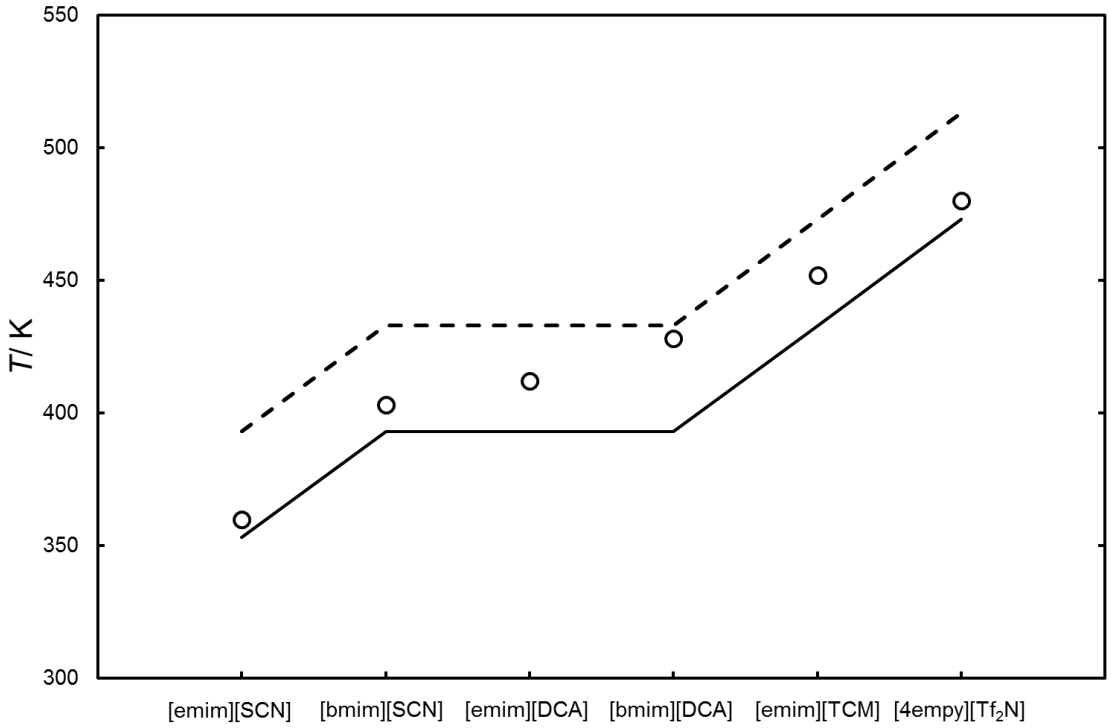

Figura 3.3. Valores de MOT (○). Las líneas continua y discontinua muestran la temperatura máxima a la que los líquidos iónicos no se descomponen y la temperatura mínima a la que los líquidos iónicos se descomponen, respectivamente, en ensayos termogravimétricos isotermos experimentales.

3.2. Calores específicos

Los calores específicos de los líquidos iónicos puros y sus mezclas se han determinado mediante calorimetría diferencial de barrido en el intervalo de temperaturas comprendido entre 296,2 K y 372,2 K. La evolución de los calores específicos con la temperatura se ha modelado mediante un polinomio de segundo orden.

En la Tabla 3.2 se recogen los calores específicos de todos los líquidos iónicos puros y sus mezclas junto con el del sulfolano a una temperatura de 308,2 K. Como se puede inferir de la comparación, todos los líquidos iónicos puros y sus mezclas han mostrado calores específicos ligeramente superiores al del sulfolano, lo que implicaría un ligero aumento de los costes energéticos a igualdad de temperaturas de operación.

Tabla 3.2. Calores específicos (C_P) para todos los líquidos iónicos puros y sus mezclas binarias a 308,2 K

Líquidos iónicos puros	
Líquidos iónicos	C_P/ J·(g·K)$^{-1}$
[emim][DCA]	1,862
[bmim][DCA]	1,775
[emim][SCN]	1,691
[bmim][SCN]	1,628
[4empy][Tf_2N]	1,591
[emim][TCM]	1,808
Mezclas binarias	
w_1	C_P/ J·(g·K)$^{-1}$
{[emim][DCA] (1) + [4empy][Tf_2N] (2)}	
0,25	1,683
0,50	1,748
0,75	1,801
{[emim][DCA] (1) + [emim][TCM] (2)}	
0,25	1,834
0,50	1,847
0,75	1,861
Disolvente de referencia	
Sulfolano	**1,518**

Con respecto a las mezclas binarias de líquidos iónicos, se aprecia claramente cómo los calores específicos fueron intermedios de los de los líquidos iónicos puros que forman las correspondientes mezclas. Para evaluar la desviación de la idealidad de esta propiedad en las dos mezclas de líquidos iónicos se han calculado los calores específicos de exceso (C_P^E):

$$C_P^E = C_{P,mezcla} - \sum_{i=1}^{I} x_i \cdot C_{P,i} \qquad (3.4)$$

donde $C_{P,mezcla}$ es el calor específico experimental obtenido para la mezcla, $C_{P,i}$ son los calores específicos de los líquidos iónicos puros que la forman y x_i sus fracciones molares en la mezcla.

En la Figura 3.4 se muestran los calores específicos de exceso en función de la temperatura y de la composición para las dos mezclas binarias de líquidos iónicos. Los calores específicos de exceso se muestran en base molar porque la evaluación de la idealidad de la ecuación 3.4 se establece así.

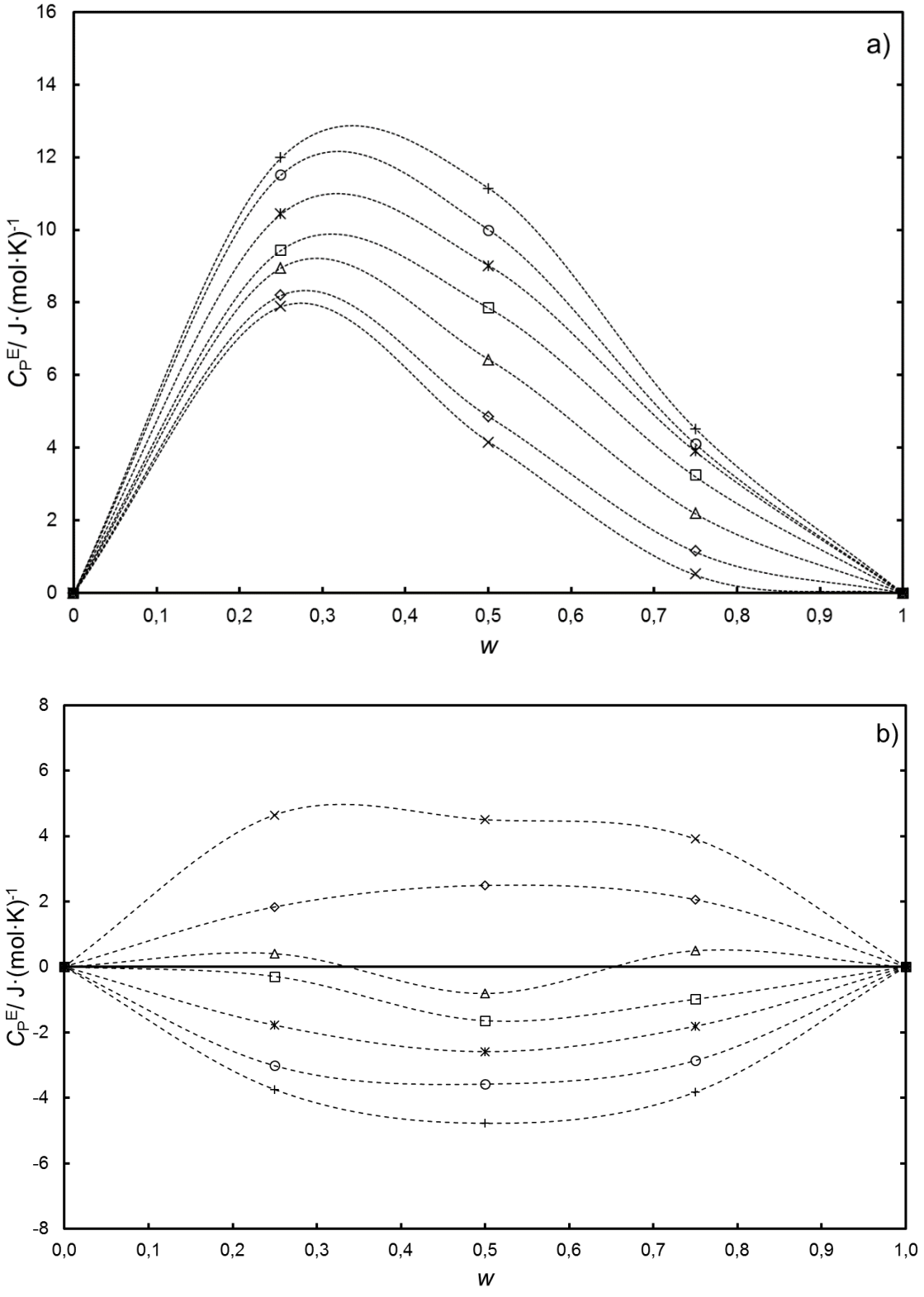

Figura 3.4. Calores específicos de exceso (C_P^E) de las mezclas binarias de líquidos iónicos: (a), {[4empy][Tf_2N] (*w*) + [emim][DCA] (1 – *w*)}; (b), {[emim][TCM] (*w*) + [emim][DCA] (1 – *w*)}. ×, *T* = 296,2 K; ◊, *T* = 308,2 K; △, *T* = 320,2 K; □, *T* = 332,2 K; ∗, *T* = 344,2 K; ○, *T* = 356,2 K; +, *T* = 368,2 K. Las líneas de trazos representan el ajuste a la ecuación de Redlich–Kister (1948).

Sabiendo que los calores específicos de las dos mezclas de líquidos iónicos han variado en el intervalo 324 – 715 $J\cdot(mol\cdot K)^{-1}$, se puede afirmar que los valores de los calores específicos de exceso calculados sugieren un comportamiento cuasi ideal de mezcla con respecto a esta propiedad para las dos mezclas.

Posteriores estudios de calores específicos de mezclas binarias de líquidos iónicos han obtenido también pequeños valores de los calores específicos de exceso (Larriba y col., 2015; Navarro y col., 2015).

3.3. Equilibrio líquido–vapor

En esta tesis doctoral se ha determinado el equilibrio líquido–vapor para mezclas representativas de corrientes de extracto obtenidas en la separación de aromáticos de sus mezclas con alcanos mediante el empleo como disolvente de líquidos iónicos.

3.3.1. Equilibrio líquido–vapor para las mezclas ternarias {*n*–heptano + tolueno + [emim][DCA] o [4empy][Tf_2N]}

El equilibrio líquido–vapor de las mezclas {*n*–heptano + tolueno + [emim][DCA] o [4empy][Tf_2N]} se ha determinado en todo el intervalo de composiciones a las temperaturas de 323,2 K, 343,2 K y 363,2 K. Estos resultados han dado lugar a las publicaciones IV y V de esta tesis doctoral.

Estas mezclas ternarias se han seleccionado con el objetivo de evaluar la recuperación de hidrocarburos de dos líquidos iónicos con propiedades extractivas muy diferentes.

El [emim][DCA] es un líquido iónico con elevada selectividad aromático/alifático, mientras que el [4empy][Tf_2N] tiene una mayor capacidad de extracción de aromáticos pero con una menor selectividad aromático/alifático (Larriba y col., 2013c).

Para evaluar la eficacia en la separación *n*–heptano (1)/tolueno (2) se han calculado las volatilidades relativas ($\alpha_{1,2}$) como:

$$\alpha_{1,2} = \frac{K_1}{K_2} = \frac{y_1 / x_1}{y_2 / x_2} \tag{3.5}$$

donde *x* e *y* representan las composiciones molares del líquido y del vapor, respectivamente, y *K* es la razón de equilibrio.

En la Figura 3.5 se recogen los valores de volatilidad relativa *n*–heptano/tolueno en la composición típica de la fase extracto de la separación de aromáticos de alifáticos. Dichos valores en las mezclas ternarias {*n*–heptano + tolueno + [emim][DCA] o [4empy][Tf_2N]} fueron muy superiores a los mostrados en las correspondientes mezclas binarias {*n*–heptano + tolueno} a las tres temperaturas ensayadas.

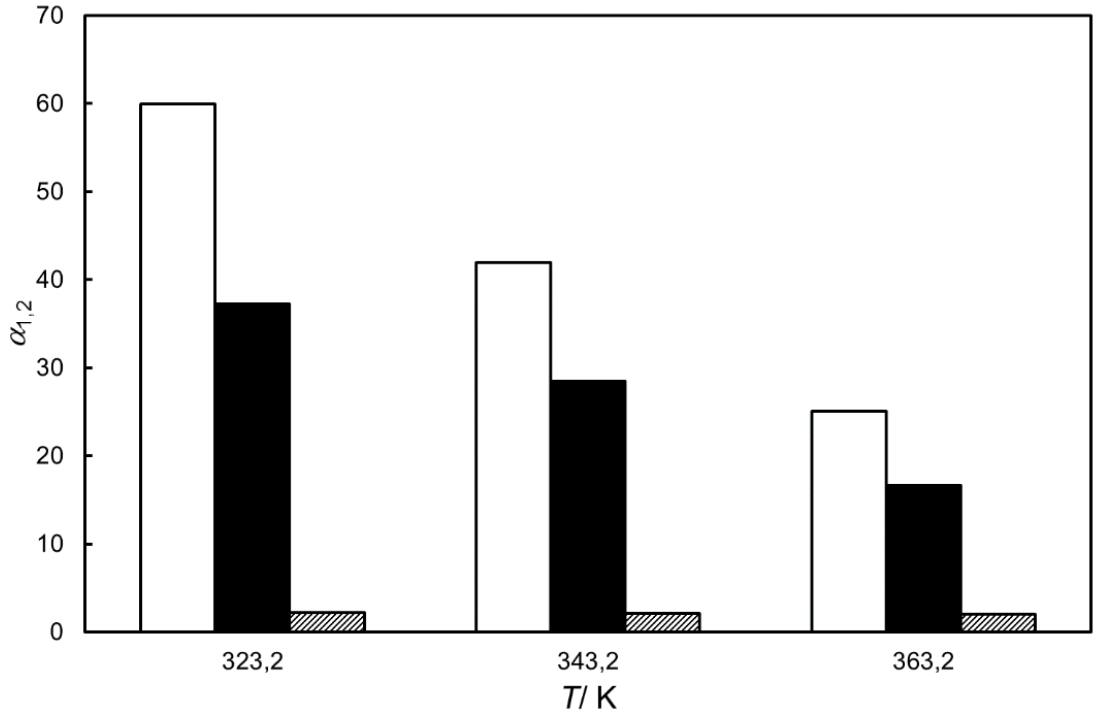

Figura 3.5. Volatilidad relativa del *n*–heptano frente al tolueno en función de la temperatura en presencia de líquidos iónicos puros ([emim][DCA], blanco; [4empy]Tf_2N], negro; sin líquido iónico, trama). Mezcla de referencia: {*n*–heptano (0,001) + tolueno (0,009) + líquido iónico (0,990)} en base másica.

Además, el líquido iónico [emim][DCA] originó los valores más elevados de volatilidad relativa *n*–heptano/tolueno. Este hecho muestra una relación entre la selectividad tolueno/*n*–heptano de un líquido iónico en extracción líquido–líquido y la volatilidad relativa *n*–heptano/tolueno a la que da lugar, ya que el líquido iónico [emim][DCA] tiene mayores valores en ambas propiedades. Posteriores estudios de equilibrios líquido–vapor alcanzaron la misma relación entre la selectividad tolueno/*n*–heptano y la volatilidad relativa *n*–heptano/tolueno (González y col., 2015).

Los datos de equilibrio líquido–vapor se correlacionaron con el modelo termodinámico *Non–Random Two Liquids* (NRTL) desarrollado por Renon y Prausnitz (1968). Esta elección se fundamente en los buenos resultados que diversos autores obtuvieron previamente para mezclas formados por compuestos orgánicos y líquidos iónicos (Andreatta y col., 2010; Li y col., 2009; Orchillés y col., 2012).

Se ha implementado un algoritmo de ajuste de los datos experimentales de equilibrio líquido–vapor al modelo NRTL en *Microsoft Excel*. Para ello se ha definido la siguiente función objetivo (*FO*) en función de las desviaciones de las fracciones molares de la fase líquida (Δx) y la presión (ΔP):

$$FO = a \cdot \Delta x + \Delta P \tag{3.6}$$

donde el parámetro *a* se emplea para corregir la diferencia de orden de magnitud de las incertidumbres de las fracciones molares de la fase líquida y las presiones, en kPa, fijándose un valor de 300.

En la Figura 3.6 se muestran los datos experimentales de equilibrio líquido–vapor de las mezclas ternarias {*n*–heptano + tolueno + [emim][DCA] o [4empy][Tf_2N]} a la temperatura de 323,2 K junto con los valores predichos a partir del modelo NRTL. Se aprecia la buena concordancia entre los datos experimentales y los calculados a partir del modelo NRTL, hecho que se extiende a las otras dos temperaturas (343,2 K y 363,2 K) como se puede observar en las publicaciones IV y V.

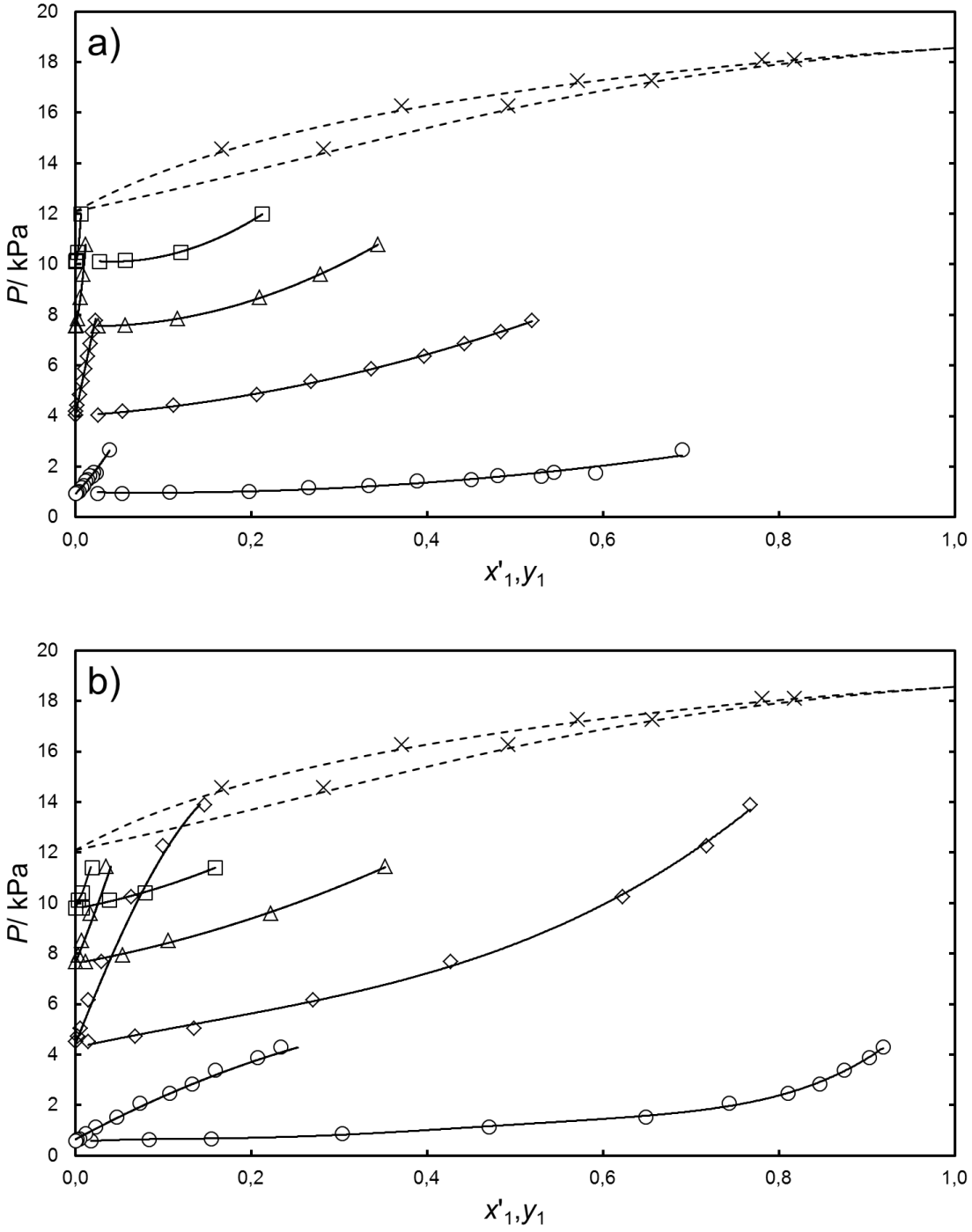

Figura 3.6. Datos experimentales y ajuste a NRTL de la mezcla {*n*–heptano (1) + tolueno (2) + líquido iónico (3)} a 323,2 K (a, [emim][DCA]; b, [4empy]Tf_2N]). La línea de trazos representa la mezcla {*n*–heptano + tolueno} y la línea sólida el ajuste a NRTL. [emim][DCA]: ○, x_3 = 0,98; ◇, x_3 = 0,92; △, x_3 = 0,84; □, x_3 = 0,77; ×, x_3 = 0,00. [4empy]Tf_2N]: ○, x_3 = 0,96; ◇, x_3 = 0,68; △, x_3 = 0,48; □, x_3 = 0,35; ×, x_3 = 0,00.

3.3.2. Efecto de la composición de la mezcla de líquidos iónicos {[4empy][Tf_2N] + [emim][DCA]} sobre el equilibrio líquido–vapor de mezclas pseudoternarias {alcano + aromático + {[4empy][Tf_2N] + [emim][DCA]}}

Los estudios previos de propiedades extractivas y físicas de la mezcla {[4empy][Tf_2N] + [emim][DCA]} habían concluido en que su composición más adecuada es aquélla con la fracción molar de [emim][DCA] de 0,7 (Larriba y col., 2013c). Sin embargo, dicha selección no había tenido en cuenta los datos de equilibrio líquido–vapor; es por ello que se ha evaluado en esta tesis doctoral, dando lugar a la publicación VI.

Se han estudiado los equilibrios líquido–vapor de diversas mezclas {alcano + aromático + {[4empy][Tf_2N] + [emim][DCA]}}. En la Figura 3.7 se muestran los valores de las volatilidades relativas *n*–heptano/tolueno de la mezcla {*n*–heptano + tolueno + {[4empy][Tf_2N] + [emim][DCA]}}.

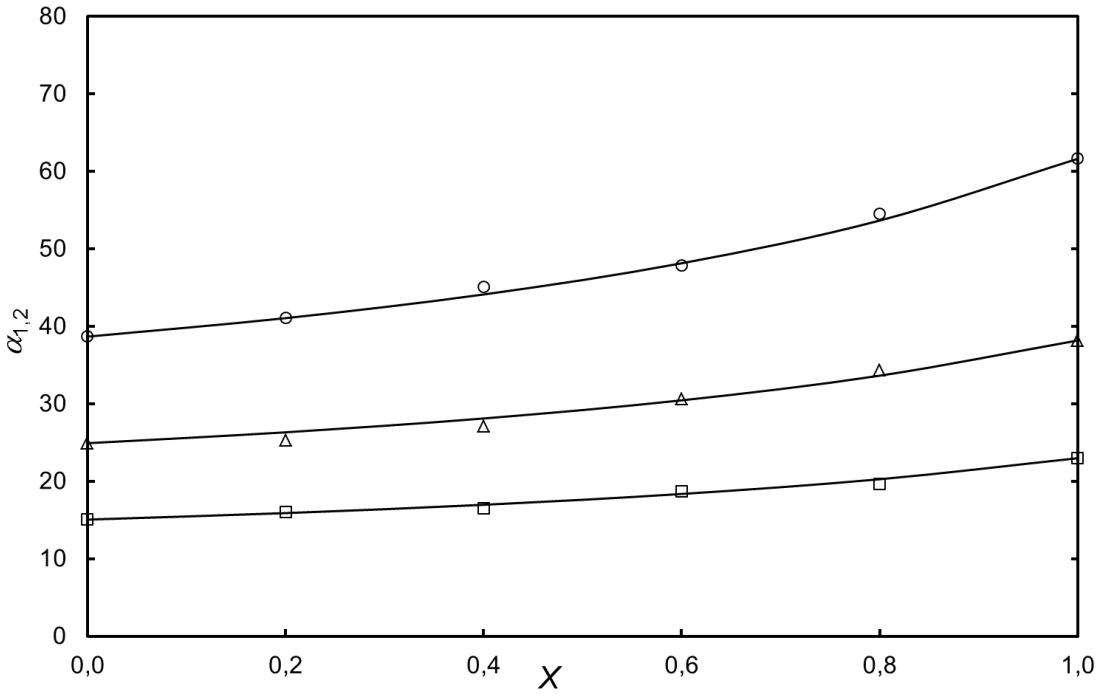

Figura 3.7. Volatilidades relativas del *n*–heptano frente al tolueno para la mezcla {*n*–heptano (1) + tolueno (2) + {[emim][DCA] (3) + [4empy]Tf_2N] (4)}} en diferentes proporciones {[emim][DCA] (*X*) + [4empy]Tf_2N] (1–*X*)} y a varias temperaturas: ○, 323,2 K; △, 343,2 K; □, 363,2 K. Mezcla de referencia: {*n*–heptano (0,001) + aromático (0,009) + {[4empy][Tf_2N] + [emim][DCA]} (0,990)} en base másica. Las líneas sólidas representan el ajuste a la regla de mezcla de Yalkowsky–Roseman.

Todas las composiciones de la mezcla binaria de líquidos iónicos dieron lugar a volatilidades relativas *n*–heptano/tolueno intermedias a aquéllas de los dos líquidos iónicos puros. Además, en todos los casos se obtuvieron valores de volatilidad relativa alifático/aromático más elevados cuanto mayor era la fracción molar de [emim][DCA] en la mezcla binaria de líquidos iónicos.

Analizando los valores de la volatilidad relativa *n*–heptano/tolueno de la Figura 3.7 para la composición de la mezcla binaria de líquidos iónicos previamente seleccionada en base a propiedades extractivas y físicas, {[4empy][Tf_2N] (0,3) + [emim][DCA] (0,7)}, se observa que dicha composición originaría valores de volatilidad relativa *n*–heptano/tolueno entre 20 y 45, aproximadamente, en función de la temperatura. Estos valores garantizarían una fácil separación del *n*–heptano del tolueno en este tipo de mezclas. En la publicación VI se puede comprobar cómo este análisis ofrece las mismas conclusiones para todas las mezclas {alcano + aromático + {[4empy][Tf_2N] (0,3) + [emim][DCA] (0,7)}}.

Además, para predecir los valores de volatilidad relativa alifático/aromático de las diversas composiciones de la mezcla a partir de los valores de los líquidos iónicos puros se empleó la regla de mezcla de Yalkowsky y Roseman (1981):

$$\ln(x, y)_{\mathrm{i,pred}} = \sum_{\mathrm{j=3}}^{4} f_{\mathrm{j}} \ln(x, y)_{\mathrm{i,j}} \qquad (3.7)$$

donde $x,y_{\mathrm{i,pred}}$ es la fracción molar de los hidrocarburos predicha para las fases líquida o vapor, respectivamente, j se refiere a los líquidos iónicos puros que forman el disolvente, f_{j} es la fracción volumétrica de los líquidos iónicos en ausencia de hidrocarburos y $x,y_{\mathrm{i,j}}$ es la fracción molar de los hidrocarburos para las fases líquida o vapor en cada líquido iónico puro que forma el disolvente. En la Figura 3.7 se comparan los valores predichos por la regla de mezcla de Yalkowsky y Roseman con los datos experimentales obtenidos en el caso de la mezcla pseudoternaria {*n*–heptano + tolueno + {[4empy][Tf_2N] + [emim][DCA]}}, observándose la buena capacidad predictiva de esta regla de mezcla.

3.3.3. Equilibrio líquido–vapor para mezclas pseudoternarias {alcano + aromático + {[4empy][Tf_2N] (0,3) + [emim][DCA] (0,7)}}

Una vez se ha comprobado que la composición de la mezcla de líquidos iónicos {[4empy][Tf_2N] (0,3) + [emim][DCA] (0,7)} es también adecuada para garantizar la separación de los alifáticos de los aromáticos, se han determinado los datos del equilibrio líquido–vapor de las mezclas pseudoternarias {alcano + aromático + {[4empy][Tf_2N] (0,3) + [emim][DCA] (0,7)}} en todo el intervalo de composiciones y a varias temperaturas. Los resultados obtenidos se han recogido en las publicaciones VII y VIII de esta tesis doctoral.

Influencia del peso molecular del aromático en la separación alifático/aromático de corrientes de extracto

En la Figura 3.8 se analiza la influencia del peso molecular del aromático (benceno, tolueno, etilbenceno y *p*–xileno) en la separación de *n*–heptano de sus mezclas con aromáticos en función de la temperatura de equilibrio.

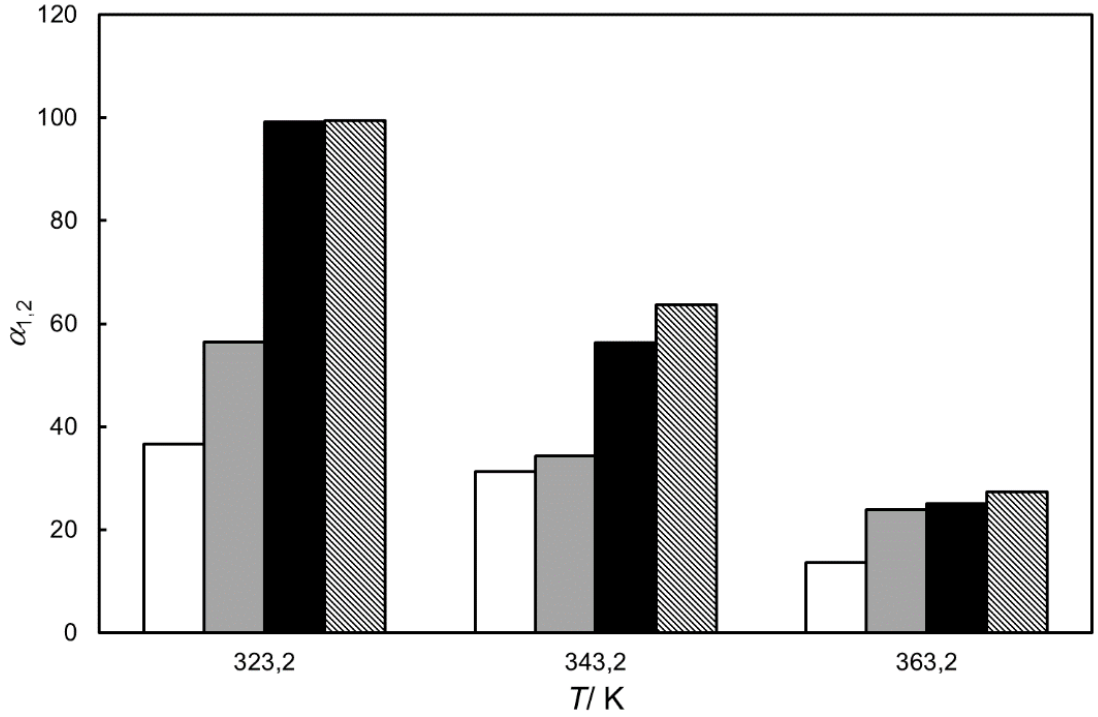

Figura 3.8. Volatilidad relativa del *n*–heptano frente al benceno (blanco), tolueno (gris), etilbenceno (negro) y *p*–xileno (trama) en mezclas {*n*–heptano (0,001) + aromático (0,009) + {[4empy][Tf_2N] (0,3) + [emim][DCA] (0,7)} (0,990)} en base másica a 323,2 K.

Como se aprecia, el aumento del peso molecular del aromático supone un incremento en la volatilidad relativa *n*–heptano/aromático, especialmente a la temperatura más baja. En cualquier caso, las volatilidades relativas *n*–heptano/aromático se vieron muy incrementadas en todas las mezclas pseudoternarias con respecto a las de las binarias {*n*–heptano + aromático}.

Además, tal y como se ve en la Figura 3.9, los valores de volatilidad relativa *n*–heptano/benceno suponen un cambio en el orden de volatilidad de los dos hidrocarburos, *n*–heptano y benceno, en favor del alcano en las mezclas {*n*–heptano + benceno + {[4empy][Tf_2N] (0,3) + [emim][DCA] (0,7)}} en comparación con la mezcla binaria {*n*–heptano + benceno} correspondiente. El aromático más ligero de la fracción BTEX, de partida más volátil que los compuestos no aromáticos, ve reducida drásticamente su volatilidad por la interacción con la mezcla de líquidos iónicos.

El benceno es el aromático que más limita la separación aromático/alifático. Sin embargo, los datos de equilibrio de la Figura 3.9 demuestran la facilidad con la que se puede llevar a cabo la recuperación de los alifáticos con la mezcla {[4empy][Tf_2N] (0,3) + [emim][DCA] (0,7)}.

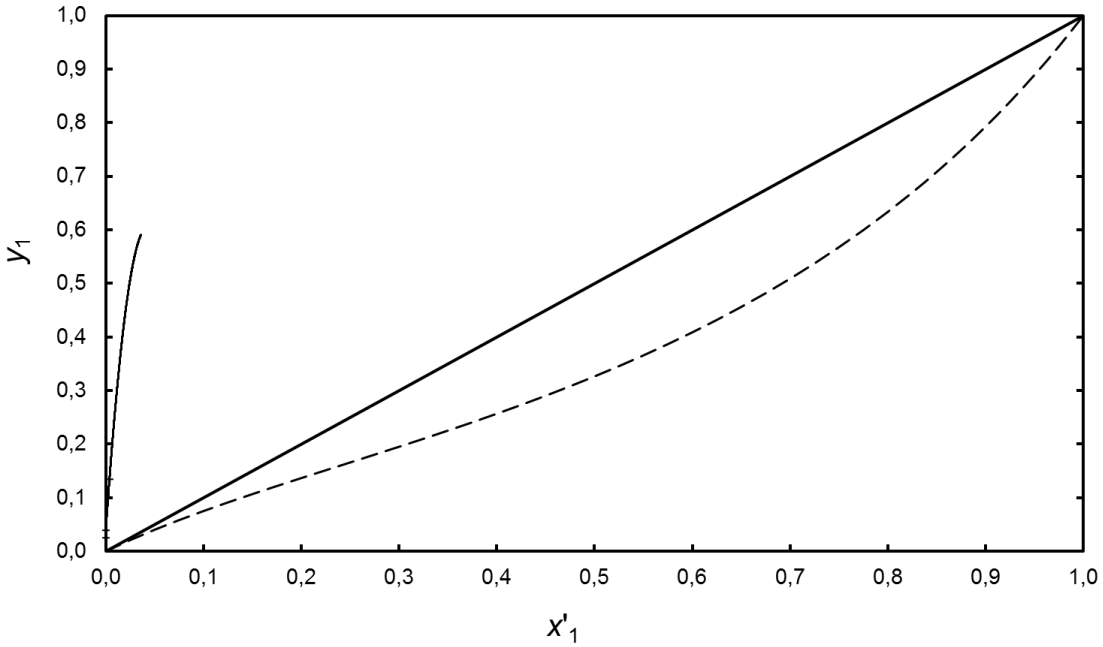

Figura 3.9. Equilibrio líquido–vapor para las mezclas pseudoternarias {*n*–heptano (1) + benceno (2) + {[4empy][Tf_2N] (3) + [emim][DCA] (4)}} con x_{3+4} = 0,98 (línea sólida) y {*n*–heptano + benceno} (línea de trazos) a 323,2 K.

Influencia de la longitud de la cadena del alcano en la separación alifático/aromático de corrientes de extracto

En la Figura 3.10 se recogen las volatilidades relativas de varios *n*–alcanos frente al tolueno, calculadas a partir del equilibrio líquido–vapor de las mezclas pseudoternarias {*n*–alcano + tolueno + {[4empy][Tf_2N] (0,3) + [emim][DCA] (0,7)}}.

Los *n*–alcanos de menor peso molecular ofrecieron mayores volatilidades relativas *n*–alcano/tolueno, especialmente a las temperaturas más reducidas. En cualquier caso, las volatilidades relativas para todos los *n*–alcanos con respecto al tolueno fueron muy elevadas.

Por tanto, se demuestra que la fracción de alcanos lineales C_6 – C_8 se podrían recuperar fácilmente y de forma selectiva de sus mezclas con tolueno o compuestos aromáticos más pesados.

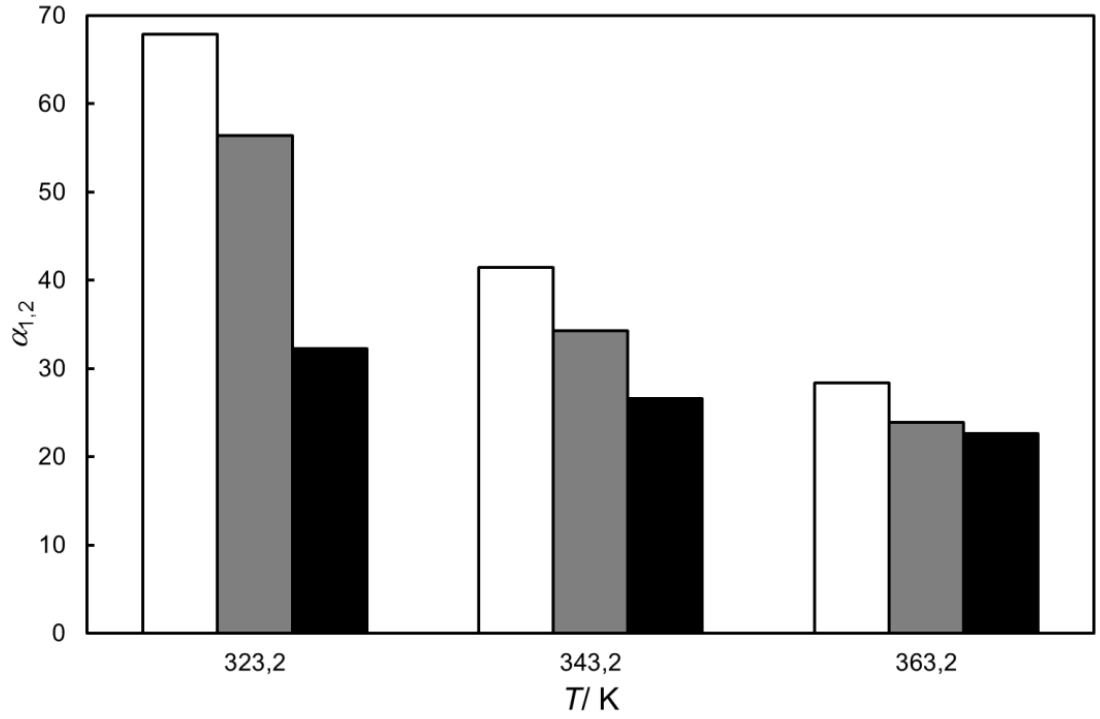

Figura 3.10. Volatilidad relativa del *n*–hexano (blanco), *n*–heptano (gris) y *n*–octano (negro) frente al tolueno en función de la temperatura para las mezclas pseudoternarias {*n*–alcano (0,001) + tolueno (0,009) + {[4empy][Tf_2N] (0,3) + [emim][DCA] (0,7)} (0,990)} en base másica a 323,2 K.

Por otro lado, los resultados obtenidos en la mezcla {*n*–octano + tolueno + {[4empy][Tf_2N] (0,3) + [emim][DCA] (0,7)}} merecen ser comentados en mayor profundidad. Como se puede apreciar en la Figura 3.11, la mezcla de líquidos iónicos cambia drásticamente el orden de volatilidades a favor del *n*–octano, ya que en la mezcla binaria {*n*–octano + tolueno} el aromático es el compuesto de mayor volatilidad..

Este punto resulta nuevamente de gran importancia en la separación de los hidrocarburos alifáticos de los aromáticos, debido a que empleando la mezcla de líquidos iónicos {[4empy][Tf_2N] (0,3) + [emim][DCA] (0,7)} como disolvente, la volatilidad de los aromáticos desciende en gran medida al interaccionar con la mezcla de líquidos iónicos en las corrientes de extracto obtenidas. Este hecho, junto con el que ya se comentó para la mezcla pseudoternaria {*n*–heptano + benceno + {[4empy][Tf_2N] (0,3) + [emim][DCA] (0,7)}} suponen un gran avance en la separación selectiva de los hidrocarburos extraídos.

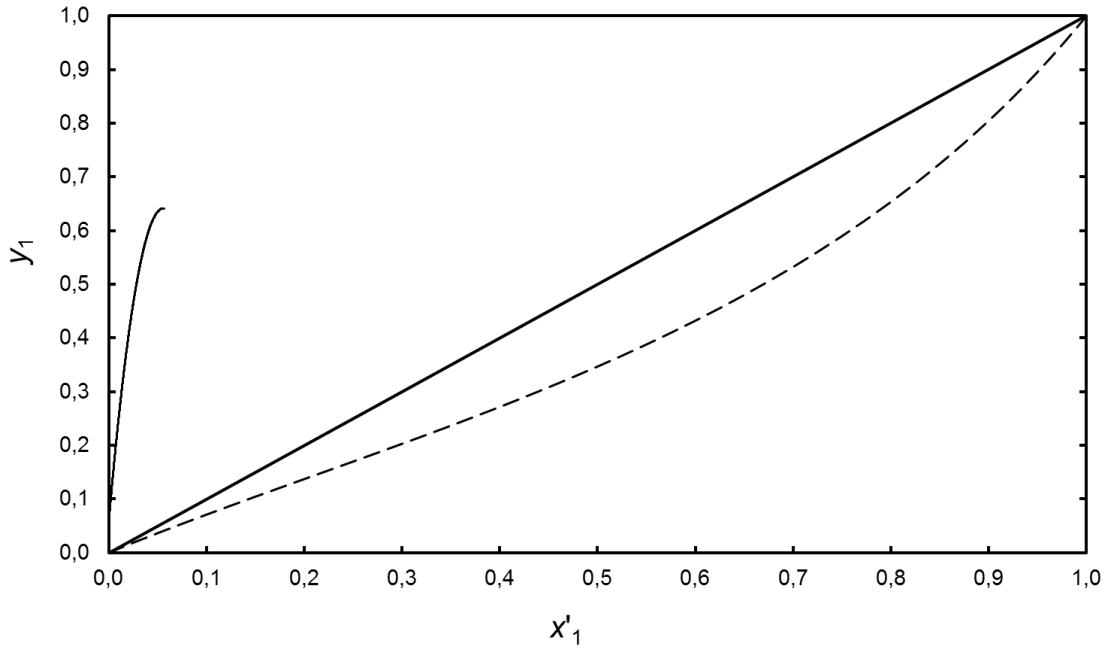

Figura 3.11. Equilibrio líquido–vapor para las mezclas {*n*–octano (1) + tolueno (2) + {[4empy][Tf_2N] (3) + [emim][DCA] (4)}} con x_{3+4} = 0,98 (línea sólida) y {*n*–octano + tolueno} (línea de trazos) a 323,2 K.

Influencia de las ramificaciones del alcano en la separación alifático/aromático de corrientes de extracto

En la Figura 3.12 se representan los valores de volatilidad relativa alcano/tolueno para las mezclas pseudoternarias {(2,3–dimetilpentano o *n*–heptano) + tolueno + {[4empy][Tf_2N] (0,3) + [emim][DCA] (0,7)}}. Se comparan, por tanto, dos alcanos con el mismo número de átomos de carbono, uno con estructura lineal y, el otro, ramificada.

Se observa un ligero incremento en el valor de la volatilidad relativa alcano/tolueno para el alcano cuya estructura es ramificada. La tendencia se explica por la mayor presión de vapor del 2,3–dimetilpentano en comparación con la del *n*–heptano, como consecuencia de una cadena principal más corta (Perry y col., 1999).

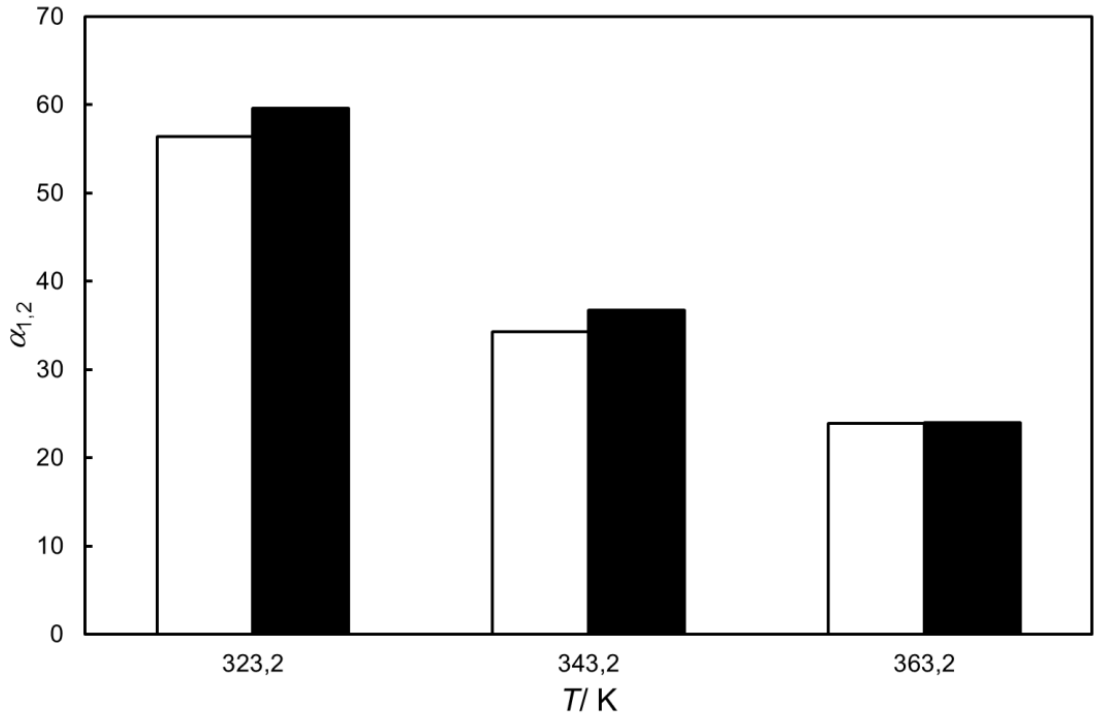

Figura 3.12. Volatilidad relativa del *n*–heptano (blanco) y 2,3–dimetilpentano (negro) frente al tolueno en las mezclas: {alcano (0,001) + tolueno (0,009) + {[4empy][Tf_2N] (0,3) + [emim][DCA] (0,7)} (0,990)} en base másica a 323,2 K.

Influencia de la naturaleza cíclica del alcano en la separación alifático/aromático de corrientes de extracto

En la Figura 3.13 se incluyen las volatilidades relativas alcano/tolueno para las mezclas {(*n*–hexano o ciclohexano) + tolueno + {[4empy][Tf_2N] (0,3) + [emim][DCA] (0,7)}}. En este caso se estudia la influencia de la naturaleza cíclica del alcano sobre la separación alcano/tolueno a partir de un alcano cíclico y uno lineal, ambos con el mismo número de átomos de carbono.

Como se aprecia, el cambio del *n*–hexano por el ciclohexano reduce el valor de la volatilidad relativa alcano/tolueno. Este hecho se explica por la mayor solubilidad del ciclohexano que la del *n*–hexano en la mezcla {[4empy][Tf_2N] (0,3) + [emim][DCA] (0,7)} (Larriba y col., 2013c).

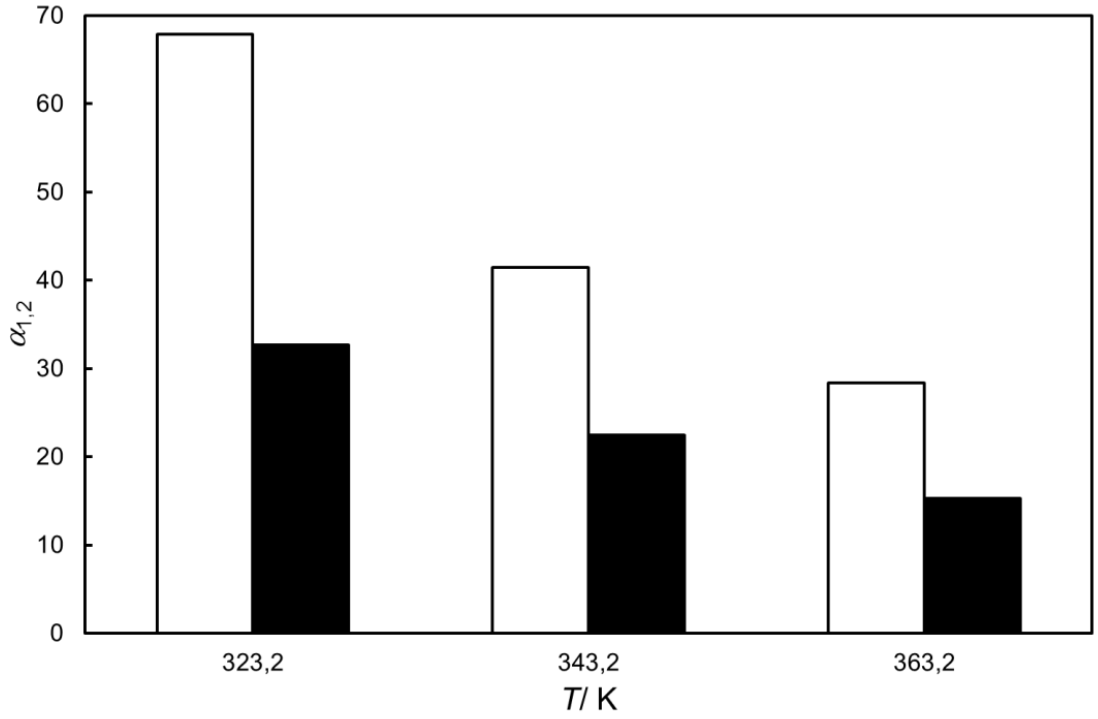

Figura 3.13. Volatilidad relativa del *n*–hexano (blanco) y ciclohexano (negro) frente al tolueno en las mezclas: {alcano (0,001) + tolueno (0,009) + {[4empy][Tf_2N] (0,3) + [emim][DCA] (0,7)} (0,990)} en base másica a 323,2 K.

3.3.4. Diseño conceptual de un proceso para el fraccionamiento del extracto de la separación de aromáticos con líquidos iónicos

En este apartado se ha estudiado el equilibrio líquido–vapor de las corrientes de extracto obtenidas en la separación de aromáticos de modelos multicomponente de tres gasolinas y una nafta empleando la mezcla {[4empy][Tf_2N] (0,3) + [emim][DCA] (0,7)} como disolvente. En la Tabla 3.3 se detallan las composiciones de las corrientes de extracto (Larriba y col., 2014e, Larriba y col., 2015b,c).

A partir de los datos de equilibrio líquido–vapor obtenidos para las cuatro corrientes de extracto se ha propuesto un proceso de fraccionamiento de las mismas formado por tres unidades de destilación súbita.

Los resultados obtenidos en esta parte del trabajo se pretenden dar a conocer a partir de las dos últimas publicaciones preparadas en el marco de esta tesis doctoral (IX y X).

Tabla 3.3. Composición másica de las corrientes de extracto usando como disolvente la mezcla binaria de líquidos iónicos {[4empy][Tf_2N] (0,3) + [emim][DCA] (0,7)} a 303,2 K y 101,3 kPa

Compuesto	*Abreviatura*	*Gasolina de reformado*	*Gasolina de pirólisis*		*Nafta alimentada al cracker de etileno*
			Craqueo Suave	*Craqueo Severo*	
Aromáticos/ %	**Arom**	**9,7**	**9,2**	**11,5**	**1,8**
Benceno/ %	Benc	0,9	4,0	6,0	0,4
Tolueno/ %	Tol	4,3	3,2	3,4	0,6
p-Xileno / %	*p*–Xil	3,8	2,0	2,2	0,3
Etilbenceno/ %	Etbenc	0,7	–	–	0,5
Alifáticos/ %	**Alif**	**0,3**	**0,3**	**0,3**	**0,3**
n-Hexano	Hexa	0,1	0,1	0,1	0,1
n-Heptano	Hepta	0,1	0,1	0,1	0,1
n-Octano	Octa	0,1	0,1	0,1	0,1
{[4empy][Tf_2N] (0,3) + [emim][DCA] (0,7)}	**LI**	**90,0**	**90,5**	**88,2**	**97,9**

Equilibrio líquido–vapor

Inicialmente se estudió el equilibrio líquido–vapor de las cuatro corrientes de extracto en el intervalo de temperaturas comprendido entre los 303,2 K y los 363,2 K.

La volatilidad relativa de la fracción alifática total frente a la fracción de aromáticos total ($\alpha_{\text{alif,arom}}$) se ha calculado a partir de los datos de equilibrio líquido–vapor obtenidos como:

$$\alpha_{\text{alif,arom}} = \frac{K_{\text{alif}}}{K_{\text{arom}}} = \left[\frac{\left(y_{\text{hexa}} + y_{\text{hepta}} + y_{\text{octa}}\right)}{\left(x_{\text{hexa}} + x_{\text{hepta}} + x_{\text{octa}}\right)}\right]\left[\frac{\left(y_{\text{benc}} + y_{\text{tol}} + y_{p\text{-xil}} + y_{\text{etbenc}}\right)}{\left(x_{\text{benc}} + x_{\text{tol}} + x_{p\text{-xil}} + x_{\text{etbenc}}\right)}\right]^{-1} \qquad (3.8)$$

donde *x* e *y* son las fracciones molares del líquido y del vapor, respectivamente, y *K* son las razones de equilibrio. En la Figura 3.14 se muestran las $\alpha_{\text{alif,arom}}$ calculadas para las cuatro corrientes en función de la temperatura.

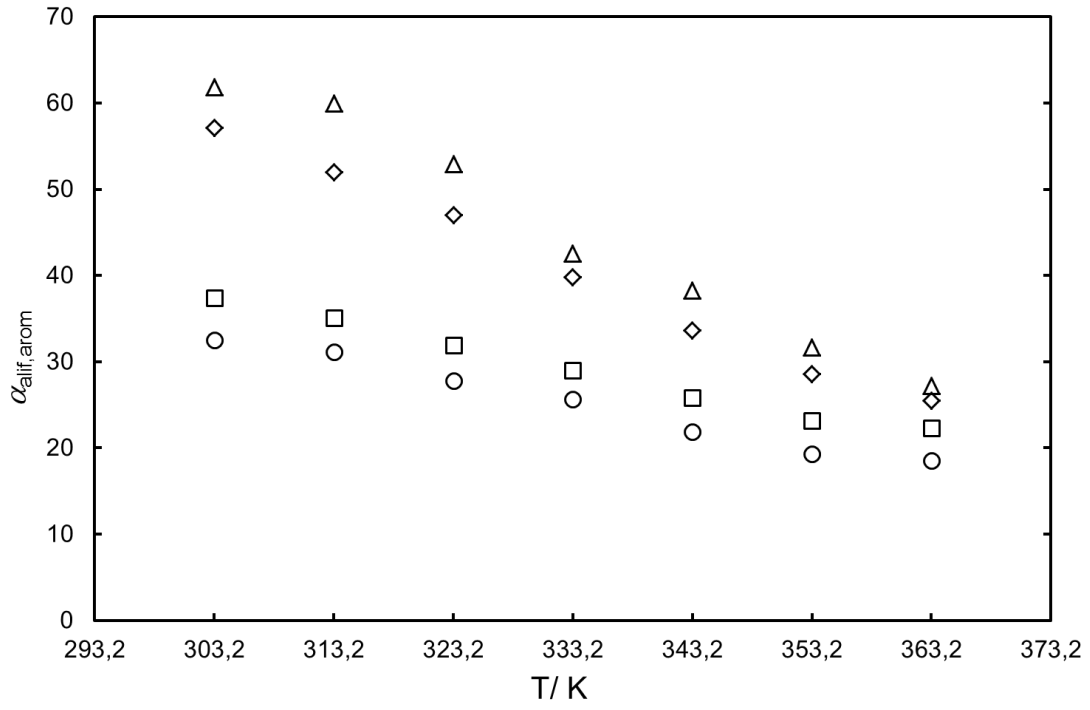

Figura 3.14. Volatilidad relativa de los alifáticos frente a los aromáticos para los extractos mostrados en la Tabla 3.3. Gasolina de reformado (◇); gasolina de pirólisis suave (□); gasolina de pirólisis severa (○); nafta alimentada al *cracker* de etileno (△).

Comparando estos valores con los obtenidos en mezclas ternarias y pseudoternarias {alifático + aromático + líquidos iónicos}, se puede aseverar que la separación de los tres compuestos alifáticos de los tres o cuatro aromáticos sigue siendo muy selectiva. Los valores más elevados de $\alpha_{alif,arom}$ se alcanzaron también a las temperaturas más bajas.

Por último, relacionando la composición de las corrientes de extracto con los valores de $\alpha_{alif,arom}$ se observa que la concentración de benceno condiciona los resultados. La separación más selectiva de alifáticos se alcanza para la nafta alimentada al *cracker* de etileno y la gasolina de reformado, ambas corrientes con una menor concentración de benceno.

Determinación de los coeficientes de actividad

Los datos de equilibrio líquido–vapor se han determinado por una técnica isoterma. Por tanto, para cada temperatura se han obtenido las composiciones de las fases vapor y líquida, así como las presiones parciales de cada componente en la fase vapor.

A partir de la ley de Raoult simplificada, se han calculado los coeficientes de actividad (γ_i) a partir de los datos de equilibrio líquido–vapor obtenidos:

$$\gamma_i = \frac{P \cdot y_i}{x_i \cdot P_i^0} \tag{3.9}$$

Se ha observado que los valores de los coeficientes de actividad de todos los hidrocarburos han variado en el intervalo de temperaturas comprendido entre 303,2 K y 363,2 K, mientras que las composiciones molares de la fase líquida apenas lo han hecho en ese intervalo.

Por tanto, sabiendo que el coeficiente de actividad es sólo función de la temperatura y de la composición de la fase líquida, se ha asumido que los valores de los coeficientes de actividad son constantes para cada valor de temperatura.

Simulación de las etapas de destilación súbita adiabáticas

Atendiendo a los elevados valores de volatilidad relativa de los alifáticos frente a los aromáticos se ha propuesto una batería de destilaciones súbitas como proceso de fraccionamiento del extracto.

En las primeras unidades se recogería la fracción de alifáticos y en las últimas se agotaría la fracción de aromáticos remanente en el extracto, que debería de alcanzar purezas en aromáticos cercanas al 99,9 % en masa (Gary y col., 2007). Se ha optado por etapas de destilación súbita adiabáticas por su menor coste en comparación con las isotermas (Branan, 2008).

La elevada concentración de la mezcla de líquidos iónicos en el extracto no permite recurrir a una operación de rectificación que sustituyese las primeras unidades de destilación súbita, ya que la corriente de extracto no ebulliría (Henley y Seader, 1981).

En la Tabla 3.4 se detalla el análisis de grados de libertad para una unidad de destilación súbita adiabática y las variables fijadas al respecto para una mezcla de 9 compuestos. Este análisis permite justificar el procedimiento implementado para calcular el reparto de fases, ya que se plantean 30 relaciones independientes para determinar otras tantas variables desconocidas. En la Figura 3.15 se incluye un diagrama de una etapa de destilación súbita adiabática para mostrar el análisis realizado de grados de libertad.

Tabla 3.4. Análisis de los grados de libertad del cálculo de las unidades de destilación súbita adiabática para el caso de 9 compuestos

Ecuación			Variables totales			
			Fijadas		Calculadas	
A	$K_i = \gamma_i \cdot P_i^0 / P$	(9)	P, T, γ_i	(11)	K_i	(9)
B	$y_i = K_i \cdot x_i$	(9)	–		x_i, y_i	(18)
C	$F \cdot z_i = L \cdot x_i + V \cdot y_i$	(9)	F, z_i	(10)	L, V	(2)
D	$\Sigma y_i = 1$	(1)	–		–	
E	$\Sigma x_i = 1$	(1)	–		–	
F	$F \cdot C_{P,F} \cdot T_F = L \cdot C_{P,L} \cdot T + V \cdot C_{P,V} \cdot T$	(1)	$C_{P,F}$, $C_{P,L}$, $C_{P,V}$, Q_{vap}	(4)	T_F	(1)
		(30)		(25)	30	(30)

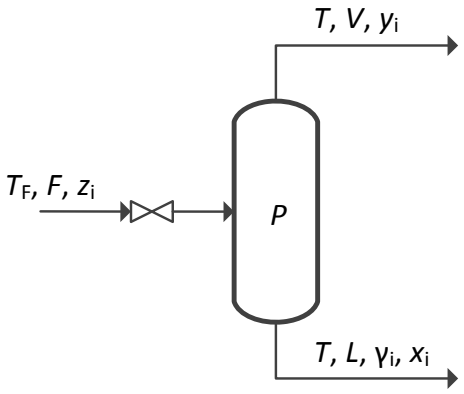

Figura 3.15. Diagrama de un destilador súbito adiabático.

Analizando las ecuaciones del balance de materia (3.10 – 3.14), se pueden plantear 29 relaciones independientes para determinar las composiciones y los caudales de las fases vapor y líquida, así como las razones de equilibrio, que ascienden también a 29. Una vez resuelto el balance de materia, se plantea de forma independiente el balance entálpico (ecuación 3.15) para determinar la temperatura del alimento (T_F). Este desacoplamiento de los balances de materia y entálpico se fundamenta en la necesidad de fijar la temperatura de equilibrio (T), ya que los datos de equilibrio sólo se conocen para valores discretos de esta variable.

El algoritmo desarrollado por Rachford y Rice (1952) no ha convergido en el cálculo de las composiciones y los caudales de las fases líquida y vapor en equilibrio, ya que el caudal molar total del vapor es muy pequeño y los valores de las razones de equilibrio muy elevados. Por tanto, ha sido necesario desarrollar la secuencia de cálculo que se recoge en la Figura 3.16.

En primer lugar se fijan los valores de la temperatura de equilibrio y la presión de operación. A continuación, se estiman los caudales molares de cada hidrocarburo en la fase vapor (V_i) y se calculan las fracciones molares de la fase vapor. Por definición, el sistema cumple con la ecuación 3.13, es decir, la suma de las fracciones molares del vapor es la unidad. A partir de estos valores, se resuelven las ecuaciones 3.10, 3.11 y 3.12 para calcular por dos vías diferentes las fracciones molares de la fase líquida.

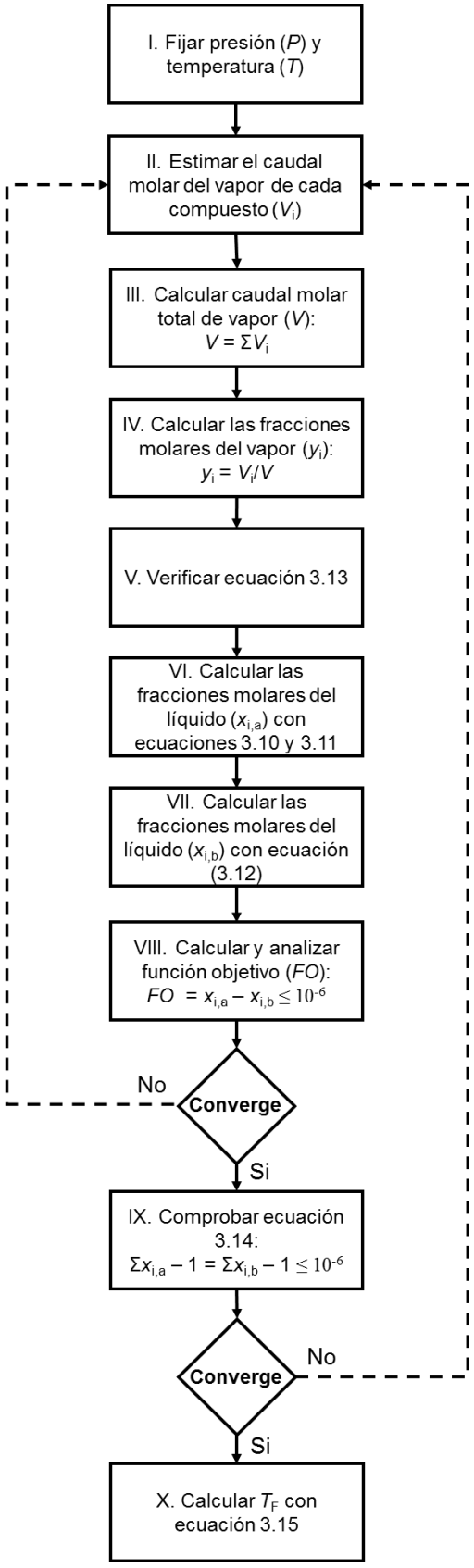

Figura 3.16. Secuencia de cálculo de los caudales y composiciones de las fases líquida y vapor de una etapa de destilación súbita.

A partir de estos dos cálculos de las fracciones molares de la fase líquida se fija la función objetivo del algoritmo, que se corresponde con la diferencia de ambas. La tolerancia de esta función objetivo se ha fijado en 10^{-6} para todos los compuestos presentes en la fase líquida. Además, se ha de cumplir la condición adicional de la ecuación 3.14, fijándose de nuevo una tolerancia de 10^{-6}. Si se cumple tanto la función objetivo como la ecuación 3.14, se calcula la temperatura del alimento (T_F) por balance entálpico; en caso contrario, se modifican los valores estimados de los caudales molares de cada hidrocarburo en la fase vapor. La resolución de este algoritmo de cálculo se ha llevado a cabo utilizando la función *Solver* de Microsoft Excel.

Proceso conceptual del fraccionamiento de la corriente de extracto de la separación de aromáticos de corrientes de refinería con líquidos iónicos

En la Figura 3.17 se incluye el diagrama de flujo simplificado para el proceso de extracción de aromáticos de un modelo de gasolina de reformado usando como disolvente la mezcla binaria de líquidos iónicos {[4empy][Tf_2N] (0,3) + [emim][DCA] (0,7)}. Como se puede ver, el tren de fraccionamiento estaría formado por tres destiladores súbitos adiabáticos dispuestos en serie. Los dos primeros se han destinado a recuperar los hidrocarburos alifáticos de la corriente de extracto, mientras que el último se ha utilizado para separar los hidrocarburos aromáticos de la mezcla de líquidos iónicos.

En las cuatro corrientes de extracto estudiadas, las temperaturas del proceso de fraccionamiento han sido muy similares, con valores comprendidos entre los 333,2 K y los 413,2 K, mientras que todas las unidades han tenido presiones de operación comprendidas en el intervalo 3 – 15 kPa.

En ningún caso se ha superado la MOT de la mezcla binaria de líquidos iónicos utilizada como disolvente, de manera que se garantiza su estabilidad térmica. Sin embargo, esta limitación en los valores de la temperatura del proceso de fraccionamiento ha llevado a trabajar en condiciones de vacío muy severas, hecho que, aunque sea técnicamente alcanzable, implica un elevado coste de operación (Fahim y col., 2010).

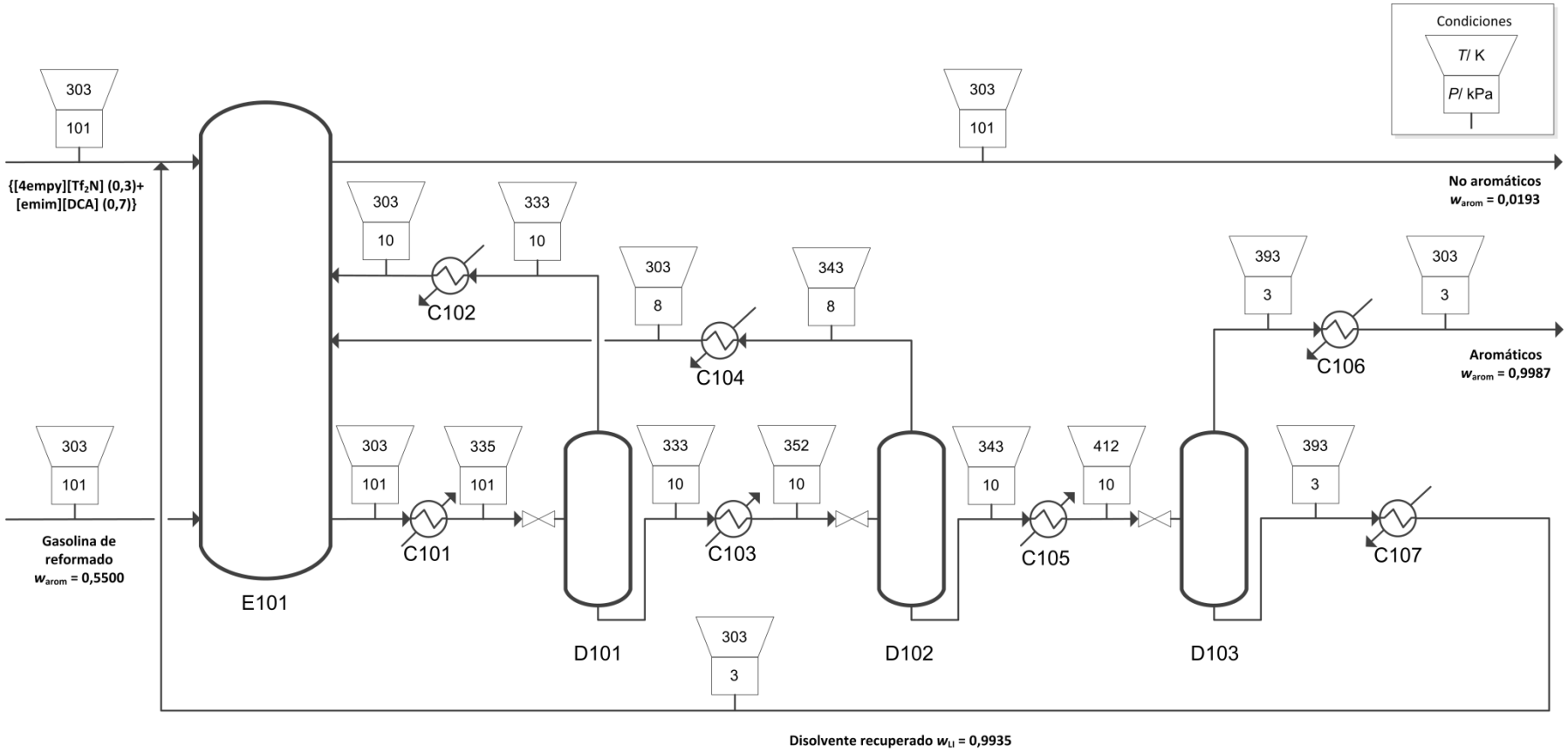

Figura 3.17. Diagrama de flujo del proceso propuesto de extracción de aromáticos para el modelo de gasolina de reformado empleando la mezcla binaria de líquidos iónicos {[4empy][Tf_2N] (0,3) + [emim][DCA] (0,7)}. Equipos: Extractor (E), destiladores súbitos (D) y cambiadores de calor (C).

En la Figura 3.18 se detalla la evolución de la pureza de los aromáticos con respecto a la concentración de los hidrocarburos para la fuente de obtención, la corriente de extracto y la corriente de aromáticos obtenida al final del proceso de fraccionamiento del extracto.

Existe una relación entre la concentración de aromáticos en la fuente y su pureza en la corriente de aromáticos. lo que justifica que las tres gasolinas dan lugar a una corriente de aromáticos con una pureza del 99,8 % en masa, superior a la alcanzada por la nafta alimentada al *cracker* de etileno (98,5 %).

Por último, destacar que la mezcla binaria de líquidos iónicos {[4empy][Tf_2N] (0,3) + [emim][DCA] (0,7)} se ha recuperado para las cuatro corrientes con una pureza superior al 99,3 % en masa.

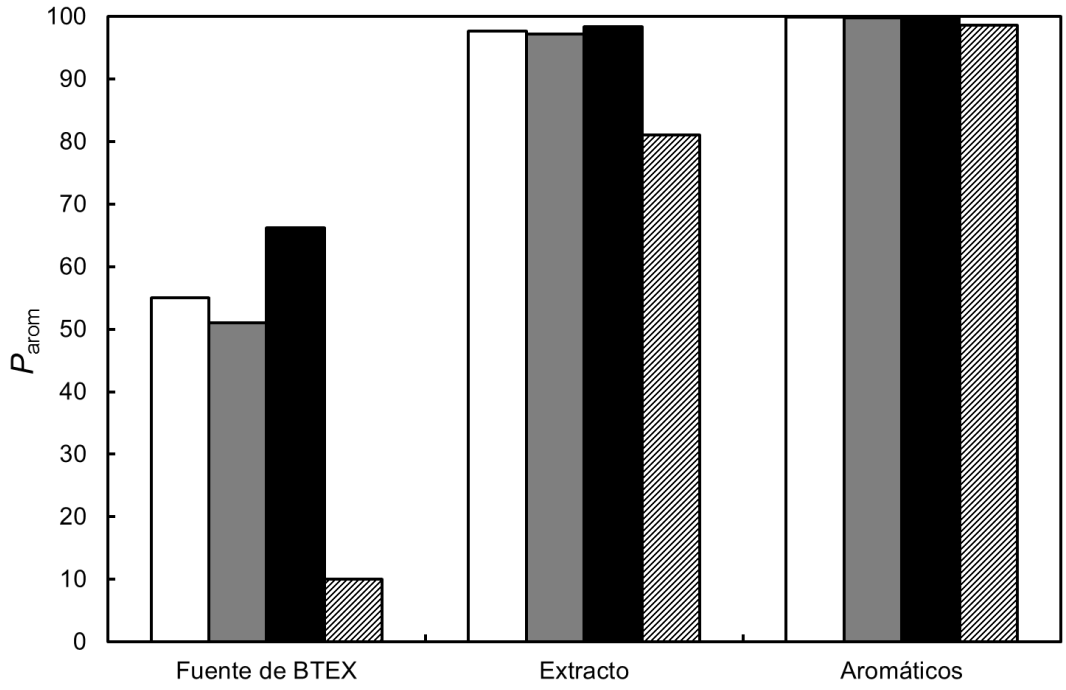

Figura 3.18. Evolución de la pureza de aromáticos dentro de la fracción hidrocarbonada, en % en masa, a lo largo del proceso de extracción para las distintas fuentes de aromáticos: reformado (blanco); pirólisis suave (gris); pirólisis severa (negro); nafta alimentada al cracker de etileno (trama).

Conclusiones y recomendaciones

Conclusiones

El estudio del fraccionamiento del extracto de la separación de aromáticos de gasolinas y naftas con líquidos iónicos se ha realizado en tres etapas: la evaluación de la estabilidad térmica de los líquidos iónicos puros y sus mezclas, la medición de sus calores específicos y la determinación del equilibrio líquido–vapor de las distintas mezclas características de las corrientes de extracto.

Los estudios de estabilidad térmica de líquidos iónicos puros han concluido en que ésta queda totalmente condicionada por la estructura del anión, matizando los resultados ligeramente tanto el catión como la longitud de sus sustituyentes. En todos los casos, el orden de estabilidad térmica de los líquidos iónicos puros atendiendo a su anión fue $[Tf_2N]$ > [TCM] > [DCA] > [SCN], mientras que el catión [bmim] ha ofrecido un ligero aumento de esta propiedad con respecto al [emim].

Los ensayos termogravimétricos dinámicos han sido útiles exclusivamente en términos comparativos, habida cuenta del elevado grado de sobreestimación de la estabilidad térmica que ofrecen. Por ello, las temperaturas máximas de operación se han definido a partir de predicciones de escenarios isotermos de larga duración validados por ensayos termogravimétricos isotermos experimentales.

Con respecto a las mezclas binarias de líquidos iónicos, {[4empy][Tf_2N] + [emim][DCA]} y {[emim][TCM] + [emim][DCA]}, destacar que su estabilidad térmica está totalmente determinada por el anión menos estable de la mezcla, a saber el [DCA]. Es decir, las dos mezclas han mostrado estabilidades térmicas muy similares entre sí y cercanas al líquidos iónico [emim][DCA].

Se ha propuesto también una regla de mezcla que ha permitido predecir con éxito la descomposición térmica de una mezcla de líquidos iónicos a partir de las de los líquidos iónicos puros que la forman.

Los estudios de la capacidad calorífica de los líquidos iónicos puros han concluido en que todos ellos presentan valores de esta propiedad comparables y ligeramente superiores a los del sulfolano, hecho que supondría un ligero incremento de los consumos energéticos a igualdad de temperaturas de operación. Con respecto a las mezclas binarias de líquidos iónicos estudiadas, reseñar que los calores específicos de exceso fueron muy bajos, comportándose por tanto las mezclas causi-idealmente con respecto a esta propiedad.

En cuanto a la estabilidad térmica y los calores específicos de la mezcla seleccionada, {[4empy][Tf_2N] (0,3) + [emim][DCA] (0,7)}, destacar que su aplicación se podría llevar a cabo hasta los 413 K, mientras que los valores de sus calores específicos se ven incrementados en un 15 % con respecto a los del sulfolano.

Los datos del equilibrio líquido–vapor de las mezclas {*n*–heptano + tolueno + [emim][DCA] o [4empy][Tf_2N]} han mostrado elevados valores de volatilidad relativa del *n*–heptano frente al tolueno, especialmente a bajas temperaturas, en comparación con la mezcla {*n*–heptano + tolueno}.

Estos estudios han permitido también relacionar la volatilidad relativa *n*–heptano/tolueno originada por un líquido iónico con sus valores de selectividad tolueno/*n*–heptano en su empleo como disolvente en la extracción líquido–líquido en mezclas {*n*–heptano + tolueno + líquidos iónicos}.

Por otro lado, se ha empleado con éxito la regla de mezcla de Yalkowsky y Roseman para predecir el equilibrio líquido–vapor de las mezclas {alcano + aromático + {[4empy][Tf_2N] + [emim][DCA]}} a partir de los datos de las mezclas {alcano + aromático + [emim][DCA] o [4empy][Tf_2N]}.

Reseñar también que el modelo termodinámico NRTL se ha empleado con resultados satisfactorios en la correlación de los datos de equilibrio líquido–vapor de las mezclas ternarias y pseudoternarias formadas por un alifático, un aromático y uno o dos líquidos iónicos.

Finalmente se han estudiado los equilibrios líquido–vapor de los extractos obtenidos de la separación de aromáticos de cuatro modelos de corrientes de refinería empleando la mezcla de líquidos iónicos {[4empy][Tf_2N] (0,3) + [emim][DCA] (0,7)}. A tenor de los datos de equilibrio obtenidos se ha propuesto un esquema de fraccionamiento formado por tres unidades de destilación súbita adiabáticas. Se ha obtenido una corriente de aromáticos con un 99,8 % de pureza en masa para los casos de las gasolinas de reformado y pirólisis y con un 98,5 % para el de la nafta alimentada al *cracker* de etileno, mientras que la mezcla binaria de líquidos iónicos {[4empy][Tf_2N] (0,3) + [emim][DCA] (0,7)} se ha recuperado con una pureza superior al 99,3 % en masa en los casos de las cuatro corrientes de refinería estudiadas.

Recomendaciones

Tras cumplir los objetivos marcados al inicio de esta tesis doctoral, se han obtenido interesantes avances en el fraccionamiento de la corriente de extracto de la separación de aromáticos con líquidos iónicos de diversas corrientes de refinería. No obstante, quedan estudios pendientes para evaluar la viabilidad y el escalado industrial del proceso.

Con respecto a los datos de equilibrio líquido–líquido y líquido–vapor del proceso, se consideran suficientes habida cuenta de los buenos resultados alcanzados con la mezcla seleccionada para los casos de gasolinas de reformado y pirólisis. Sin embargo, se sugiere ampliar el estudio para el caso de la nafta alimentada al *cracker* de etileno con disolventes iónicos de mayor selectividad aromático/alifático para aumentar así la pureza de aromáticos.

Asimismo, como mejora de los resultados obtenidos, la búsqueda de nuevos líquidos iónicos con mayor estabilidad térmica, mostrando iguales o superiores propiedades extractivas y físicas que la mezcla {[4empy][Tf_2N] (0,3) + [emim][DCA] (0,7)}, podría suavizar las condiciones de vacío requeridas en las etapas de destilación súbita, al permitir operar a mayores temperaturas, abaratando así los costes de operación. En cualquiera de estos casos, se debería realizar una integración energética del proceso para minimizar sus consumos energéticos y evaluar sus costes de operación.

Sin embargo, los mayores esfuerzos deben recaer en la cinética del proceso de extracción, indispensable en el dimensionado del extractor. Para ello se ha de realizar un estudio de la difusión de los hidrocarburos en los líquidos iónicos durante su extracción.

Tras obtener todos los datos necesarios que hoy en día no están disponibles, se podría abordar el diseño riguroso del proceso, pudiendo estimar así los costes de inmovilizado y de operación. En este punto se evaluaría la viabilidad del proceso y su potencial implantación como sustituto de los actualmente empleados a escala industrial.

Bibliografía

Andreatta, A.E.; Arce, A.; Rodil, E.; Soto, A. Physical properties and phase equilibria of the system isopropyl acetate + isopropanol + 1–octyl–3–methyl–imidazolium bis(trifluoromethylsulfonyl)imide. Fluid Phase Equilib. **2010**, 287, 84–94.

Anjan, S.T. Ionic Liquid for Aromatic Extraction: Are They Ready? Chem. Eng. Prog. **2006**, 102, 30–39.

Aparicio, S.; Atilhan, M.; Karadas, F. Thermophysical Properties of Pure Ionic Liquids: Review of Present Situation. Ind. Eng Chem. Res. **2010**, 49, 9580–9595.

Arce, A.; Earle, M.J; Rodríguez, H.; Seddon, K.R. Separation of Benzene and Hexane by Solvent Extraction with 1–Alkyl–3–methylimidazolium Bis(trifluoromethyl)sulfonylamide Ionic Liquids: Effect of the Alkyl–Substituent Length. J. Phys. Chem. B **2007**, 111, 4732–4736.

Aspen Plus Versión 7.1, Database, Aspen Technology, **2004**.

ASTM International. ASTM E 1269 – 01. Standard Test Method for Determining Specific Heat Capacity by Differential Scanning Calorimetry. **2001**.

Branan, C.R. Soluciones prácticas para el ingeniero químico. 2nd Ed.; McGraw–Hill: New York, **2008**.

Carvalho, P.J.; Regueira, T.; Santos, L.M.N.B.F.; Fernández, J.; Coutinho, J.A.P. Effect of Water on the Viscosities and Densities of 1–Butyl–3–methylimidazolium Dicyanamide and 1–Butyl–3–methylimidazolium Tricyanomethane at Atmospheric Pressure. J. Chem. Eng. Data **2010**, 55, 645–652.

Corderi, S. Gonzalez. E.J.; Calvar N.; Dominguez, A. Application of [HMim][NTf_2], [HMim][TfO] and [BMim][TfO] Ionic Liquids on the Extraction of Toluene from Alkanes: Effect of the Anion and the Alkyl Chain Length of the Cation on the LLE. J. Chem. Thermodyn. **2012**, 53, 60–66.

Crosthwaite, J.M.; Muldoon, M.J.; Dixon, J.K.; Anderson, J.L.; Brennecke, J.F. Phase transition and decomposition temperatures, heat capacities and viscosities of pyridinium ionic liquids. J. Chem. Thermodyn. **2005**, 37, 559–568.

DeSimone, J.M. Practical Approaches to Green Solvents. Science **2002**, 297, 799–803.

EIA (Energy Information Administration) of U.S. Annual Energy Outlook 2015 with projections to 2040. **2015**.

Esperança, J.M.M.S.; Visak, Z.P.; Plechkova, N.V.: Seddon, K.R.; Guedes, H.J.R.; Rebelo, L.P.N. Density, Speed of Sound, and Derived Thermodynamic Properties of Ionic Liquids over an Extended Pressure Range. 4. [C_3mim][NTf_2] and [C_5mim][NTf_2]. J. Chem. Eng. Data **2006**, 51, 2009–2015.

Fahim, M.; Al–Sahhaf, T.; Elkilani, A. Fundamentals of Petroleum Refining. Elsevier. Amsterdam. **2010**.

Fernández, A.; Torrecilla, J.S.; García, J.; Rodríguez, F. Thermophysical Properties of 1–Ethyl–3–methylimidazolium Ethylsulfate and 1–Butyl–3–methylimidazolium Methylsulfate Ionic Liquids. J. Chem. Eng. Data **2007**, 52, 1979–1984.

Ficke, L.E.; Novak, R.; Brennecke, J.F. Thermodynamic and Thermophysical Properties of Ionic Liquid + Water Systems. J. Chem. Eng. Data **2010**, 55, 4946–4953.

Franck, H.G.; Staldelhofer, J.W. Industrial Aromatic Chemistry; Springer–Verlag: Berlin, **1988**.

França, J.M.P.; Nieto de Castro, C.A.; Matos Lopes, M.; Nunes, V.M.B. Influence of Thermophysical Properties of Ionic Liquids in Chemical Process Design. J. Eng. Chem. Data **2009**, 54, 2569–2575.

Fredlake, C.P.; Crosthwaite, J.M.; Hert, D.G.; Aki, S.N.V.K.; Brennecke, J.F. Thermophysical Properties of Imidazolium–Based Ionic Liquids. J. Chem. Eng. Data **2004**, 49, 954–964.

García, J.; García, S.; Torrecilla, J.S.; Oliet, M.; Rodríguez, F. Liquid–liquid Equilibria for the Ternary Systems {Heptane + Toluene + N–Butylpyridinium Tetrafluoroborate or N–Hexylpyridinium Tetrafluoroborate} at T = 313.2 K. J. Chem. Eng. Data **2010**, 55, 2862–2865.

García, S.; Larriba, M.; García, J.; Torrecilla, J.S.; Rodríguez, F. Liquid−Liquid Extraction of Toluene from Heptane Using 1−Alkyl−3−methylimidazolium Bis(trifluoromethylsulfonyl)imide Ionic Liquids. J. Chem. Eng. Data **2011a**, 56, 113–118.

García, J.; García, S.; Torrecilla, J.S.; Rodríguez, F. N–butylpyridinium bis–(trifluormethylsulfonyl)imide Ionic Liquids as Solvents for the Liquid–liquid Extraction of Aromatic from Their Mixtures with Alkanes: Isomeric Effect of the Cation. Fluid Phase Equilib. **2011b**, 301, 62–66.

García, S.; Larriba, M.; García, J.; Torrecilla, J.S.; Rodríguez, F. Liquid–liquid Extraction of Toluene from Heptane Using Binary Mixtures of N–butylpyridinium Tetrafluoroborate and N–butylpyridinium Bis(trifluoromethylsulfonyl)imide Ionic Liquids. Chem. Eng. J. **2012a**, 180, 210−215.

García, S.; Larriba, M.; García, J.; Torrecilla, J.S.; Rodríguez, F. Alkylsulfate–based Ionic Liquids in the Liquid–liquid Extraction of Aromatic Hydrocarbons. J. Chem. Thermodyn. **2012b**, 45, 68–74.

García, S.; Larriba, M.; García, J.; Torrecilla, J.S.; Rodríguez, F. Separation of toluene from *n*–heptane by liquid–liquid extraction using binary mixtures of [bpy][BF_4] and [4bmpy][Tf_2N] ionic liquids as solvent. J. Chem. Thermodyn. **2012c**, 53, 119−124.

García, S.; Larriba, M.; Casas, A.; García, J.; Rodríguez, F. Separation of Toluene and Heptane by Liquid−Liquid Extraction Using Binary Mixtures of the Ionic Liquids 1–Butyl–4–methylpyridinium Bis(trifluoromethylsulfonyl)imide and 1–Ethyl–3–methylimidazolium Ethylsulfate. J. Chem. Eng. Data **2012d**, 57, 2472–2478.

García, S.; García, J.; Larriba, M.; Casas, A.; Rodríguez, F. Liquid-liquid Extraction of Toluene from Heptane by {[4bmpy][Tf_2N] + [emim][$CHF_2CF_2SO_3$]} Ionic Liquid Mixed Solvents. Fluid Phase Equilib. **2013**, 337, 47–52.

Gary, J.; Handwerk, G.; Kaiser, M. Petroleum Refining Technology and Economics, 5th ed.; CRC Press: Boca Raton, FL, **2007**.

Ge, Y.; Zhang, L.; Yuan, X.; Geng, W.; Ji, J. Selection of ionic liquids as entrainers for the separation of (water + ethanol). J. Chem. Thermodyn. **2008**, 40, 1248–1252.

González, E.J.; González, B.; Calvar, N.; Domínguez, A. Study of [EMim][ESO_4] Ionic Liquid as Solvent in the Liquid–liquid Extraction of Xylenes from their Mixtures with Hexane. Fluid Phase Equilib. **2011**, 305, 227–232.

González, E.J.; Navarro, P.; Larriba, M.; García, J.; Rodríguez, F. Use of selective ionic liquids and ionic liquid/salt mixtures as entrainer in a (vapor + liquid) system to separate *n*–heptane from toluene. J. Chem. Thermodyn. **2015**, 91, 156–164.

Hao, Y.; Peng, J.; Hu, S.; Li, J.; Zhai, M. Thermal decomposition of allyl–imidazolium–based ionic liquid studied by TGA–MS analysis and DFT calculations. Thermochim. Acta **2010**, 501, 78–85.

Hansmeier, A.R.; Minoves Ruiz, M.; Meindersman, G.W.; de Haan, A.B. Liquid–Liquid Equilibria for the Three Ternary Systems (3–Methyl–N–butylpyridinium Dicyanamide + Toluene + Heptane), (1–Butyl–3–methylimidazolium Dicyanamide + Toluene + Heptane) and (1–Butyl–3–methylimidazolium Thiocyanate + Toluene + Heptane) at T = (313.15 and 348.15) K and p = 0.1 MPa. J. Chem. Eng. Data **2010**, 55, 708–713.

Henley, E.J.; **Seader**, J.D. Equilibrium-Stage Separation Operations in Chemical Engineering; John Wiley and Sons: New York, **1981**.

Jacquemin, J.; Husson, P.; Mayer, V.; Cibulka, I. High–Pressure Volumetric Properties of Imidazolium-Based Ionic Liquids: Effect of the Anion. J. Chem. Eng. Data **2007**, 52, 2204–2211.

Kim, M.J.; Shin, S.H.; Kim, Y.J.; Cheong, M.; Lee, J.S.; Kim, H.S. Role of Alkyl Group in the Aromatic Extraction using Pyridinium–Based Ionic Liquids. Phys. Chem B **2013**, 117, 14827–14834.

Kirk, R.E.; **Othmer**, D.F. Encyclopaedia of Chemical Technology. Wiley: New York, **1998**.

Kolb, B.; **Ettre** L.S. Static Headspace–Gas Chromatography: Theory and Practice; Wiley–VCH: New York, **1997**.

Larriba, M.; García, S.; García, J.; Torrecilla, J.S.; Rodríguez, F. Thermophysical Properties of 1–Ethyl–3–methylimidazolium 1,1,2,2–Tetrafluoroethanesulfonate and 1–Ethyl–3–methylimidazolium Ethylsulfate Ionic Liquids as a Function of Temperature. J. Chem. Eng. Data **2011**, 56, 3589–3597.

Larriba, M.; García, S.; Navarro, P.; García, J.; Rodríguez, F. Physical Properties of N–butylpyridinium Tetrafluoroborate and N–butylpyridinium Bis(trifluoromethylsulfonyl)imide Binary Ionic Liquid Mixtures. J. Chem. Eng. Data **2012**, 57, 1318–1325.

Larriba, M.; García, S.; Navarro, P.; García, J.; Rodríguez, F. Physical Physical Characterization of an Aromatic Extraction Solvent Formed by [bpy][BF_4] and [4bmpy][Tf_2N] Mixed Ionic Liquids. J. Chem. Eng. Data **2013a**, 58, 1496–1504.

Larriba, M.; Navarro, P.; García, J.; Rodríguez, F. Liquid-liquid extraction of toluene from heptane using [emim][DCA], [bmim][DCA], and [emim][TCM] ionic liquids. Ind. Chem. Eng. Res. **2013b**, 52, 2714–2720.

Larriba, M.; Navarro, P.; García, J.; Rodríguez, F. Separation of toluene from *n*-heptane, 2,3–dimethylpentane, and cyclohexane using binary mixtures of [4empy][Tf_2N] and [emim][DCA] ionic liquids as extraction solvents. Sep. Purif. Technol. **2013c**, 120, 392–401.

Larriba, M.; Navarro, P.; García, J.; Rodríguez, F. Liquid–liquid extraction of toluene from *n*–heptane by {[emim][TCM] + [emim][DCA]} binary ionic liquid mixtures. Fluid Phase Equilib. **2014a**, 364, 48–54.

Larriba, M.; Navarro, P.; García, J.; Rodríguez, F. Extraction of benzene, ethylbenzene, and xylenes from *n*–heptane using binary mixtures of [4empy][Tf_2N] and [emim][DCA] ionic liquids. Fluid Phase Equilib. **2014b**, 380, 1–10.

Larriba, M.; Navarro, P.; García, J.; Rodríguez, F. Liquid−Liquid Extraction of Toluene from *n*–Alkanes using {[4empy][Tf_2N] + [emim][DCA]} Ionic Liquid Mixtures. J. Chem. Eng. Data **2014c**, 59, 1692–1699.

Larriba, M.; Navarro, P.; García, J.; Rodríguez, F. Selective extraction of toluene from *n*–heptane using [emim][SCN] and [bmim][SCN] ionic liquids as solvents. J. Chem. Thermodyn. **2014d**, 79, 266–271.

Larriba, M.; Navarro, P.; García, J.; Rodríguez, F. Liquid−Liquid Extraction of BTEX from Reformer Gasoline Using Binary Mixtures of [4empy][Tf_2N] and [emim][DCA] Ionic Liquids. Energy Fuels **2014e**, 28, 6666–6676.

Larriba, M.; Navarro, P.; Beigbeder, J.B.; García, J.; Rodríguez, F. Mixing and Decomposition Behavior of {[4bmpy][Tf_2N] + [emim][$EtSO_4$]} and {[4bmpy][Tf_2N] + [emim][TFES]} Ionic Liquid Mixtures. J. Chem. Thermodyn. **2015a**, 82, 58–75.

Larriba, M.; Navarro, P.; González, E.J.; García, J.; Rodríguez, F. Separation of BTEX from a naphtha feed to ethylene crackers using a binary mixture of [4empy][Tf_2N] and [emim][DCA] ionic liquids. Sep. Purif. Technol. **2015b**, 144, 54–62.

Larriba, M.; Navarro, P.; González, E.J.; García, J.; Rodríguez, F. Dearomatization of pyrolysis gasolines from mild and severe cracking by liquid–liquid extraction using a binary mixture of [4empy][Tf_2N] and [emim][DCA] ionic liquids. Fuel Process. Technol. **2015c**, 137, 269–282.

Li, Q.; Zhang, J.; Lei, J.; Zhu, J.; Wang, B.; Huang, X. Isobaric Vapor-Liquid Equilibirum for (Propa–2–ol + Water + 1–Butyl–3–methylimidazolium Tetrafluoroborate). J. Chem. Eng. Data **2009**, 54, 2785–2788.

Meindersma, G.W.; Podt, A.J.G.; de Haan, A.B. Selection of Ionic Liquids for the Extraction of Aromatic Hydrocarbons from Aromatic/aliphatic Mixtures. Fuel Process. Technol. **2005**, 87, 59–70.

Meindersma, G.W.; de Haan, A.B. Conceptual Process Design for Aromatic/aliphatic Separation with Ionic Liquids. Chem. Eng. Res. Des. **2008**, 86, 745–752.

Meindersma, G.W.; Hansmeier, A.R.; de Haan, A.B. Ionic Liquids for Aromatics Extraction. Present Status and Future Outlook. Ind. Eng. Chem. Res. **2010**, 49, 7530–7540.

Meindersma, G.W.; de Haan, A.B. Cyano–containing Ionic Liquids for the Extraction of Aromatic Hydrocarbons from an Aromatic/aliphatic Mixture. Sci. China Chem. **2012**, 55, 1488–1499.

Meyers, R.A. Handbook of Petroleum Refining Processes, 3rd Ed.; McGraw–Hill: New York, **2004**.

Navarro, P.; Larriba, M.; Beigbeder, J.B.; García, J.; Rodríguez, F. Thermal stability and specific heats of {[bpy][BF_4] + [bpy][Tf_2N]} and {[bpy][BF_4] + [4bmpy][Tf_2N]} mixed ionic liquid solvents. J. Therm. Anal. Calorim. **2015**, 119, 1235–1243.

Orchillés, A.V.; Miguel, J.P.; González-Alfaro, V.; Vercher, E. 1–Ethyl–3–methylimidazolium Dicyanamide as a Very Efficient Entrainer for the Extractive Distillation of the Acetone + Methanol System. J. Chem. Eng. Data **2012**, 57, 394–399.

Perry, R.H.; Green, D.W.; Maloney, J.O. Perry's Chemical Engineers' Handbook. McGraw–Hill. New York, 1999.

Plechkova, N.V.; Seddon, K.R. Applications of Ionic Liquids in the Chemical Industry. Chem. Soc. Rev. **2008**, 37, 123–150.

Rachford, H.H.; **Rice**, J.D. J. Pet. Trans. **1952**, 195, 327–328.

Ramos Carpio, M.A. Refino de Petróleo, Gas Natural y Petroquímica. Ed. Ramos Carpio. **1997**.

Redlich, O.; **Kister** A.T. Thermodynamics of nonelectrolyte solutions, Ind. Eng. Chem. **1948**, 40, 345–348.

Renon, H.; **Prausnitz**, J.M. Local Compositions in Thermodynamic Excess Functions for Liquid Mixtures. AIChE J. **1968**, 14, 135–142.

Rogers, R.D.; **Seddon**, K.R. Ionic Liquids-Solvents of the Future? Science **2003**, 302, 792–793.

Seeberger, A.; Andresen, A.K.; Jess, A. Prediction of long–term stability of ionic liquids at elevated temperatures by means of non–isothermal thermogravimetrical analysis. Phys. Chem. Chem. Phys. **2009**, 11, 9375–9383.

ThyssenKrupp. Aromatics, Sources, Demand and Applications. **2014**.

Wauquier, J.P. Petroleum Refining. Vol. 2. Separation Processes. Editions Technip: Paris, **2000**.

Yalkowsky, S.H.; **Roseman**, T.J. Chapter 3: Solubilization of drugs by cosolvents, in: Techniques of Solubilization of Drugs; Dekker: New York, **1981**.

Publicaciones

Listado de publicaciones

Publicación I: Navarro, P.; Larriba, M.; Rojo, E.; García, J.; Rodríguez, F. Thermal properties of cyano–based ionic liquids. J. Chem. Eng. Data 58 (2013) 2187 – 2193.

Publicación II: Navarro, P.; Larriba, M.; García, J.; Rodríguez, F. Thermal stability, specific heats, and surface tensions of ([emim][DCA] + [4empy][Tf_2N]) ionic liquid mixtures. J. Chem. Thermodyn. 76 (2014) 152 – 160.

Publicación III: Navarro, P.; Larriba, M.; García, J.; Rodríguez, F. Thermal stability and specific heats of {[emim][DCA] + [emim][TCM]} mixed ionic liquids. Thermochim. Acta 588 (2014) 22 – 27.

Publicación IV: Navarro, P.; Larriba, M.; García, J.; González, E.J.; Rodríguez, F. Vapor–liquid equilibria of {*n*–heptane + toluene + [emim][DCA]} system by headspace gas chromatography. Fluid Phase Equilib. 387 (2015) 209 – 216.

Publicación V: Navarro, P.; Larriba, M.; García, J.; González, E.J.; Rodríguez, F. Vapor–liquid equilibria of *n*–heptane + toluene + 1–ethyl–4–methylpyridinium bis(trifluoromethylsulfonyl)imide ionic liquid. J. Chem. Eng. Data 61 (2016) 458 – 465.

Publicación VI: Navarro, P.; Larriba, M.; García, J.; González, E.J.; Rodríguez, F. Selective recovery of aliphatics from aromatics in the presence of the {[4empy][Tf_2N] + [emim][DCA]} ionic liquid mixture. J. Chem. Thermodyn. 96 (2016) 134 – 142.

Publicación VII: Navarro, P.; Larriba, M.; García, J.; Rodríguez, F. Vapor–liquid equilibria for *n*–heptane + (benzene, toluene, *p*–xylene, or ethylbenzene) + {[4empy][Tf_2N] (0.3) + [emim][DCA] (0.7)} binary ionic liquid mixture. Fluid Phase Equilib. 417 (2016) 41 – 49.

Publicación VIII: Navarro, P.; Larriba, M.; García, J.; Rodríguez, F. Vapor–liquid equilibria for (*n*–hexane, *n*–octane, cyclohexane, or 2,3–dimethylpentane) + toluene + {[4empy][Tf_2N] (0.3) + [emim][DCA] (0.7)} mixed ionic liquids. J. Chem. Eng. Data 61 (2016) 2440 – 2449.

Publicación IX: Navarro, P.; Larriba, M.; García, J.; Rodríguez, F. Design of the hydrocarbon recovery section from the extract stream of the aromatic separation from reformer and pyrolysis gasolines using a binary mixture of [4empy][Tf_2N] + [emim][DCA] ionic liquids. EnergyFuels 31 (2017) 1035 – 1043.

Publicación X: Navarro, P.; Larriba, M.; García, J.; Rodríguez, F. Design of the recovery section of the extracted aromatics in the separation of BTEX from naphtha feed to ethylene crackers using [4empy][Tf_2N] and [emim][DCA] mixed ionic liquids as solvent. Sep. Purif. Technol. 180 (2017) 149 – 156.

Journal of chemical & engineering data

Article

pubs.acs.org/jced

Thermal Properties of Cyano-Based Ionic Liquids

Pablo Navarro, Marcos Larriba, Ester Rojo, Julián García,* and Francisco Rodríguez

Department of Chemical Engineering, Complutense University of Madrid, E−28040 Madrid, Spain

ABSTRACT: Nowadays, extraction of aromatics from aromatic/aliphatic mixtures is being investigated using cyano-based ionic liquids (ILs) as a new green alternative to currently used conventional organic extraction solvents, such as sulfolane. In this process, the maximum operation temperature (MOT) of the IL is a decisive property to know. Thus, thermal behavior of ILs is a target issue to study. The MOTs of cyano-based ILs 1-ethyl-3-methylimidazolium dicyanamide ([emim][DCA]), 1-butyl-3-methylimidazolium dicyanamide ([bmim][DCA]), 1-ethyl-3-methylimidazolium thiocyanate ([emim][SCN]), 1-butyl-3-methylimidazolium thiocyanate ([bmim][SCN]), and 1-ethyl-3-methylimidazolium tricyanomethanide ([emim][TCM]) have been determined using dynamic and isothermal thermogravimetric analyses. In addition, specific heats from (296.2 to 372.2) K of all ILs included in this work have been also measured using differential scanning calorimetry (DSC). The MOT for [emim][TCM] was the highest, whereas the MOT for [emim][DCA], [bmim][DCA], and [bmim][SCN] were a little lower, the [emim][SCN] MOT being the lowest found. Specific heats of all ILs analyzed were higher than that of sulfolane.

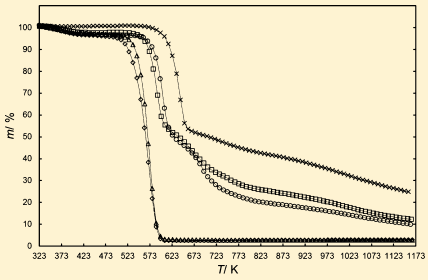

INTRODUCTION

Ionic liquids (ILs) are a current alternative to volatile organic compounds (VOCs), because of their properties, specifically their negligible vapor pressure.[1] In the liquid−liquid extraction of aromatics from aromatic/aliphatic mixtures the most promising ILs employed are cyano-based ILs, which have shown good extractive properties (both selectivity and aromatic distribution ratio) in comparison with sulfolane.[2−4] In addition to the extractive properties, other IL properties have to be determined to confirm their potential uses as solvents for aromatic extraction. This way, one of the more relevant IL properties is the maximum operation temperature (MOT), which is defined as the maximum temperature that a substance can support without decomposition.

The common way to determine the thermal properties of a substance is a non-isothermal thermogravimetric analysis (TGA) known as dynamic analysis.[5−7] A dynamic analysis consists of a quick temperature ramp during a known short time. In dynamic analyses, the MOT is assumed to be the onset temperature, which is the cross point between the tangent straight lines to the TGA curve before and after decomposition started. However, this claim is not altogether correct, since the onset temperature is a function of evaporation and decomposition processes, and also because its value is also completely dependent on the heating rate used. Furthermore, the onset temperature has been experimentally determined to be an overestimated MOT, because dynamic analyses are performed for a short time.[5,8−10] On the other hand, isothermal TGA is made at a constant temperature for longer times.[5,8−10] This method produces a real MOT, close to the run time required by the application studied. Isothermal analyses for very long periods of time are needed when a good precision is required for the MOT. Nevertheless, prediction of long-term stability of ionic liquids at elevated temperatures by means of non-isothermal TGA is also possible. Seeberger et al.[8] outlined non-isothermal TGA method to estimate a MOT.

Thus, the aim of this work has been to determine MOTs of the cyano-based ILs 1-ethyl-3-methylimidazolium dicyanamide ([emim][DCA]), 1-butyl-3-methylimidazolium dicyanamide ([bmim][DCA]), 1-ethyl-3-methylimidazolium thiocyanate ([emim][SCN]), 1-butyl-3-methylimidazolium thiocyanate ([bmim][SCN]), and 1-ethyl-3-methylimidazolium tricyanomethanide ([emim][TCM]). All the ILs investigated here have proven to have both selectivity and aromatic distribution ratios that make them promising ILs in the liquid−liquid extraction of aromatics.[2−4] Dynamic and isothermal experiments by TGA have been carried out in this work. Specifically, dynamic decomposition parameters (onset temperature, $T_{10\ \%}$, $T_{50\ \%}$, and ashes remained at critical temperatures), the influence of different heating rates on dynamic values, and the ILs dependence on time through isothermal conditions have been studied. In addition, the Seeberger et al. model has been applied in order to estimate the behavior of each IL at extremely long times from nonisothermal TGA. Finally, the specific heats of all ILs from (296.2 to 372.2) K, necessary properties from a process design point of view, have been determined as well.

EXPERIMENTAL SECTION

Chemicals. [emim][DCA], [bmim][DCA], [emim][SCN], [bmim][SCN], and [emim][TCM] ILs were purchased from Iolitec GmbH with mass purities higher than 0.98, whereas halides are less than 0.02 and water content is no more than 0.002, in mass fraction. To prevent water absorption, all ILs were stored in a desiccator and handed inside a glovebox under

Received: February 11, 2013
Accepted: June 25, 2013
Published: July 9, 2013

Table 1. Chemicals: Specifications and Properties. Densities (ρ) and Dynamic Viscosities (η)

chemical	source	purity	analysis method	ρ, at 298.2 K/(g·cm^{-3})	η, at 298.2 K/(mPa·s)
[emim][DCA]	Iolitec GmbH	0.98	NMR[a], IC[b]	1.1013[c]	15.1[c]
[bmim][DCA]	Iolitec GmbH	0.98	NMR[a], IC[b]	1.0607[c]	27.3[c]
[emim][SCN]	Iolitec GmbH	0.98	NMR[a], IC[b]	1.1170	23.8
[bmim][SCN]	Iolitec GmbH	0.98	NMR[a], IC[b]	1.0710	59.8
[emim][TCM]	Iolitec GmbH	0.98	NMR[a], IC[b]	1.0816[c]	15.0[c]
Sulfolane	Sigma-Aldrich	0.99	GC[d]	1.2620[c,e]	10.8[c,e]
Sapphire	Mettler Toledo	0.9999	Verneuil[f]	3.99	

[a]Nuclear magnetic resonance. [b]Ion chromatography. [c]From ref 2. [d]Gas chromatography. [e]Measured at 303.2 K due to its melting point. [f]Purity is assessed by this production method.

an inert atmosphere of dry nitrogen. Sulfolane was supplied by Sigma-Aldrich with mass fraction purity higher than 0.99. Sapphire employed was supplied by Mettler Toledo with mass purity higher than 0.9999. Specifications and properties of all chemicals employed in this work are shown in Table 1. It is important to stress that chemicals were used without further purification.

Thermal Analysis. Both dynamic and isothermal TGA were made in a thermogravimetric analyzer Mettler Toledo TGA/DSC 1. Indium and aluminum melting points were checked at (5, 10, and 20) K·min^{-1} heating rates to calibrate this equipment, which has ± 0.1 K and ± 10^{-3} mg precisions on temperature and mass measurement, respectively. Runs were carried out into 70 μL alumina pans and under an inert atmosphere of nitrogen. Nitrogen reaction flow was 20 mL·min^{-1}, whereas nitrogen protection flow was 50 mL·min^{-1}. Initial mass introduced in the pan was set in (20 ± 1) mg, because between 10 mg and 40 mg no influence was seen in the results, and because this mass fully covers the button surface of the pan. Dynamic measurements were done from (313.2 to 1,173.2) K; a temperature near the maximum specification temperature of the alumina pans employed. Used heating rates in this work were 5, 10, and 20 K·min^{-1}. The mean of three replicated measurements was reported. Isothermal determinations were made at 313.2 K, 353.2 K, 393.2 K, 433.2 K, and 473.2 K. A time of 48 h is set as suitable to take into account decomposition or no decomposition processes at each constant temperature. In addition, it is important to underline that this equipment was used before by our research group and results obtained were successfully published.[5,11,12]

Specific Heats. Specific heats of ILs were determined by differential scanning calorimetry (DSC) in a Mettler Toledo DSC821^e. The sapphire method was followed to improve accuracy (2 %) from the direct measurement (4 %). Thus, ASTM E 1269-01 was applied in this work.[13] Experiments were done into 40 μL stainless steel pans and under an inert atmosphere of nitrogen. The nitrogen reaction flow was 20 mL·min^{-1}, whereas the nitrogen protection flow was 50 mL·min^{-1}. Initial mass introduced in the pan was (25 ± 1) mg, to produce better results by reducing the pan resistance over heat transfer and to be similar to the mass standard of sapphire (24.4 mg). Water content was eliminated in a treatment before each experiment that consists of isothermal heating at 378.2 K for 0.5 h, where these conditions are optimimal to remove all the water presented in the IL matrix while not modifying the IL identity. The experiments were then performed from (296.2 to 372.2) K, with a 20 K·min^{-1} heating rate, doing an isothermal measurement of 5 min before the experiment at lower temperature and after the experiment at the upper temperature. Blank simulations and sapphire determination in the same range of temperatures were also needed to achieve accurate results. This equipment was also used in previous publications of our research group.[5,11,12]

Densities and Dynamic Viscosities. Densities were measured using an Anton Paar DMA-5000 U-tube density meter, whereas viscosities were analyzed using an Anton Paar AMVn automated viscometer. These determinations were done in order to characterize solvents [emim][SCN] and [bmim][SCN], which our research group had not determined until now. The estimated uncertainty of the measured densities was 1 × 10^{-4} g·cm^{-3}, where 1.1 % is the estimated uncertainty of the analyzed dynamic viscosities. Both density meter and viscometer were used by our research group before for measuring physical properties of pure substances and mixtures.[14−17]

RESULTS AND DISCUSSION

Dynamic TGA. Dynamic runs were done for all ILs cited previously as explained above in Experimental Section. The determination of all characteristic parameters is graphically explained in Figure 1. In Figure 2, 10 K·min^{-1} heating rate experiments are presented in order to show the differences between all cyano-based ILs studied. All dynamic comparisons are done at 10 K·min^{-1} heating rate, because it is the most commonly used.[5−7,11,12] However, in Table 2, the most characteristic parameters of dynamic experiments done are summarized for the ILs employed at every heating rate.

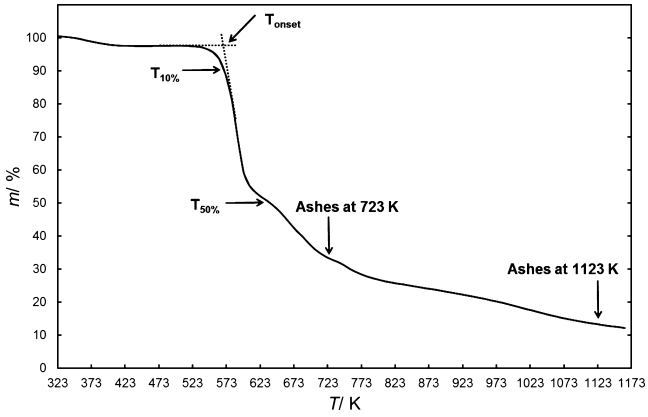

Figure 1. The graphical determination of characteristic parameters for ILs form a dynamic TGA curve.

The [emim][TCM] IL has shown the highest onset temperature, whereas those of both dicyanamide-based ILs are a little below. Thiocyanate-based ILs onset temperatures are the lowest obtained in this work. The IL cation change from 1-

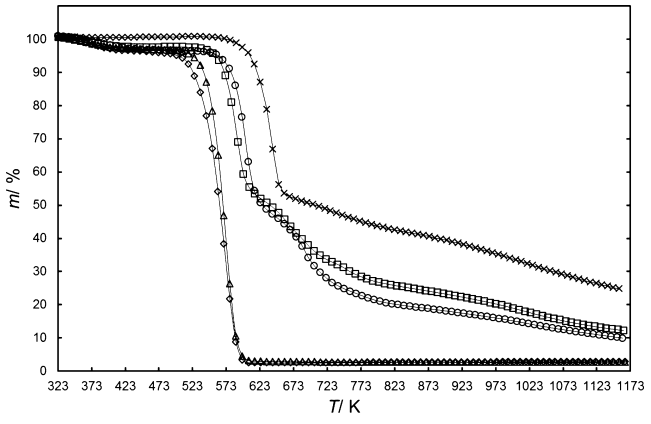

Figure 2. Dynamic TGA thermograms for ILs: □, [emim][DCA]; ○, [bmim][DCA]; ◇, [emim][SCN]; Δ, [bmim][SCN]; ×, [emim]-[TCM]. Heating rate: 10 K·min^{-1}.

Table 2. Dynamic TGA Characteristic Parameters for [emim][DCA], [bmim][DCA], [emim][SCN], [bmim][SCN], and [emim][TCM] Ionic Liquids

		ionic liquid				
parameter	HR[a]	[emim] [DCA]	[bmim] [DCA]	[emim] [SCN]	[bmim] [SCN]	[emim] [TCM]
T_{onset}/K	5	557.4	560.2	525.5	533.0	602.5
	10	569.7	569.4	538.6	547.2	616.0
	20	583.0	580.8	553.7	555.3	631.2
$T_{10\ \%}$[b]/K	5	557.0	551.8	505.5	524.5	605.6
	10	569.6	568.4	523.3	538.8	618.9
	20	582.2	579.3	535.4	551.4	629.1
$T_{50\ \%}$[c]/K	5	614.6	591.0	547.8	552.8	700.3
	10	638.0	617.8	563.1	568.1	705.1
	20	647.9	625.3	576.9	581.1	710.4
$ashes_{723\ K}$/%	5	33.1	25.7	2.2	2.2	48.2
	10	33.5	27.9	2.5	2.7	48.9
	20	33.5	27.8	2.5	2.8	49.1
$ashes_{1,123\ K}$/%	5	11.9	8.7	2.1	2.2	26.1
	10	13.3	12.2	2.5	2.7	26.4
	20	13.6	13.0	2.5	2.7	26.4

[a]Heating rate in K·min^{-1}. [b]Temperature that provides a mass loss equal to 10 % of the initial mass introduced. [c]Temperature that provides a mass loss equal to 50 % of the initial mass introduced.

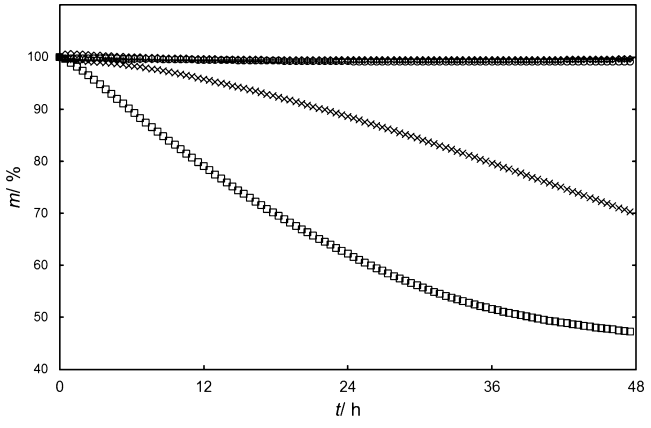

Figure 3. Isothermal TGA data for [emim][DCA] at several temperatures for 48 h: ◇, T = 313.2 K; +, T = 353.2 K; ○, T = 393.2 K; ×, T = 433.2 K; □, T = 473.2 K.

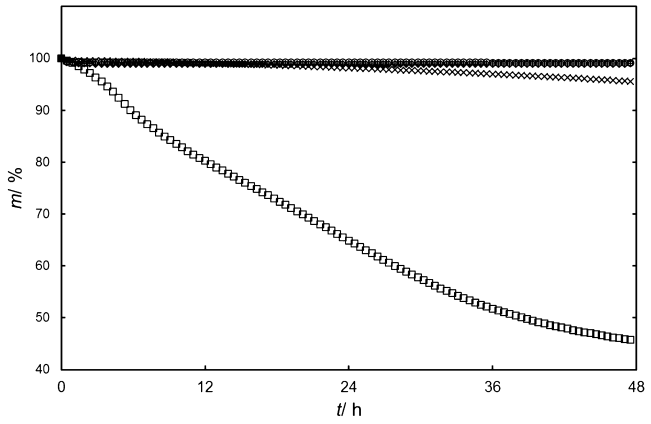

Figure 4. Isothermal TGA data for [bmim][DCA] at several temperatures for 48 h: ◇, T = 313.2 K; +, T = 353.2 K; ○, T = 393.2 K; ×, T = 433.2 K; □, T = 473.2 K.

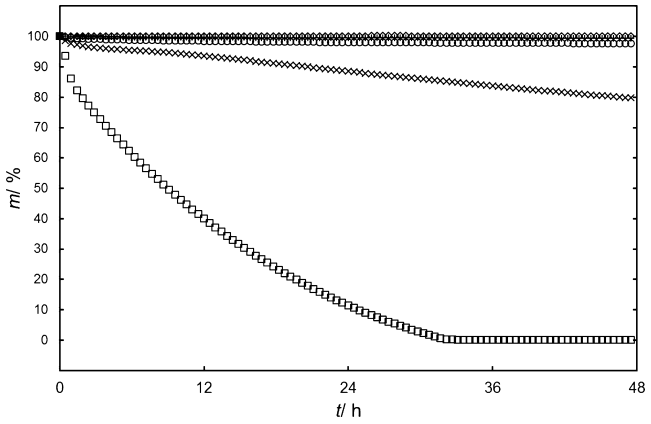

Figure 5. Isothermal TGA data for [emim][SCN] at several temperatures for 48 h: ◇, T = 313.2 K; +, T = 353.2 K; ○, T = 393.2 K; ×, T = 433.2 K; □, T = 473.2 K.

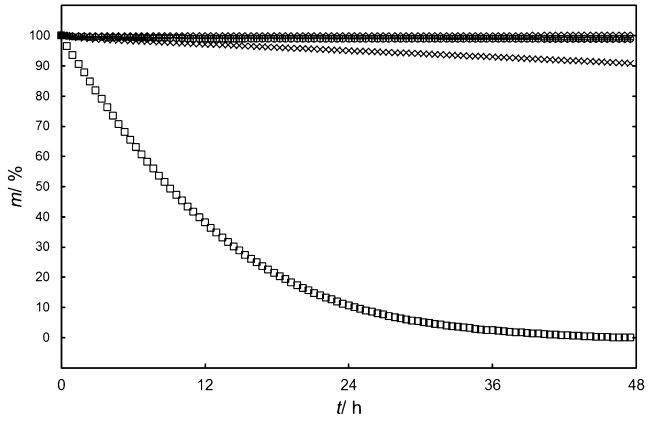

Figure 6. Isothermal TGA data for [bmim][SCN] at several temperatures for 48 h: ◇, T = 313.2 K; +, T = 353.2 K; ○, T = 393.2 K; ×, T = 433.2 K; □, T = 473.2 K.

ethyl-3-methylimidazolium ([emim]) to 1-butyl-3-methylimidazolium ([bmim]) causes a slight influence on onset temperature. Thus, it is possible to claim that imidazolium ILs with tricyanomethanide anion are more stable than ILs with dicyanamide anion, and these are more stable than those containing thiocyanate anion.

dx.doi.org/10.1021/je400140n | J. Chem. Eng. Data 2013, 58, 2187−2193

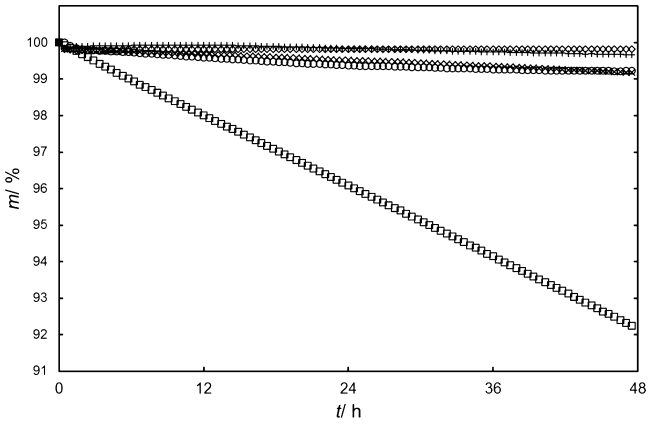

Figure 7. Isothermal TGA data for [emim][TCM] at several temperatures for 48 h: ◇, T = 313.2 K; +, T = 353.2 K; ○, T = 393.2 K; ×, T = 433.2 K; □, T = 473.2 K.

Table 3. Frequency Factors (k_0) and Activations Energies (E_A) for Adjustments Using eq 1 and Experimental Dynamic Data at 5 K·min^{-1} Heating Rate. MOT Experimental (exptl) and Calculated (calc) from eq 3

IL	k_0/s^{-1}	E_A/J·mol^{-1}	MOT$_{exptl}$, for 48 h/K	MOT$_{calc}$, for 8000 h/K
[emim][DCA]	$7.31\cdot10^{13}$	$1.83\cdot10^{8}$	393.2 to 433.2	412
[bmim][DCA]	$5.11\cdot10^{16}$	$2.14\cdot10^{8}$	393.2 to 433.2	428
[emim][SCN]	$5.19\cdot10^{10}$	$1.39\cdot10^{8}$	353.2 to 393.2	360
[bmim][SCN]	$2.47\cdot10^{16}$	$1.99\cdot10^{8}$	393.2 to 433.2	403
[emim][TCM]	$1.86\cdot10^{14}$	$2.05\cdot10^{8}$	433.2 to 473.2	452

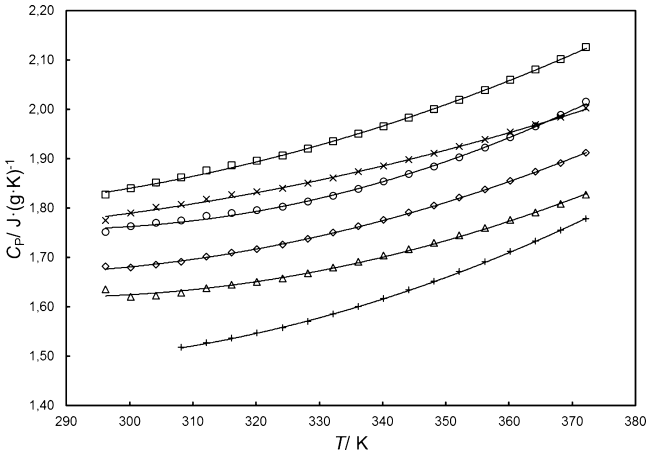

Figure 8. Specific heat (C_P) versus temperature (T): □, [emim][DCA]; ○, [bmim][DCA]; ◇, [emim][SCN]; Δ, [bmim][SCN]; ×, [emim][TCM]; +, Sulfolane. Solid lines denote adjustments of experimental data to eq 4.

In addition to this, $T_{10\ \%}$ and $T_{50\ \%}$, included in Table 2 show the same behavior commented to onset temperature, but they are relevant parameters that provide information of the behavior the IL follows in its decomposition. This way, the difference between onset temperature and $T_{10\ \%}$ or $T_{50\ \%}$ is a type of measure of the decomposition tax, and, because of this, thiocyanate-based ILs have the lowest difference between temperatures, as a consequence of their quick decomposition. On the other hand, the highest difference between temperatures was found for [emim][TCM], which has the highest onset temperature and is apparently the most stable.

Table 2 also includes the comparison between the ashes remaining in the pan at 723.2 K and at 1123.2 K. These results are related to inorganic compounds formed in the decomposition processes. A high inorganic character is directly related

Table 4. Results of Specific Heats[a] for ILs and Sulfolane

	C_P/J·(g·K)$^{-1}$					
T/K	[emim][DCA]	[bmim][DCA]	[emim][SCN]	[bmim][SCN]	[emim][TCM]	Sulfolane
296.2	1.827	1.751	1.681	1.620	1.775	
300.2	1.839	1.763	1.679	1.620	1.790	
304.2	1.851	1.769	1.685	1.623	1.801	
308.2	1.862	1.775	1.691	1.628	1.808	1.518
312.2	1.876	1.783	1.701	1.637	1.818	1.527
316.2	1.886	1.789	1.709	1.644	1.826	1.537
320.2	1.895	1.796	1.717	1.650	1.833	1.547
324.2	1.906	1.803	1.726	1.657	1.840	1.557
328.2	1.920	1.813	1.737	1.668	1.849	1.571
332.2	1.935	1.824	1.750	1.679	1.861	1.585
336.2	1.950	1.839	1.762	1.691	1.873	1.601
340.2	1.965	1.853	1.776	1.703	1.885	1.617
344.2	1.982	1.869	1.791	1.716	1.897	1.634
348.2	2.000	1.884	1.805	1.729	1.910	1.652
352.2	2.019	1.902	1.821	1.745	1.924	1.671
356.2	2.038	1.922	1.837	1.759	1.939	1.691
360.2	2.059	1.943	1.855	1.775	1.953	1.712
364.2	2.080	1.965	1.874	1.791	1.969	1.733
368.2	2.102	1.989	1.891	1.808	1.984	1.755
372.2	2.126	2.015	1.911	1.826	2.003	1.778

[a]Standard uncertainty calculated to specific heat is $u(C_P)$ = 0.01 J·(g·K)$^{-1}$.

dx.doi.org/10.1021/je400140n | J. Chem. Eng. Data 2013, 58, 2187−2193

Table 5. Adjustment Parameters of Specific Heats[a] for ILs and Sulfolane

chemical	a/J·(g·K)$^{-1}$	b/J·g^{-1}·K^{-2}	c/J·g^{-1}·K^{-3}	R^2	T range/K
[emim][DCA]	3.35	$-1.22\cdot10^{-2}$	$2.41\cdot10^{-5}$	0.9994	296.2 to 372.2
[bmim][DCA]	4.82	$-2.12\cdot10^{-2}$	$3.66\cdot10^{-5}$	0.9985	296.2 to 372.2
[emim][SCN]	3.72	$-1.48\cdot10^{-2}$	$2.68\cdot10^{-5}$	0.9995	296.2 to 372.2
[bmim][SCN]	3.65	$-1.45\cdot10^{-2}$	$2.58\cdot10^{-5}$	0.9995	296.2 to 372.2
[emim][TCM]	2.72	$-7.95\cdot10^{-3}$	$1.62\cdot10^{-5}$	0.9983	296.2 to 372.2
Sulfolane	3.82	$-1.70\cdot10^{-2}$	$3.10\cdot10^{-5}$	0.9999	308.2 to 372.2

[a]Standard uncertainty calculated to specific heat is $u(C_P) = 0.01$ J·(g·K)$^{-1}$.

to a high thermal stability. At both temperatures, [emim]-[TCM] has the lowest mass lost, whereas dicyanamide-based ILs have less mass lost than thiocyanate-based ILs, which have negligible mass remaining at 1123.2 K.

In Table 2, the results at the different heating rates studied are presented. The lowest heating rate (5 K·min^{-1}, in this work) has the lowest decomposition temperatures. Thermal stability is closely dependent on time, and thus, thermal stability parameters decrease when experimental time increases, at low heating rates.

Another important characteristic during the decomposition of an ionic substance is the behavior of the ions. Using the relationship between the molecular weight of each anion to the IL molecular weight, it is possible to know what ion decomposes first. This way, the relative weight of the anion over the IL structure was calculated, the values for each IL being 37 % for [emim][DCA], 32 % for [bmim][DCA], 34 % for [emim][SCN], 29 % for [bmim][SCN], and 45 % for [emim][TCM]. Only the 10 K·min^{-1} heating rate is presented here, but the conclusions at other heating rates are identical.

As can be seen in Figure 2, both thiocyanate-based ILs decompose without a difference between the anion and cation. Thus, only dicyanamide-based and tricyanomethanide-based ILs can be studied. Dicyanamide-based ILs show an initial decrease of weight at about 513 K that ends with a change of slope of the TGA curve at about 600 K, a period that for [emim][DCA] involves approximately 40 % of lost mass and 35 % for [bmim][DCA]. In a comparison of these values with the relative weight of the anion, it is possible to claim that first the anion and then the cation decompose in the dicyanamide-based ILs studied, taking into account that a little overlap takes place. There is also a difference between anion and cation decomposition in [emim][TCM]. In this case, decomposition started at about 600 K and a change of slope of the TGA curve is found at 650 K where 45 % of the mass was lost, a mass which is closely near to the relative weight of the tricyanomethanide anion.

It is then important to highlight that the anion could modify the beginning of the cation decomposition. In this work, imidazolium-based cations have started to decompose from (560 to 650) K, describing different shapes in their decomposition, as it can be observed in Figure 2. Thus, the behavior of the IL in thermal decomposition is closely depended on the decomposition of the anion.

To end with dynamics experiments, a comparison with published values is done. Data for dicyanamide ILs set the onset temperature of both [emim][DCA] and [bmim][DCA] at 573.2 K[3,6] and 566 K[18] and the start of mass loss at 513.2 K.[3,6,19,20] These data are in close agreement with the results included in this study, where the deviation of these values is below 1 %.

Isothermal TGA. Isothermal TGA experiments were carried out as explain in the Experimental Section. The results of the isothermal analysis of the five ILs studied here are graphically represented in Figures 3 to 7. These runs show that all ILs measured in this study lose mass at quite lower temperature than the onset temperature determined by dynamic TGA. Thus, the time effect on decomposition is demonstrated experimentally again. The MOT for [emim][TCM] is between (433.2 and 473.2) K, whereas for [emim][DCA], [bmim]-[DCA], and [bmim][SCN] the MOTs are between (393.2 and 433.12) K, and for [bmim][SCN] the MOT is between (353.2 and 393.2) K.

Thus, onset temperature from dynamic analysis over-estimates no less than 150 K experimental MOT from isothermal runs. Because of this, it is important to know the behavior of the IL at extremely long-term runs. The main drawback of these experiments is the long time demanded. Therefore, the employment of prediction models from short time dynamic analysis, such as the model of Seeberger et al.,[8] could be a solution.

Prediction of MOT. The main contribution of a thermal analysis of an IL or any compound should be the acquisition of a quite accurate value of MOT that would be able to secure that under this temperature no IL decomposition could take place.

As commented before, dynamic data from TGA analysis are needed for carrying out this prediction model. This cited method consists of considering both decomposition and evaporation processes, because they are the processes that occur in a heating experiment. However, in this study the employment of high heating rates and the very low vapor pressure of ILs set values of evaporation that could be considered as negligible.[8]

This way, the decomposition process is assumed to be the only process that affects mass loss. Then, a first order model was proposed, where the constant of decomposition is developed to fit Arrhenius law:[8]

$$\frac{-\mathrm{d}m}{\mathrm{d}t} = k_0 \exp\left(-\frac{E_A}{RT}\right)m \qquad (1)$$

where $-\mathrm{d}m/\mathrm{d}t$ is the decomposition rate, k_0 denotes the frequency factor, E_A is the activation energy, R refers to the ideal gas law constant, T is the temperature, and m denotes the mass of the substance.

Adjusting the dynamic data to eq 1, k_0 and E_A are calculated and listed in Table 3. Data from experiments at 5 K·min^{-1} have been fitted, as they have a lineal zone enough to do this, because they were done during a larger period of time. With these decomposition parameters, the next expression can be used to predict decomposition temperatures at extremely long-term analysis:[8]

$$\mathrm{MOT} = \frac{E_A}{R\left\{ -\ln\left[\ln\left(\frac{m}{m_0}\right)\right] + \ln(k_0 t_{max})\right\}} \quad (2)$$

where t_{max} is the time at which MOT value is calculated and m_0 denotes initial mass. To obtain a representative MOT, the prediction of decomposition has to ensure a lower decomposition than 1 %, in mass. In other words, the relation m/m_0 has a value of 0.99. Thus, eq 2 is simplified to eq 3:[8]

$$\mathrm{MOT} = \frac{E_A}{R[4.6 + \ln(k_0 t_{max})]} \quad (3)$$

As can be seen in Table 3, predicted values are in agreement with experimental data, as they are into the experimentally MOT range obtained from isothermal analysis. This means that the use of dynamic TGA data fitted to the Seeberger et al. model makes it possible to predict an accurate value of the MOT. This prediction method for long-term runs is a good tool to correct the onset temperature from dynamic thermal analysis, but isothermal runs are actually important to check the values experimentally. Therefore, this method could be applied to other ILs to predict the MOT. However, more dynamic and isothermal experiments over different ILs would be needed.

Specific Heats. The determination of all specific heats of the ILs involved in this study was done from (296.2 to 372.2) K. A second order model was used to correlate specific heats (C_P) against temperature (T):

$$C_P = a + bT + cT^2 \quad (4)$$

The results of the specific heats are tabulated in Table 4 and graphically represented in Figure 8, whereas the correlations of specific heats as function of temperature are listed in Table 5. The studied ILs have been shown to possess higher specific heats than sulfolane. Thiocyanate-based ILs have lower specific heat than dicyanamide-based ILs and [emim][TCM]. When [bmim] is replaced by [emim] an increase in the specific heat value has been observed in dicyanamide and thiocyanate ILs. The same behavior was previously commented by Fredlake et al.[6] in their study about specific heats of imidazolium-based ILs and by Gómez et al.[21] in their investigation about specific heats of several 1-alkyl-3-methylimidazolium-based ILs.

To validate the specific heats gathered in this work, a comparison with published data was made. The mean absolute deviation between the results of this work and published specific heats for [emim][DCA] were 1.7 %[7] and 4.3 %;[22] for [bmim][DCA] were 0.9 %,[23] 3.6 %,[24] 3.8 %,[25] and 3.2 %;[26] and for [emim][SCN] were 1.3 %[22] and 0.6 %.[27] In addition, sulfolane values are compared to bibliographic data, and the mean absolute deviation calculated was lower than 0.7 %,[28] 1.8 %,[29] and 3.0 %, respectively.

CONCLUSIONS

This study has shown that a thermal analysis has to consider both time and temperature to reach realistic MOT values. This way, results obtained for [emim][DCA], [bmim][DCA], [emim][SCN], [bmim][SCN], and [emim][TCM] through dynamic analysis overestimate the real MOT values at which they are thermally stable, experimentally checked by isothermal analysis, and theoretically predicted using the Seeberger et al. model. In other words, MOT dependence on time has been demonstrated. In addition to this, dynamic experiments have been shown to be effective in a comparison of several substances, but not in a determination of the temperature a substance without the substance suffering decomposition processes.

Specific heats of all ILs studied were measured from (296.2 to 372.2) K, and they were successfully fitted to a second order model. It is remarkable that all the ILs studied here have higher specific heats than sulfolane.

AUTHOR INFORMATION

Corresponding Author

*Tel.: +34 91 394 51 19. Fax: +34 91 394 42 43. E-mail: jgarcia@quim.ucm.es.

Funding

Authors are grateful to the Ministerio de Economía y Competitividad (MINECO) of Spain and the Comunidad de Madrid for financial support of Projects CTQ2011−23533 and S2009/PPQ-1545, respectively. Pablo Navarro also thanks MINECO for awarding him an FPI grant (Reference BES-2012-052312). Marcos Larriba thanks Ministerio de Educación, Cultura y Deporte of Spain for awarding him an FPU grant (Reference AP2010-0318).

Notes

The authors declare no competing financial interest.

REFERENCES

(1) Plechkova, N. V.; Seddon, K. R. Applications of ionic liquids in the chemical industry. *Chem. Soc. Rev.* **2008**, *37*, 123.

(2) Larriba, M.; Navarro, P.; García, J.; Rodríguez, F. Liquid−liquid extraction of toluene from heptane using [emim][DCA], [bmim][DCA], and [emim][TCM] ionic liquids. *Ind. Chem. Eng. Res.* **2013**, *52*, 2714.

(3) Meindersma, G. W.; De Haan, A. B. Cyano-containing ionic liquids for the extraction of aromatic hydrocarbons from an aromatic/aliphatic mixture. *Sci. China Chem.* **2012**, *55*, 1488.

(4) Hansmeier, A. R.; Minoves Ruiz, M.; Meindersma, G. W.; de Haan, A. B. Liquid−liquid equilibria for the three ternary systems (3-methyl-*N*-butylpyridinium dicyanamide + toluene + heptane), (1-butyl-3-methylimidazolium dicyanamide + toluene + heptane), and (1-butyl-3-methylimidazolium thiocyanate + toluene + heptane) at T = (313.15 and 348.15) K and p = 0.1 MPa. *J. Chem. Eng. Data* **2010**, *55*, 708.

(5) Fernández, A.; Torrecilla, J. S.; García, J.; Rodríguez, F. Thermophysical properties of 1-ethyl-3-methylimidazolium ethylsulfate and 1-butyl-3-methylimidazolium methylsulfate ionic liquids. *J. Chem. Eng. Data* **2007**, *52*, 1979.

(6) Fredlake, C. P.; Crosthwaite, J. M.; Hert, D. G.; Aki, S. N. V. K.; Brennecke, J. F. Thermophysical properties of imidazolium-based ionic liquids. *J. Chem. Eng. Data* **2004**, *49*, 954.

(7) Crosthwaite, J. M.; Muldoon, M. J.; Dixon, J. K.; Anderson, J. L.; Brennecke, J. F. Phase transition and decomposition temperatures, heat capacities and viscosities of pyridinium ionic liquids. *J. Chem. Thermodyn.* **2005**, *37*, 559.

(8) Seeberger, A.; Andresen, A. K.; Jess, A. Prediction of long-term stability of ionic liquids at elevated temperatures by means of non-isothermal thermogravimetrical analysis. *Phys. Chem. Chem. Phys.* **2009**, *11*, 9375.

(9) Hao, Y.; Peng, J.; Hu, S.; Li, J.; Zhai, M. Thermal decomposition of allyl-imidazolium-based ionic liquid studied by TGA−MS analysis and DFT calculations. *Thermochim. Acta* **2010**, *501*, 78.

(10) Aparicio, S.; Atilhan, M.; Karadas, F. Thermophysical properties of pure ionic liquids: Review of present situation. *Ind. Eng. Chem. Res.* **2010**, *49*, 9580.

(11) Casas, A.; Oliet, M.; Alonso, M. V.; Rodríguez, F. Dissolution of *Pinus radiata* and *Eucalyptus globulus* woods in ionic liquids under microwave radiation: Lignin regeneration and characterization. *Sep. Purif. Technol.* **2012**, *97*, 115.

(12) Casas, A.; Alonso, M. V.; Oliet, M.; Santos, T. M.; Rodríguez, F. Characterization of cellulose regenerated from solutions of pine and eucalyptus woods in 1-allyl-3-methilimidazolium chloride. *Carbohydr. Polym.* **2013**, *92*, 1946.
(13) Standard test method for determining specific heat capacity by differential scanning calorimetry. *ASTM E 1269-01*; ASTM International: West Conshohocken, PA, 2001.
(14) Larriba, M.; García, S.; Navarro, P.; García, J.; Rodríguez, F. Physical properties of *N*-butylpyridinium tetrafluoroborate and *N*-butylpyridinium bis(trifluoromethylsulfonyl)imide binary ionic liquid mixtures. *J. Chem. Eng. Data* **2012**, *57*, 1318.
(15) Larriba, M.; García, S.; Navarro, P.; García, J.; Rodríguez, F. Physical characterization of an aromatic extraction solvent formed by [bpy][BF_4] and [4bmpy][Tf_2N] mixed ionic liquids. *J. Chem. Eng. Data* **2013**, *58*, 1496−.
(16) Larriba, M.; García, S.; García, J.; Torrecilla, J. S.; Rodríguez, F. Thermophysical Properties of 1-ethyl-3-methylimidazolium 1,1,2,2-tetrafluoroethanesulfonate and 1-ethyl-3-methylimidazolium ethylsulfate ionic liquids as a function of temperature. *J. Chem. Eng. Data* **2011**, *56*, 3589.
(17) Navarro, P.; Larriba, M.; García, S.; García, J.; Rodríguez, F. Physical properties of binary and ternary mixtures of 2-propanol, water, and 1-butyl-3-methylimidazolium tetrafluoroborate ionic liquid. *J. Chem. Eng. Data* **2012**, *57*, 1165.
(18) Zech, O.; Stoppa, A.; Buchner, R.; Kunz, W. The Conductivity of imidazolium-based ionic liquids from (248 to 468) K. B. Variation of the Anion. *J. Chem. Eng. Data* **2010**, *55*, 1774.
(19) Yoshida, Y.; Muroi, K.; Otsuka, A.; Saito, G.; Takahashi, M.; Yoko, T. 1-ethyl-3-methylimidazolium based ionic liquids containing cyano groups: Synthesis, characterization, and crystal structure. *Inorg. Chem.* **2004**, *43*, 1458.
(20) Yoshida, Y.; Baba, O.; Yoko, T. Ionic liquids based on dicyanamide anion: Influence of structural variations in cationic structures on ionic conductivity. *J. Phys. Chem. B* **2007**, *111*, 4742.
(21) Gómez, E.; Calvar, N.; Domínguez, A.; Macedo, E. A. Themal analysis and heat capacities of 1-alkyl-3-methylimidazolium ionic liquids with NTf_2^-, TFO^-, and DCA^- anions. *Ind. Eng. Chem. Res.* **2013**, *52*, 2103−.
(22) Freire, M. G.; Teles, A. R. R.; Rocha, M. A. A.; Schroder, B.; Neves, C. M. S. S.; Carvalho, P. J.; Evtuguin, D. V.; Santos, L. M. N. B. F.; Coutinho, J. A. P. Thermophysical characterization of ionic liquids able to dissolve biomass. *J. Chem. Eng. Data* **2011**, *56*, 4813.
(23) Yu, Y. H.; Soriano, A. N.; Li, M. H. Heat capacities and electrical conductivities of 1-ethyl-3-methylimidazolium-based ionic liquids. *J. Chem. Thermodyn.* **2009**, *41*, 103.
(24) de Castro, C. A. N.; Langa, E.; Morais, A. L.; Lopes, M. L. S. M.; Lourenco, M. J. V.; Santos, F. J. V.; Santos, M. S.; Lopes, J. N. C.; Veiga, H. M.; Macatrao, M.; Esperanca, J. M. S. S.; Marques, C. S.; Rebelo, L. P. N.; Afonso, C. A. M. Studies on the density, heat capacity, surface tension and infinite dilution diffusion with the ionic liquids [C_4mim][NTf_2], [C_4mim][dca], [C_2mim][$EtOSO_3$] and [Aliquat][dca]. *Fluid Phase Equilib.* **2010**, *294*, 157.
(25) Gonzalez, E. J.; Dominguez, A.; Macedo, E. A. Physical and excess properties of eight binary mixtures containing water and ionic liquids. *J. Chem. Eng. Data* **2012**, *57*, 2165.
(26) Paulechka, Y. U.; Kabo, A. G.; Blokhin, A. V.; Kabo, G. J.; Shevelyova, M. P. Heat capacity of ionic liquids: Experimental determination and correlations with molar volume. *J. Chem. Eng. Data* **2010**, *55*, 2719.
(27) Ficke, L. E.; Novak, R.; Brennecke, J. F. Thermodynamic and thermophysical properties of ionic liquid + water systems. *J. Chem. Eng. Data* **2010**, *55*, 4946.
(28) Mundhwa, M.; Elmahmundi, S.; Maham, Y.; Henni, A. Molar heat capacity of aqueous sulfolane, 4-formylmorpholine, 1-methil-2-pyrrolidinone, and triethylene glycol dimethyl ether solutions from (303.15 to 353.15) K. *J. Chem. Eng. Data* **2009**, *54*, 2895.
(29) Fulem, M.; Ruzicka, K.; Ruzicka, M. Recommended vapor pressures for thiophene, sulfolane, and dimethyl sulfoxide. *Fluid Phase Equilib.* **2011**, *303*, 205.
(30) Steele, W. V.; Chirico, R. D.; Knipmeyer, S. E.; Nguyen, A. Vapor pressure, heat capacity, and density along the saturted line, measurements for cyclohexanol, 2- cyclohexen-1-one, 1,2-dichloropropane, 1,4-di-*tert*-butylbenzene, (±)-2-ethylhexanoic acid, 2-(methylamino)ethanol, perfluoro-*n*-heptane, and Sulfolane. *J. Chem. Eng. Data* **1997**, *42*, 1021.

J. Chem. Thermodynamics 76 (2014) 152–160

Contents lists available at ScienceDirect

J. Chem. Thermodynamics

journal homepage: www.elsevier.com/locate/jct

Thermal stability, specific heats, and surface tensions of ([emim][DCA] + [4empy][Tf_2N]) ionic liquid mixtures

Pablo Navarro, Marcos Larriba, Julián García *, Francisco Rodríguez

Department of Chemical Engineering, Complutense University of Madrid, E-28040 Madrid, Spain

ARTICLE INFO

Article history:
Received 13 January 2014
Received in revised form 14 March 2014
Accepted 21 March 2014
Available online 31 March 2014

Keywords:
Mixtures of ionic liquids
Thermal stability
Specific heats
Surface tensions

ABSTRACT

Lately, mixing ionic liquids (ILs) is a current trend in the investigation of the potential use of ILs as solvents in the liquid–liquid extraction of aromatics from aliphatic/aromatic mixtures. Several mixtures have shown high values of both aromatic/aliphatic selectivity and aromatic distribution ratio, which are the essential parameters an IL or a mixtures of ILs have to accomplish. However, it is also important to know the behavior of relevant aspects of the IL mixtures whether extraction results are of interest. The maximum operation temperature (MOT) is a key property to determine, because it limits the applicability of ILs to work without thermal decomposition. [emim][DCA] and [4empy][Tf_2N] IL mixtures have shown good properties in liquid–liquid extraction of toluene from alkane/toluene mixtures. Isothermal analyses of the IL mixture were carried out to obtain an experimental decomposition interval for long-terms, whereas dynamic runs were performed to study several interesting parameters of the IL mixture and were also used to apply Seeberger *et al.* prediction model for long-terms behaviors. An ideal model to predict the behavior of the mixture was proposed and used in order to predict the MOT of the IL mixture from dynamic data of pure ILs involved in the mixture. To complete this study, specific heats and surface tensions of the mixture were measured and the ideality of the mixture in both cases was also evaluated through their excess properties.

1. Introduction

Ionic liquids (ILs) are liquid salts at temperatures lower than 373 K formed by an organic cation and an organic or inorganic anion [1]. The main aspect that shows ILs as promising substances in order to replace conventional solvents is their negligible vapor pressures. The non-volatile character of ILs could simplify several separation and purification processes [1,2]. Also the high number of combinations forming IL structures permits to design adequate ILs to several applications [1–3]. However, although IL properties could be tuned through the IL structure, several applications demand a whole number of requirements. Therefore, the trend of mixing ILs is nowadays carried out, looking for intermediate properties between those of the ILs forming the mixture [4–6].

Among others, one of the research lines that involve the study of ILs as alternative substances is the aromatic extraction [4–15]. Several studies deal with the liquid–liquid extraction of aromatics from aliphatic/aromatic mixtures, but also there are many works that are focused on measuring other important aspects of the ILs involved in this field. Specifically, the most studied properties are density, dynamic viscosity, and maximum operation temperature (MOT) [16–32]. It is difficult to find an IL that shows both good extractive and physical properties. Thus, the actual trend is the commented tuning of both groups of properties by mixing ILs. Then, the composition of the mixture is an additional variable to obtain the desired IL-based solvent.

The performance of binary IL mixtures has been studied in the liquid–liquid extraction of aromatics, and also the characterization of several properties as density, viscosity, refractive index, and surface tension has been performed [4–6,17,18,28–31]. However, to the best of our knowledge, the study of thermal stability and specific heats of binary mixtures of ILs has not been carried out until now.

Thus, the aim of this work was the evaluation of the thermal stability of the binary mixture of 1-ethyl-3methylimidazolium dicyanamide ([emim][DCA]) and 1-ethyl-4-methylpyridinium bis(trifluoromethylsulfonyl)imide ([4empy][Tf_2N]), which is a good mixed IL solvent in the separation of aromatic hydrocarbons considering its extractive and physical properties [4]. For the purpose of determining thermal resistance, both dynamic and isothermal thermogravimetrical analyses (TGA) were used. Dynamic runs were done from $T = (293.2$ to $1173.2)$ K at different heating rates of (5, 10, and 20) $K \cdot min^{-1}$, whereas isothermal experiments were

* Corresponding author. Tel.: +34 91 394 51 19; fax: +34 91 394 42 43.
E-mail address: jgarcia@quim.ucm.es (J. García).

http://dx.doi.org/10.1016/j.jct.2014.03.023
0021-9614/

TABLE 1
Chemicals: specifications and properties. Densities (ρ) and dynamic viscosities (η).

Chemical	Source	Purity	Analysis method	ρ, at 298.2 K/g · cm^{-3}	η, at 298.2 K/mPa · s
[emim][DCA]	Iolitec GmbH	0.98	NMR[a], IC[b]	1.1013[c]	15.1[c]
[4empy][Tf_2N]	Iolitec GmbH	0.99	NMR[a], IC[b]	1.4919[c]	42.4[c]
Sapphire	Mettler Toledo	0.9999	Verneuil[d]	3.99	–

[a] Nuclear Magnetic Resonance.
[b] Ion Chromatography.
[c] From reference [4].
[d] Purity is assessed by this production method.

TABLE 2
Dynamic TGA characteristic parameters obtained for ([emim][DCA] (1) + [4empy][Tf_2N] (2)) mixture.

Parameter	HR[a]	w_1				
		0.00	0.25	0.5	0.75	1.00[b]
T_{onset}/K	5	675.7	539.4	550.8	556.4	557.4
	10	704.4	553.8	560.7	568.8	569.7
	20	715.9	565.1	573.6	579.7	583.0
$T_{10\%}$[c]/ K	5	667.4	577.8	557.9	557.7	557.0
	10	696.2	594.9	577.0	574.3	569.6
	20	713.2	610.1	591.0	585.2	582.2
$T_{50\%}$[d]/ K	5	708.9	703.1	679.5	671.4	614.6
	10	722.7	720.3	714.4	687.6	638.0
	20	738.5	734.5	728.0	698.1	647.9
$Ashes_{723\ K}$/%	5	14.7	29.6	37.25	36.5	33.1
	10	48.7	47.0	44.4	40.3	33.5
	20	79.8	63.4	52.3	43.6	33.5
$Ashes_{1123\ K}$/%	5	2.5	9.2	9.5	14.8	11.9
	10	3.8	11.4	14.0	16.0	13.3
	20	6.5	13.0	14.6	16.0	13.6

[a] Heating rate in K · min^{-1}.
[b] From reference [24].
[c] Temperature that provides a mass lose equal to 10% of the initial mass introduced.
[d] Temperature that provides a mass lose equal to 50% of the initial mass introduced.

carried out during 48 h at constant temperatures of (313.2, 353.2, 393.2, 433.2, and 473.2) K. Moreover the temperature of 513.2 K was proved in the case of the pure [4empy][Tf_2N].

Dynamic data were analyzed to compare the behavior of the mixture with those of the pure components forming the mixture, and to predict long-term stabilities of ([emim][DCA] + [4empy][Tf_2N]) mixtures using the method proposed by Seeberger *et al.* [26]. Isothermal runs were planned in order to have an experimental reference of MOT and to check predicted values from dynamic data [24–27]. Moreover a linear mixing rule was proposed to predict dynamic thermograms of mixed ILs from data of the pure ILs. MOTs were also calculated from predicted dynamic thermograms of mixture in order to check if it is possible to predict MOT directly from pure dynamic data.

Specific heats and surface tensions of the IL mixture as function of temperature were also measured. As cited above, specific heat study of an IL mixture is determined for the first time here, whereas this work is also one of the first that includes surface tension data of mixed ILs [28–30]. The evaluation of the ideality of mixture through specific heats and surface tension excess deviations was done and excess properties were fitted to Redlich–Kister equation model.

2. Experimental

2.1. Chemicals

[emim][DCA] and [4empy][Tf_2N] ILs were supplied by Iolitec GmbH. Their purities were higher than 0.98 in mass basis, whereas halides and moisture impurities were less than 0.02 and 0.002, respectively in mass according to the certification of analysis provided by the manufacter. Both ILs were stored in their original vessels into a desiccator and carefully handling inside a glove box under an inert atmosphere of dry nitrogen. Sapphire disc employed in the specific heat determination was purchased from Mettler Toledo with 0.9999 of purity in mass. Table 1 includes a description

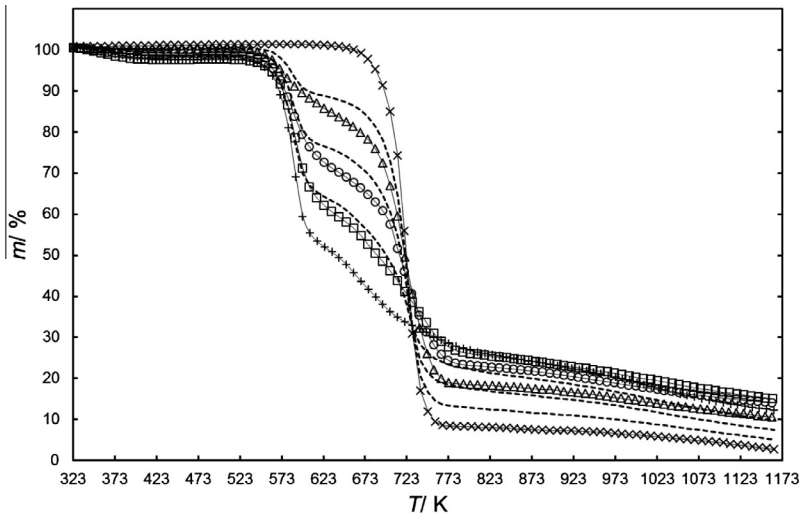

FIGURE 1. Dynamic TGA thermograms for binary mixtures of ([emim][DCA] (1) + [4empy][Tf_2N] (2)) as a function of [emim][DCA] mass fraction: ×, w_1 = 0.00; Δ, w_1 = 0.25; ○, w_1 = 0.50; □, w_1 = 0.75; +, w_1 = 1.00. Data for pure [emim][DCA] from reference [24]. Heating rate used: 10 K·min^{-1}. Dashed lines refer to the TGA ideal mixing rule from equation (1).

TABLE 3
Experimental thermal stability intervals for ([emim][DCA] (1) + [4empy][Tf_2N] (2)) mixtures.

w_1	T_{stable}/K[a]	$T_{unstable}$/K[b]
0.00	473.2	513.2
0.25	393.2	433.2
0.50	393.2	433.2
0.75	393.2	433.2
1.00[c]	393.2	433.2

[a] T_{stable} is the maximum experimental temperature at which the IL or the mixture of ILs are stable in long-terms.
[b] $T_{unstable}$ is the minimum experimental temperature at which the IL or the mixture of ILs are unstable in long-terms.
[c] From reference [24].

of each chemical. They were used here without being purified after purchasing.

2.2. Mixtures of ILs

Mixtures have been prepared by mass employing a Mettler Toledo XS 205 balance, with a precision of $1 \cdot 10^{-5}$ g. The uncertainty in the mass fraction was estimated to be $5 \cdot 10^{-5}$ g.

2.3. Thermal stability

Both dynamic and isothermal TGA were made into a Mettler Toledo TGA/DSC 1 thermogravimetric analyzer, which assesses precisions of ±0.1 K on temperature and $\pm 10^{-3}$ mg in mass measurement. Dynamic and isothermal methods were described in more detail in our last work [24].

2.4. Specific heat

Using differential scanning calorimetry (DSC), specific heats were obtained. The equipment employed was a Mettler Toledo DSC821[e]. Sapphire method has been used to determine specific heats, as recommended in ASTM E 1269-01 [33]. A full description of the experimental method was written in our previous work [24].

2.5. Surface tension

Surface tensions were measured using a Dataphysics OCA 15 plus tensiometer. A pendant drop of the IL was formed into a thermostatic chamber controlling the temperature by employing a Julabo F12-EC bath. The shape of the drop was focused and

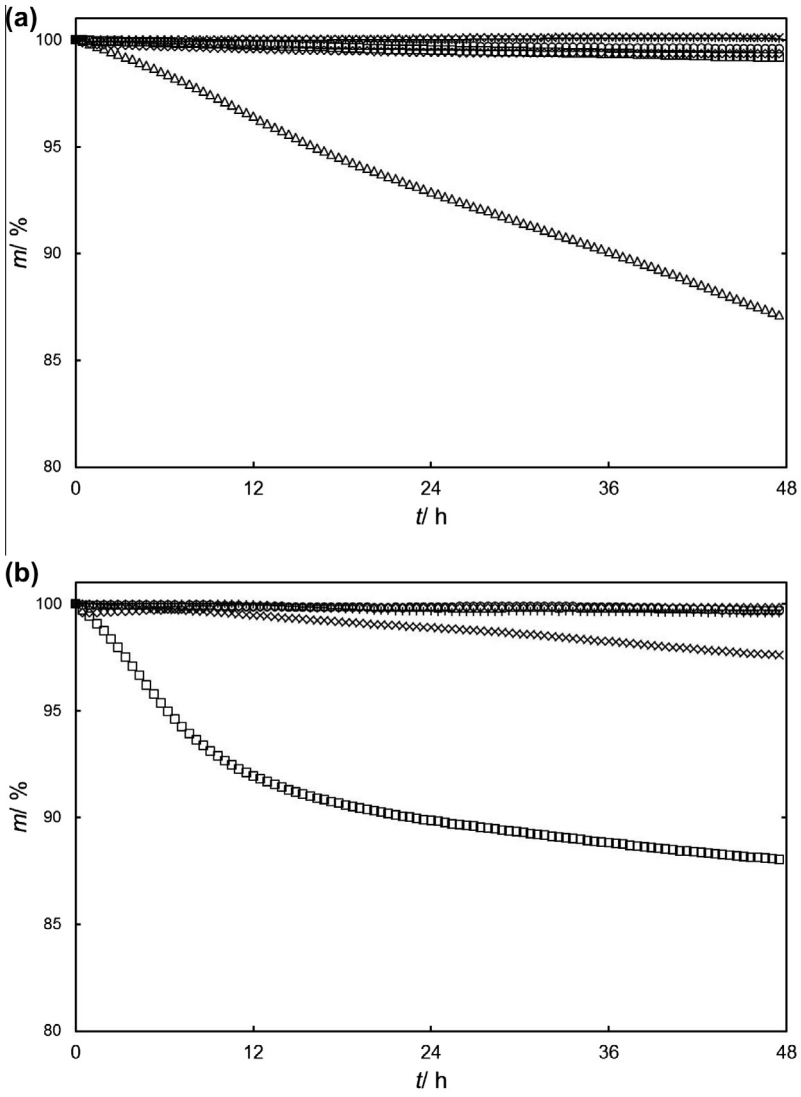

FIGURE 2. Isothermal TGA data for binary mixtures of ([emim][DCA] (1) + [4empy][Tf_2N] (2)). ◇, T = 313.2 K; +, T = 353.2 K; ○, T = 393.2 K; ×, T = 433.2 K; □, T = 473.2 K; Δ, T = 513.2 K. (a), w_1 = 0.00; (b), w_1 = 0.25; (c), w_1 = 0.50; (d), w_1 = 0.75.

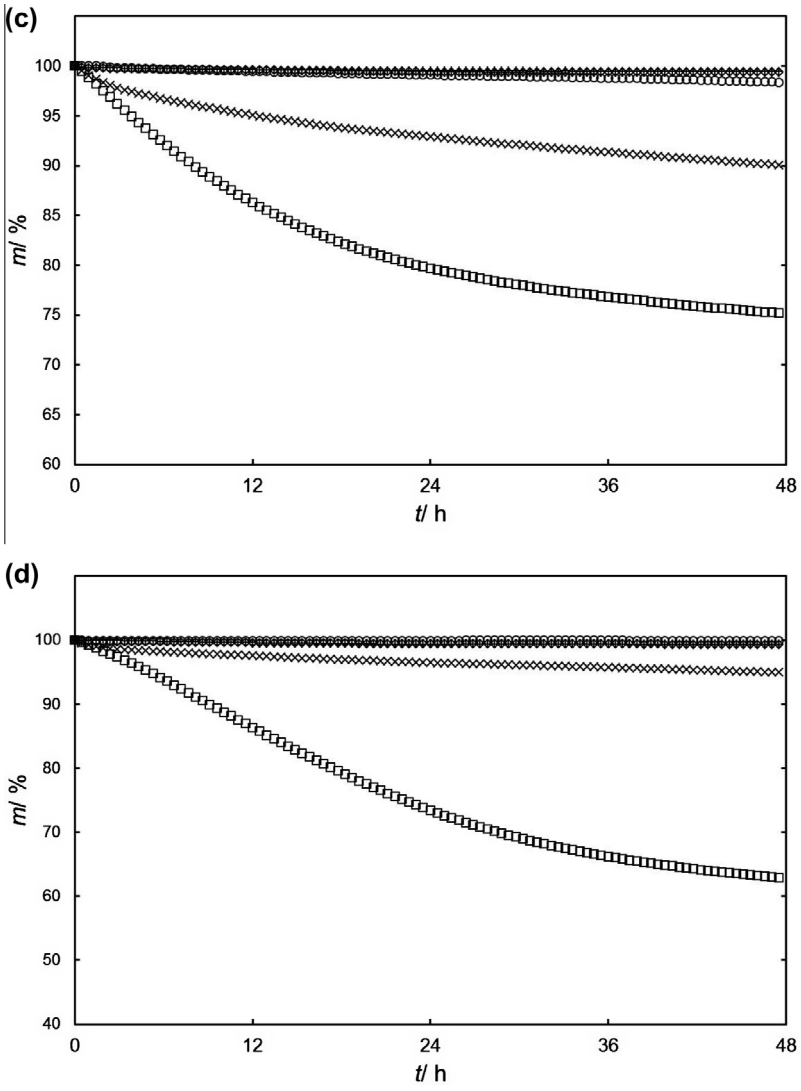

Fig. 2 (*continued*)

determined by a charge-coupled device (CCD) video camera. Surface tension was calculated by the software SCA 20 OCA, employing for this purpose the Young–Laplace equation. Experiments were done at $T = (298.2, 303.2, 313.2, \text{and } 323.2)$ K, being the results showed here the mean of three independent measurements. Mean deviations of pure [emim][DCA] surface tension between values obtained in this work with those published in the literature were calculated. Values determined here are in the middle of the literature range, being the deviations 6.4% for Almeida *et al.* [34], 11.2% for Klomfar *et al.* [35], and 25.4% for Quijada *et al.* [36].

3. Results and discussion

3.1. Dynamic TGA

In this work, binary mixtures of [emim][DCA] and [4empy][Tf_2N] with [emim][DCA] mass fractions of 0.25, 0.50, and 0.75 were measured using different heating rates, specifically at (5, 10, and 20) $K \cdot min^{-1}$. Pure [4empy][Tf_2N] was also evaluated in this work at all heating rates cited above, whereas [emim][DCA] data were published in our previous work [24]. Results obtained were summarized in table 2. In figure 1, a graphical comparison was also done at a heating rate of 10 $K \cdot min^{-1}$, which is the most employed in dynamic TGA [24–27,33,37,38].

In order to try to avoid experimental determinations of TGA for binary mixtures of ILs an ideal TGA mixing rule, which corresponds to a degradation of the mixture proportionally to the pondered degradation of both ILs separately, was proved using pure IL data:

$$m_{\text{mixture}} = \sum_{i=1}^{I} w_i \cdot m_i, \tag{1}$$

where m_{mixture} is the mass that the mixture would lose in an ideal case at each temperature, m_i denotes the experimental mass lost by each compound forming the mixture at each temperature, and w_i refers to the IL mass fraction in the mixture, being I the number of compounds presented in the mixture. Then, the ideal thermograms were graphically shown in figure 1 for the three compositions proved here at cited heating rate.

As showed in figure 1, experimental thermograms for ([emim][DCA] + [4empy][Tf_2N]) binary mixtures follow an intermediate behavior between experimental thermograms of the pure ILs forming the mixture at 10 $K \cdot min^{-1}$. This behavior is also observed in table 2 for all heating rates proved here. First the anion and then the cation decomposed in pure [emim][DCA] [24],

whereas the decomposition process for pure [4empy][Tf_2N] is only in one step. In the case of the mixture, first the [DCA] anion and then both [emim] cation and the pure [4empy][Tf_2N] IL decomposed. This aspect can be observed in figure 1, as a result of the mass loses that are approximately 10%, 20%, and 30% in the first decomposition step for [emim][DCA] mass fractions of 0.25, 0.50, and 0.75, respectively. The relative weights of the anion at these compositions of mixture are 9.3%, 18.5%, and 27.8%, respectively, values that are very close to those cited above. Both temperatures of 10% and 50% loss of mass for mixed ILs are intermediate between those of pure ILs. However, onset temperatures for IL binary mixtures are somewhat lower than those of [emim][DCA] and also remained ashes at (723 and 1123) K are slightly higher in any mixture than for the two pure ILs. Onset temperatures were determined by the cross point between the tangents after and before the decomposition starts, being affected by the slope of the first step of degradation of the [emim][DCA]. The high amount of ashes at determined temperatures in comparison with pure data could be related to interactions between degradation products of the decomposition of both [emim][DCA] and [4empy][Tf_2N].

In comparison with the ideal TGA mixing rule from equation (1), experimental trend is in agreement until 723 K, especially at the start of the decomposition. Thus, the dynamic behavior of the ([emim][DCA] + [4empy][Tf_2N]) mixtures can be assumed to be almost ideal during the first steps of the decomposition. At higher temperatures, the behavior of ([emim][DCA] + [4empy][Tf_2N]) mixtures cannot be estimated by the ideal mixing rule proposed, possibly because of the cited interaction between decomposition products of [emim][DCA] and those corresponding to [4empy][Tf_2N].

3.2. Isothermal TGA

Isothermal TGA experiments were done for all compositions analyzed in this work for binary mixtures of ([emim][DCA] + [4empy][Tf_2N]) and for pure [4empy][Tf_2N] at temperatures of (313.2, 353.2, 393.2, 433.2, and 473.2) K. Temperature of 513.2 K was only checked in the case of [4empy][Tf_2N] because of its higher thermal stability. Stability parameters obtained were included in table 3 jointly to literature data for [emim][DCA], whereas TGA results were graphically represented in figure 2.

All binary mixtures showed a decomposition interval for long-terms equal to that corresponding to [emim][DCA], which was T = (393.2 to 433.2) K [24], being experimental decomposition interval for pure [4empy][Tf_2N] T = (473.2 to 513.2) K. Therefore, the decomposition for long-terms is also conditioned by the less stable IL, which is [emim][DCA].

3.3. Prediction of MOT

In order to obtain a clear comparison, MOT prediction using dynamic data at 5 K · min^{-1} were done employing for this purpose the Seeberger *et al.* model. The decomposition process of an IL or a mixture of ILs is assumed to be the only process that affect to the mass loss process that occurs in a TGA experiment, due to the negligible vapor pressure of ILs [24]. Therefore, the decomposition tax ($-dm/dt$) was explained by a first order model, being the constant of decomposition developed to Arrhenius law [26]:

$$\frac{-dm}{dt} = k_0 \cdot \exp\left(-\frac{E_A}{R \cdot T}\right) \cdot m, \tag{2}$$

where k_0 denotes the frequency factor, E_A is the activation energy, R is the ideal gas law constant, T refers to the temperature in K, and m denotes the mass of the substance.

Adjusting experimental dynamic data to equation (2), k_0 and E_A were calculated and listed in table 4. Additionally to this, decomposition parameters were also determined for thermograms predicted by the ideal mixing rule, due to the good prediction showed by this method. Parameters obtained by ideal predicted curves were also included in table 4.

The next equation can be employed to predict MOTs at any desirable long-term [26]:

$$\mathrm{MOT} = \frac{E_A}{R \cdot [4.6 + \ln(k_0 \cdot t_{max})]}, \tag{3}$$

where t_{max} is the time at which MOT value is calculated, set here in 8000 h. A full description of this method was done by Seeberger

TABLE 5
Specific heats[a] (C_P) and surface tensions[b] (γ) for ([emim][DCA] (1) + [4empy][Tf_2N] (2)) mixtures.

T/K	w_1 = 0.00	w_1 = 0.25	w_1 = 0.50	w_1 = 0.75	w_1 = 1.00[c]
			C_P/J · (mol · K)$^{-1}$		
296.2	627	504	421	363	324
300.2	634	509	425	366	326
304.2	637	512	427	369	328
308.2	640	514	430	371	330
312.2	644	517	433	374	332
316.2	647	520	436	376	334
320.2	649	522	438	378	336
324.2	652	524	441	381	338
328.2	655	528	444	383	340
332.2	659	532	448	387	343
336.2	665	537	451	390	346
340.2	669	541	455	393	348
344.2	674	546	459	397	351
348.2	679	550	463	400	355
352.2	685	555	467	404	358
356.2	691	560	472	407	361
360.2	697	565	477	411	365
364.2	703	570	481	415	369
368.2	708	576	486	419	372
372.2	715	584	492	424	377
			γ/mN · m^{-1}		
298.2	24.3	40.8	45.8	52.0	56.4
303.2	23.9	40.3	45.3	51.5	56.0
313.2	23.1	39.2	44.1	50.3	54.8
323.2	22.2	38.0	42.8	49.0	53.5

[a] Standard uncertainty calculated to specific heat is u(C_P) = 5 J · (mol · K)$^{-1}$.
[b] Standard uncertainty calculated to surface tension is u(γ) = 0.1 mN · m^{-1}.
[c] Specific heat data from reference [24].

TABLE 4
Frequency factors (k_0) and activations energies (E_A) for ([emim][DCA] (1) + [4empy][Tf_2N] (2)) mixtures for adjustments using equation (2) and experimental dynamic data (exptl) or predicted dynamic data using equation (1) (pred) at 5 K · min^{-1} heating rate. MOT calculated from equation (3).

w_1	$k_{0,\ exptl}$/s^{-1}	$k_{0,\ pred}$/s^{-1}	$E_{A,\ exptl}$/J · mol^{-1}	$E_{A,\ pred}$/J · mol^{-1}	$MOT_{exptl,\ 8000\ h}$/K	$MOT_{pred,\ 8000\ h}$/K
0.00	$1.45 \cdot 10^{11}$	–	$1.89 \cdot 10^5$	–	480	–
0.25	$1.59 \cdot 10^{14}$	$1.28 \cdot 10^{14}$	$1.87 \cdot 10^5$	$1.87 \cdot 10^5$	415	415
0.50	$1.44 \cdot 10^{14}$	$1.12 \cdot 10^{14}$	$1.87 \cdot 10^5$	$1.86 \cdot 10^5$	413	413
0.75	$1.07 \cdot 10^{14}$	$7.90 \cdot 10^{13}$	$1.85 \cdot 10^5$	$1.84 \cdot 10^5$	412	412
1.00[a]	$7.31 \cdot 10^{13}$	–	$1.83 \cdot 10^5$	–	412	–

[a] From reference [24].

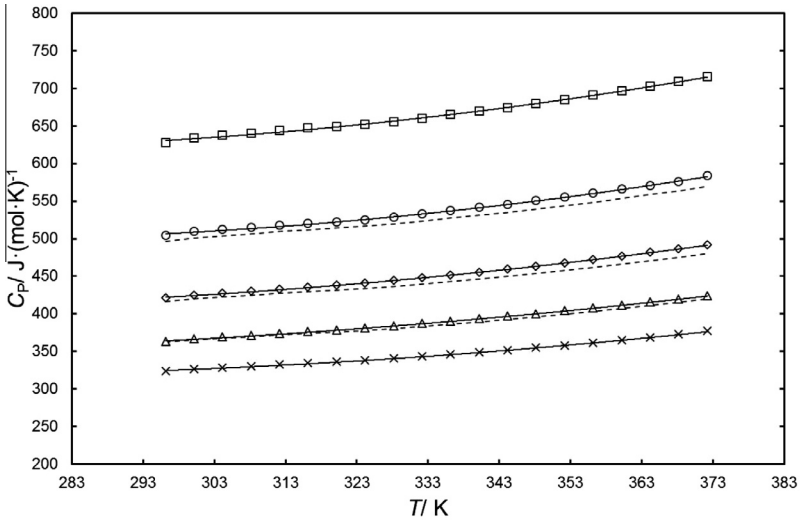

FIGURE 3. Specific heat (C_P) against temperature for binary mixtures of ([emim][DCA] (1) + [4empy][Tf_2N] (2)) as a function of [emim][DCA] mass fraction: □, w_1 = 0.00; ○, w_1 = 0.25; ◇, w_1 = 0.50; Δ, w_1 = 0.75; ×, w_1 = 1.00. Solid lines denote adjustments of experimental data to equation (4) and dashed lines refer to ideal specific heat of mixture. Data for pure [emim][DCA] from reference [24].

TABLE 6
Adjustment parameters of specific heats[a] (C_P) and surface tensions[b] (γ) for ([emim][DCA] (1) + [4empy][Tf_2N] (2)) mixtures as function of temperature.

w_1	a/J · g^{-1} · K^{-1}	b/J · g^{-1} · K^{-2}	c/J · g^{-1} · K^{-3}	R^2	T_{range}/K
		C_P/J · (g · K)$^{-1}$			
0.00	1114	−3.66	7.23 · 10^{-3}	0.998	296.2 to 372.2
0.25	1029	−3.79	7.16 · 10^{-3}	0.998	296.2 to 372.2
0.50	714	−2.36	4.89 · 10^{-3}	0.999	296.2 to 372.2
0.75	629	−2.12	4.33 · 10^{-3}	0.999	296.2 to 372.2
1.00[c]	593	−2.16	4.27 · 10^{-3}	0.999	296.2 to 372.2
		γ/mN · m^{-1}			
	a/mN · m^{-1}	b/mN · m^{-1} · K^{-1}			
0.00	4.97 · 10^{-2}	8.52 · 10^{-5}		0.999	298.2 to 323.2
0.25	7.51 · 10^{-2}	1.15 · 10^{-4}		0.998	298.2 to 323.2
0.50	8.13 · 10^{-2}	1.19 · 10^{-4}		0.999	298.2 to 323.2
0.75	8.81 · 10^{-2}	1.21 · 10^{-4}		0.996	298.2 to 323.2
1.00	9.14 · 10^{-2}	1.17 · 10^{-4}		0.995	298.2 to 323.2

[a] Standard uncertainty calculated to specific heat is u(C_P) = 5 J · (mol · K)$^{-1}$.
[b] Standard uncertainty calculated to surface tension is u(γ) = 0.1 mN · m^{-1}.
[c] From reference [24].

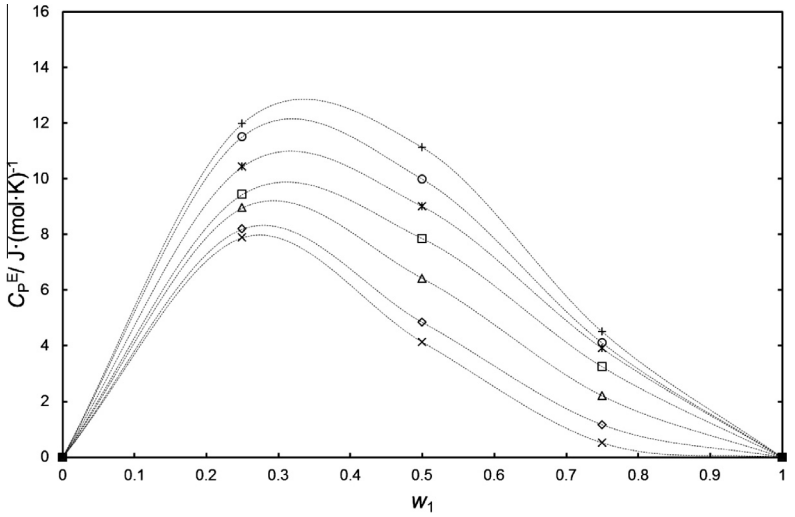

FIGURE 4. Excess specific heat (C_P^E) for binary mixtures of ([emim][DCA] (1) + [4empy][Tf_2N] (2)) as a function of temperature: ×, T = 296.2 K; ◇, T = 308.2 K; Δ, T = 320.2 K; □, T = 332.2 K; ∗, T = 344.2 K; ○, T = 356.2 K; +, T = 368.2 K. Dashed lines correspond to adjustments to Redlich–Kister model showed in equation (6).

et al. and in our previous work [24,26]. MOT values were also shown in table 4. MOT for the ([emim][DCA] + [4empy][Tf_2N]) mixtures are almost the same as MOT estimated for [emim][DCA]. Only a little difference was found in activation energies and frequency factors by adding [4empy][Tf_2N] to [emim][DCA] pure IL.

3.4. Specific heats

The determination of specific heats of all mixtures of ILs involved in this study was done from T = (296.2 to 372.2) K. Results of experimental specific heats were collected in table 5 and graphically showed in figure 3. Specific heats were included here in molar basis because the study of the ideality of a mixture should be done in these units.

A second order model was used to correlate specific heats (C_P) against temperature (T):

$$C_P = a + b \cdot T + c \cdot T^2, \quad (4)$$

Results obtained from the fitting were included in table 6 and also in figure 3 as solid lines. Specific heats for [4empy][Tf_2N] were higher than those of [emim][DCA], being the values of all IL mixtures intermediate between the data of pure ILs proved here. Furthermore, the ideality of specific heats of mixtures of [emim][DCA] and [4empy][Tf_2N] ILs was also evaluated through excess specific heat (C_P^E), which is defined as:

$$C_P^E = C_{P,m} - \sum_{i=1}^{2} C_{P,i} \cdot x_i, \quad (5)$$

where $C_{P,m}$ is the specific heat of the mixture, $C_{P,i}$ denotes the specific heat of the pure IL at the same temperature, and x_i refers to the IL mole fraction in the mixture. Values of excess specific heats were shown graphically in figure 4 and properly correlated using Redlich–Kister polynomial equation model, which could be defined as [39]:

$$Q = x_1 \cdot x_2 \sum_{k=0}^{K} A_k \cdot (2 \cdot x_1 - 1)^k, \quad (6)$$

where Q is the property that is adjusted, x_1 and x_2 are the mole fractions of the ILs involved in the mixture, A_k are the fitting parameters, and k refers to the order of the adjustment. Fitting parameters and standard deviations of the adjustment were including in table 7.

The low values of excess specific heats imply a quite ideal behavior of the specific heat of the IL mixture. The trend observed was that the higher values of excess specific heats were found at the higher temperatures. Another important fact is that the maximum of excess specific heat appears near to [emim][DCA] mass fraction of 0.3 at any temperature, which is the equimolar composition of the IL binary mixture.

TABLE 7
Adjustment parameters of excess specific heats (C_P^E) and surface tension deviations ($\Delta\gamma$) for ([emim][DCA] (1) + [4empy][Tf_2N] (2)) mixtures to Redlich–Kister polynomial model (n = 2).

T	A_0	A_1	A_2	s
		$C_P^E/J \cdot (g \cdot K)^{-1}$		
296.2	30.037	−18.316	−21.692	$2 \cdot 10^{-2}$
300.2	31.475	−17.918	−22.229	$6 \cdot 10^{-2}$
304.2	30.071	−13.079	−17.920	$2 \cdot 10^{-2}$
308.2	31.642	−15.341	−18.305	$2 \cdot 10^{-2}$
312.2	31.674	−6.1116	−25.891	$9 \cdot 10^{-3}$
316.2	32.206	−0.3544	−28.296	$6 \cdot 10^{-3}$
320.2	36.026	−6.4190	−21.179	$1 \cdot 10^{-2}$
324.2	36.009	−2.8808	−19.987	$3 \cdot 10^{-3}$
328.2	38.727	−2.6005	−19.527	$1 \cdot 10^{-2}$
332.2	39.342	2.9849	−23.338	$2 \cdot 10^{-2}$
336.2	40.015	4.2466	−20.552	$1 \cdot 10^{-2}$
340.2	41.937	2.7108	−16.096	$3 \cdot 10^{-2}$
344.2	43.826	5.9848	−24.234	$1 \cdot 10^{-2}$
348.2	45.161	5.9109	−27.333	$4 \cdot 10^{-2}$
352.2	46.701	8.1210	−33.378	$1 \cdot 10^{-2}$
356.2	48.811	8.7949	−33.681	$1 \cdot 10^{-2}$
360.2	50.143	14.047	−45.050	$8 \cdot 10^{-3}$
364.2	50.796	13.936	−46.067	$1 \cdot 10^{-1}$
368.2	52.306	18.516	−46.201	$2 \cdot 10^{-2}$
372.2	57.767	−2.9728	−21.780	$3 \cdot 10^{-7}$
		$\Delta\gamma/mN \cdot m^{-1}$		
298.2	−9.3249	16.540	−12.061	$3 \cdot 10^{-13}$
303.2	−9.5846	14.762	−9.8252	$6 \cdot 10^{-4}$
313.2	−9.8635	15.092	−10.928	$5 \cdot 10^{-3}$
323.2	−10.462	15.582	−11.867	$3 \cdot 10^{-6}$

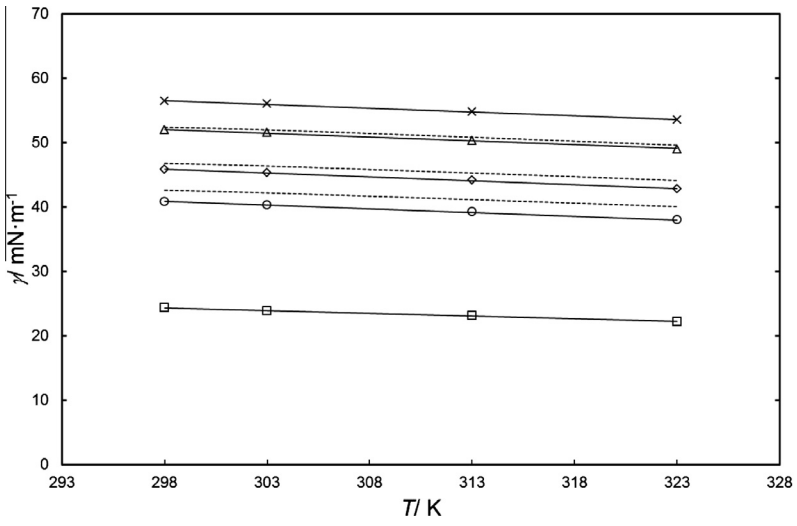

FIGURE 5. Surface tension (γ) against temperature for binary mixtures of ([emim][DCA] (1) + [4empy][Tf_2N] (2)) as a function of [emim][DCA] mass fraction: □, w_1 = 0.00; ○, w_1 = 0.25; ◇, w_1 = 0.50; Δ, w_1 = 0.75; ×, w_1 = 1.00. Straight lines correspond to the adjustments to the linear trend as function of temperature proposed in equation (7) and dashed lines refer to ideal surface tension of mixture.

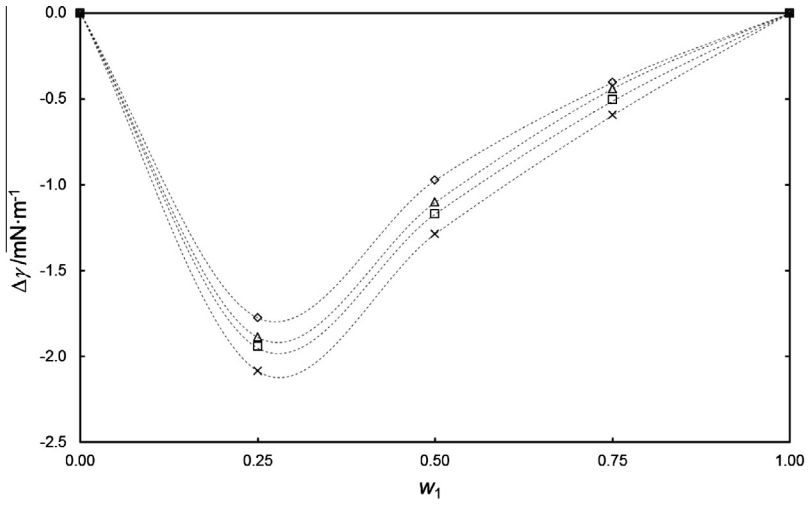

Fig. 6. Surface tension deviations ($\Delta\gamma$) for binary mixtures of ([emim][DCA] (1) + [4empy][Tf_2N] (2)). ◇, T = 298.2 K; Δ, T = 303.2 K; □, T = 313.2 K; ×, T = 323.2 K. Dashed lines correspond to adjustments to Redlich–Kister model described in equation (6).

3.5. Surface tensions

The measurement of surface tensions of all binary mixtures of ILs included in this study was carried out from T = (298.2 to 323.2) K. Results obtained were listed in table 5 and plotted in figure 5. A linear model was proposed in order to correlate surface tension (γ) as function of temperature:

$$\gamma = a + b \cdot T. \tag{7}$$

Fitting parameters and correlation coefficients of the fitting were written in table 6. Results obtained showed that [4empy][Tf_2N] has a substantially lower surface tension than [emim][DCA], whereas binary mixtures of ([emim][DCA] + [4empy][Tf_2N]) have intermediate values of this property.

To study the behavior of the surface tension of ([emim][DCA] + [4empy][Tf_2N]) IL mixtures, deviations of surface tension ($\Delta\gamma$) were calculated as:

$$\Delta\gamma = \gamma_m - \sum_{i=1}^{2} \gamma_i \cdot x_i, \tag{8}$$

where γ_m denotes the experimental surface tension of the mixture and γ_i is the surface tension of the pure IL at the same temperature. Deviations of surface tension were graphically represented in figure 6, and correlated using Redlich–Kister polynomial equation model, which was described in equation (6). Fitting parameters and standard deviations of the adjustment were listed in table 7.

Values of deviation of surface tension for ([emim][DCA] + [4empy][Tf_2N]) binary mixtures imply a low deviation from the ideality of mixture, especially high at the equimolar composition of both ILs, which correspond to the [emim][DCA] mass fraction of 0.3. This result is in agreement with published surface tension data for binary mixtures of ILs [28–30]. It is also remarkable that the higher deviations from ideality were at the higher temperatures.

4. Conclusions

Thermal stability, specific heats, and surface tensions of binary mixtures of [emim][DCA] and [4empy][Tf_2N] have been studied in this work. Moreover, the ideality of the decomposition behavior, specific heats, and surface tensions of ([emim][DCA] + [4empy][Tf_2N]) mixture has also been investigated.

Dynamic TGA analysis has been carried out at (5, 10, and 20) K · min^{-1}. ([emim][DCA] + [4empy][Tf_2N]) binary mixtures followed a decomposition proportionally to the ILs forming the mixture. Hence, the proposed ideal mixing rule has been properly predicted the behavior of mixture as function of the pure IL data. In addition to this, using Seeberger *et al.* prediction model, MOT for all binary mixtures were determined by both experimental and predicted dynamic TGA thermograms. As a result of the identical results obtained in both cases, it is possible to claim that MOT of IL mixtures can be predicted from pure IL dynamic TGA data. This behavior should be evaluated in other systems in order to find a general trend.

Isothermal TGA evaluation was successfully done and predicted values of MOT obtained by using Seeberger *et al.* model were in agreement with those measured experimentally. [emim][DCA] limits the thermal stability of the mixture with [4empy][Tf_2N] because of its less thermal stability. Thus, MOT of binary mixtures of ([emim][DCA] + [4empy][Tf_2N]) are completely dependent on MOT of [emim][DCA], which is T = 412 K. Therefore, ([emim][DCA] + [4empy][Tf_2N]) binary mixture and pure [emim][DCA] IL have shown the same thermal resistance from an industrial point of view.

Specific heats were measured from T = (296.2 to 372.2) K for ([emim][DCA] + [4empy][Tf_2N]) binary mixtures and were adjusted as function of temperature with a second order model. Excess specific heats were calculated and correctly adjusted to Redlich–Kister polynomial model. The low deviation from the ideality has demonstrated a quasi-ideal behavior of the IL mixture for this property, being the maximum deviation found at the equimolar composition of the IL mixture.

Surface tensions were measured from T = (298.2 to 323.2) K for ([emim][DCA] + [4empy][Tf_2N]) mixed ILs and were also adjusted as function of temperature with a linear model. Deviations of surface tension were calculated and properly adjusted to the Redlich–Kister polynomial model. The deviation from the ideality was found to be low and the maximum of surface tension deviation was in the equimolar composition of the IL mixture.

Acknowledgments

Authors are grateful to the Ministerio de Economía y Competitividad of Spain and the Comunidad de Madrid for financial support of Projects CTQ2011-23533 and S2009/PPQ-1545, respectively.

Pablo Navarro also thanks Ministerio de Economía y Competitividad of Spain for awarding him an FPI grant (Reference BES-2012-052312). Marcos Larriba thanks Ministerio de Educación, Cultura y Deporte of Spain for awarding him an FPU grant (Reference AP2010-0318).

References

[1] R.D. Rogers, K.R. Seddon, Science 302 (2003) 792–793.
[2] N.V. Plechkova, K.R. Seddon, Chem. Soc. Rev. 37 (2008) 123–150.
[3] S.T. Anjan, Chem. Eng. Prog. 102 (2006) 30–39.
[4] M. Larriba, P. Navarro, J. García, F. Rodríguez, Sep. Purif. Technol. 120 (2013) 392–401.
[5] S. García, M. Larriba, J. García, J.S. Torrecilla, F. Rodríguez, J. Chem. Thermodyn. 53 (2012) 119–124.
[6] S. García, M. Larriba, J. García, J.S. Torrecilla, F. Rodríguez, Chem. Eng. J. 180 (2012) 210–215.
[7] M. Larriba, P. Navarro, J. García, F. Rodríguez, Ind. Chem. Eng. Res. 52 (2013) 2714–2720.
[8] M. Larriba, P. Navarro, J. García, F. Rodríguez, J. Chem. Thermodyn. 76 (2014) 152–160.
[9] A. Marciniak, M. Krolikowski, J. Chem. Thermodyn. 49 (2012) 154–158.
[10] G.W. Meindersma, A.J.G. Podt, A.B. de Haan, Fuel Process. Technol. 87 (2005) 59–70.
[11] G.W. Meindersma, A.R. Hansmeier, A.B. de Haan, Ind. Eng. Chem. Res. 49 (2010) 7530–7540.
[12] S. Corderí, E.J. González, N. Calvar, A. Domínguez, J. Chem. Thermodyn. 53 (2012) 60–66.
[13] G.W. Meindersma, A.B. de Haan, Sci. China Chem. 55 (2012) 1488–1499.
[14] G.W. Meindersma, A.B. de Haan, Chem. Eng. Res. Des. 86 (2008) 745–752.
[15] F. Farshad, M. Iravaninia, N. Kasiri, T. Mohammadi, J. Ivakpour, Chem. Eng. J. 173 (2011) 11–18.
[16] P. Navarro, M. Larriba, S. García, J. García, F. Rodríguez, J. Chem. Eng. Data 57 (2012) 1165–1174.
[17] M. Larriba, S. García, P. Navarro, J. García, F. Rodríguez, J. Chem. Eng. Data 57 (2012) 1318–1325.
[18] M. Larriba, S. García, P. Navarro, J. García, F. Rodríguez, J. Chem. Eng. Data 58 (2013) 1496–1504.
[19] M. Larriba, S. García, J. García, J.S. Torrecilla, F. Rodríguez, J. Chem. Eng. Data 56 (2011) 3589–3597.
[20] O. Zech, A. Stoppa, R. Buchner, W. Kunz, J. Chem. Eng. Data 55 (2010) 1774–1778.
[21] C.A. Nieto de Castro, E. Langa, A.L. Morais, M.L.S.M. Lopes, M.J.V. Lourenco, F.J.V. Santos, M.S. Santos, J.N.C. Lopes, H.M. Veiga, M. Macatrao, J.M.S.S. Esperanca, C.S. Rebelo, L.P.N. Marques, C.A.M. Afonso, Fluid Phase Equilib. 294 (2010) 157–179.
[22] E.J. Gonzalez, A. Dominguez, E.A. Macedo, J. Chem. Eng. Data 57 (2012) 2165–2176.
[23] M.G. Freire, A.R.R. Teles, M.A.A. Rocha, B. Schroder, C.M.S.S. Neves, P.J. Carvalho, D.V. Evtuguin, L.M.N.B.F. Santos, J.A.P. Coutinho, J. Chem. Eng. Data 56 (2011) 4813–4822.
[24] P. Navarro, M. Larriba, E. Rojo, J. García, F. Rodríguez, J. Chem. Eng. Data 58 (2013) 2187–2193.
[25] A. Fernández, J.S. Torrecilla, J. García, F. Rodríguez, J. Chem. Eng. Data 52 (2007) 1979–1983.
[26] A. Seeberger, A.K. Andresen, A. Jess, Phys. Chem. Chem. Phys. 11 (2009) 9375–9381.
[27] S. Aparicio, M. Atilhan, F. Karadas, Ind. Eng. Chem. Res. 49 (2010) 9580–9595.
[28] M.G. Freire, A.R.R. Teles, R.A.S. Ferreira, L.D. Carlos, J.A. Lopes-da-Silva, J.A.P. Coutinho, Green Chem. 13 (2011) 3173–3180.
[29] M.B. Oliveira, M. Domínguez-Pérez, M.G. Freire, F. Llovell, O. Cabeza, J.A. Lopes-da-Silva, L.F. Vega, J.A. Coutinho, Phys. Chem. B 116 (2012) 12133–12141.
[30] M.B. Oliveira, M. Domínguez-Pérez, O. Cabeza, J.A. Lopes-da-Silva, M.G. Freire, J.A.P. Coutinho, J. Chem. Thermodyn. 64 (2013) 22–27.
[31] E.T. Fox, J.E.F. Weaver, W.A. Henderson, Phys. Chem. C 116 (2012) 5270–5274.
[32] H. Rodríguez, A. Arce, A. Soto, Sci. China Chem. 55 (2012) 1519–1524.
[33] ASTM International, ASTM E 1269–01, Standard Test Method for Determining Specific Heat Capacity by Differential Scanning Calorimetry, 2001.
[34] H.F.D. Almeida, A.R.R. Teles, J.A. Lopes-da-Silva, J.A.P. Coutinho, M.G. Freire, J. Chem. Thermodyn. 54 (2012) 49–54.
[35] J. Klomfar, M. Souckova, J. Patek, J. Chem. Eng. Data 56 (2011) 3454–3462.
[36] E. Quijada, S.v.d. Boogaart, J.H. Lijbers, G.W. Meindersma, A.B.d. Haan, J. Chem. Thermodyn. 51 (2012) 51–58.
[37] A. Casas, M. Oliet, M.V. Alonso, F. Rodríguez, Sep. Purif. Technol. 97 (2012) 115–122.
[38] A. Casas, M.V. Alonso, M. Oliet, T.M. Santos, F. Rodríguez, Carbohydr. Polym. 92 (2013) 1946–1952.
[39] O. Redlich, A.T. Kister, Ing. Eng. Res. 40 (1948) 345–348.

JCT 14–27

Thermochimica Acta 588 (2014) 22–27

Contents lists available at ScienceDirect

Thermochimica Acta

journal homepage: www.elsevier.com/locate/tca

Thermal stability and specific heats of {[emim][DCA] + [emim][TCM]} mixed ionic liquids

Pablo Navarro, Marcos Larriba, Julián García *, Francisco Rodríguez

Department of Chemical Engineering, Complutense University of Madrid, E-28040 Madrid, Spain

ARTICLE INFO

Article history:
Received 31 March 2014
Received in revised form 22 April 2014
Accepted 25 April 2014
Available online 4 May 2014

Keywords:
Mixtures of ionic liquids
Thermal stability
Specific heats
TGA
DSC

ABSTRACT

Ionic liquids (ILs) have been revealed as promising solvents, specifically in the liquid–liquid extraction of aromatics from aliphatics. Nowadays, the use of binary mixtures of ILs is a usual trend looking for improving results achieved by pure ILs. {[emim][DCA] + [emim][TCM]} mixtures have shown good extractive properties. Thus, the goal of this work has been the study of the thermal stability and specific heats of the {[emim][DCA] + [emim][TCM]} IL mixtures. Isothermal TGA analyses were done to experimentally check the long term thermal stability, whereas dynamic TGA analyses were done to compare target parameters for the mixtures and to apply Seeberger et al. prediction method to calculate maximum operation temperatures (MOTs). Moreover, an ideal TGA mixing rule was proposed to describe the decomposition of the mixtures. Specific heats were also measured from 296.2 to 372.2 K and the deviation from ideality of mixture was evaluated.

1. Introduction

Ionic liquids (ILs) are salts at temperatures below 373 K or even at room temperatures [1]. ILs are usually formed by an organic cation and an organic or inorganic anion [1,2]. The potential use of these compounds is completely dependent on its non-volatile character, which is one of its most relevant properties in order to replace volatile organic compounds (COVs) in several industrial processes [2]. Thus, the incorporation of ILs at industrial scale would reduce atmospheric emissions and also operational and investment costs because of the easier separation units associated to these compounds [1,2].

One of the most promising fields in which ILs have been researched is the extraction of aromatics from aromatic/aliphatic mixtures [3–16]. Several works related to this issue have concluded that only a few pure ILs could be competitive in comparison with actual employed sulfolane, in both extractive and physical properties [8,14]. In the recent years, also binary mixtures of ILs, which were proposed in order to improve individual properties achieved with pure ILs, have demonstrated that mixed ILs could be also good alternative solvents [4,5]. However, the thermal stability of ILs and mixed ILs has not been evaluated as far asother properties such as density or viscosity, being also a key value to know [17–26]. The necessity of determining the maximum resistance of mixed ILs against temperature, which is the definition for maximum operation temperature (MOT), has been only involved in several works using pure ILs [27–33]. However, there has been only one study about the thermal behavior of a mixture of ILs, which concerns on the 1-ethyl-3-methyimizadolium dicyanamide ([emim][DCA]) + 1-ethyl-4-methylpyridinium bis(trifluoromethylsulfonyl)imide ([4empy][Tf_2N]) mixed solvent [34].

Because of this, the aim of this work was the study of the thermal behavior of the binary mixture of 1-ethyl-3-methyimizadolium dicyanamide ([emim][DCA]) and 1-ethyl-3-methylimidazolium tricyanomethanide ([emim][TCM]). This mixture has been evaluated as solvent in the extraction of toluene from *n*-heptane/toluene mixtures with promising results [4]. Also, densities and viscosities of this mixture have been measured, showing adequate values for the purpose of using this mixture as an extractive solvent [4]. In the present paper, both dynamic and isothermal TGA were used to determined target dynamic parameters and to experimentally obtain and to predict a value of MOT for [emim][DCA] + [emim][TCM] binary mixtures. Furthermore, to complete this study the determination of specific heats for [emim][DCA] + [emim][TCM] mixed solvent was carried out. Excess specific heats were calculated in order to evaluate the deviation from the ideality of the mixture from the specific heat point of view, which has been hitherto done only for the {[emim][DCA] + [4empy][Tf_2N]} binary mixture [34].

* Corresponding author. Tel.: +34 91 394 51 19; fax: +34 91 394 42 43.
E-mail address: jgarcia@quim.ucm.es (J. García).

http://dx.doi.org/10.1016/j.tca.2014.04.026
0040-6031/

Table 1
Chemicals: specifications and properties. densities (ρ) and dynamic viscosities (η).

Chemical	Source	Purity	Analysis method	ρ, at 298.2 K/g cm^{-3}	η, at 298.2 K/mPa s
[emim][DCA]	Iolitec GmbH	0.98	NMR[a], IC[b]	1.1013[c]	15.1[c]
[emim][TCM]	Iolitec GmbH	0.98	NMR[a], IC[b]	1.0816[c]	15.0[c]
Sapphire	Mettler Toledo	0.9999	Verneuil[d]	3.99	–

[a] Nuclear magnetic resonance.
[b] Ion chromatography.
[c] From Ref. [4].
[d] Purity is assessed by this production method.

2. Experimental

2.1. Chemicals

[emim][DCA] and [emim][TCM] ILs were purchased from Iolitec GmbH, both with purity higher than 0.98 in mass basis, being halides and water content less than 0.02 and 0.002, respectively in mass. ILs were kept in their original vessels into a desiccator filled with silica gel. The handling of ILs was always done inside a glove box under an inert atmosphere of dry nitrogen. Sapphire disc employed in the measurement of specific heats was supplied by Mettler Toledo with 0.9999 of purity in mass. Table 1 shows a brief description of each chemical. It is important to mention that all chemicals were used in this work as received without being purified after purchasing.

2.2. Mixtures of ILs

Mixed ILs were prepared by mass using a Mettler Toledo XS 205 balance, with a precision of 1×10^{-5} g. The uncertainty in the mass fraction of the IL mixtures was estimated to be 5×10^{-5}.

2.3. Thermal stability

Both dynamic and isothermal TGA were carried out into a Mettler Toledo TGA/DSC 1 thermogravimetric analyzer with a temperature precision of ±0.1 K and a mass measurement precision of $\pm 10^{-3}$ mg. A complete description of both methods can be found elsewhere [27,34].

2.4. Specific heats

Specific heats were determined by employing differential scanning calorimetry (DSC) technique, specifically the sapphire method. For this purpose, we followed ASTM E 1269 – 01 [35], whereas the equipment employed was a Mettler Toledo DSC821^e, which follows the disc heat flow principle. A full description of the experimental method was included in our recent works [27,34].

3. Results and discussion

3.1. Dynamic TGA

In this work, {[emim][DCA] + [emim][TCM]} binary mixtures with [emim][DCA] mass fractions of 0.25, 0.50, and 0.75 were measured employing different heating rates, specifically 5, 10, and 20 K min^{-1}. Results obtained were listed in Table 2, including all key parameters calculated, whereas a graphical comparison was also done in Fig. 1 at the most employed heating rate of 10 K min^{-1} [27–30,34–39].

In addition to this, an ideal mixing rule of TGA was evaluated using pondered pure IL data to predict those of the mixtures [34]:

$$m_{\text{mixture}} = \sum_{i=1}^{I} w_i \cdot m_i \quad (1)$$

where m_{mixture} denotes the mass that the mixture would lose in an ideal case at each temperature, m_i refers to the experimental mass lost by each IL forming the mixture at each temperature, w_i is the mass fraction of each IL in the mixture, and I is the number of ILs presented in the mixture. Predicted thermograms were also shown in Fig. 1 for the three compositions evaluated in this work at the cited heating rate of 10 K min^{-1}. The same trend was observed for the other heating rates proved here.

Onset temperatures for the three mixtures evaluated at any heating rate used were near and even below to the less stable IL values. This fact is related to the slope of decomposition, because the start of the decomposition is the same whereas the loss of mass is more quickly for [emim][DCA] than for its binary mixtures with [emim][TCM]. The lower the slope of the decomposition is, the lower the value of the onset temperature is. Therefore, taking into account that onset temperatures were determined as the cross point between the tangent lines before and after the decomposition starts, this slower process of decomposition for the binary mixtures of {[emim][DCA] + [emim][TCM]} implies a lower value of onset temperature calculated. This trend is less pronounced in the IL mixture evaluated here than in {[emim][DCA] + [4empy][Tf$_2$N]} binary

Table 2
Dynamic TGA characteristic parameters obtained for {[emim][DCA] (1) + [emim][TCM] (2)} mixtures.

Parameter	HR[a]	w_1				
		0.00[b]	0.25	0.50	0.75	1.00[b]
T_{onset}/K	5	602.5	555.5	554.1	552.0	557.4
	10	616.0	570.4	569.1	564.7	569.7
	20	631.2	584.7	579.0	575.9	583.0
$T_{10\%}$[c]/K	5	605.6	574.9	560.4	555.1	557.0
	10	618.9	589.6	579.8	574.1	569.6
	20	629.1	606.3	581.2	580.3	582.2
$T_{50\%}$[d]/K	5	700.3	732.6	689.5	655.3	614.6
	10	705.1	736.1	710.8	661.2	638.0
	20	710.4	739.9	713.4	663.6	647.9
$\text{Ashes}_{723\text{ K}}$/%	5	48.2	51.2	47.5	42.3	33.1
	10	48.9	51.6	49.3	43.3	33.5
	20	49.1	51.8	49.5	43.8	33.5
$\text{Ashes}_{1123\text{ K}}$/%	5	26.1	26.6	21.6	20.1	11.9
	10	26.4	26.7	25.2	20.7	13.3
	20	26.4	28.1	25.3	21.4	13.6

[a] Heating rate in K min^{-1}.
[b] Ref. [27].
[c] Temperature that provides a mass lose equal to 10% of the initial mass introduced.
[d] Temperature that provides a mass lose equal to 50% of the initial mass introduced.

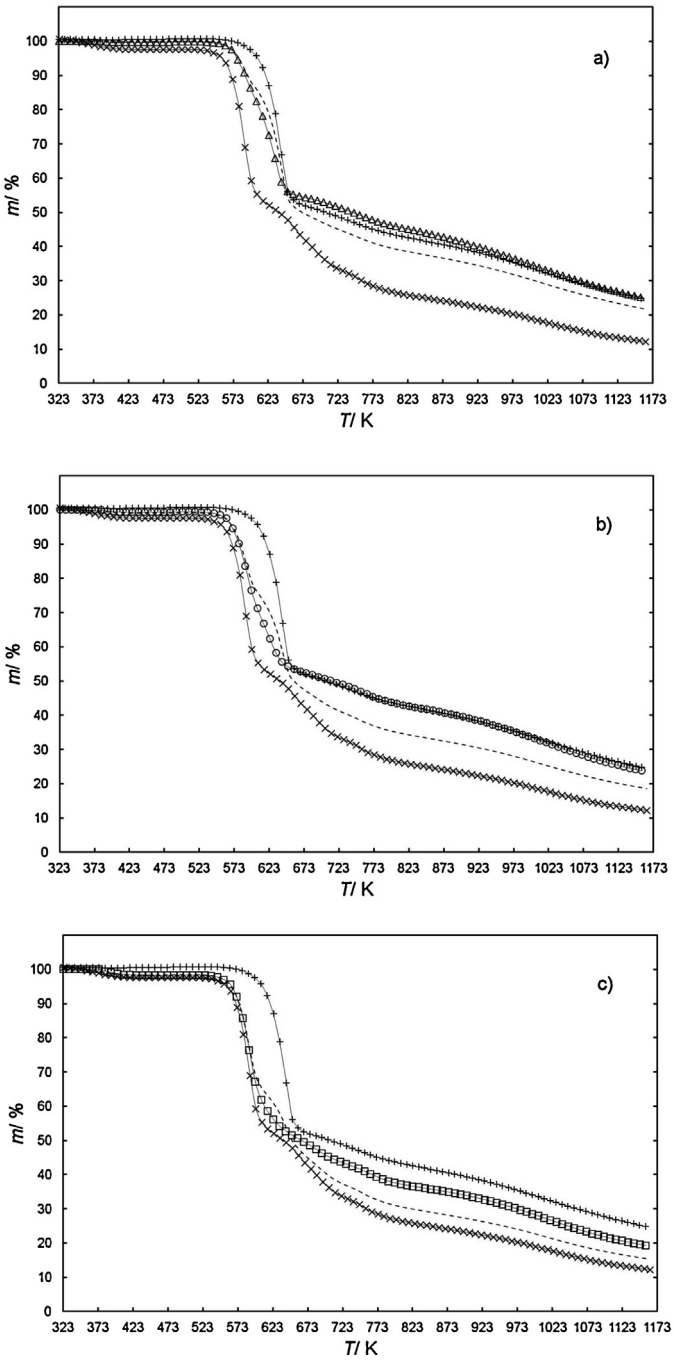

Fig. 1. Dynamic TGA thermograms for binary mixtures of {[emim][DCA] (1) + [emim][TCM] (2)}: (a) $w_1 = 0.25$ (△); (b) $w_1 = 0.50$ (○); (c) $w_1 = 0.75$ (□). Data for pure [emim][DCA] (×) and [emim][TCM] (+) from Ref. [27]. Dashed lines denote the TGA ideal mixing rule from Eq. (1). Heating rate: 10 K min^{-1}.

mixtures, possibly because of the lower stability of [emim][TCM] in comparison with [4empy][Tf_2N] [34].

Temperatures for a loss of mass of the 10% of the initial mass follow an intermediate behavior between both pure ILs forming the mixture, because the first steps of decomposition describe a proportional trend of [emim][DCA] and [emim][TCM]. Thus, this aspect, which can be seen in Fig. 1, confirms that the model proposed in Eq. (1) is a good tool to predict the behavior of the mixture in the initial processes of decomposition.

However, the intermediate behavior showed at low temperatures is not the same at temperatures near to 723 K. At elevated temperatures, determined parameters $T_{50\%}$, ashes at 723 K, and ashes at 1123 K are near or even above those parameters calculated for [emim][TCM] that is the most stable IL in the mixture. This behavior at elevated temperatures could be related to the interaction between decompositions products of both ILs [34]. Thus, it could be useful to fully study the decomposition process of IL mixtures in the future to understand the decomposition mechanism as function of the composition of the mixture.

Table 3
Experimental MOT intervals for {[emim][DCA] (1) + [emim][TCM] (2)} mixtures.

w_1	T_{stable}/K[a]	$T_{unstable}$/K[b]
0.00[c]	433.2	473.2
0.25	393.2	433.2
0.50	393.2	433.2
0.75	393.2	433.2
1.00[c]	393.2	433.2

[a] T_{stable} is the maximum experimental temperature at which the IL or the mixture of ILs are stable in long-terms.
[b] $T_{unstable}$ is the minimum experimental temperature at which the IL or the mixture of ILs are unstable in long-terms.
[c] Ref. [27].

3.2. Isothermal TGA

Isothermal TGA experiments were carried out for all compositions included in this work for binary mixtures of {[emim][DCA] + [4empy][Tf_2N]} at temperatures of 353.2, 393.2, and 433.2 K. Results gathered here were included in Table 3 jointly to literature data for pure ILs forming the mixture, whereas they also were graphically represented together in Fig. 2 [27].

Binary mixtures showed the same decomposition interval for 48 h as [emim][DCA], which was 393.2–433.2 K [27], because of the mixture thermal stability dependence on the less stable substance forming the mixture, specifically [DCA] anion [34].

3.3. Prediction of MOT

The prediction of MOT was done using dynamic data at the lowest heating rate of 5 K min^{-1} and the Seeberger et al. model [29]. The decomposition process of an IL-based substance is assumed to be the only process that occurs in a TGA experiment, because of the negligible vapor pressure of ILs. Hence, the decomposition tax ($-dm/dt$) was described by a first order model, being the constant of decomposition explained by Arrhenius law:

$$-\frac{dm}{dt} = k_0 \cdot \exp\left[-\frac{E_A}{(R \cdot T)}\right] \cdot m \quad (2)$$

where k_0 refers to the frequency factor, E_A is the activation energy, R denotes the ideal gas law constant, T is the temperature in K, and m refers to the mass of the substance. Adjusting experimental dynamic data to Eq. (2), k_0 and E_A were calculated and listed in Table 4 for all binary mixtures proved here. Additionally to this, decomposition parameters were also determined for predicted curves by the ideal mixing rule obtained from Eq. (1), due to the trend seen in the comparison between experimental and predicted thermograms at low temperatures. Also, determined parameters to ideal predicted curves were included in Table 4. Through these decomposition parameters it is possible to calculate MOTs at any desirable long-term:

$$\mathrm{MOT} = \left(\frac{E_A}{R}\right) \cdot [4.6 + \ln(k_0 \cdot t_{max})] \quad (3)$$

where t_{max} is the time at which MOT value was calculated. Time used to this calculus was set in 8000 h (one industrial year). A full explanation of this method was done by Seeberger et al. [29] and in our previous works [27,29,34]. MOT results were listed in Table 4.

Table 4
Frequency factors (k_0) and activations energies (E_A) for {[emim][DCA] (1) + [emim][TCM] (2)} mixtures for adjustments using Eq. (2) and experimental dynamic data or predicted dynamic data using Eq. (1) at 5 K min^{-1} heating rate. MOT calculated from Eq. (3).

w_1	$k_{0,\,exptl}$/s^{-1}	$k_{0,\,pred}$/s^{-1}	$E_{A,\,exptl}$/J mol^{-1}	$E_{A,\,pred}$/J mol^{-1}	$MOT_{exptl,\,8000\,h}$/K	$MOT_{pred,\,8000\,h}$/K
0.00[a]	1.86×10^{14}	–	2.05×10^{5}	–	452	–
0.25	8.73×10^{13}	8.47×10^{13}	1.86×10^{5}	1.85×10^{5}	414	414
0.50	8.55×10^{13}	8.14×10^{13}	1.85×10^{5}	1.84×10^{5}	413	412
0.75	7.90×10^{13}	6.21×10^{13}	1.84×10^{5}	1.83×10^{5}	412	412
1.00[a]	7.31×10^{13}	–	1.83×10^{5}	–	412	–

[a] Ref. [27].

As was cited above, the closely dependence on the less stable IL for binary mixtures of ILs is also true in the analysis of MOT. Values for all mixed ILs evaluated here showed almost the same MOT value as pure [emim][DCA], which is the less stable IL forming the mixture. The activation energies for all binary mixtures of {[emim][DCA] + [emim][TCM]} are also closely near to the activation energy determined for pure [emim][DCA], and consequently the frequency factors are also of the same order of that corresponding to pure [emim][DCA]. The proximity of both decompositions parameters means that [emim][DCA] decomposes in the first step, being slightly influenced by the other IL presented in the mixture. The main conclusion obtained from the analysis of the binary mixtures of {[emim][DCA] + [emim][TCM]} and just published {[emim][DCA] + [4empy][Tf$_2$N]} is that the thermal stability for a mixture of ILs could be considered as the same as the less stable IL for long-terms, the [emim][DCA] in both cases studied [34].

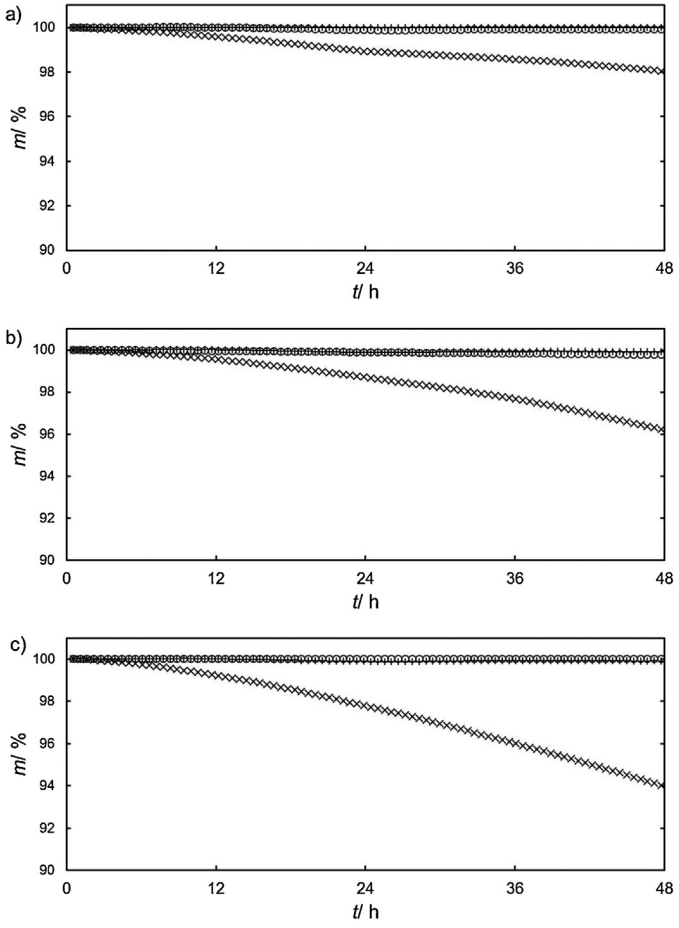

Fig. 2. Isothermal TGA data for binary mixtures of {[emim][DCA] (1) + [emim][TCM] (2)}. +, T = 353.2 K; ◯, T = 393.2 K; ×, T = 433.2 K. (a) w_1 = 0.25; (b) w_1 = 0.50; (c) w_1 = 0.75.

However, more experimental data would be needed to confirm this behavior.

On the other hand, calculation done for MOT from predicted dynamic TGA data using Eq. (1) showed almost the same results by using experimental or predicted dynamic TGA thermograms. This trend was also observed in our previous work involving {[emim][DCA] + [4empy][Tf$_2$N]} [34].

3.4. Specific heats

The measurement of specific heats for {[emim][DCA] + [emim][TCM]} binary mixtures was done from 296.2 to 372.2 K. Thus, values of experimental specific heats were listed in Table 5 and graphically showed in Fig. 3. Also specific heats (C_P) were correlated against temperature (T) by a second order model:

$$C_P = a + b \cdot T + c \cdot T^2 \quad (4)$$

Parameters obtained from the adjustment were collected in Table 6 and the correlation was represented in Fig. 3 as solid lines. In addition to this, excess specific heats of {[emim][DCA] + [4empy][Tf$_2$N]} mixtures were calculated to evaluate the deviation from ideality of mixture as:

$$C_P^E = C_{P,m} - \sum_{i=1}^{2} C_{P,i} \cdot x_i \quad (5)$$

where $C_{P,m}$ denotes the specific heat of the mixture, $C_{P,i}$ is the specific heat of the pure ILs forming the mixture, and x_i refers to the IL mole fraction in the mixture. Values of excess specific heats were

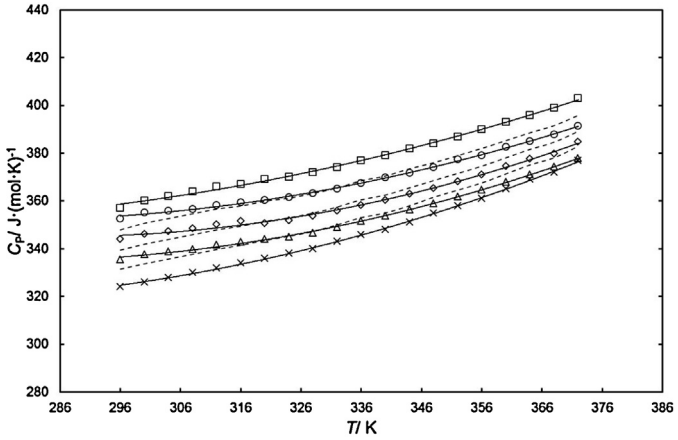

Fig. 3. Specific heat (C_P) against temperature for binary mixtures of {[emim][DCA] (1) + [emim][TCM] (2)} as a function of [emim][DCA] mass fraction: □, w_1 = 0.00; ◯, w_1 = 0.25; ◇, w_1 = 0.50; △, w_1 = 0.75; ×, w_1 = 1.00. Solid lines denote adjustments of experimental data to Eq. (4) and dashed lines refer to ideal specific heat of mixture. Data for pure [emim][DCA] and [emim][TCM] from Ref. [27].

Table 5
Specific heats[a] (C_P) and excess specific heats (C_P^E) for {[emim][DCA] (1) + [emim][TCM] (2)} mixtures.

T/K	$w_1 = 0.00$[b]	$w_1 = 0.25$	$w_1 = 0.50$	$w_1 = 0.75$	$w_1 = 1.00$[b]
	C_P/J mol^{-1} K^{-1}				
296.2	357	354	344	335	324
300.2	360	355	346	338	326
304.2	362	356	347	339	328
308.2	364	357	348	340	330
312.2	366	358	350	342	332
316.2	367	359	352	343	334
320.2	369	360	352	344	336
324.2	370	361	354	345	338
328.2	372	363	356	347	340
332.2	374	365	358	349	343
336.2	377	367	360	352	346
340.2	379	370	362	354	348
344.2	382	372	365	356	351
348.2	384	374	367	359	355
352.2	387	377	370	362	358
356.2	390	381	373	365	361
360.2	393	383	376	368	365
364.2	396	385	380	371	369
368.2	399	388	383	374	372
372.2	403	391	387	378	377
	C_P^E/J mol^{-1} K^{-1}				
296.2	–	4	5	5	–
300.2	–	4	4	5	–
304.2	–	3	3	3	–
308.2	–	2	2	2	–
312.2	–	2	2	2	–
316.2	–	1	2	1	–
320.2	–	1	−1	0	–
324.2	–	0	−1	0	–
328.2	–	−1	−1	0	–
332.2	–	−1	−2	0	–
336.2	–	−2	−2	−1	–
340.2	–	−1	−2	−1	–
344.2	–	−2	−3	−2	–
348.2	–	−3	−3	−2	–
352.2	–	−3	−3	−2	–
356.2	–	−3	−4	−3	–
360.2	–	−3	−4	−3	–
364.2	–	−4	−4	−3	–
368.2	–	−4	−5	−4	–
372.2	–	−5	−5	−5	–

[a] Standard uncertainty calculated to specific heat is $u(C_P) = 5$ J mol^{-1} K^{-1}.
[b] Ref. [27].

Table 6
Adjustment parameters of specific heats for {[emim][DCA] (1) + [emim][TCM] (2)} mixtures as function of temperature with Eq. (4).

w_1	a/J mol^{-1} K^{-1}	b/J mol^{-1} K^{-2}	c/J mol^{-1} K^{-3}	R^2	T_{range}/K
0.00[a]	548	−1.61	3.26×10^{-3}	0.998	296.2–372.2
0.25	694	−2.46	4.41×10^{-3}	0.999	296.2–372.2
0.50	707	−2.62	4.73×10^{-3}	0.999	296.2–372.2
0.75	689	−2.57	4.66×10^{-3}	0.999	296.2–372.2
1.00[a]	593	−2.16	4.27×10^{-3}	0.999	296.2–372.2

[a] Ref. [27].

shown in Fig. 4 and adjusted to Redlich Kister polynomial expansion model, which can be expressed as [40]:

$$Q = x_1 \cdot x_2 \sum_{k=0}^{K} A_k \cdot (2 \cdot x_1 - 1)^k \quad (6)$$

where Q is the adjusted property, x_1 and x_2 refer to the mole fractions of the ILs involved in the mixture, A_k denotes the fitting parameters, and k refers to the order of the adjustment. Fitting parameters and standard deviations of the fit were listed in Table 7.

Results of specific heats of {[emim][DCA] + [emim][TCM]} binary mixtures are intermediate between both pure ILs forming the mixture. Moreover, the low values of excess specific heats denote an almost ideal behavior of this property for the binary mixtures of [emim][DCA] and [emim][TCM]. Other important fact is that the maximum deviation from the ideality was found near to the equimolar composition. This behavior of mixture has just observed in our previous study [34].

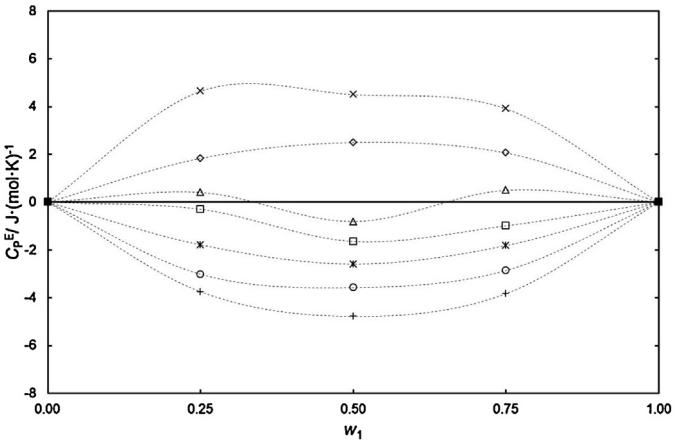

Fig. 4. Excess specific heat (C_P^E) for binary mixtures of {[emim][DCA] (1) + [emim][TCM] (2)} as a function of temperature: ×, $T = 296.2$ K; ◊, $T = 308.2$ K; △, $T = 320.2$ K; □, $T = 332.2$ K; ∗, $T = 344.2$ K; ○, $T = 356.2$ K; +, $T = 368.2$ K. Dashed lines correspond to adjustments to Redlich–Kister model showed in Eq. (6).

Table 7
Adjustment parameters of excess specific heats for {[emim][DCA] (1) + [emim][TCM] (2)} mixtures to the Redlich–Kister polynomial model ($n = 2$) from Eq. (6).

T	A_0	A_1	A_2	s
296.2	18.185	−2.8516	18.963	6×10^{-5}
300.2	16.828	−3.0675	22.680	3×10^{-6}
304.2	13.870	0.5858	10.706	9×10^{-7}
308.2	9.8756	2.3488	1.9752	1×10^{-6}
312.2	9.0190	2.8839	−0.0790	9×10^{-7}
316.2	8.3281	1.0776	−2.6694	2×10^{-3}
320.2	−3.2440	−1.3950	23.011	8×10^{-7}
324.2	−4.2461	−4.7244	17.372	4×10^{-7}
328.2	−4.7903	−4.1520	13.001	1×10^{-3}
332.2	−6.2940	−5.3029	11.972	3×10^{-7}
336.2	−9.1926	−4.4055	10.135	5×10^{-6}
340.2	−8.1926	−4.3979	11.812	1×10^{-6}
344.2	−10.307	−1.6756	2.9616	2×10^{-7}
348.2	−12.569	−6.5677	1.3016	3×10^{-5}
352.2	−13.224	−8.3281	5.7418	6×10^{-7}
356.2	−14.295	−0.6203	−5.4992	6×10^{-7}
360.2	−14.197	−5.5052	−8.5992	3×10^{-4}
364.2	−15.840	−4.0690	−17.394	5×10^{-7}
368.2	−19.014	−2.5659	−4.6815	4×10^{-7}
372.2	−17.504	−2.5734	−32.765	1×10^{-6}

4. Conclusions

Thermal stability and specific heats of binary mixtures of [emim][DCA] and [emim][TCM] have been studied in this work. Moreover, the deviation from ideality of the {[emim][DCA] + [emim][TCM]} mixture was also investigated from both decomposition and specific heats points of view.

Dynamic TGA evaluation has been done at 5, 10, and 20 K min^{-1} and has shown that {[emim][DCA] + [emim][TCM]} binary mixtures follow a decomposition almost proportionally to the pure ILs involved in the mixture at low temperatures. Therefore, the ideal mixing rule of TGA has correctly predicted this behavior. Furthermore, the employment of Seeberger et al. prediction model to calculate MOT for all mixture proved here was carried out by using both experimental and predicted dynamic TGA

data. As a result of the almost identical values achieved in both cases, it could be claimed that it is possible to determine MOT of mixtures by knowing only pure dynamic TGA data forming the mixture. This behavior should be evaluated in other systems in order to find a general conclusion, but was also observed for the {[emim][DCA] + [4empy][Tf_2N]} IL binary mixture.

Isothermal TGA analysis was successfully carried out and predicted values of MOT by employing Seeberger et al. model were in agreement with the stability interval checked experimentally. {[emim][DCA] + [emim][TCM]} binary mixtures and pure [emim][DCA] IL have shown the same thermal stability from an industrial point of view. This trend is also in agreement with that previously observed for {[emim][DCA] + [4empy][Tf_2N]}.

Specific heats were determined from 296.2 to 372.2 K for all binary mixtures of {[emim][DCA] + [emim][TCM]} and were correctly fitted as function of temperature with a second order model. Excess specific heats have shown a quasi-ideal behavior of mixture from the specific heat point of view, whereas the maximum of deviation was found at the equimolar composition, as in the just cited case of {[emim][DCA] + [4empy][Tf_2N]}.

Funding sources

Authors are grateful to the Ministerio de Economía y Competitividad of Spain and the Comunidad de Madrid for financial support of Projects CTQ2011-23533 and S2009/PPQ-1545, respectively. Pablo Navarro also thanks Ministerio de Economía y Competitividad of Spain for awarding him an FPI grant (Reference BES-2012-052312). Marcos Larriba thanks Ministerio de Educación, Cultura y Deporte of Spain for awarding him an FPU grant (Reference AP2010-0318).

References

[1] R.D. Rogers, K.R. Seddon, Ionic liquids–solvents of the future? Science 302 (2003) 792–793.
[2] N.V. Plechkova, K.R. Seddon, Applications of ionic liquids in the chemical industry, Chem. Soc. Rev. 37 (2008) 123–150.
[3] S.T. Anjan, Ionic liquid for aromatic extraction: are they ready? Chem. Eng. Progr. 102 (2006) 30–39.
[4] M. Larriba, P. Navarro, J. García, F. Rodríguez, Liquid–liquid extraction of toluene from *n*-heptane by {[emim][TCM] + [emim][DCA]} binary ionic liquid mixtures, Fluid Phase Equilib. 364 (2014) 48–54.
[5] M. Larriba, P. Navarro, J. García, F. Rodríguez, Separation of toluene from *n*-heptane, 2,3-dimethylpentane, and cyclohexane using binary mixtures of [4empy][Tf_2N] and [emim][DCA] ionic liquids as extraction solvents, Sep. Purif. Technol. 120 (2013) 392–401.
[6] S. García, M. Larriba, J. García, J.S. Torrecilla, F. Rodríguez, Separation of toluene from *n*-heptane by liquid–liquid extraction using binary mixtures of [bpy][BF_4] and [4bmpy][Tf_2N] ionic liquids as solvent, J. Chem. Thermodyn. 53 (2012) 119–124.
[7] S. García, M. Larriba, J. García, J.S. Torrecilla, F. Rodríguez, Liquid–liquid extraction of toluene from *n*-heptane using binary mixtures of N-butylpyridium tetrafluoroborate and N-butylpyridinium bis(trifluoromethylsulfonyl)imide ionic liquids, Chem. Eng. J. 180 (2012) 210–215.
[8] M. Larriba, P. Navarro, J. García, F. Rodríguez, Liquid–liquid extraction of toluene from heptane using [emim][DCA], [bmim][DCA], and [emim][TCM] ionic liquids, Ind. Chem. Eng. Res. 52 (2013) 2714–2720.
[9] M. Larriba, P. Navarro, J. García, F. Rodríguez, Selective extraction of toluene from *n*-heptane using [emim][SCN] and [bmim][SCN] ionic liquids as solvents, J. Chem. Thermodyn. (2013), http://dx.doi.org/10.1016/j.jct.2013.11.005.
[10] A. Marciniak, M. Krolikowski, Ternary (liquid + liquid) equilibria of {trifluorotris(perfluoroethyl)phosphate based ionic liquids + thiophene + heptane}, J. Chem. Thermodyn. 49 (2012) 154–158.
[11] G.W. Meindersma, A.J.G. Podt, A.B. de Haan, Selection of ionic liquids for the extraction of aromatic hydrocarbons from aromatic/aliphatic mixtures, Fuel Process. Technol. 87 (2005) 59–70.
[12] G.W. Meindersma, A.R. Hansmeier, A.B. de Haan, Ionic liquids for aromatics extraction. Present status and future outlook, Ind. Eng. Chem. Res. 49 (2010) 7530–7540.
[13] S. Corderi, E.J. González, N. Calvar, A. Domínguez, Application of [HMim][NTf2], [HMim][TfO] and [BMim][TfO] ionic liquids on the extraction of toluene from alkanes: effect of the anion and the alkyl chain length of the cation on the LLE, J. Chem. Thermodyn. 53 (2012) 60–66.
[14] G.W. Meindersma, A.B. de Haan, Cyano-containing ionic liquids for the extraction of aromatic hydrocarbons from an aromatic/aliphatic mixture, Sci. Chin. Chem. 55 (2012) 1488–1499.
[15] G.W. Meindersma, A.B. de Haan, Conceptual process design for aromatic/aliphatic separation with ionic liquids, Chem. Eng. Res. Des. 86 (2008) 745–752.
[16] F. Farshad, M. Iravaninia, N. Kasiri, T. Mohammadi, J. Ivakpour, Separation of toluene/*n*-heptane mixtures experimental, modeling and optimization, Chem. Eng. J. 173 (2011) 11–18.
[17] P. Navarro, M. Larriba, S. García, J. García, F. Rodríguez, Physical properties of binary and ternary mixtures of 2-propanol, water, and 1-butyl-3-methylimidazolium tetrafluoroborate ionic liquid, J. Chem. Eng. Data 57 (2012) 1165–1174.
[18] M. Larriba, S. García, P. Navarro, J. García, F. Rodríguez, Physical properties of N-butylpyridinium tetrafluoroborate and N-butylpyridinium bis(trifluoromethylsulfonyl)imide binary ionic liquid mixtures, J. Chem. Eng. Data 57 (2012) 1318–1325.
[19] M. Larriba, S. García, P. Navarro, J. García, F. Rodríguez, Physical characterization of an aromatic extraction solvent formed by [bpy][BF_4] and [4bmpy][Tf_2N] mixed ionic liquids, J. Chem. Eng. Data 58 (2013) 1496–1504.
[20] M. Larriba, S. García, J. García, J.S. Torrecilla, F. Rodríguez, Thermophysical properties of 1-ethyl-3-methylimidazolium 1,1,2,2-tetrafluoroethanesulfonate and 1-ethyl-3-methylimidazolium ethylsulfate ionic liquids as a function of temperature, J. Chem. Eng. Data 56 (2011) 3589–3597.
[21] O. Zech, A. Stoppa, R. Buchner, W. Kunz, The conductivity of imidazolium-based ionic liquids from (248–468) K. B. Variation of the anion, J. Chem. Eng. Data 55 (2010) 1774–1778.
[22] C.A. Nieto de Castro, E. Langa, A.L. Morais, M.L.S.M. Lopes, M.J.V. Lourenco, F.J.V. Santos, M.S. Santos, J.N.C. Lopes, H.M. Veiga, M. Macatrao, J.M.S.S. Esperanca, C.S. Rebelo, L.P.N. Marques, C.A.M. Afonso, Studies on the density, heat capacity, surface tension and infinite dilution diffusion with the ionic liquids [C_4mim][NTf_2], [C_4mim][dca], [C_2mim][$EtOSO_3$] and [Aliquat][dca], Fluid Phase Equilib. 294 (2010) 157–179.
[23] E.J. González, A. Domínguez, E.A. Macedo, Physical and excess properties of eight binary mixtures containing water and ionic liquids, J. Chem. Eng. Data 57 (2012) 2165–2176.
[24] M.G. Freire, A.R.R. Teles, M.A.A. Rocha, B. Schroder, C.M.S.S. Neves, P.J. Carvalho, D.V. Evtuguin, L.M.N.B.F. Santos, J.A.P. Coutinho, Thermophysical characterization of ionic liquids able to dissolve biomass, J. Chem. Eng. Data 56 (2011) 4813–4822.
[25] M. García-Mardones, P. Cea, M.C. López, C. Lafuente, Refractive properties of binary mixtures containing pyridinium-based ionic liquids and alkanols, Thermochim. Acta 572 (2013) 39–44.
[26] M. Królikowska, T. Hofman, Densities, isobaric expansivities and isothermal compressibilities of the thiocyanate-based ionic liquids at temperatures (298.15–338.15 K) and pressures up to 10 MPa, Thermochim. Acta 530 (2012) 1–3.
[27] P. Navarro, M. Larriba, E. Rojo, J. García, F. Rodríguez, Thermal properties of cyano-based ionic liquids, J. Chem. Eng. Data 58 (2013) 2187–2193.
[28] A. Fernández, J.S. Torrecilla, J. García, F. Rodríguez, Thermophysical properties of 1-ethyl-3-methylimidazolium ethylsulfate and 1-butyl-3-methylimidazolium methylsulfate ionic liquids, J. Chem. Eng. Data 52 (2007) 1979–1983.
[29] A. Seeberger, A.K. Andresen, A. Jess, Prediction of long-term stability of ionic liquids at elevated temperatures by means of non-isothermal thermogravimetrical analysis, Phys. Chem. Chem. Phys. 11 (2009) 9375–9381.
[30] S. Aparicio, M. Atilhan, F. Karadas, Thermophysical properties of pure ionic liquids: review of present situation, Ind. Eng. Chem. Res. 49 (2010) 9580–9595.
[31] R.E. Del Sesto, T.M. McCleskey, C. Macomber, K.C. Ott, A.T. Koppisch, G.A. Baker, A.K. Burrell, Limited thermal stability of imidazolium and pyrrolidinium ionic liquids, Thermochim. Acta 491 (2009) 118–120.
[32] A. Efimova, G. Hubrig, P. Schmidt, Thermal stability and crystallization behavior of imidazolium halide ionic liquids, Thermochim. Acta 573 (2013) 162–169.
[33] N. Calvar, E. Gómez, E.A. Macedo, A. Domínguez, Thermal analysis and heat capacities of pyridinium and imidazolium ionic liquids, Thermochim. Acta 565 (2013) 178–182.
[34] P. Navarro, M. Larriba, J. García, F. Rodríguez, Thermal stability, specific heats, and surface tensions of ([emim][DCA] + [4empy][Tf_2N]) ionic liquid mixtures, J. Chem. Thermodyn. (2014), http://dx.doi.org/10.1016/j.jct.2014.03.023.
[35] ASTM International, ASTM E 1269-01. Standard Test Method for Determining Specific Heat Capacity by Differential Scanning Calorimetry, 2001.
[36] Y. Zhang, X. Sheng, F. Huang, Thermal stability and degradation products analysis of benzocyclobutene-terminated imide polymers, Thermochim. Acta 430 (2005) 15–22.
[37] A. Casas, M. Oliet, M.V. Alonso, F. Rodríguez, Dissolution of *Pinus radiata* and *Eucalyptus globulus* woods in ionic liquids under microwave radiation: lignin regeneration and characterization, Sep. Purif. Technol. 97 (2012) 115–122.
[38] A. Casas, M.V. Alonso, M. Oliet, T.M. Santos, F. Rodríguez, Characterization of cellulose regenerated from solutions of pine and eucalyptus woods in 1-allyl-3-methilimidazolium chloride, Carbohydr. Polym. 92 (2013) 1946–1952.
[39] S.M. Lomakin, S.Z. Rogovina, A.V. Grachev, E.V. Prut, Ch.V. Alexanyan, Thermal degradation of biodegradable blends of polyethylene with cellulose and ethylcellulose, Thermochim. Acta 521 (2011) 66–73.
[40] O. Redlich, A.T. Kister, Thermodynamics of nonelectrolyte solutions, Ind. Eng. Chem. 40 (1948) 345–348.

Fluid Phase Equilibria 387 (2015) 209–216

Contents lists available at ScienceDirect

Fluid Phase Equilibria

journal homepage: www.elsevier.com/locate/fluid

Vapor–liquid equilibria of {*n*-heptane + toluene + [emim][DCA]} system by headspace gas chromatography

Pablo Navarro, Marcos Larriba, Julián García *, Emilio J. González, Francisco Rodríguez

Department of Chemical Engineering, Complutense University of Madrid, Madrid E-28040, Spain

ARTICLE INFO

Article history:
Received 24 October 2014
Received in revised form 9 December 2014
Accepted 15 December 2014
Available online 19 December 2014

Keywords:
Ionic liquids
Aromatic/aliphatic separation
VLE
HS-GC

ABSTRACT

The potential use of ionic liquids (ILs) in the extraction of aromatics from aromatic/aliphatic mixtures has been widely evaluated in the last decade. In addition to the good results obtained in the extraction step, the non-volatile character of ILs could simplify the aromatic recovery unit. However, the scarce vapor–liquid equilibria (VLE) data for {aliphatic + aromatic + IL} systems demand additional experimental VLE data for such systems to correctly define the aromatic recovery from the extract stream. Only then, it will be possible to assess as a whole if the application of ILs as replacement to conventional organic solvents could represent a real improvement of the present aromatic extraction industrial methods. Thus, the aim of this work has been to measure the VLE for the {*n*-heptane + toluene + 1-ethyl-3-methylimidazolium dicyanamide ([emim][DCA])} system. This mixture includes one of the most promising IL-based solvents reported previously for aromatic extraction. Static headspace gas chromatography (HS-GC) was employed to measure isothermal VLE at 323.2 K, 343.2 K, and 363.2 K over the whole range of compositions within the rich-IL miscibility region. Also, the correlation of the VLE data to non-random two liquids (NRTL) thermodynamic model was successfully done. A high increase in the *n*-heptane relative volatility from toluene was achieved under the presence of [emim][DCA].

1. Introduction

Ionic liquids (ILs) are liquid salts at temperatures lower than 373.2 K or even at room temperature. ILs are conformed by an organic cation and an organic or inorganic anion. The main property associated to ILs, in addition to be liquids at low temperatures, is their almost negligible vapor pressure [1,2].

Among other applications related to the use of ILs, the effort in the research of aromatic extraction processes is quite relevant. A high number of works deals with the extraction of aromatics from aliphatics, in order to find out an IL that could be considered as a good candidate to replace conventional solvents used nowadays, such as sulfolane [3–17]. In addition to the extractive properties, physical and thermal properties have been also taken into consideration for evaluating IL-based solvents [18–24]. Density completely sets the hydrodynamic behavior in the extractor, and viscosity is associated to mixing and pumping costs, whereas thermal stability and specific heats determine maximum operation temperatures (MOTs) and heating costs in the whole process, respectively. However, only a low number of vapor–liquid equilibria (VLE) works has been done in order to experimentally evaluate the recovery of the extracted hydrocarbons from extract streams that are composed by {aliphatics + aromatics + ILs} mixtures and the regeneration of the IL [25–27]. Therefore, the aim of the present work was the measurement of the VLE of the {*n*-heptane + toluene + 1-ethyl-3-methylimidazolium dicyanamide ([emim][DCA])} system in order to determine its thermodynamic behavior. Both hydrocarbons have been the most proved in the works dealing with LLE determinations, whereas [emim][DCA] is a pure IL with high extractive properties, specifically its aromatic/aliphatic selectivity [3,9].

VLE of all binary and ternary mixtures involving these three compounds were determined in this work. Isothermal VLE measurements were carried out using a static headspace gas chromatography (HS-GC) technique. Temperatures were set at 323.2 K, 343.2 K, and 363.2 K due to these values are intermediate between the MOT of [emim][DCA] (412 K) [18] and the common equilibrium temperature used in the liquid–liquid extraction employing ILs (313.2 K) [9]. Feed compositions prepared in this work for the ternary mixture were limited by the miscibility region in the LLE of the {*n*-heptane + toluene + [emim][DCA]} system [3].

Results revealed [emim][DCA] as a high mass agent in the separation of *n*-heptane from toluene, fact that means the possibility of easily separating aromatics and aliphatics. In addition

* Corresponding author. Tel.: +34 91 394 51 19; fax: +34 91 394 42 43.
E-mail address: jgarcia@quim.ucm.es (J. García).

http://dx.doi.org/10.1016/j.fluid.2014.12.025
0378-3812/

Table 1
Specifications of chemicals.

Chemical	Source	Purity	Analysis method
[emim][DCA]	Iolitec GmbH	0.98	NMR[a], IC[b]
n-Heptane	Sigma–Aldrich	0.997	GC[c]
Toluene	Sigma–Aldrich	0.995	GC[c]

[a] Nuclear magnetic resonance.
[b] Ion chromatography.
[c] Gas chromatography.

to this, VLE data were successfully correlated to non-random two liquids (NRTL) thermodynamic model, which has been revealed as a good model for similar systems that those included here containing ILs [25,26,28].

2. Experimental

2.1. Chemicals

[emim][DCA] was purchased from Iolitec GmbH. Its purity was higher than 0.98, being halides and water content in mass fraction below than 0.02 and 0.002, respectively. Both storage and handling of [emim][DCA] were done in order to prevent water absorption. The IL was kept inside a desiccator and handled into a glove box filled with dry nitrogen. Toluene and *n*-heptane were acquired from Sigma–Aldrich with mass fraction purities of 0.995 and 0.997, respectively. To keep their identity, both hydrocarbons were preserved in their original vessels over molecular sieves. Specifications of all chemicals, which were employed in this work without further purification, are shown in Table 1.

2.2. Apparatus and procedure

VLE can be measured by isothermal and isobaric methods, both in static or dynamic conditions. In general, the most commonly employed method for VLE determinations is the dynamic isobaric method [28–31], but in the present work we have used a static isothermal method since the IL viscosity and the only partial miscibility of hydrocarbons in ILs affect negatively the mixing process in a dynamic isobaric apparatus. In addition to the advantage just commented, the method used in this work considerably reduces the consumption of chemicals.

The equipment employed to measure VLE was a gas chromatographer (GC) equipped with a headspace injector (HS). Specifically, VLE determinations were carried out using an Agilent HS 7697A injector coupled to an Agilent GC 7890A. The GC is equipped with a flame ionization detector (FID) and a HP-5 Agilent column, whereas the HS injector uses a loop system to extract the vapor sample. A detailed description of additional parameters of the GC is summarized in Table 2.

Binary and ternary mixtures involving the two hydrocarbons and [emim][DCA] were prepared by mass, using a Mettler Toledo XS 205 balance with a precision of $\pm 10^{-5}$ g. First the IL and then the hydrocarbons were added into 20.0 mL vials. In the case of ternary mixtures, it is important to underline that the *n*-heptane + toluene mixtures were separately mixed before they were added to the IL in order to minimize uncertainties. Once the vial was sealed, the mixture was vigorously mixed using a Labnet Vortex Mixer and then inserted in the thermostated oven of the HS sampler at the equilibrium temperature for an enough time of 2 h. The oven agitation was selected to 100 rpm, due to the negligible influence that a higher value implies in the sensitivity of the method. After phase equilibrium was reached, a sample from the vapor phase was taken by the sampling device of the HS injector and analyzed by GC.

Since the vapor pressure of an IL is negligible, in the vapor phase only a peak area is obtained for the binary {hydrocarbon + IL} mixtures. Hence, the partial pressure (P_i) of the hydrocarbon dissolved in the IL can be determined as follows [32]:

$$P_i = \frac{P_i^0 \times A_i}{A_i^0} \quad (1)$$

where A_i represents the peak area of the hydrocarbon i measured from the {hydrocarbon + IL} mixture, A_i^0 is the peak area of the hydrocarbon i when the hydrocarbon alone is maintained at the measurement temperature, and P_i^0 denotes the saturated vapor pressure of the hydrocarbons taken from the literature [33].

Table 2
Key parameters for Agilent GC 7890A.

Agilent GC 7890A	
Inlet	523.2 K, 100:1 split
Detector	573.2 K, FID
Carrier gas	He 3X, supplied by Praxair
Column	Agilent HP-5, 30 m × 0.32 mm × 0.25 μm
Oven	348.2 K

Table 3
VLE[a] data for {*n*-heptane + [emim][DCA]} and {toluene + [emim][DCA]} binary systems.

n-Heptane (1) + [emim][DCA] (2)		Toluene (1) + [emim][DCA] (2)	
x_1	P (kPa)	x_1	P (kPa)
$T/K = 323.2$			
0.0007	1.2	0.0092	0.4
0.0011	1.8	0.0350	1.7
0.0021	3.7	0.0664	3.2
0.0055	7.9	0.1204	5.9
0.0076	11.6	0.1616	8.0
0.0128	15.0	0.2360	10.2
0.0254	18.0	0.3796	11.4
0.0510	18.4	0.4405	11.6
0.1291	18.7	0.5520	11.9
0.2777	18.8	0.6500	12.0
0.6199	18.9	0.7367	12.2
1.0000	18.8[b]	1.0000	12.3[b]
$T/K = 343.2$			
0.0002	0.9	0.0087	0.9
0.0003	1.5	0.0332	3.5
0.0006	3.1	0.0487	5.1
0.0013	6.0	0.1291	13.0
0.0036	12.5	0.1555	15.5
0.0060	27.8	0.2280	21.2
0.0157	36.2	0.3720	24.9
0.0460	38.2	0.4336	25.3
0.1205	40.0	0.5466	25.9
0.2740	39.9	0.6457	26.9
0.6219	40.7	0.7336	27.1
1.0000	40.4[b]	1.0000	27.2[b]
$T/K = 363.2$			
0.0001	0.5	0.0074	1.4
0.0004	1.6	0.0304	6.1
0.0006	2.9	0.0458	9.1
0.0015	6.3	0.1198	24.6
0.0036	12.2	0.1475	29.7
0.0050	27.4	0.2162	40.9
0.0063	41.5	0.3551	49.1
0.0150	67.6	0.4177	50.4
0.0913	73.9	0.5343	53.5
0.2459	76.2	0.6357	53.1
0.6055	78.9	0.7283	53.4
1.0000	78.6[b]	1.0000	54.3[b]

[a] Standard uncertainty (u) are $u(x) = 0.0001$ and $u(P) = 0.1$ kPa.
[b] From Ref. [33].

Table 4
VLE[a] data for {*n*-heptane (1) + toluene (2) + [emim][DCA] (3)} ternary system.

x_3	x'_1	y_1	P (kPa)	a_{12}
$T/K = 323.2$				
0.9844	0.0390	0.6900	2.7	54.8
0.9863	0.0234	0.5918	1.7	60.6
0.9851	0.0209	0.5445	1.8	56.1
0.9848	0.0191	0.5297	1.6	57.9
0.9836	0.0165	0.4806	1.6	55.2
0.9836	0.0140	0.4506	1.5	57.6
0.9829	0.0123	0.3884	1.4	51.1
0.9838	0.0093	0.3339	1.3	53.6
0.9827	0.0075	0.2649	1.2	47.5
0.9834	0.0048	0.1977	1	50.8
0.9826	0.0023	0.1074	1	52.3
0.9821	0.0008	0.0535	0.9	70.6
0.9817	0.0003	0.0258	0.9	88.3
0.9242	0.0233	0.5193	7.8	45.2
0.9235	0.0191	0.4844	7.3	48.3
0.9213	0.0171	0.4428	6.9	45.6
0.9192	0.0142	0.3967	6.4	45.5
0.9191	0.0111	0.3369	5.9	45.2
0.9184	0.0082	0.2681	5.4	44.3
0.9167	0.0050	0.2064	4.9	51.3
0.9171	0.0023	0.1120	4.4	55
0.9176	0.0010	0.0542	4.2	59
0.9188	0.0004	0.0259	4	71.9
0.8445	0.0121	0.3444	10.8	42.9
0.8438	0.0091	0.2790	9.6	42.2
0.8449	0.0056	0.2097	8.7	47
0.8408	0.0027	0.1163	7.8	48.6
0.8379	0.0011	0.0570	7.6	54.4
0.8409	0.0004	0.0264	7.6	61.6
0.7695	0.0065	0.2128	12	41.3
0.768	0.0031	0.1202	10.5	44.5
0.7735	0.0012	0.0570	10.2	48.9
0.7684	0.0005	0.0277	10.1	59.9
$T/K = 343.2$				
0.9881	0.0336	0.5614	2.9	36.9
0.9862	0.0196	0.4549	2.6	42
0.986	0.0171	0.4239	2.6	42.4
0.9856	0.0153	0.3897	2.5	41.8
0.9856	0.0125	0.3517	2.3	42.5
0.9864	0.0117	0.3194	2.1	40.8
0.9847	0.0098	0.2853	2.2	41.2
0.9845	0.0077	0.2272	2.1	37.6
0.9844	0.0064	0.1856	2	37
0.9839	0.0037	0.1287	1.9	37.2
0.9824	0.0017	0.0601	2	40.9
0.9845	0.0006	0.0344	1.6	48.2
0.9819	0.0003	0.0170	1.9	75.1
0.9255	0.0177	0.3973	12.2	36.6
0.9239	0.0148	0.3591	11.6	37.3
0.9233	0.0129	0.3280	11.1	37.5
0.9227	0.0110	0.2863	10.7	35.9
0.9214	0.0085	0.2340	10.1	35.7
0.9202	0.0065	0.1915	9.7	36.3
0.9191	0.0042	0.1341	9.2	37.2
0.917	0.0012	0.0667	8.9	59.3
0.9188	0.0006	0.0370	8.3	59.4
0.9182	0.0002	0.0180	8.3	85.1
0.8613	0.0091	0.2254	18.3	31.7
0.8435	0.0072	0.1961	18	33.6
0.8464	0.0046	0.1358	17.1	34.5
0.8424	0.0013	0.0700	16	55.9
0.8416	0.0008	0.0380	15.8	53.8
0.8406	0.0003	0.0185	15.6	72.9
0.7756	0.0048	0.1408	23.8	34.3
0.775	0.0017	0.0692	22.1	43.5
0.771	0.0009	0.0391	21.5	46.5
0.7737	0.0003	0.0193	20.8	65.4
$T/K = 363.2$				
0.9877	0.0325	0.4337	4.8	22.7
0.9854	0.0212	0.3510	4.3	25.1
0.9864	0.0184	0.3231	3.9	25
0.9866	0.0164	0.2924	3.7	24.6

Table 4 (*Continued*)

x_3	x'_1	y_1	P (kPa)	a_{12}
0.9859	0.0134	0.2619	3.7	25.6
0.9867	0.0113	0.2252	3.6	24.9
0.9852	0.0094	0.2084	3.6	27
0.9847	0.0072	0.1672	3.5	28.3
0.9862	0.0051	0.1271	3.3	27.4
0.9847	0.0033	0.0911	3.3	30.5
0.9839	0.0012	0.0437	3.3	41.9
0.9873	0.0008	0.0199	3.1	34.1
0.9837	0.0001	0.0113	3.1	46
0.9307	0.0195	0.2822	19.3	19.8
0.9341	0.0161	0.2411	18.5	19.4
0.9334	0.0140	0.2182	18	19.8
0.9282	0.0114	0.1988	17.7	21.4
0.9303	0.0087	0.1554	16.8	20.8
0.9281	0.0065	0.1283	16.3	22.2
0.9275	0.0043	0.0869	15.6	22.2
0.9268	0.0014	0.0413	15.3	31.3
0.9336	0.0006	0.0210	15.2	35.5
0.9274	0.0003	0.0107	14.9	41.5
0.8541	0.0110	0.1526	33.4	16.1
0.8639	0.0079	0.1187	31.8	16.9
0.8584	0.0049	0.0827	31.4	18.3
0.8586	0.0018	0.0379	30.7	21.1
0.8579	0.0008	0.0217	30.4	29.3
0.8549	0.0003	0.0104	30.1	33.5
0.79	0.0061	0.0874	40.1	15.4
0.7894	0.0027	0.0411	36.2	16.1
0.7852	0.0011	0.0246	36.1	22.8
0.7841	0.0003	0.0127	35.8	40.9

[a] Standard uncertainty (u) are $u(x) = 0.0001$, $u(x') = 0.0002$, $u(y) = 0.00005$, and $u(P) = 0.1$ kPa.

For the ternary system {*n*-heptane + toluene + [emim][DCA]}, two peaks are obtained from the vapor phase analysis. In order to measure the composition of the vapor phase, a GC response factor (RF) was determined to both volatile compounds involved in the mixtures, i.e., *n*-heptane and toluene. Thereby, several compositions of both hydrocarbons have been prepared by mass and determined by a simple GC analysis to relate peak areas and compositions. Then, the RF determined was employed to correct peak areas obtained from the GC and thus to calculate the vapor compositions. The total pressure of the vapor phase was calculated as the sum of partial pressures of both volatile compounds, which was determined by the Eq. (1).

Table 5
VLE[a] data for {*n*-heptane (1) + toluene (2)} binary system.

x_1	y_1	P (kPa)	a_{12}
T/K = 323.2			
0.1670	0.2822	14.6	2.0
0.3716	0.4922	16.3	1.6
0.5716	0.6559	17.3	1.4
0.7809	0.8181	18.1	1.3
T/K = 343.2			
0.1889	0.3099	31.8	1.9
0.3811	0.4893	34.8	1.6
0.5733	0.6550	37.1	1.4
0.7882	0.8280	38.7	1.3
T/K = 363.2			
0.1862	0.2928	63.7	1.8
0.3779	0.4777	69.4	1.5
0.5704	0.6491	73.0	1.4
0.7874	0.8142	75.0	1.2

[a] Standard uncertainty (u) are $u(x) = 0.0001$, $u(y) = 0.00005$, and $u(P) = 0.1$ kPa.

In order to determine the composition of the liquid phase when VLE was reached, the true mole fraction of liquid (x_i) of the each component (i) was calculated as follows:

$$x_i = \frac{z_i \times F - P_i \times V_G/(R \times T)}{\sum_{i=1}^{3}(z_i \times F - P_i \times V_G/(R \times T))} \quad (2)$$

where z_i denotes the mole fraction of the component i in the VLE feed (1 for *n*-heptane, 2 for toluene, and 3 for [emim][DCA]), F is the molar amount of the feed, and V_G refers to the vapor (headspace) volume of the vial, which was 19.0 mL for all experiments carried out in this work.

3. Results and discussion

The VLE data for the {*n*-heptane + toluene}, {*n*-heptane + [emim][DCA]}, {toluene + [emim][DCA]}, and {*n*-heptane + toluene + [emim][DCA]} systems were determined at 323.2 K,

Table 6
NRTL parameters from the adjustment of VLE data for {*n*-heptane + [emim][DCA]}, {toluene + [emim][DCA]}, and {*n*-heptane + toluene + [emim][DCA]} systems.

i–j	Δg_{ij} (J mol^{-1})	Δg_{ji} (J mol^{-1})	Δx	ΔP (kPa)
n-Heptane (1) + [emim][DCA] (2)				
1–2	9828.5	−385.83	0.001	0.001
Toluene (1) + [emim][DCA] (2)				
1–2	3576.2	−3192.0	0.010	0.004
n-Heptane (1) + toluene (2) + [emim][DCA] (3)				
1–2	7122.4	5872.5	0.003	0.020
1–3	3545.4	17309		
2–3	3612.3	381.59		

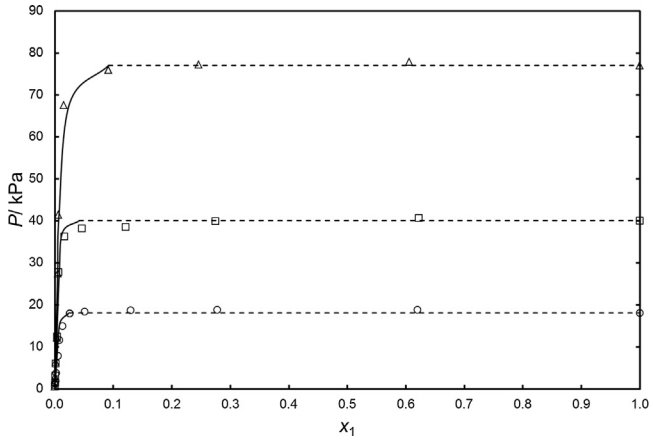

Fig. 1. Experimental VLE for the binary system {*n*-heptane (1) + [emim][DCA] (2)} at several temperatures: ○, T = 323.2 K; □, T = 343.2 K; Δ, T = 363.2 K. Solid lines denote the NRTL adjustment and dashed lines refer to constant pressure equal to pure component pressure from Ref. [33].

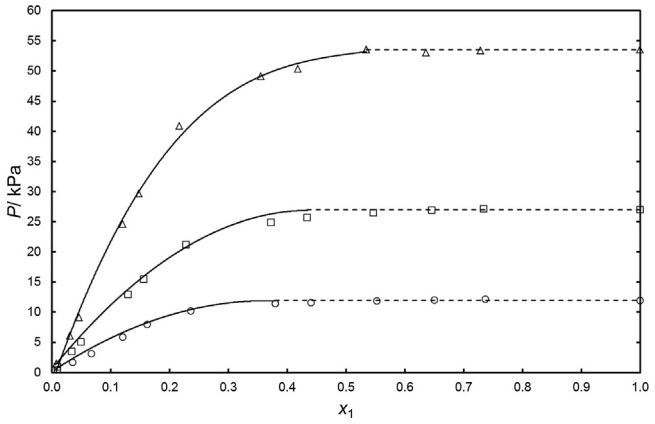

Fig. 2. VLE data for binary system {toluene (1) + [emim][DCA] (2)} at several temperatures. ○, T = 323.2 K; □, T = 343.2 K; Δ, T = 363.2 K. Solid lines denote the NRTL adjustment and dashed lines refer to constant pressure equal to pure component pressure from Ref. [33].

343.2 K, and 363.2 K by the HS-GC method described previously. The x–P data obtained for the systems {*n*-heptane + [emim][DCA]} and {toluene + [emim][DCA]} are listed in Table 3. The x,y–P data obtained for the systems {*n*-heptane + toluene + [emim][DCA]} and {*n*-heptane + toluene} are listed in Tables 4 and 5, respectively, the first based on a solvent-free basis (x'_i).

In order to evaluate the effect of the IL on the VLE of the ternary system, the relative volatility (α_{12}) of *n*-heptane (1) from toluene

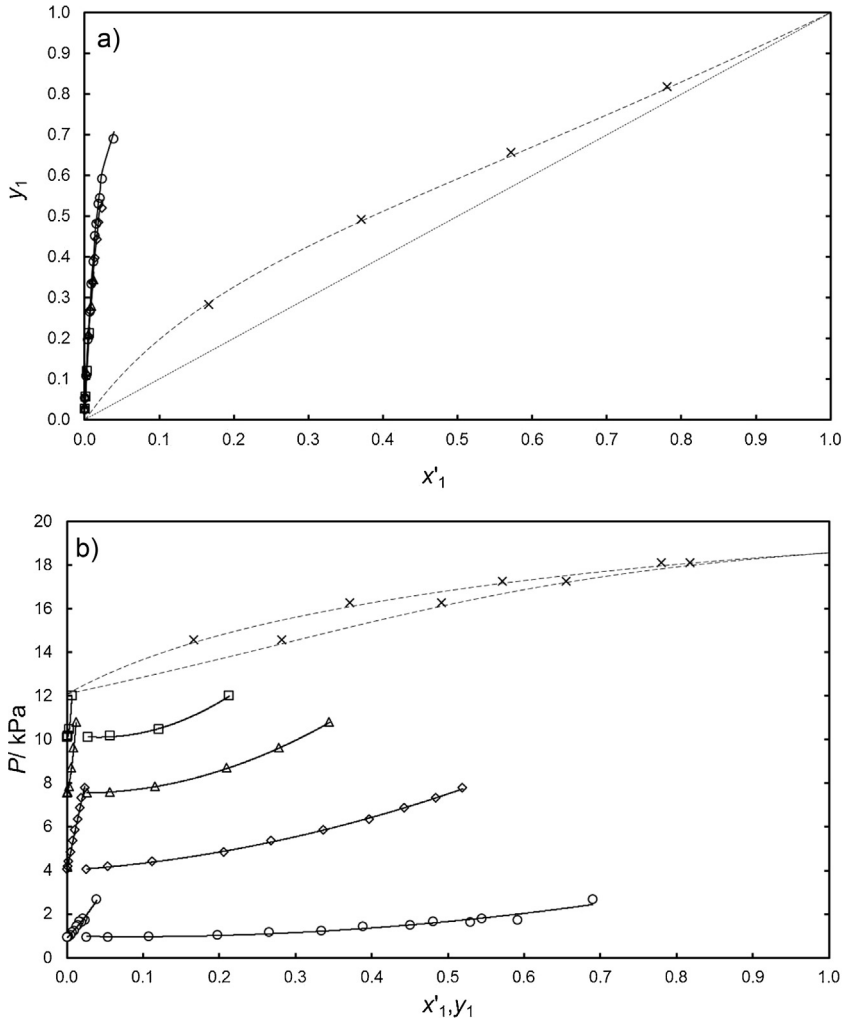

Fig. 3. VLE data for ternary system {*n*-heptane (1) + toluene (2) + [emim][DCA] (3)} at T = 323.2 K. x'-y diagram (a) and x',y-P diagram (b). IL mole fraction (x_3): ○, $x_3 \approx 0.98$; ◇, $x_3 \approx 0.92$; Δ, $x_3 \approx 0.84$; □, $x_3 \approx 0.77$; x, binary system of {*n*-heptane (1) + toluene (2)}. Solid lines denote the NRTL adjustment and dashed lines refer to VLE data from Aspen Plus Simulator Software Database at 323.2 K for the binary system of {*n*-heptane (1) + toluene (2)}.

(2) was calculated as follows:

$$\alpha_{12} = \frac{K_1}{K_2} = \frac{y_1/x_1}{y_2/x_2} \tag{3}$$

where K is the K-value for each volatile compound. The values of n-heptane relative volatility from toluene are listed in Tables 4 and 5 for the {n-heptane + toluene + [emim][DCA]} and {n-heptane + toluene} systems, respectively.

The NRTL thermodynamic model was employed to correlate the experimental VLE data. This model has been widely used in modeling VLE [25,26,28–30,34–36]. The objective function (OF) used in order to minimize the global deviation is defined following the next expression:

$$\mathrm{OF} = \frac{\alpha \times \sum_{i=1}^{I} |x_{i,\mathrm{calc}} - x_{i,\mathrm{exptl}}| + \sum_{i=1}^{I} |P_{i,\mathrm{calc}} - P_{i,\mathrm{exptl}}|}{N} \tag{4}$$

where a is the weighting coefficient of mole fraction deviations for minimizing the deviation of the adjustment and N refers to the number of VLE points included in the adjustment. The best adjustment was achieved for $a = 300$, balancing the difference of magnitude between x and P. The experimental data were correlated by the Solver tool in the Microsoft Excel spreadsheet software. The value of the nonrandomness parameter, α, in the NRTL model was set to 0.3 [25,26,28–30,34–36] for all the systems. The interaction parameters are listed in Table 6, jointly with the deviations of the compositions, Δx, and the pressures, ΔP, calculated as:

$$\Delta x = \frac{\sum_{i=1}^{I} |x_{i,\mathrm{calc}} - x_{i,\mathrm{exptl}}|}{N} \tag{5}$$

$$\Delta P = \frac{\sum_{i=1}^{I} |P_{i,\mathrm{calc}} - P_{i,\mathrm{exptl}}|}{N} \tag{6}$$

As can be inferred from Table 6, the NRTL model describes quite accurately the experimental values. The experimental results are compared with the values obtained from the NRTL adjustments in Figs. 1–5 as can be seen, the NRTL model satisfactorily correlates the experimental results for the VLE of all systems.

Figs. 1 and 2 show the x–P data for the binary systems {n-heptane (1) + [emim][DCA] (2)} and {toluene (1) + [emim][DCA] (2)}. Both figures show that there is a miscibility gap for n-heptane

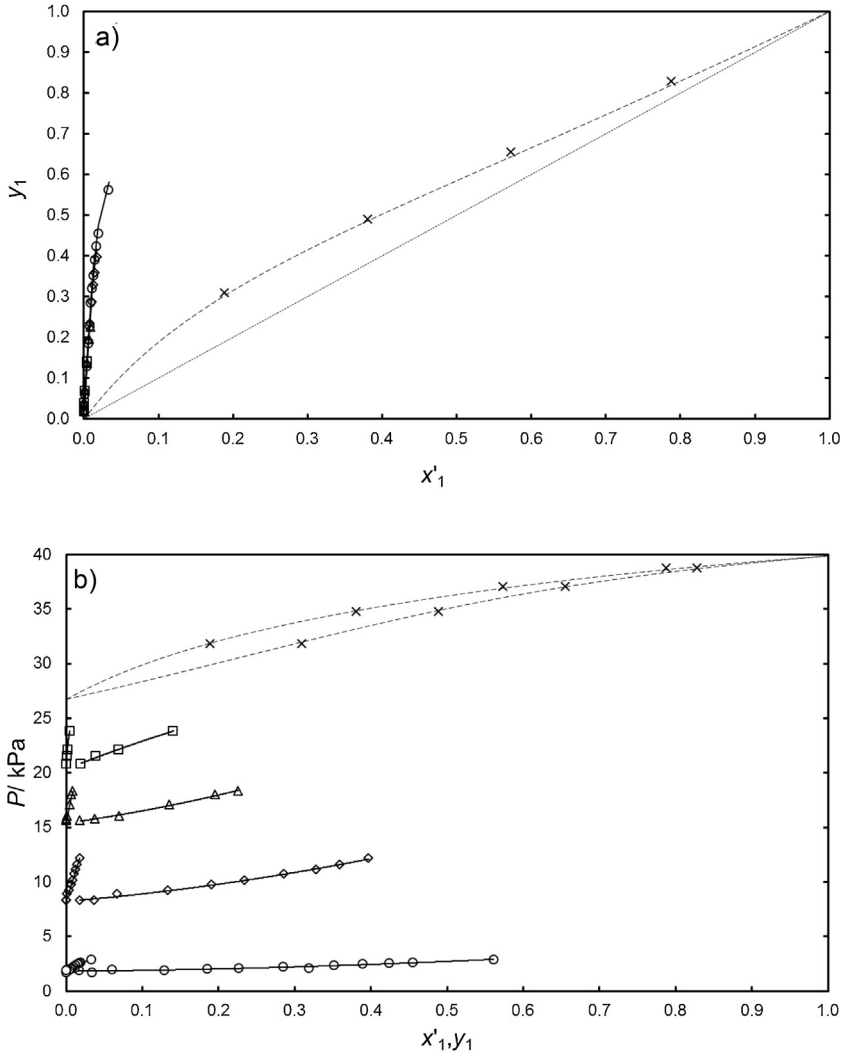

Fig. 4. VLE data for ternary system {n-heptane (1) + toluene (2) + [emim][DCA] (3)} at $T = 343.2$ K. x'-y diagram (a) and x',y-P diagram (b). IL mole fraction (x_3): ○, $x_3 \approx 0.98$; ◇, $x_3 \approx 0.92$; Δ, $x_3 \approx 0.84$; □, $x_3 \approx 0.77$; x, binary system of {n-heptane (1) + toluene (2)}. Solid lines denote the NRTL adjustment and dashed lines refer to VLE data from Aspen Plus Simulator Software Database at 343.2 K for the binary system of {n-heptane (1) + toluene (2)}.

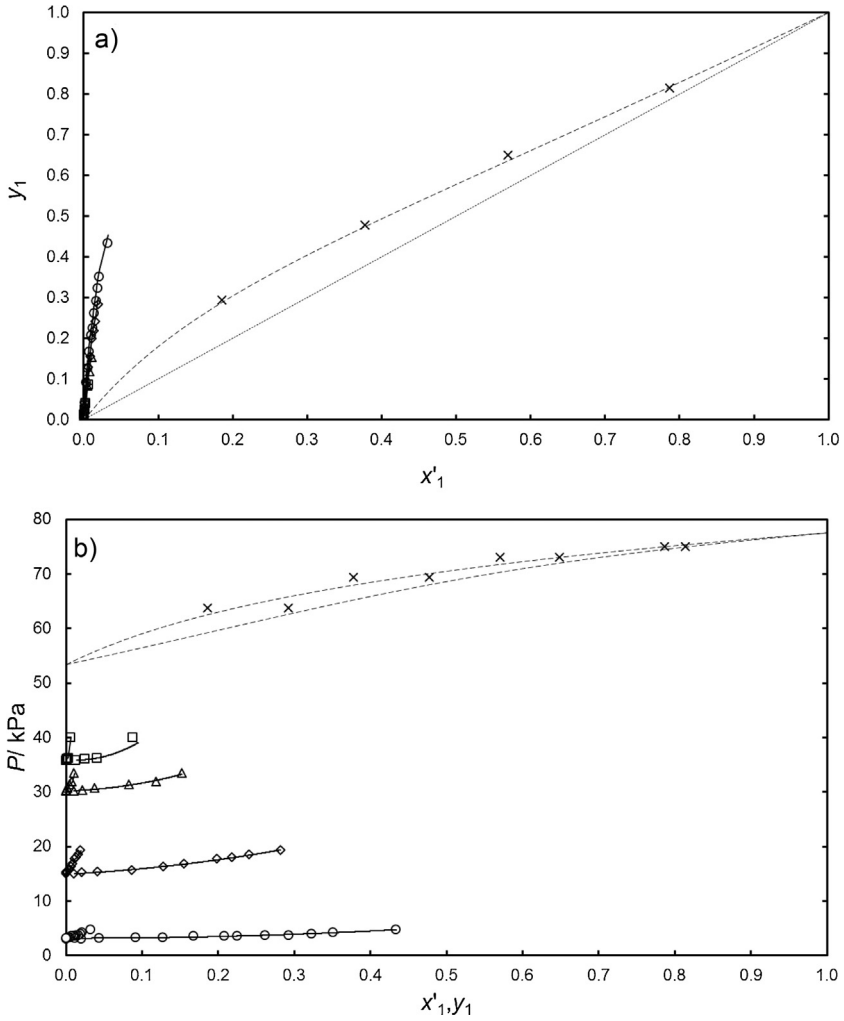

Fig. 5. VLE data for ternary system {*n*-heptane (1) + toluene (2) + [emim][DCA] (3)} at $T = 363.2$ K. x'-y diagram (a) and x', y-P diagram (b). IL mole fraction (x_3): ○, $x_3 \approx 0.98$; ◇, $x_3 \approx 0.92$; Δ, $x_3 \approx 0.84$; □, $x_3 \approx 0.77$; x, binary system of {*n*-heptane (1) + toluene (2)}. Solid lines denote the NRTL adjustment and dashed lines refer to VLE data from Aspen Plus Simulator Software Database at 363.2 K for the binary system of {*n*-heptane (1) + toluene (2)}.

or toluene + [emim][DCA]. The shape of all pressure curves is clearly divided in two parts. The first includes a growing pressure zone until reaching the solubility limit of *n*-heptane or toluene in the IL. An increase in the hydrocarbon fraction causes an increase in the vapor pressure of the binary mixture. The end of this first zone developed a pressure identical to that of the pure hydrocarbons. Because of the high affinity of toluene to [emim][DCA], the miscibility zone in the case of {toluene + [emim][DCA]} system is higher than that of the {*n*-heptane + [emim][DCA]} system, increasing the value of solubility in both cases as temperature does. The same conclusion was predicted by Mutelet et al. and Ma et al. in their studies about hydrocarbon activity coefficients at infinite dilution in the same IL [38,39]. Results gathered in this work are in agreement with those published at 313.2 K, as the solubilities were 0.003 for *n*-heptane and 0.320 for toluene, in mole basis [3].

The x', y–P data for the {*n*-heptane + toluene + [emim][DCA]} system is shown in Figs. 3–5. Also the x, y–P data for {*n*-heptane + toluene} is shown in Figs. 3–5 together with VLE data provided by Aspen Plus Simulator Software Database included in Table 7 [37] to validate experimental method used in this work. The experimental and literature data were in agreement as can be graphically observed or making a comparison between the values of Tables 5 and 7.

The presence of [emim][DCA] in the {*n*-heptane + toluene} system highly increased the *n*-heptane relative volatility from toluene at any temperature proved in this work. This effect is related to the aromatic character of the IL, which has a higher affinity to the toluene than to the *n*-heptane. The higher values of the relative volatility of *n*-heptane from toluene were achieved at the lowest temperature and with the highest fraction of [emim][DCA].

Table 7
VLE data for {*n*-heptane (1) + toluene (2)} binary system from Ref. [37].

x_1	y_1	P (kPa)	y_1	P (kPa)	y_1	P (kPa)
	$T/K = 323.2$		$T/K = 343.2$		$T/K = 363.2$	
0.0000	0.0000	12.1	0.0000	26.7	0.0000	53.4
0.1000	0.1982	13.7	0.1890	29.9	0.1805	59.1
0.2000	0.3272	14.8	0.3156	32.1	0.3048	63.0
0.3000	0.4266	15.6	0.4153	33.7	0.4049	66.0
0.4000	0.5125	16.3	0.5028	35.1	0.4940	68.5
0.5000	0.5924	16.8	0.5851	36.2	0.5784	70.5
0.6000	0.6705	17.3	0.6658	37.1	0.6615	72.3
0.7000	0.7492	17.7	0.7468	38.0	0.7447	73.8
0.8000	0.8299	18.0	0.8294	38.7	0.8289	75.2
0.9000	0.9134	18.3	0.9137	39.3	0.9141	76.4
1.0000	1.0000	18.6	1.0000	39.9	1.0000	77.5

The promising results gathered here could permit to plan and simulate a whole alternative process of extraction of aromatics with ILs as solvents including the purification section for the first time. Thus, the influence of both extraction and purification sections on the operational and fixed costs of the process can be together evaluated in future works. The NRTL parameters predict the values of *n*-heptane relative volatility from toluene with a mean deviation of 8.7% from the experimental values; thus, the NRTL parameters can be used to estimate a simplified aromatic extraction process involving {*n*-heptane + toluene + [emim][DCA]}.

Recently, we have simulated the extraction process involving ILs in order to remove the BTEX fraction from a reformer gasoline [40]; the low presence of aliphatics in the extract stream obtained and the high *n*-heptane relative volatility from toluene achieved here suggest the possibility of separating the low amount of extracted aliphatics by a flash distillation process, as advanced Anjan years ago [7]. Also the values obtained for toluene + [emim][DCA] are valuable to study the removing of aromatics from the IL-based solvent. Then, the advances achieved in this work permit to deeply study the aromatic extraction from gasolines from an aromatic recovery point of view.

4. Conclusions

In this study, VLE measurements have been done for {*n*-heptane + [emim][DCA]}, {toluene + [emim][DCA]}, and {*n*-heptane + toluene + [emim][DCA]} systems at 323.2 K, 343.2 K, and 363.2 K. VLE of {*n*-heptane + toluene} binary mixtures have been also measured to validate the HS-GC method employed by comparing the experimental data with those in Aspen Plus Simulator Software Database. The HS-GC methodology has been revealed as a potential way for future VLE determinations of {aliphatic + aromatic + IL} systems. Moreover, VLE data of {*n*-heptane + [emim][DCA]}, {toluene + [emim][DCA]}, and {*n*-heptane + toluene + [emim][DCA]} systems have been successfully fitted to NRTL.

The results gathered in this work have revealed [emim][DCA] as a potential mass agent in the separation of *n*-heptane from toluene. Relative volatilities of *n*-heptane from toluene highly increased under the presence of [emim][DCA]. Low temperature and high concentration of [emim][DCA] were the best conditions observed.

Funding sources

Authors are grateful to the Ministerio de Economía y Competitividad (MINECO) of Spain and the Comunidad de Madrid for financial support of Projects CTQ2011-23533 and S2013/MAE-2800, respectively. Pablo Navarro also thanks MINECO for awarding him an FPI grant (Reference BES-2012-052312). Marcos Larriba thanks Ministerio de Educación, Cultura y Deporte of Spain for awarding him an FPU grant (Reference AP2010-00318). Emilio J. González also thanks MINECO for awarding him a Juan de la Cierva Contract (Reference JCI-2012-12005).

References

[1] R.D. Rogers, K.R. Seddon, Science 302 (2003) 792–793.
[2] N.V. Plechkova, K.R. Seddon, Chem. Soc. Rev. 37 (2008) 123–150.
[3] M. Larriba, P. Navarro, J. García, F. Rodríguez, Ind. Chem. Eng. Res. 52 (2013) 2714–2720.
[4] Y. Nie, C. Li, H. Meng, Z. Wang, Fuel Process. Technol. 89 (2008) 978–983.
[5] L. Alonso, A. Arce, M. Francisco, A. Soto, J. Chem. Thermodyn. 40 (2008) 966–972.
[6] A. Marciniak, M. Krolikowski, J. Chem. Thermodyn. 49 (2012) 154–158.
[7] S.T. Anjan, Ionic liquid for aromatic extraction: are they ready? Chem. Eng. Prog. 102 (2006) 30–39.
[8] G.W. Meindersma, A.J.G. Podt, A.B. de Haan, Fuel Process. Technol. 87 (2005) 59–70.
[9] G.W. Meindersma, A.R. Hansmeier, A.B. de Haan, Ind. Eng. Chem. Res. 49 (2010) 7530–7540.
[10] G.W. Meindersma, A.J.G. Podt, A.B. de Haan, Fluid Phase Equilib. 247 (2006) 158–168.
[11] S. Corderí, E.J. González, N. Calvar, A. Domínguez, J. Chem. Thermodyn. 53 (2012) 60–66.
[12] M. Larriba, P. Navarro, J. García, F. Rodríguez, Fluid Phase Equilib. 380 (2014) 1–10.
[13] G.W. Meindersma, A.B. de Haan, Chem. Eng. Res. Des. 86 (2008) 745–752.
[14] A.R. Hansmeier, M. Minoves Ruiz, G.W. Meindersma, A.B. de Haan, J. Chem. Eng. Data 55 (2010) 708–713.
[15] M. Larriba, P. Navarro, J. García, F. Rodríguez, Fluid Phase Equilib. 364 (2013) 48–54.
[16] F. Farshad, M. Iravaninia, N. Kasiri, T. Mohammadi, J. Ivakpour, Chem. Eng. J. 173 (2011) 11–18.
[17] M. Larriba, P. Navarro, J. García, F. Rodríguez, Sep. Purif. Technol. 120 (2013) 392–401.
[18] P. Navarro, M. Larriba, E. Rojo, J. García, F. Rodríguez, J. Chem. Eng. Data 58 (2013) 2187–2193.
[19] P. Navarro, M. Larriba, J. García, F. Rodríguez, J. Chem. Thermodyn. 76 (2014) 152–160.
[20] A. Fernández, J.S. Torrecilla, J. García, F. Rodríguez, J. Chem. Eng. Data 52 (2007) 1979–1983.
[21] A. Seeberger, A.K. Andresen, A. Jess, Phys. Chem. Chem. Phys. 11 (2009) 9375–9381.
[22] S. Aparicio, M. Atilhan, F. Karadas, Ind. Eng. Chem. Res. 49 (2010) 9580–9595.
[23] M. Larriba, S. García, P. Navarro, J. García, F. Rodríguez, J. Chem. Eng. Data 57 (2012) 1318–1325.
[24] M. Larriba, S. García, P. Navarro, J. García, F. Rodríguez, J. Chem. Eng. Data 58 (2013) 1496–1504.
[25] B. Mokhtarani, J. Gmehling, J. Chem. Thermodyn. 42 (2010) 1036–1038.
[26] B. Mokhtarani, L. Valialahi, K.T. Heidar, H.R. Mortaheb, A. Sharifi, M. Mirzaei, J. Chem. Thermodyn. 51 (2012) 77–81.
[27] E. Alvarez-Guerra, S.P.M. Ventura, J.A.P. Coutinho, A. Irabien, Fluid Phase Equilib. 371 (2014) 67–74.
[28] A.V. Orchillés, J.P. Miguel, V. González-Alfaro, E. Vercher, J. Chem. Eng. Data 57 (2012) 394–399.
[29] A.E. Andreatta, A. Arce, E. Rodil, A. Soto, Fluid Phase Equilib. 287 (2010) 84–94.
[30] Y. Ge, L. Zhang, X. Yuan, W. Geng, J. Ji, J. Chem. Thermodyn. 40 (2008) 1248–1252.
[31] L. Zhang, J. Han, D. Deng, J. Ji, Fluid Phase Equilib. 255 (2007) 179–185.
[32] B. Kolb, L.S. Ettre, Static Headspace-Gas Chromatography: Theory and Practice, Wiley-VCH, New York, 1997.
[33] R.H. Perry, D.W. Green, J.O. Maloney, Perry's Chemical Engineers' Handbook, McGraw-Hill, 1999.
[34] P. Luis, C. Wouters, N. Sweygers, C. Creemers, B. Van der Bruggen, J. Chem. Thermodyn. 49 (2012) 128–136.
[35] Z. Jiqin, C. Jian, L. Chengyue, F. Weiyang, Fluid Phase Equilib. 247 (2006) 102–106.
[36] H. Renon, J.M. Prausnitz, AlChE J. 14 (1968) 135–144.
[37] Aspen Plus Version 7.1, Database, Aspen Technology, 2004.
[38] F. Mutelet, A.-L. Revelli, J.-N. Jaubert, L.M. Sprunger Jr., W.E. Acree, G.A. Baker, J. Chem. Eng. Data 55 (2010) 234–242.
[39] L. Ma, W.-R. Ji, J.-B. Ji, J. Chem. Eng. Chin. Univ. 22 (2008) 547–552.
[40] M. Larriba, P. Navarro, J. García, F. Rodríguez, Energy Fuels 28 (2014) 6666–6676.

Journal of chemical & engineering data

Article

pubs.acs.org/jced

Vapor−Liquid Equilibria of *n*-Heptane + Toluene +1-Ethyl-4-methylpyridinium Bis(trifluoromethylsulfonyl)imide Ionic Liquid

Pablo Navarro, Marcos Larriba, Julián García,* Emilio J. González, and Francisco Rodríguez

Department of Chemical Engineering, Complutense University of Madrid, E−28040 Madrid, Spain

ABSTRACT: Ionic liquids (ILs) are considered as promising solvents in aromatic extraction because of their high extractive capacities, and a large number of experimental liquid−liquid equilibrium (LLE) data can be found in the literature for systems containing hydrocarbons and ionic liquids. However, the vapor−liquid equilibrium (VLE) data of {aliphatic + aromatic + IL} mixtures are scarce and essential to evaluate the feasibility of the global process. In this work, the VLE data for {*n*-heptane + toluene + [4empy][Tf_2N]} ternary system were experimental measured at 323.2, 343.2, and 363.2 K using a headspace gas chromatography (HS-GC) technique. The selection of this ionic liquid was made taking into account its high ability to extract aromatic compounds, in order to evaluate the relationship between the extractive properties for an IL and its performance as mass agent. The experimental VLE data was successfully modeled using the non-random two liquids (NRTL) model.

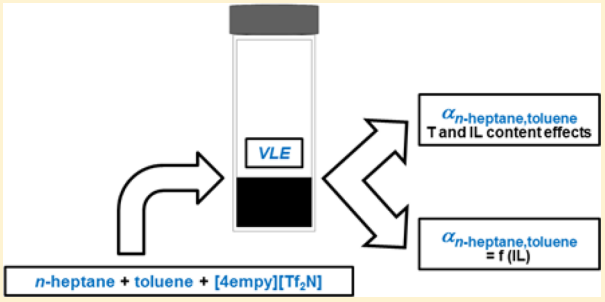

1. INTRODUCTION

Ionic liquids (ILs) are commonly defined as liquid salts at temperatures lower 373.2 K formed by an organic cation and an inorganic anion.[1,2] These compounds are mainly characterized by the possibility of synthesizing a large number of ILs families and their negligible vapor pressure, which become them as one of the most promising alternative solvents.[2]

One important field in which ILs are extensively studied is the separation of aromatic and aliphatic hydrocarbons.[3−19] However, most of these studied are focused on the extraction processes and the characterization of the ILs, leaving aside the IL recovery step, which would complete the global separation process.

Taking into account the negligible vapor pressure of the ILs, the separation of these compounds from the extracted hydrocarbons could be simply performed by a flash distillation. However, the aliphatic/aromatic/IL separation should be evaluated to selectively recover the extracted hydrocarbons. For that, new experimental vapor−liquid equilibrium (VLE) data are required. Although some studies about experimental VLE data for {aliphatic + aromatic + IL} systems have been recently carried out,[20−22] they are still scarce. So, efforts are needed to ensure the proper knowledge of the VLE for {aliphatic + aromatic + IL} systems that would allow the design of the global extraction process.

In a previous work, the experimental VLE data for a ternary mixture containing *n*-heptane, toluene, and a high aromatic/aliphatic selective ionic liquid 1-ethyl-3-methylimidazolium dicyanamide ([emim][DCA]) were determined at several temperatures.[20] The results showed that a highly selective ionic liquid from an extractive point of view, as [emim][DCA], is also a high selective mass agent.

Now, the aim of this work is to extend this study using a less selective ionic liquid but with a high capacity to extract aromatics from their mixtures with aliphatic. For that, the ionic liquid selected was 1-ethyl-4-methylpyridinium bis-(trifluoromethylsulfonyl)imide ([4empy][Tf_2N]), which has these characteristics as can be observed in our previous work.[3]

Table 1. Specifications of Chemicals

chemical	source	final mass fraction purity	purification method	analysis method
[4empy][Tf_2N]	Iolitec GmbH	0.99	none	NMR[a], IC[b]
n-heptane	Sigma-Aldrich	0.997	molecular sieves	GC[c]
toluene	Sigma-Aldrich	0.995	molecular sieves	GC[c]

[a]Nuclear magnetic resonance. [b]Ion chromatography. [c]Gas chromatography.

The experimental VLE data of the {*n*-heptane + toluene + [4empy][Tf_2N]} mixture were measured at 323.2, 343.2, and 363.2 K over the whole range of compositions in the miscibility region. A high *n*-heptane relative volatility from toluene under the presence of [4empy][Tf_2N] was observed. In addition, a comparison between *n*-heptane relative volatility from toluene using [4empy][Tf_2N] and [emim][DCA] was made, confirming the results obtained by Jongmans et al.[27] who had observed a relationship between the selectivity of ILs as solvents and the relative volatility as mass agent. This fact suggests that the use of ILs with high aromatic/aliphatic selectivity as solvents could simplify the purification steps in a whole aromatic extraction process.

Finally, the experimental VLE data measured in this work were correctly fitted to the non-random two liquids (NRTL)

Received: July 27, 2015
Accepted: December 22, 2015
Published: January 4, 2016

DOI: 10.1021/acs.jced.5b00650
J. Chem. Eng. Data 2016, 61, 458−465

thermodynamic model,[28] confirming that this model can be successfully used to fit VLE data in systems with ILs.[20−26]

2. EXPERIMENTAL SECTION

2.1. Chemicals. The ionic liquid [4empy][Tf_2N] was acquired from Iolitec GmbH with a purity of 0.99 and their halides and water content were below 0.001 in mass fractions. It was used as received without further purifications. To prevent water absorption in the IL, a desiccator was used to store it and its handling was done in a glovebox filled with dry nitrogen. Toluene and *n*-heptane were purchased from Sigma-Aldrich with mass fraction purities of 0.995 and 0.997, respectively. The storage of the hydrocarbons was done in their original vessels over molecular sieves. A summary of the chemicals is shown in Table 1.

2.2. Apparatus and Procedure. The isothermal determination of VLE for systems containing ILs is a good option in order to avoid mixing problems caused by their high viscosity. Thus, the VLE experiments were done using an Agilent headspace 7697A injector coupled to an Agilent gas chromatograph 7890A. The gas chromatograph is equipped with a flame ionization detector (FID) and an HP-5 Agilent column, whereas the headspace injector has a loop system to extract the vapor sample. A detailed description of additional parameters of the HS-GC could be found in our previous work.[20]

Binary and ternary mixtures were prepared by mass, employing a Mettler Toledo XS205 balance with a standard uncertainty of 10^{-5} g. First, the [4empy][Tf_2N] and then the hydrocarbons were added in 20 mL vials. After sealing the vials, the mixture was vigorously mixed using a Labnet Vortex Mixer. For the ternary mixtures, the feed compositions were prepared in order to guarantee miscibility between all compounds.[3] After that, the vials were heated in the oven of the HS sampler at the desirable temperature for a time of 2 h to reach the equilibrium, whereas the oven agitation was set in 100 rpm.

Taking into account that the vapor pressures of the ILs are negligible; the vapor phase only develops one peak area for the binary {hydrocarbon + IL} mixtures. Hence, the partial pressure (P_i) of the hydrocarbon dissolved in the IL can be calculated as follows:[29]

$$P_i = \frac{P_i^0 \cdot A_i}{A_i^0} \quad (1)$$

where A_i is the peak area of the hydrocarbon i from the {hydrocarbon + IL} mixture, A_i^0 is the peak area developed by a sample of the pure hydrocarbon i at the same temperature, and P_i^0 denotes the saturated vapor pressure of the hydrocarbon taken from the literature.[30,31] The repeatability of peak areas was lower than 1% for both hydrocarbons.

In the case of the ternary system {*n*-heptane + toluene + [4empy][Tf_2N]}, two peaks are obtained. In order to analyze the composition of the vapor phase, a response factor was determined for both volatile compounds involved in the mixtures. The total pressure of the vapor phase of the ternary systems was calculated as the sum of partial pressures of the volatile compounds calculated using eq 1. On the other hand, the composition of the liquid phase when the VLE was reached was recalculated as follows:[28]

$$x_i = \frac{z_i \cdot F - (P_i \cdot V_G / R \cdot T)}{\sum_{i=1}^{3} (z_i \cdot F - (P_i \cdot V_G / R \cdot T))} \quad (2)$$

Table 2. VLE[a] for {*n*-Heptane + [4empy][Tf_2N]} and {Toluene + [4empy][Tf_2N]} Binary Systems at Several Temperatures, *T*, Mole Fractions of Hydrocarbon in the Liquid Phase, x_1, and Total Pressures, *P*

{*n*-heptane (1) + [4empy][Tf_2N] (2)}		{toluene (1) + [4empy][Tf_2N] (2)}	
x_1	*P*/kPa	x_1	*P*/kPa
	T/K = 323.2		
0.0047	2.4	0.0101	1.2
0.0099	5.2	0.0566	2.8
0.0169	10.3	0.1070	5.0
0.0419	18.2	0.2279	6.8
0.0794[b]	18.7	0.3778	8.8
0.1138[b]	18.8	0.4997	10.5
0.1339[b]	18.8	0.6175	11.7
0.2375[b]	18.8	0.7382[b]	12.2
0.2735[b]	18.8	0.8098[b]	12.2
0.4831[b]	18.8	0.9077[b]	12.2
0.7952[b]	18.8	0.9761[b]	12.2
1.0000	18.8[c]	1.0000	12.3[c]
	T/K = 343.2		
0.0014	1.0	0.0113	2.4
0.0089	6.4	0.0514	5.9
0.0171	12.4	0.0984	10.5
0.0333	25.4	0.2441	15.6
0.0491	36.4	0.3764	19.3
0.0837	39.1	0.4857	22.7
0.1222[b]	40.4	0.6328	25.2
0.1859[b]	40.4	0.7350[b]	26.9
0.2490[b]	40.3	0.8083[b]	27.0
0.4300[b]	40.4	0.9043[b]	27.0
0.7885[b]	40.4	0.9747[b]	27.2
1.0000	40.4[c]	1.0000	27.2[c]
	T/K = 363.2		
0.0002	1.0	0.0109	5.8
0.0061	6.6	0.0463	12.0
0.0130	13.5	0.1009	18.9
0.0298	25.8	0.2438	31.3
0.0358	43.6	0.3753	38.5
0.0450	58.8	0.4799	46.5
0.0566	70.2	0.6459	52.1
0.1272	76.8	0.7325[b]	53.2
0.2014[b]	78.2	0.8047[b]	53.6
0.4302[b]	78.3	0.9089[b]	54.1
0.7768[b]	78.5	0.9745[b]	54.3
1.0000	78.6[c]	1.0000	54.3[c]

[a]Standard uncertainties (u) were $u(x)$ = 0.0004, $u_r(P)$ = 0.02, and $u(T)$ = 0.1 K. [b]Overall hydrocarbon liquid compositions for vapor−liquid−liquid equilibria (VLLE) experiments. [c]From ref 30.

where x_i is the mole fraction of the liquid phase, z_i refers to the mole fraction of the component i in the VLE feed (1 for *n*-heptane, 2 for toluene, and 3 for [4empy][Tf_2N]), F denotes the molar amount of the feed, and V_G is the vapor (headspace) volume of the vial, which was 19.0 mL for all experiments carried out.

3. RESULTS AND DISCUSSION

The experimental VLE data for the {*n*-heptane + [4empy][Tf_2N]}, {toluene + [4empy][Tf_2N]}, and {*n*-heptane + toluene + [4empy][Tf_2N]} systems were measured at 323.2, 343.2, and 363.2 K. The $x-p$ data for the binary systems {*n*-heptane + [4empy][Tf_2N]} and {toluene + [4empy][Tf_2N]} are listed in

DOI: 10.1021/acs.jced.5b00650
J. Chem. Eng. Data 2016, 61, 458−465

Table 3. VLE[a] for {*n*-Heptane (1) + Toluene (2) + [4empy][Tf_2N] (3)} Ternary System at Several Temperatures, *T*, IL Mole Fractions in the Liquid Phase, x_3, IL-free *n*-Heptane Mole Fractions in the Liquid Phase, x'_1, *n*-Heptane Vapor Mole Fractions, y_1, Total Pressures, *P*, and *n*-Heptane/Toluene Relative Volatilities, $\alpha_{1,2}$

x_3	x'_1	y_1	*P*/ kPa	$\alpha_{1,2}$
		T/K = 323.2		
0.9701	0.2341	0.9184	4.3	36.9
0.9688	0.2083	0.9032	3.9	35.7
0.9667	0.1592	0.8741	3.4	36.6
0.9664	0.1339	0.8463	2.8	35.9
0.9635	0.1068	0.8103	2.5	35.6
0.9608	0.0740	0.7433	2.1	36.7
0.9622	0.0476	0.6489	1.5	37.3
0.9558	0.0226	0.4704	1.1	37.4
0.9551	0.0111	0.3035	0.9	36.9
0.9576	0.0047	0.1546	0.7	38.6
0.9557	0.0023	0.0842	0.6	43.7
0.9547	0.0000	0.0180	0.6	42.7
0.6867	0.1471	0.7672	13.9	19.1
0.6875	0.0998	0.7179	12.3	22.9
0.6895	0.0638	0.6227	10.2	24.2
0.6803	0.0297	0.4268	7.7	24.3
0.6747	0.0148	0.2703	6.1	24.5
0.6820	0.0060	0.1348	5.0	25.3
0.6775	0.0028	0.0680	4.7	25.3
0.6692	0.0006	0.0149	4.5	26.0
0.4830	0.0352	0.3524	11.4	14.9
0.4832	0.0174	0.2227	9.6	16.1
0.4748	0.0072	0.1058	8.5	16.2
0.4795	0.0035	0.0536	7.9	16.6
0.4714	0.0008	0.0115	7.7	16.8
0.3468	0.0197	0.1592	11.4	9.4
0.3503	0.0080	0.0794	10.4	10.7
0.3455	0.0038	0.0389	10.1	10.6
0.3428	0.0008	0.0083	9.8	10.8
		T/K = 343.2		
0.9695	0.1934	0.8718	6.3	28.2
0.9698	0.1788	0.8529	5.5	26.7
0.9681	0.1348	0.8124	4.8	27.9
0.9665	0.1104	0.7723	4.2	27.3
0.9658	0.0877	0.7240	3.7	27.7
0.9636	0.0604	0.6427	3.0	27.6
0.9616	0.0391	0.5403	2.6	28.5
0.9573	0.0187	0.3482	2.1	28.0
0.9561	0.0091	0.2126	1.7	28.1
0.9558	0.0045	0.0994	1.5	28.1
0.9559	0.0023	0.0496	1.4	27.7
0.9560	0.0000	0.0102	1.4	27.6
0.7025	0.1146	0.7271	27.5	20.6
0.6947	0.0780	0.6463	24.1	21.6
0.6858	0.0528	0.5136	20.4	19.0
0.6869	0.0252	0.3281	15.2	19.0
0.6935	0.0124	0.1981	12.6	19.8
0.6629	0.0053	0.0904	12.0	18.1
0.6721	0.0021	0.0515	11.4	25.3
0.6753	0.0003	0.0109	11.0	25.7
0.6935	0.0124	0.1981	12.6	19.8
0.6629	0.0053	0.0904	12.0	18.1
0.6721	0.0021	0.0515	11.4	25.3
0.6753	0.0003	0.0109	11.0	25.7
0.4901	0.0308	0.2914	23.6	13.0
0.4962	0.0153	0.1680	21.2	13.0
0.4787	0.0063	0.0753	20.2	12.6
0.4765	0.0031	0.0376	19.3	13.1
0.4775	0.0006	0.0080	18.9	13.2
0.3536	0.0179	0.1351	25.8	8.5
0.3335	0.0077	0.0586	24.7	8.1
0.3518	0.0035	0.0294	24.2	8.7
0.3476	0.0008	0.0063	23.8	9.0
		T/K = 363.2		
0.9723	0.1986	0.8096	7.3	17.1
0.9703	0.1785	0.7823	6.8	16.6
0.9678	0.1398	0.7182	6.2	15.8
0.9689	0.1093	0.6711	5.3	16.7
0.9674	0.0890	0.6151	4.7	16.6
0.9655	0.0609	0.5208	4.2	16.9
0.9625	0.0400	0.4141	3.8	16.7
0.9607	0.0178	0.2453	3.3	17.3
0.9588	0.0097	0.1401	3.0	17.3
0.9597	0.0050	0.0636	2.7	17.9
0.9581	0.0024	0.0305	2.7	18.1
0.9581	0.0000	0.0062	2.7	17.1
0.7087	0.0949	0.6071	49.7	14.7
0.6673	0.0703	0.5197	44.5	14.3
0.6896	0.0470	0.4058	34.2	13.8
0.6857	0.0232	0.2355	27.6	13.0
0.6846	0.0117	0.1335	24.5	13.0
0.6835	0.0047	0.0586	23.1	12.7
0.6850	0.0022	0.0294	22.0	13.5
0.6849	0.0003	0.0063	21.9	14.5
0.4937	0.0277	0.2192	45.6	9.9
0.4884	0.0141	0.1192	42.5	9.5
0.4961	0.0058	0.0532	39.2	9.7
0.4879	0.0027	0.0261	38.8	9.8
0.4877	0.0006	0.0054	38.5	9.8
0.3684	0.0163	0.1070	50.2	7.2
0.3621	0.0069	0.0465	47.6	7.1
0.3552	0.0033	0.0225	46.6	7.1
0.3550	0.0006	0.0047	46.3	7.2

[a]Standard uncertainties (u) were $u(x)$ = 0.0004, $u(x')$ = 0.0009, $u(y)$ = 0.0010, $u_r(P)$ = 0.02, and $u(T)$ = 0.1 K.

Table 2, whereas the x',y–P data for the {*n*-heptane + toluene + [4empy][Tf_2N]} ternary system are listed in Table 3. In the ternary system, the free-solvent mole fraction (x') was used to graphically show the IL content dependence on the *n*-heptane separation from toluene. In order to quantify this IL effect on the {*n*-heptane + toluene} VLE, the relative volatility (α_{12}) of *n*-heptane (1) from toluene (2) was calculated as follows:

$$\alpha_{12} = \frac{K_1}{K_2} = \frac{y_1/x_1}{y_2/x_2} \quad (3)$$

DOI: 10.1021/acs.jced.5b00650
J. Chem. Eng. Data 2016, 61, 458−465

Table 4. NRTL Parameters[a] from the Adjustment of VLE of {*n*-Heptane + [4empy][Tf_2N]}, {Toluene + [4empy][Tf_2N]}, and {*n*-Heptane + Toluene + [4empy][Tf_2N]} Systems[b]

i−*j*	Δg_{ij}/J·mol^{-1}	Δg_{ji}/J·mol^{-1}	Δx	ΔP/ kPa
	{*n*-heptane (1) + [4empy][Tf_2N] (2)}			
1−2	5317.3	−64.156	0.007	0.16
	{toluene (1) + [4empy][Tf_2N] (2)}			
1−2	2557.9	−308.59	0.009	0.19
	{*n*-heptane (1) + toluene (2) + [4empy][Tf_2N] (3)}			
1−2	−2432.7	3735.9		
1−3	791.01	8048.9	0.006	0.13
2−3	759.99	−1682.2		

[a] α_{12}, α_{13}, and α_{23} were set in 0.3 for all systems [b] Deviations of the adjustment in liquid mole fraction (Δx) and in pressure (ΔP).

where *K* is the *K*-value and *y* is the vapor mole fraction for each volatile compound. The relative volatilities of *n*-heptane from toluene are also listed in Table 3.

The NRTL thermodynamic model was employed to correlate the experimental VLE data, as it has been successfully used before in the correlation of VLE for systems containing ILs.[20−26] The objective function (OF) used here was proposed in order to minimize both pressures and liquid fractions

$$\mathrm{OF} = \frac{a \cdot \sum_{i=1}^{i} |x_{i,\mathrm{calc}} - x_{i,\mathrm{exp\,tl}}| + \sum_{i=1}^{i} |P_{i,\mathrm{calc}} - P_{i,\mathrm{exp\,tl}}|}{N} \quad (4)$$

where *a* denotes the weighting coefficient of mole fraction deviations and was set to 300, whereas *N* is the number of VLE

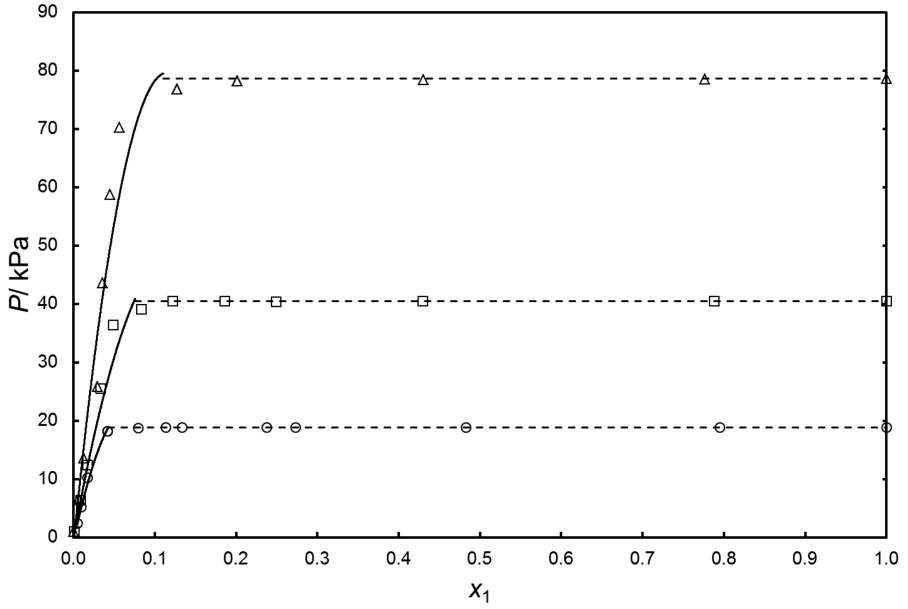

Figure 1. VLE data for binary system {*n*-heptane (1) + [4empy][Tf_2N] (2)} at several temperatures: ○, T = 323.2 K; □, T = 343.2 K; △, T = 363.2 K. Solid lines denote the NRTL adjustment, and dashed lines refer to constant pressure equal to pure component pressure from ref 30.

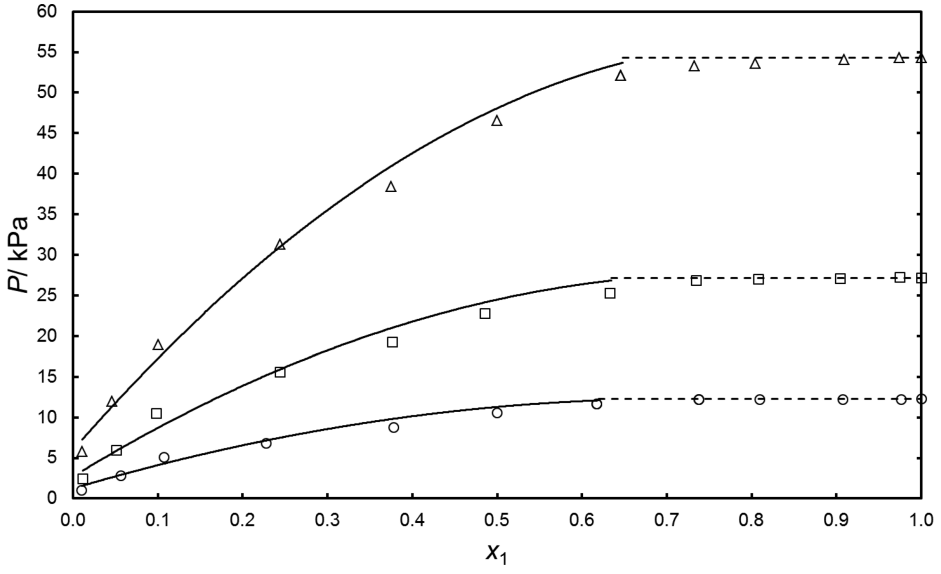

Figure 2. VLE data for binary system {toluene (1) + [4empy][Tf_2N] (2)} at several temperatures: ○, T = 323.2 K; □, T = 343.2 K; △, T = 363.2 K. Solid lines denote the NRTL adjustment, and dashed lines refer to constant pressure equal to pure component pressure from ref 30.

DOI: 10.1021/acs.jced.5b00650
J. Chem. Eng. Data 2016, 61, 458−465

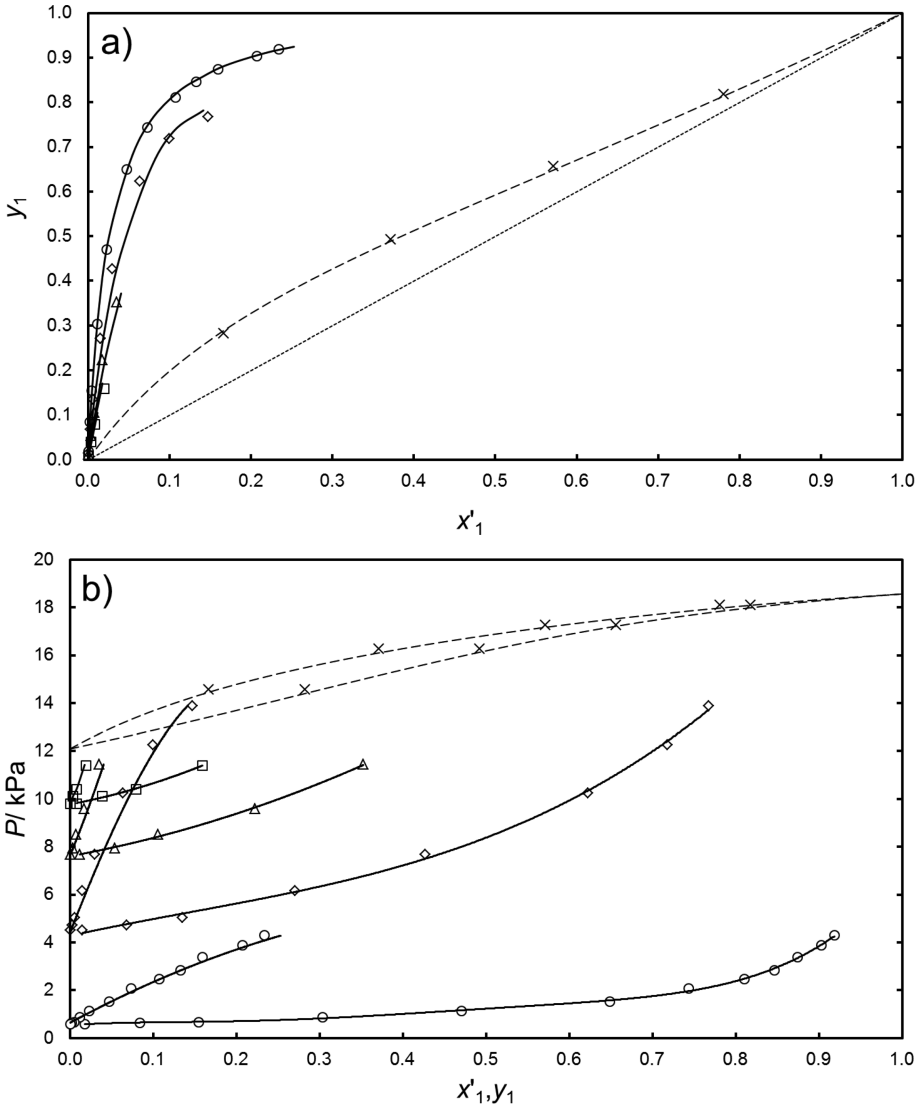

Figure 3. VLE data for ternary system {*n*-heptane (1) + toluene (2) + [4empy][Tf_2N] (3)} at T = 323.2 K. x'−y diagram (a) and x',y−P diagram (b). IL mole fraction (x_3): ○, $x_3 \approx 0.96$; ◇, $x_3 \approx 0.68$; △, $x_3 \approx 0.48$; □, $x_3 \approx 0.35$; ×, binary system of {*n*-heptane (1) + toluene (2)} from ref 20. Solid lines denote the NRTL adjustment, and dashed lines refer to VLE data from Aspen Plus Simulator Software Database at 323.2 K for the binary system of {*n*-heptane (1) + toluene (2)} from ref 32.

points included in the adjustment. The selection of the value of a is based on gathering compensate deviations for the liquid composition and pressure, in addition to minimizing the OF. The experimental data were fitted by using the Solver tool in the Microsoft Excel spreadsheet software. For all systems studied, the value of the nonrandomness parameter in the NRTL model (α) was set to 0.3 due to this is the most used value for α in the VLE correlation for systems containing ILs.[20−26] The binary interaction parameters obtained in the correlation are listed in Table 4, jointly to the composition deviations, Δx, and the pressure deviations, ΔP, both calculated as follows:

$$\Delta x = \frac{\sum_{i=1}^{i} |x_{i,\mathrm{calc}} - x_{i,\mathrm{exptl}}|}{N} \quad (5)$$

$$\Delta P = \frac{\sum_{i=1}^{i} |P_{i,\mathrm{calc}} - P_{i,\mathrm{exptl}}|}{N} \quad (6)$$

As reported in Table 4 and as can be seen in Figures 1 to 5, the NRTL model accurately describes the experimental values.

As can be observed in Figures 1 and 2, two well-differentiated zones define the phase equilibria of the binary mixtures. The first one includes the VLE data until the hydrocarbon maximum solubility in [4empy][Tf_2N] where the pressure is a function of the fraction of the hydrocarbon, whereas the second part corresponds to the two-liquid-phase zone. This last one shows constant pressure because hydrocarbons are not fully dissolved in the IL. The high affinity of the IL with the aromatics leads to a higher miscibility zone in the case of toluene than for *n*-heptane. Moreover, an increase in temperature seems to imply a slight increase of the solubility of both hydrocarbons in the IL. The solubility regions described at all temperatures are completely in agreement with the results previously obtained by our research group in the liquid−liquid equilibria for the {*n*-heptane + toluene + [4empy][Tf_2N]} system at 313.2 K.[3]

The VLE data for the ternary mixture {*n*-heptane + toluene + [4empy][Tf_2N]}at 323.2, 343.2, and 363.2 K are plotted in Figures 3 to 5. The most relevant effect associated with the use of [4empy][Tf_2N] as agent mass is the improvement in the *n*-heptane/toluene relative volatility in comparison with the VLE

DOI: 10.1021/acs.jced.5b00650
J. Chem. Eng. Data 2016, 61, 458−465

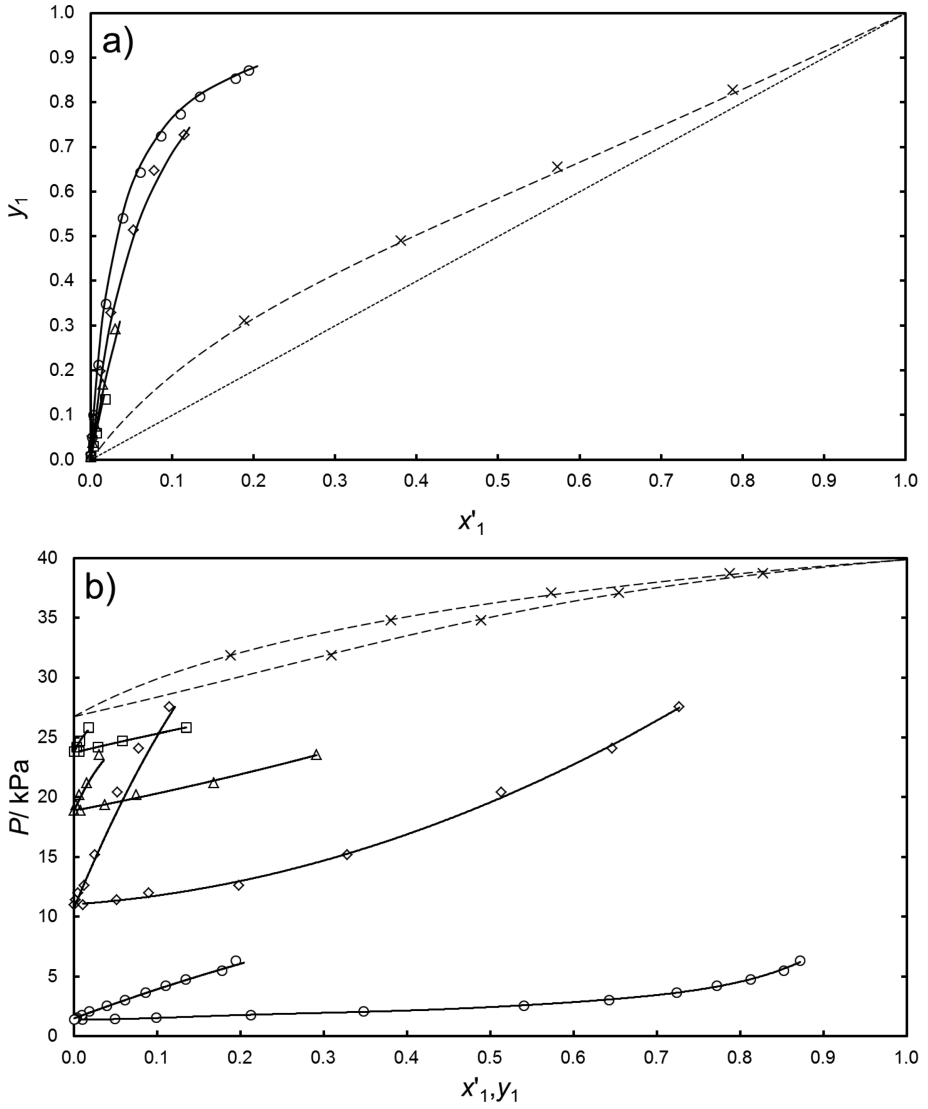

Figure 4. VLE data for ternary system {*n*-heptane (1) + toluene (2) + [4empy][Tf_2N] (3)} at T = 343.2 K. x'−y diagram (a) and x',y−P diagram (b). IL mole fraction (x_3): ○, $x_3 \approx 0.96$; ◇, $x_3 \approx 0.68$; △, $x_3 \approx 0.48$; □, $x_3 \approx 0.35$; ×, binary system of {*n*-heptane (1) + toluene (2)} from ref 20. Solid lines denote the NRTL adjustment and dashed lines refer to VLE data from Aspen Plus Simulator Software Database at 343.2 K for the binary system of {*n*-heptane (1) + toluene (2)} from ref 32.

of {*n*-heptane + toluene} mixture, which is higher at high IL concentrations. On the other hand, the temperature causes the opposite effect in the *n*-heptane relative volatility from toluene, being its highest value at the lowest temperature. The high value of the aliphatic relative volatility from the aromatic would imply a simplified purification unit in an alternative global process of extraction of aromatics from aliphatics using ILs instead of common organic solvents.

Finally, in order to evaluate the nature of the ILs in the phase equilibrium, the experimental VLE data obtained in this work for {*n*-heptane + toluene + [4empy][Tf_2N]} were compared with those previously published with [emim][DCA].[20] To the best of our knowledge, these two works are the only experimental researches focused on the VLE of an extract stream from an aromatic extraction process using ILs as solvents. The *n*-heptane relative volatilities from toluene with [4empy][Tf_2N] and [emim][DCA] systems as a function of temperature are shown in Figure 6. As can be seen, this parameter is higher using [emim][DCA] than [4empy][Tf_2N] at all temperatures. Although both ILs improve the *n*-heptane relative volatility from toluene, the better results were achieved using an IL with higher toluene/*n*-heptane selectivity, such as [emim][DCA]. This behavior was also found in the separation of ethylbenzene and styrene by using ILs.[27]

Taking into account the selective recovery of *n*-heptane from toluene and the negligible vapor pressures for ILs, it is possible to conclude that the use of this liquid salts in the aromatic extraction seems to be feasible. The recovery of alkanes seems to be more selective at low temperatures and employing ILs with higher aromatic/aliphatic selectivity in the liquid−liquid extraction.

4. CONCLUSIONS

Isothermal VLE determinations carried out here have been done for {*n*-heptane + [4empy][Tf_2N]}, {toluene + [4empy][Tf_2N]}, and {*n*-heptane + toluene + [4empy][Tf_2N]} systems at 323.2, 343.2, and 363.2 K.

The [4empy][Tf_2N] IL has been revealed as a good mass agent in the separation of *n*-heptane from toluene, specifically at low temperatures. However, the results obtained for

DOI: 10.1021/acs.jced.5b00650
J. Chem. Eng. Data 2016, 61, 458−465

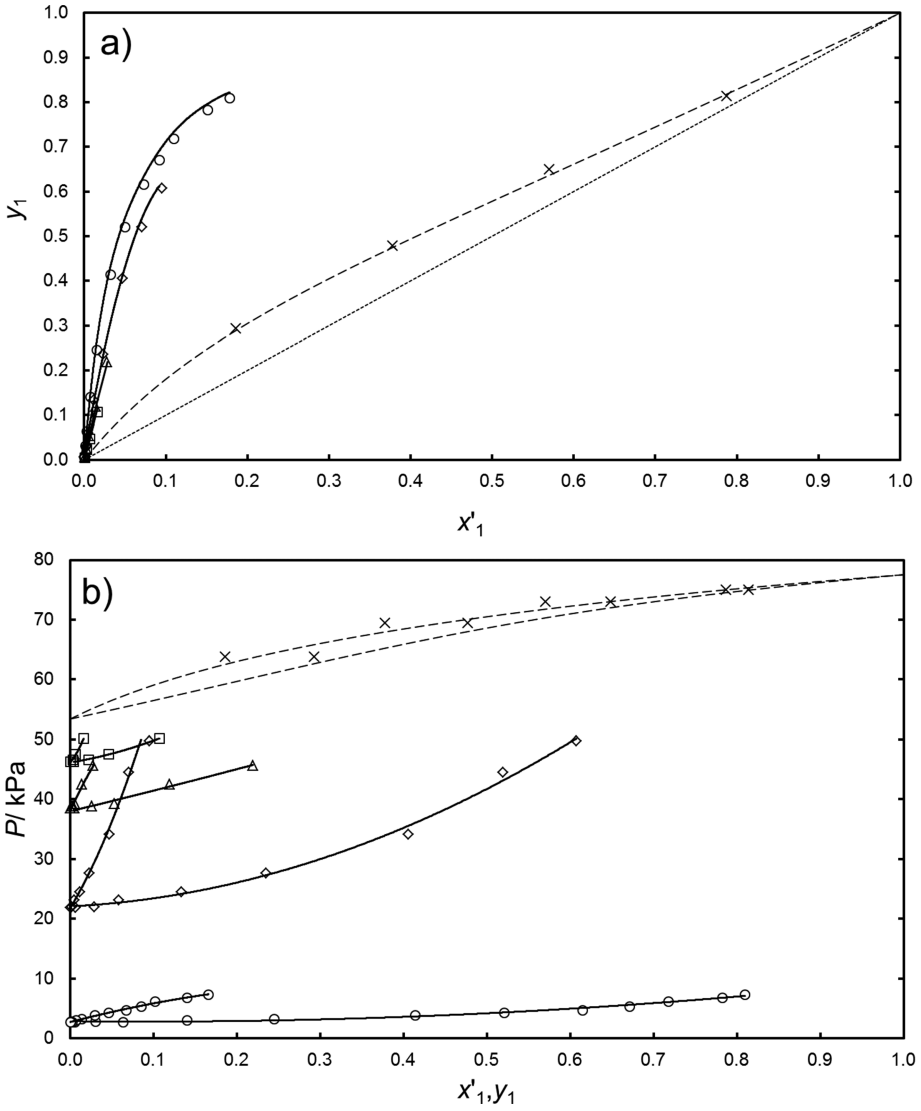

Figure 5. VLE data for ternary system {*n*-heptane (1) + toluene (2) + [4empy][Tf_2N] (3)} at $T = 363.2$ K. $x'-y$ diagram (a) and $x', y-P$ diagram (b). IL mole fraction (x_3): ○, $x_3 \approx 0.96$; ◇, $x_3 \approx 0.68$; △, $x_3 \approx 0.48$; □, $x_3 \approx 0.35$; ×, binary system of {*n*-heptane (1) + toluene (2)} from ref 20. Solid lines denote the NRTL adjustment, and dashed lines refer to VLE data from Aspen Plus Simulator Software Database at 363.2 K for the binary system of {*n*-heptane (1) + toluene (2)} from ref 32.

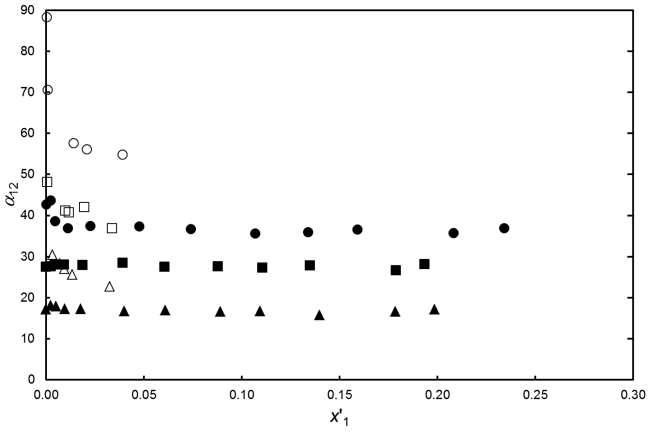

Figure 6. Values of *n*-heptane relative volatility from toluene (α_{12}) under the presence of ILs in {*n*-heptane (1) + toluene (2) + IL (3)} ternary systems for $x_3 \approx 0.98$ as a function of temperature: 323.2 K, circle; 343.2 K, square; 363.2 K, triangle. Full symbols represent the $\alpha_{1,2}$ values in presence of [4empy][Tf_2N], whereas empty symbols denote those achieved by using [emim][DCA], taken from ref 20.

[4empy][Tf_2N] showed lower *n*-heptane relative volatility from toluene than those obtained using ILs with a higher aromatic/aliphatic selectivity in the liquid−liquid extraction of aromatics from aliphatics such as dicyanamide-based ILs. In addition to these measurements, VLE data of binary and ternary systems have been properly correlated to NRTL thermodynamic model.

AUTHOR INFORMATION

Corresponding Author

*Tel.: +34 91 394 51 19. Fax: +34 91 394 42 43. E-mail: jgarcia@quim.ucm.es.

Funding

Authors are grateful to the Ministerio de Economía y Competitividad (MINECO) of Spain and the Comunidad de Madrid for financial support of Projects CTQ2011-23533 and S2013/MAE-2800, respectively. P.N. also thanks MINECO for awarding him an FPI grant (Reference BES-2012-052312). Marcos Larriba thanks Ministerio de Educación, Cultura y Deporte of Spain for awarding him an FPU grant (Reference AP2010-0318). E.J.G. also thanks MINECO for awarding him a Juan de la Cierva Contract (Reference JCI-2012-12005).

DOI: 10.1021/acs.jced.5b00650
J. Chem. Eng. Data 2016, 61, 458−465

Notes

The authors declare no competing financial interest.

REFERENCES

(1) Rogers, R. D.; Seddon, K. R. Ionic Liquids-Solvents of the Future? *Science* **2003**, *302*, 792.

(2) Plechkova, N. V.; Seddon, K. R. Applications of Ionic Liquids in the Chemical Industry. *Chem. Soc. Rev.* **2008**, *37*, 123−150.

(3) García, J.; García, S.; Torrecilla, J. S.; Rodríguez, F. Solvent Extraction of Toluene from Heptane with the Ionic Liquids N-Ethylpyridinium Bis(trifluoromethylsulfonyl)imide and z-Methyl-N-ethylpyridinium Bis(trifluoromethylsulfonyl)imide (z = 2, 3, or 4) at T = 313.2 K. *J. Chem. Eng. Data* **2010**, *55*, 4937−4942.

(4) Larriba, M.; Navarro, P.; García, J.; Rodríguez, F. Liquid-liquid extraction of toluene from heptane using [emim][DCA], [bmim]-[DCA], and [emim][TCM] ionic liquids. *Ind. Eng. Chem. Res.* **2013**, *52*, 2714−2720.

(5) Corderí, S.; Gómez, E.; Calvar, N.; Domínguez, A. Measurement and Correlation of Liquid-Liquid Equilibria for Ternary and Quaternary Systems of Heptane, Cyclohexane, Toluene, and [EMim][OAc] at 298.15 K. *Ind. Eng. Chem. Res.* **2014**, *53*, 9471−9477.

(6) Alonso, L.; Arce, A.; Francisco, M.; Soto, A. Solvent extraction of thiophene from n-alkanes (C7, C12, and C16) using the ionic liquid $[C_8mim][BF_4]$. *J. Chem. Thermodyn.* **2008**, *40*, 966−972.

(7) Marciniak, A.; Krolikowski, M. Ternary (Liquid + liquid) Equilibria of {Trifluorotris(perfluoroethyl)phosphate based Ionic Liquids + Thiophene + Heptane}. *J. Chem. Thermodyn.* **2012**, *49*, 154−158.

(8) Meindersma, G. W.; Podt, A. J. G.; de Haan, A. B. Selection of Ionic Liquids for the Extraction of Aromatic Hydrocarbons from Aromatic/aliphatic Mixtures. *Fuel Process. Technol.* **2005**, *87*, 59−70.

(9) Meindersma, G. W.; Hansmeier, A. R.; de Haan, A. B. Ionic liquids for aromatics extraction. Present status and future outlook. *Ind. Eng. Chem. Res.* **2010**, *49*, 7530−7540.

(10) Meindersma, G. W.; de Haan, A. B. Cyano-containing ionic liquids for the extraction of aromatic hydrocarbons from an aromatic/aliphatic mixture. *Sci. China: Chem.* **2012**, *55*, 1488−1499.

(11) García, S.; García, J.; Larriba, M.; Torrecilla, J. S.; Rodríguez, F. Sulfonate-based ionic liquids in the liquid-liquid extraction of aromatic hydrocarbons. *J. Chem. Eng. Data* **2011**, *56*, 3188−3193.

(12) Meindersma, G. W.; de Haan, A. B. Conceptual process design for aromatic/aliphatic separation with ionic liquids. *Chem. Eng. Res. Des.* **2008**, *86*, 745−752.

(13) García, S.; Larriba, M.; García, J.; Torrecilla, J. S.; Rodríguez, F. 1-Alkyl-2,3-dimethylimidazolium Bis(trifluoromethylsulfonyl)imide ionic liquids for the liquid−liquid extraction of toluene from heptane. *J. Chem. Eng. Data* **2011**, *56*, 3468−3474.

(14) Hansmeier, A. R.; Minoves Ruiz, M.; Meindersma, G. W.; de Haan, A. B. Liquid−liquid Equilibria for the Three Ternary Systems (3-Methyl-N-butylpyridinium Dicyanamide + Toluene + Heptane), (1-Butyl-3-Methylimidazolium Dicyanamide + Toluene + Heptane), and (1-Butyl-3-Methylimidazolium Thiocyanate + Toluene + Heptane) at T = (313.15 and 348.15) K and p = 0.1 MPa. *J. Chem. Eng. Data* **2010**, *55*, 708−713.

(15) Navarro, P.; Larriba, M.; Rojo, E.; García, J.; Rodríguez, F. Thermal properties of cyano-based ionic liquids. *J. Chem. Eng. Data* **2013**, *58*, 2187−2193.

(16) Seeberger, A.; Andresen, A. K.; Jess, A. Prediction of long-term stability of ionic liquids at elevated temperatures by means of non-isothermal thermogravimetrical analysis. *Phys. Chem. Chem. Phys.* **2009**, *11*, 9375−9381.

(17) Aparicio, S.; Atilhan, M.; Karadas, F. Thermophysical Properties of Pure Ionic Liquids: Review of Present Situation. *Ind. Eng. Chem. Res.* **2010**, *49*, 9580−9595.

(18) Larriba, M.; García, S.; Navarro, P.; García, J.; Rodríguez, F. Physical Properties of N−butylpyridinium Tetrafluoroborate and N−butylpyridinium Bis(trifluoromethylsulfonyl)imide Binary Ionic Liquid Mixtures. *J. Chem. Eng. Data* **2012**, *57*, 1318−1325.

(19) Navarro, P.; Larriba, M.; García, J.; Rodríguez, F. Thermal stability, specific heats, and surface tensions of {[emim][DCA] + [4empy][Tf_2N]} ionic liquid mixtures. *J. Chem. Thermodyn.* **2014**, *76*, 152−160.

(20) Navarro, P.; Larriba, M.; García, J.; González, E. J.; Rodríguez, F. Vapor-liquid equilibria of {*n*-heptane + toluene + [emim][DCA]} system using headspace gas chromatography. *Fluid Phase Equilib.* **2015**, *387*, 209−216.

(21) Mokhtarani, B.; Gmehling, J. Vapour + liquid) equilibria of ternary systems with ionic liquids using headspace gas chromatography. *J. Chem. Thermodyn.* **2010**, *42*, 1036−1038.

(22) Mokhtarani, B.; Valialahi, L.; Heidar, K. T.; Mortaheb, H. R.; Sharifi, A.; Mirzaei, M. Experimental study on vapor-liquid equilibria of ternary systems of hydrocarbons/ionic liquid using headspace gas chromatography. *J. Chem. Thermodyn.* **2012**, *51*, 77−81.

(23) Orchillés, A. V.; Miguel, J. P.; González-Alfaro, V.; Vercher, E.; Martínez-Andreu, A. 1-Ethyl-3-methylimidazolium Dicyanamide as a Very Efficient Entrainer for the Extractive Distillation of the Acetone + Methanol System. *J. Chem. Eng. Data* **2012**, *57*, 394−399.

(24) Andreatta, A. E.; Arce, A.; Rodil, E.; Soto, A. Physical properties and phase equilibria of the system isopropyl acetate + isopropanol + 1-octyl-3-methyl-imidazolium bis(trifluoromethylsulfonyl)imide. *Fluid Phase Equilib.* **2010**, *287*, 84−94.

(25) Ge, Y.; Zhang, L.; Yuan, X.; Geng, W.; Ji, J. Selection of ionic liquids as entrainers for the separation of (water + ethanol). *J. Chem. Thermodyn.* **2008**, *40*, 1248−1252.

(26) Zhang, L.; Han, J.; Deng, D.; Ji, J. Selection of ionic liquids as entrainers for separation of water + 2-propanol. *Fluid Phase Equilib.* **2007**, *255*, 179−185.

(27) Jongmans, M. T. G.; Schuur, B.; de Haan, A. B. Ionic Liquid Screening for Ethylbenzene/Styrene Separation by Extractive Distillation. *Ind. Eng. Chem. Res.* **2011**, *50*, 10800−10810.

(28) Renon, H.; Prausnitz, J. M. Local compositions in thermodynamic excess functions for liquid mixtures. *AIChE J.* **1968**, *14*, 135−144.

(29) Kolb, B.; Ettre, L. S. *Static Headspace-Gas Chromatography: Theory and Practice*; Wiley-VCH: New York, 1997.

(30) Perry, R. H.; Green, D. W.; Maloney, J. O. *Perry's Chemical Engineers' Handbook*; McGraw-Hill: New York, 1999.

(31) Jiqin, Z.; Jian, C.; Chengyue, L.; Weiyang, F. Study on the separation of 1-hexene and trans-3-hexene using ionic liquids. *Fluid Phase Equilib.* **2006**, *247*, 102−106.

(32) *Aspen Plus*, Version 7.1, Aspen Technology: Burlington, MA, 2004.

DOI: 10.1021/acs.jced.5b00650
J. Chem. Eng. Data 2016, 61, 458−465

J. Chem. Thermodynamics 96 (2016) 134–142

Contents lists available at ScienceDirect

J. Chem. Thermodynamics

journal homepage: www.elsevier.com/locate/jct

Selective recovery of aliphatics from aromatics in the presence of the {[4empy][Tf_2N] + [emim][DCA]} ionic liquid mixture

Pablo Navarro, Marcos Larriba, Julián García *, Emilio J. González, Francisco Rodríguez

Department of Chemical Engineering, Complutense University of Madrid, E-28040 Madrid, Spain

ARTICLE INFO

Article history:
Received 4 September 2015
Received in revised form 30 November 2015
Accepted 30 December 2015
Available online 9 January 2016

Keywords:
Ionic liquids mixtures
Aromatic/aliphatic separation
(Vapor + liquid) equilibria
Head-space gas chromatography

ABSTRACT

Lately, the use of binary mixtures of ionic liquids (ILs) has been revealed as an interesting election in order to find alternative solvents in the liquid–liquid extraction of aromatics from aliphatics. Specifically, the {[4empy][Tf_2N] + [emim][DCA]} mixture has exhibited both aromatic selectivity and distribution ratios higher than sulfolane in the BTEX separation from several gasolines and naphthas. Moreover, its density and viscosity are comparable with those showed by sulfolane, and its thermal stability is also quite high. However, the absence of (vapor + liquid) equilibria (VLE) studies concerning aliphatics/aromatics mixtures in ILs has not led to propose a recovery section to selectively separate aliphatics, aromatics, and the IL-based solvent. For that reason, the aim of this work is to study the VLE of several {aliphatic + aromatic} systems in the presence of {[4empy][Tf_2N] + [emim][DCA]} mixture over the whole composition range of the IL mixture and also at several temperatures. The results showed high aliphatic relative volatility from all aromatics, fact that would facilitate the selective separation of aliphatics, BTEX, and ILs. On the other hand, the Yalkowsky–Roseman log-linear model was successfully apply to predict the phase behavior of {aliphatic + aromatic + [4empy][Tf_2N] + [emim][DCA]} systems.

1. Introduction

The current interest about the use of ionic liquids (ILs) as extraction solvents is mainly caused by their high extraction performance. However, very few pure ILs has simultaneously showed adequate extractive and physical properties [1–15]. Specifically, several ILs have shown high aromatic/aliphatic selectivity values and low viscosities, as dicyanamide-based ILs, whereas their densities and aromatic distribution ratios were low in comparison with the sulfolane values. On the other hand, there are ILs with high aromatic distribution ratios and densities, as bis(trifluoromethyl)sulfonylimide-based ionic liquids, which have shown quite high viscosities and low aromatic/aliphatic selectivity values. To solve this drawback, lastly, the strategy of mixing ILs is been used to tune extractive and physical properties [16–32]. As a result of using binary mixtures of ILs, the extractive and physical properties of the solvent are dependent on the IL mixture composition. Then, it is possible to choose an IL mixture composition that implies the best combination between extractive and physical properties.

The selection of the pure ILs that will form a mixture should be done to find an intermediate behavior. In this work, the 1-ethyl-3-methylimidazolium dicyanamide ([emim][DCA]) IL was chosen due to its high aromatic/aliphatic selectivities and low viscosity, whereas 1-ethyl-4-methylpyridinium bis(trifluoromethyl sulfonyl)imide ([4empy][Tf_2N]) was selected because of its high aromatic distribution ratios and its high density. Taking into account only extractive and physical properties, the mixture composition was optimized to a 0.7 mol fraction of [emim][DCA] [17]. However, the (vapor + liquid) equilibria (VLE) data of {aliphatics + aromatics + [4empy][Tf_2N] + [emim][DCA]} systems are not available; then, it is not possible to confirm this mixture composition as the best for the global extraction process neither the feasibility of the recovery section with a {[4empy][Tf_2N] (0.3) + [emim][DCA] (0.7)} IL-based solvent.

Because of that, the aim of this work is to determine the VLE for pseudo-ternary mixtures containing toluene with (*n*-hexane, *n*-heptane, *n*-octane, cyclohexane, or 2,3-dimethylpentane) and the *n*-heptane with (benzene, *p*-xylene, or ethylbenzene) in {[4empy][Tf_2N] + [emim][DCA]} mixtures. The experimental VLE was carried out over the whole composition range of the IL mixture at $T = (323.2, 343.2, \text{and } 363.2)$ K. In all cases, the hydrocarbon mixtures were prepared with a mass fraction of the aliphatic compound equal to 10 wt.%, whereas the IL mixture was selected to a 99 wt.% in the feed composition for all experiments.

* Corresponding author. Tel.: +34 91 394 51 19; fax: +34 91 394 42 43.
E-mail address: jgarcia@quim.ucm.es (J. García).

http://dx.doi.org/10.1016/j.jct.2015.12.033
0021-9614/

On the other hand, the Yalkowsky and Roseman log-linear mixing rule was apply here to predict the VLE behavior of the hydrocarbons in the IL mixtures from the VLE data for the pure ILs constituting the mixture [33]. This point is interesting because it could help to reduce experimental efforts in future works involving binary IL mixtures in (vapor + liquid) systems.

The IL mixture considerably increased the values of the aliphatic relative volatilities from aromatics for all the systems reported in this work, which comes to confirm the feasibility of the recovery section. For each system, the best results were obtained at the lowest temperature, 323.2 K, and with the highest concentration of [emim][DCA] in the IL mixture, trends in agreement with the works that can be found elsewhere [34–36]. Because of that, the {[4empy][Tf_2N] (0.3) + [emim][DCA] (0.7)} mixture could be considered as a potential aromatic solvent taking also into account VLE data.

2. Experimental

2.1. Chemicals

The ILs [emim][DCA] and [4empy][Tf_2N] were acquired from Iolitec GmbH. [emim][DCA] had a mass fraction purity of 0.98 and its water content and halide content were 937 ppm and <0.02 in mass fraction, respectively, whereas [4empy][Tf_2N] had a mass fraction purity of 0.99, a water content of 89 ppm, and a halide content <100 ppm. Both ILs were used as received without further purifications. They were kept and handled using a desiccator filled with silica gel and a glove box filled with dry nitrogen, respectively, in order to avoid water absorption in the ILs. Aliphatic and aromatic hydrocarbons studied in this work were purchased from Sigma–Aldrich with 0.99 mass fraction purities. All chemical specifications are listed in table 1.

2.2. VLE preparation and measurement

The VLE was determined using a static technique combining an Agilent headspace 7697A injector and an Agilent gas chromatograph 7890A. A detailed description of the equipments used in this work can be found in our previous study [35].

All mixtures of ILs and hydrocarbons were made by mass, employing a Mettler Toledo XS205 balance with a precision of $1{\cdot}10^{-5}$ g. The binary mixtures of ILs were done under a controlled dry atmosphere then mixing with a Labnet Vortex Mixer. The feed of the VLE experiments was prepared adding first the IL or the IL mixture and then the hydrocarbon mixture just before hermetically closing the vial.

In our last work, [emim][DCA] has been used with slightly different specifications in anion and cation purities and in water and halide contents [35]. Because of that, the three {*n*-heptane + toluene + [emim][DCA]} VLE points have been repeated for this work in order to correctly analyze the behavior of ionic liquid mixtures and study the effect of impurities [37].

After reaching the equilibrium, the vapor composition was directly determined from the GC analysis of the vapor phase as can be found elsewhere [35]. Once the compositions of the vapor phase have been obtained, the composition of the liquid phase was recalculated as follows:

$$x_i = \frac{z_i \cdot F - (P_i \cdot V_G/R \cdot T)}{\sum_{i=1}^{3}(z_i \cdot F - (P_i \cdot V_G/R \cdot T))}, \quad (1)$$

where x_i is the mole fraction of the component i in the liquid phase, z_i is the mole fraction of the component i in the VLE feed, F denotes the molar amount of the feed, V_G refers to the vapor volume of the vial (19.0 mL), and P_i is the partial pressure of the component i calculated as follows:

$$P_i = \frac{A_i}{A_i^0} P_i^0, \quad (2)$$

where A_i are the peak areas of the hydrocarbons, whereas P_i^0 and A_i^0 are the vapor pressures and the peak areas of the pure hydrocarbons in the same conditions than those used to reach the equilibrium, respectively.

3. Results and discussion

In this work the VLE data were determined for the (*n*-hexane, *n*-heptane, *n*-octane, cyclohexane, or 2,3-dimethylpentane) + toluene + {[4empy][Tf_2N] + [emim][DCA]} and the *n*-heptane + (benzene, *p*-xylene, or ethylbenzene) + {[4empy][Tf_2N] + [emim][DCA]} pseudoternary systems. The VLE was studied at T = (323.2, 343.2, and 363.2) K and using (0.0, 0.2, 0.4, 0.6, 0.8, and 1.0) mol fractions of [emim][DCA] ($\phi_{[emim][DCA]}$) in the {[4empy][Tf_2N] + [emim][DCA]} binary mixtures. The VLE data are summarized in tables 2 and 3. The aliphatic relative volatility from aromatics ($\alpha_{1,2}$) was calculated from the VLE data as follows:

$$\alpha_{1,2} = \frac{K_1}{K_2} = \frac{y_1/x_1}{y_2/x_2}, \quad (3)$$

where subscript 1 represents an aliphatic compound and subscript 2 an aromatic hydrocarbon. The aliphatic relative volatilities from aromatics obtained in this work are also included in tables 2 and 3 and graphically represented at several temperatures in figures 1 and 2 as a function of [emim][DCA] mole fraction.

TABLE 1
Specifications of chemicals.

Chemical	Supplier	Mass fraction purity	Analysis method
[emim][DCA]	Iolitec GmbH	0.98	NMR[a], IC[b]
[4empy][Tf_2N]	Iolitec GmbH	0.99	NMR[a], IC[b]
n-Hexane	Sigma–Aldrich	0.995	GC[c]
n-Heptane	Sigma–Aldrich	0.997	GC[c]
n-Octane	Sigma–Aldrich	0.990	GC[c]
Cyclohexane	Sigma–Aldrich	0.995	GC[c]
2,3-Dimethylpentane	Sigma–Aldrich	0.990	GC[c]
Benzene	Sigma–Aldrich	0.995	GC[c]
Toluene	Sigma–Aldrich	0.995	GC[c]
p-Xylene	Sigma–Aldrich	0.990	GC[c]
Ethylbenzene	Sigma–Aldrich	0.998	GC[c]

[a] Nuclear magnetic resonance.
[b] Ion chromatography.
[c] Gas chromatography.

TABLE 2
VLE[a] of *n*-heptane/*n*-heptane/*n*-octane/cyclohexane/2,3-dimethylpentane (1) + toluene (2) + [4empy][Tf_2N] (3) + [emim][DCA] (4) at several temperatures (T). Mole fraction of [emim][DCA] in the IL mixture ($\phi_{[emim][DCA]}$), overall IL mixture liquid mole fraction (x_{3+4}), IL-free mole fraction of alkane in the liquid phase (x'_1), alkane vapor mole fraction (y_1), total pressure (P), and alkane/aromatic relative volatility ($\alpha_{1,2}$).

$\phi_{[emim][DCA]}$	x_{3+4}	x'_1	y_1	P/kPa	$\alpha_{1,2}$
n-Hexane (1) + toluene (2) + [4empy][Tf_2N] (3) + [emim][DCA] (4)					
T/K = 323.2					
0.00	0.9854	0.0460	0.6837	1.55	44.8
0.20	0.9691	0.0414	0.6732	1.86	47.7
0.40	0.9698	0.0369	0.6681	2.15	52.5
0.60	0.9733	0.0312	0.6621	2.32	60.8
0.80	0.9796	0.0246	0.6412	2.23	70.9
1.00	0.9833	0.0179	0.6084	2.41	85.4
T/K = 343.2					
0.00	0.9855	0.0438	0.5344	2.33	25.1
0.20	0.9710	0.0400	0.5320	2.50	27.3
0.40	0.9730	0.0353	0.5201	2.82	29.6
0.60	0.9761	0.0300	0.4993	3.12	32.2
0.80	0.9797	0.0244	0.4787	3.37	36.7
1.00	0.9855	0.0189	0.4514	3.42	42.7
T/K = 363.2					
0.00	0.9855	0.0407	0.3972	3.68	15.5
0.20	0.9704	0.0387	0.4034	3.93	16.8
0.40	0.9743	0.0341	0.3889	4.21	18.0
0.60	0.9776	0.0300	0.3856	4.33	20.3
0.80	0.9808	0.0250	0.3726	4.68	23.2
1.00	0.9844	0.0193	0.3454	5.12	26.8
n-Heptane (1) + toluene (2) + [4empy][Tf_2N] (3) + [emim][DCA] (4)					
T/K = 323.2					
0.00	0.9821	0.0462	0.6519	1.35	38.7
0.20	0.9739	0.0423	0.6447	1.37	41.1
0.40	0.9749	0.0380	0.6401	1.58	45.0
0.60	0.9782	0.0330	0.6204	1.68	47.9
0.80	0.9806	0.0282	0.6122	1.89	54.4
1.00	0.9857	0.0233	0.5949	2.21	61.6
T/K = 343.2					
0.00	0.9818	0.0414	0.5182	2.10	24.9
0.20	0.9718	0.0385	0.5023	2.26	25.2
0.40	0.9734	0.0345	0.4920	2.60	27.1
0.60	0.9775	0.0297	0.4836	2.63	30.6
0.80	0.9791	0.0243	0.4603	3.27	34.2
1.00	0.9863	0.0196	0.4330	3.36	38.2
T/K = 363.2					
0.00	0.9823	0.0408	0.3901	3.17	15.0
0.20	0.9744	0.0365	0.3776	3.22	16.0
0.40	0.9762	0.0336	0.3648	3.60	16.5
0.60	0.9791	0.0279	0.3489	4.05	18.7
0.80	0.9836	0.0249	0.3342	4.05	19.7
1.00	0.9848	0.0209	0.3287	4.98	22.9
n-Octane (1) + toluene (2) + [4empy][Tf_2N] (3) + [emim][DCA] (4)					
T/K = 323.2					
0.00	0.9837	0.0479	0.5423	1.28	23.6
0.20	0.9679	0.0454	0.5546	1.37	26.2
0.40	0.9738	0.0389	0.5402	1.49	29.0
0.60	0.9735	0.0338	0.5393	1.88	33.5
0.80	0.9765	0.0284	0.5353	2.09	39.4
1.00	0.9798	0.0219	0.5359	2.32	51.6
T/K = 343.2					
0.00	0.9843	0.0411	0.4409	1.93	18.4
0.20	0.9689	0.0369	0.4465	2.26	21.1
0.40	0.9717	0.0328	0.4401	2.51	23.2
0.60	0.9764	0.0282	0.4295	2.62	25.9
0.80	0.9777	0.0229	0.4100	3.22	29.7
1.00	0.9808	0.0171	0.3856	3.54	36.1
T/K = 363.2					
0.00	0.9850	0.0345	0.3473	3.21	14.9
0.20	0.9708	0.0316	0.3362	3.60	15.5
0.40	0.9733	0.0294	0.3306	3.85	16.3
0.60	0.9761	0.0262	0.3225	4.20	17.7
0.80	0.9791	0.0221	0.3070	4.69	19.6
1.00	0.9814	0.0174	0.2784	5.71	21.8

TABLE 2 (*continued*)

$\phi_{[emim][DCA]}$	x_{3+4}	x'_1	y_1	P/kPa	$\alpha_{1,2}$
Cyclohexane (1) + toluene (2) + [4empy][Tf_2N] (3) + [emim][DCA] (4)					
T/K = 323.2					
0.00	0.9822	0.0674	0.6061	1.39	21.3
0.20	0.9671	0.0650	0.6011	1.47	21.7
0.40	0.9689	0.0620	0.6021	1.65	22.9
0.60	0.9718	0.0577	0.5900	1.86	23.5
0.80	0.9772	0.0527	0.5779	1.91	24.6
1.00	0.9803	0.0448	0.5488	2.32	25.9
T/K = 343.2					
0.00	0.9823	0.0629	0.4702	2.32	13.2
0.20	0.9652	0.0599	0.4620	2.60	13.5
0.40	0.9696	0.0584	0.4573	2.60	13.6
0.60	0.9681	0.0551	0.4500	3.31	13.9
0.80	0.9771	0.0509	0.4273	3.10	13.9
1.00	0.9816	0.0432	0.3971	3.59	14.6
T/K = 363.2					
0.00	0.9822	0.0614	0.3601	3.77	8.6
0.20	0.9677	0.0583	0.3534	3.79	8.8
0.40	0.9712	0.0563	0.3442	4.02	8.8
0.60	0.9747	0.0540	0.3375	4.17	8.8
0.80	0.9763	0.0509	0.3184	5.12	8.9
1.00	0.9814	0.0449	0.2990	5.81	9.1
2,3-Dimethylpentane (1) + toluene (2) + [4empy][Tf_2N] (3) + [emim][DCA] (4)					
T/K = 323.2					
0.00	0.9825	0.0425	0.6456	1.62	41.0
0.20	0.9671	0.0393	0.6428	1.67	44.0
0.40	0.9688	0.0340	0.6327	1.98	48.9
0.60	0.9755	0.0277	0.6108	2.00	55.1
0.80	0.9762	0.0229	0.6073	2.34	66.0
1.00	0.9811	0.0164	0.5777	2.45	82.0
T/K = 343.2					
0.00	0.9860	0.0366	0.5023	2.12	26.6
0.20	0.9661	0.0339	0.4971	2.77	28.2
0.40	0.9704	0.0311	0.4891	2.85	29.8
0.60	0.9718	0.0274	0.4753	3.29	32.2
0.80	0.9775	0.0233	0.4548	3.31	35.0
1.00	0.9823	0.0172	0.4171	3.59	40.9
T/K = 363.2					
0.00	0.9843	0.0360	0.3840	3.72	16.7
0.20	0.9723	0.0342	0.3755	3.40	17.0
0.40	0.9696	0.0311	0.3653	4.44	17.9
0.60	0.9746	0.0274	0.3601	4.46	20.0
0.80	0.9764	0.0233	0.3391	5.40	21.5
1.00	0.9825	0.0183	0.3110	5.73	24.2

[a] Standard uncertainty (u) are u(x) = 0.0002, u(x') = 0.0004, u(y) = 0.0010, u(P) = 0.1 kPa, and u(T) = 0.1 K.

3.1. Temperature and IL mixture composition effects on the aliphatic/aromatic relative volatilities

As can be seen in figures 1 and 2, the values of the aliphatic relative volatility from aromatics calculated for all pseudoternary systems studied in this work have shown an important increase in comparison with the same hydrocarbon systems without the IL mixture summarized in table 4. The higher values for the aliphatic relative volatility from aromatic in all systems were achieved at the lowest temperature, 323.2 K, and with the highest mole fraction of [emim][DCA] in the {[4empy][Tf_2N] + [emim][DCA]} mixture. The [emim][DCA] has shown quite higher values of aromatic/aliphatic selectivity than those gathered with [4empy][Tf_2N] in the liquid–liquid extraction of aromatics from aliphatics [17]. Therefore, the use of ILs with high aromatic/aliphatic selectivities in liquid–liquid extraction seems to show higher aliphatic/aromatic relative volatilities in VLE. The temperature dependence was just observed elsewhere [35], whereas the relation between the aromatic/aliphatic selectivity in liquid–liquid extraction and the aliphatic/aromatic relative volatility in VLE was also found in related studies [34]. The higher aliphatic/aromatic relative volatilities obtained at the higher mole fractions of [emim][DCA] used in this work are related to the lower capacity and more aromatic selectivity associated to [emim][DCA] in comparison with those of [4empy][Tf_2N]. This means that the aliphatic compound presence is greater in the vapor phase and lower in the liquid phase when [emim][DCA] instead of [4empy][Tf_2N] is present. Therefore, the alkane K-value highly increase in the presence of [emim][DCA] and, consequently, the aliphatic/relative relative volatility.

Taking into account the VLE data obtained in this work and the extractive and physical properties just available in the literature [17], it is possible to claim that the {[4empy][Tf_2N] (0.3) + [emim][DCA] (0.7)} mixture is a potential solvent in the aromatic extraction. Moreover, the high aliphatic relative volatilities from aromatic suggest a selective recovery of the aliphatic hydrocarbons from the extract stream obtained in the liquid–liquid extraction of aromatics from aliphatics using ILs [39]. After that, the separation of the aromatic hydrocarbons from the IL-based solvent would be feasible as a result of the negligible vapor pressure of ILs.

TABLE 3
VLE[a] of *n*-heptane (1) + benzene/*p*-xylene/ethylbenzene (2) + [4empy][Tf_2N] (3) + [emim][DCA] (4) at several temperatures (T). Mole fraction of [emim][DCA] in the IL mixture ($\phi_{[emim][DCA]}$), overall IL mixture liquid mole fraction (x_{3+4}), IL-free mole fraction of alkane in the liquid phase (x'_1), alkane vapor mole fraction (y_1), total pressure (P), and alkane/aromatic relative volatility ($\alpha_{1,2}$).

$\phi_{[emim][DCA]}$	x_{3+4}	x'_1	y_1	P/kPa	$\alpha_{1,2}$
n-Heptane (1) + benzene (2) + [4empy][Tf_2N] (3) + [emim][DCA] (4)					
T/K = 323.2					
0.00	0.9834	0.0433	0.4800	1.69	20.4
0.20	0.9706	0.0390	0.4787	1.73	22.6
0.40	0.9695	0.0359	0.4859	2.09	25.4
0.60	0.9750	0.0304	0.4860	2.12	30.2
0.80	0.9778	0.0245	0.4808	2.39	36.9
1.00	0.9785	0.0184	0.4691	2.93	47.1
T/K = 343.2					
0.00	0.9858	0.0355	0.3869	2.54	17.1
0.20	0.9706	0.0329	0.3823	2.77	18.2
0.40	0.9746	0.0305	0.3776	2.82	19.3
0.60	0.9772	0.0265	0.3745	3.10	22.0
0.80	0.9801	0.0222	0.3551	3.45	24.3
1.00	0.9825	0.0181	0.3419	3.92	28.2
T/K = 363.2					
0.00	0.9861	0.0341	0.2924	4.15	11.7
0.20	0.9719	0.0321	0.2885	4.14	12.2
0.40	0.9757	0.0307	0.2879	4.06	12.8
0.60	0.9776	0.0273	0.2821	4.57	14.0
0.80	0.9818	0.0236	0.2663	4.78	15.0
1.00	0.9851	0.0194	0.2543	5.38	17.2
n-Heptane (1) + p-xylene (2) + [4empy][Tf_2N] (3) + [emim][DCA] (4)					
T/K = 323.2					
0.00	0.9839	0.0551	0.8009	1.27	69.0
0.20	0.9708	0.0510	0.7992	1.32	74.1
0.40	0.9731	0.0455	0.7890	1.49	78.4
0.60	0.9724	0.0389	0.7781	1.91	86.6
0.80	0.9774	0.0323	0.7674	1.95	98.8
1.00	0.9811	0.0247	0.7481	2.05	117.3
T/K = 343.2					
0.00	0.9865	0.0459	0.6467	1.77	38.0
0.20	0.9716	0.0425	0.6507	1.99	42.0
0.40	0.9761	0.0386	0.6388	2.00	44.0
0.60	0.9790	0.0337	0.6288	2.15	48.6
0.80	0.9801	0.0278	0.6049	2.57	53.5
1.00	0.9813	0.0212	0.5747	3.11	62.4
T/K = 363.2					
0.00	0.9863	0.0448	0.4946	2.67	20.9
0.20	0.9722	0.0417	0.4826	3.01	21.4
0.40	0.9764	0.0380	0.4835	2.97	23.7
0.60	0.9756	0.0337	0.4668	3.81	25.1
0.80	0.9806	0.0279	0.4465	3.88	28.1
1.00	0.9812	0.0211	0.3963	5.16	30.5
n-Heptane (1) + ethylbenzene (2) + [4empy][Tf_2N] (3) + [emim][DCA] (4)					
T/K = 323.2					
0.00	0.9846	0.0560	0.7822	1.22	60.5
0.20	0.9679	0.0513	0.7784	1.49	65.0
0.40	0.9730	0.0439	0.7701	1.58	73.0
0.60	0.9771	0.0386	0.7664	1.61	81.7
0.80	0.9785	0.0305	0.7463	1.96	93.5
1.00	0.9790	0.0230	0.7285	2.41	114.0
T/K = 343.2					
0.00	0.9847	0.0476	0.6318	1.95	34.3
0.20	0.9697	0.0432	0.6241	2.23	36.8
0.40	0.9701	0.0394	0.6141	2.61	38.8
0.60	0.9746	0.0340	0.5988	2.75	42.4
0.80	0.9799	0.0278	0.5708	2.77	46.5
1.00	0.9827	0.0206	0.5273	3.06	53.0
T/K = 363.2					
0.00	0.9859	0.0436	0.4705	2.84	19.5
0.20	0.9715	0.0409	0.4627	3.32	20.2
0.40	0.9751	0.0372	0.4555	3.44	21.7
0.60	0.9762	0.0334	0.4421	4.01	22.9
0.80	0.9808	0.0274	0.4082	4.35	24.5
1.00	0.9815	0.0206	0.3698	5.22	27.9

[a] Standard uncertainty (u) are u(x) = 0.0002, u(x') = 0.0004, u(y) = 0.0010, u(P) = 0.1 kPa, and u(T) = 0.1 K.

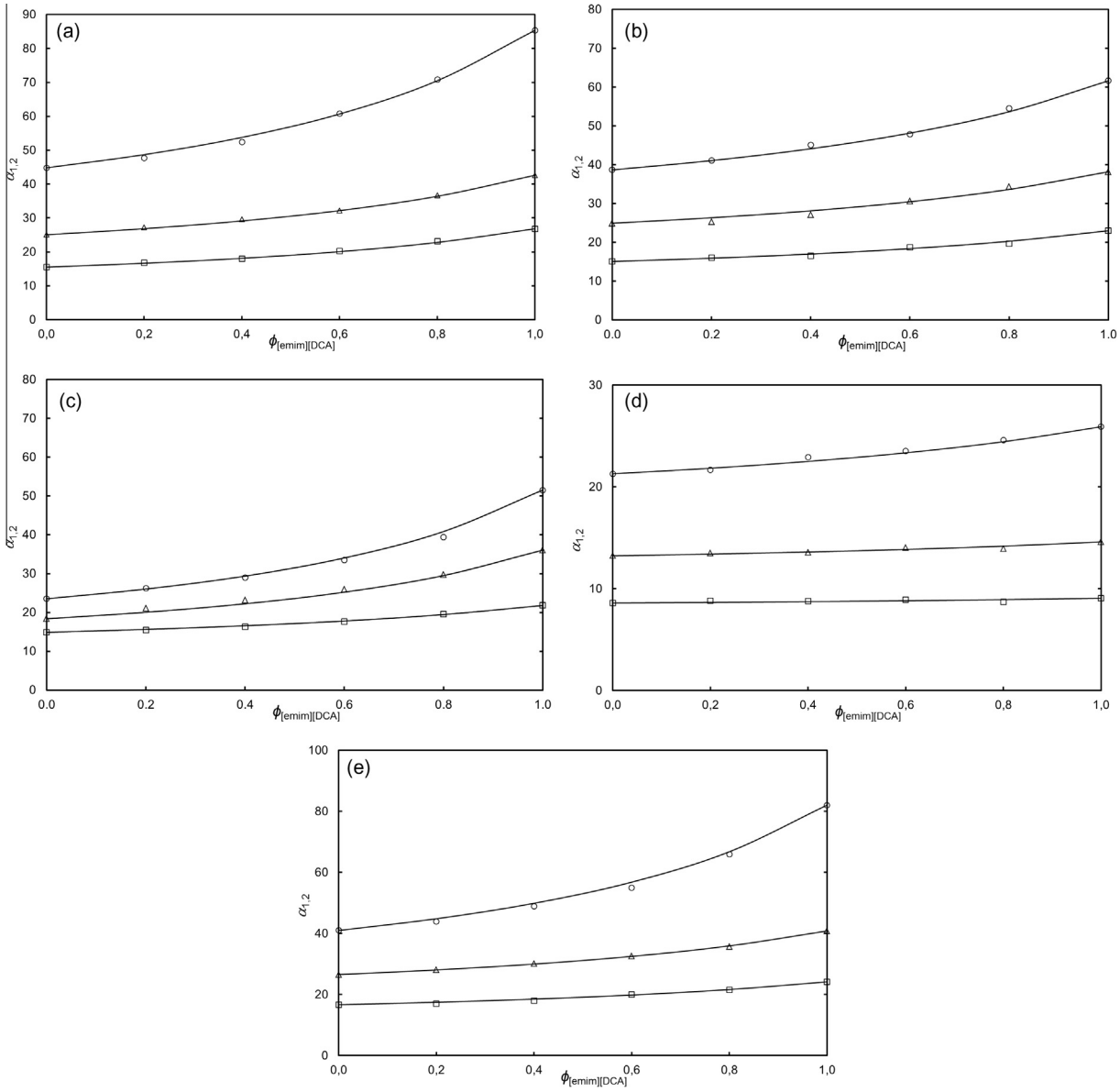

FIGURE 1. Relative volatility ($\alpha_{1,2}$) of aliphatic (1) from toluene (2): (a) *n*-hexane (1) + toluene (2) + [4empy][Tf_2N] (3) + [emim][DCA] (4); (b) *n*-heptane (1) + toluene (2) + [4empy][Tf_2N] (3) + [emim][DCA] (4); (c) *n*-octane (1) + toluene (2) + [4empy][Tf_2N] (3) + [emim][DCA] (4); (d) cyclohexane (1) + toluene (2) + [4empy][Tf_2N] (3) + [emim][DCA] (4); (e) 2,3-dimethylpentane (1) + toluene (2) + [4empy][Tf_2N] (3) + [emim][DCA] (4). Temperatures: ○, 323.2 K; △, 343.2 K; □, 363.2 K. Solid lines denote Yalkowsky–Roseman log-linear mixing rule.

3.2. Effect of the aliphatic structure on the aliphatic/toluene relative volatility

In figure 3, the aliphatic influence in the aliphatic relative volatility from toluene is shown at $T = 323.2$ K. As expected, the increase in the alkyl chain length of the *n*-alkanes leaded to a decrease in the *n*-alkane relative volatility from toluene, whereas the cyclohexane relative volatility from toluene was much lower than for *n*-hexane. The analysis of a branched-chain alkane, 2,3-dimethylpentane, concluded with a higher relative volatility from toluene for the branched-chain alkane than for the linear alkane with the same carbon atoms, *n*-heptane.

The alkyl chain length effect is explained as a consequence of the higher volatility associated to short *n*-alkanes, which has lower boiling points [38]. It is true that the solubility of *n*-alkanes in ILs increases as the alkyl chain length decreases [40], but in this work the main effect is demonstrated to be the volatile character of the aliphatic compound. The increase in the aliphatic/aromatic relative volatility associated to the use of 2,3-dimethylpentane instead of *n*-heptane is also explained as a result of the higher effect associated to the volatile character than for the solubility in the IL mixture. In addition to this, the results obtained for the cyclohexane case are caused by the intermediate behavior, between aliphatic and aromatics, associated to cycloalkanes. Then, the IL mixture composition hardly affects the cyclohexane/toluene relative volatility, as showed in figure 1d.

3.3. Effect of the aromatic structure on the n-heptane/aromatic relative volatility

In figure 4, the *n*-heptane relative volatility from benzene, toluene, ethylbenzene, and *p*-xylene was evaluated at $T = 323.2$ K. Analyzing the *n*-heptane relative volatilities from aromatics, the highest values were achieved in presence of those aromatics with

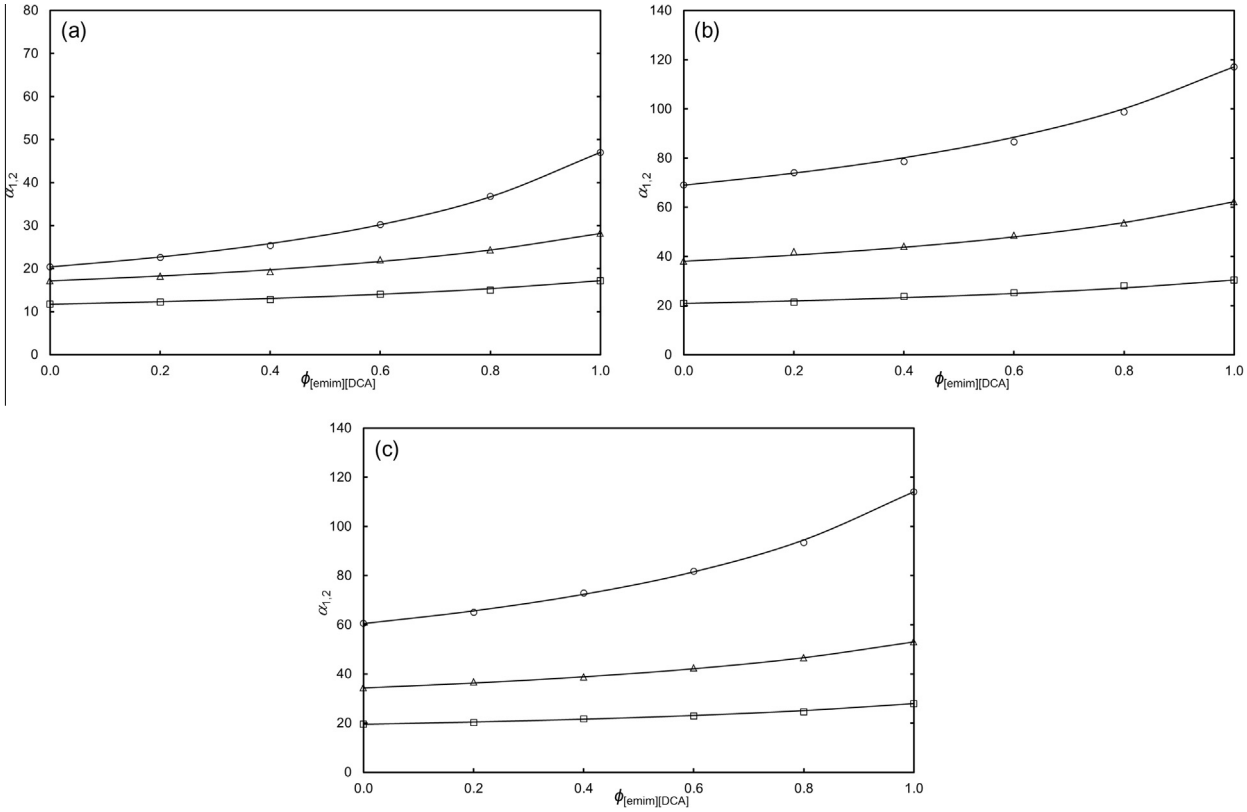

FIGURE 2. Relative volatility ($\alpha_{1,2}$) of *n*-heptane (1) from aromatic (2): (a) *n*-heptane (1) + benzene (2) + [4empy][Tf_2N] (3) + [emim][DCA] (4); (b) *n*-heptane (1) + *p*-xylene (2) + [4empy][Tf_2N] (3) + [emim][DCA] (4); (c) *n*-heptane (1) + ethylbenzene (2) + [4empy][Tf_2N] (3) + [emim][DCA] (4). Temperatures: ○, 323.2 K; △, 343.2 K; □, 363.2 K. Solid lines denote Yalkowsky–Roseman log-linear mixing rule.

TABLE 4
Aliphatic relative volatilities from aromatics[a] for several {aliphatic (1) + aromatic (2)} systems from the literature as a function of temperature with a mass fraction for the aliphatic equal to 10%.

Hydrocarbons		*T*/K		
1	2	323.2	343.2	363.2
n-Hexane	Toluene	6.8	5.6	4.7
n-Heptane	Toluene	2.2	2.1	2.0
n-Octane	Toluene	0.7	0.7	0.8
n-Heptane	Benzene	0.7	0.8	0.8
n-Heptane	*p*-Xylene	5.7	4.9	4.3
n-Heptane	Ethylbenzene	5.7	4.8	4.2
2,3-Dimethylpetane	Toluene	2.2	2.0	1.9
Cyclohexane	Toluene	3.9	3.4	3.0

[a] Literature values obtained from Aspen Plus Database (Ref. [38]).

a larger molecular weight. In addition, the *n*-heptane relative volatilities from ethylbenzene were slightly lower than those values from *p*-xylene.

On the other hand, the VLE data for the {*n*-octane + toluene} and {*n*-heptane + benzene} systems with {[4empy][Tf_2N] + [emim][DCA]} mixture deserves to be highlighted. In both systems, as is known, the aromatic hydrocarbon is more volatile than the alkane (table 4). Nevertheless, an important flipping phenomenon was observed in this work in favor to the alkane in both systems; in fact, the *n*-heptane relative volatility from benzene and the *n*-octane relative volatility from toluene were much higher than 1. This means that the IL mixtures strongly and selectively decrease the volatile character of the aromatics in favor to the alkanes, even when the aliphatic hydrocarbons showed higher boiling points than those of the aromatics in {aliphatic + aromatic} systems.

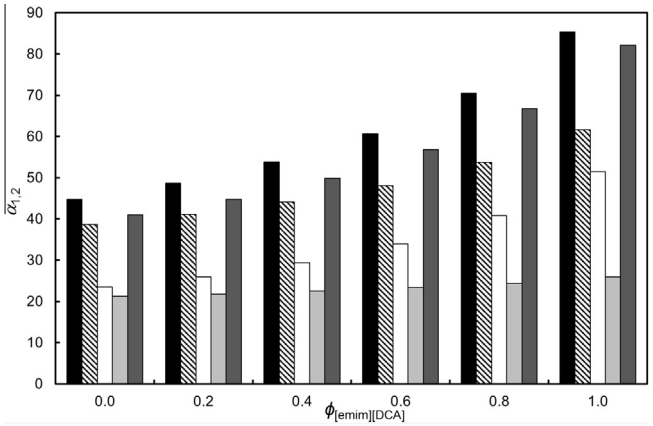

FIGURE 3. Influence of the alkane in the relative volatility ($\alpha_{1,2}$) of aliphatic (1) from toluene (2) at *T* = 323.2 K in (alkane (1) + toluene (2) + [4empy][Tf_2N] (3) + [emim][DCA]) (4): black for *n*-hexane; lined for *n*-heptane; white for *n*-octane; light gray for cyclohexane; dark gray for 2,3-dimethylpentane.

3.4. Prediction of VLE using binary IL mixtures

The suitability of the Yalkowsky–Roseman log-linear mixing rule was evaluated in all mixtures included in this work as was also done in similar VLE systems [41]. This mixing rule is based on the prediction of the VLE data for a system in the presence of two solvents by knowing the VLE data for the same system in both solvents separately. This relationship is collected in the next expression:

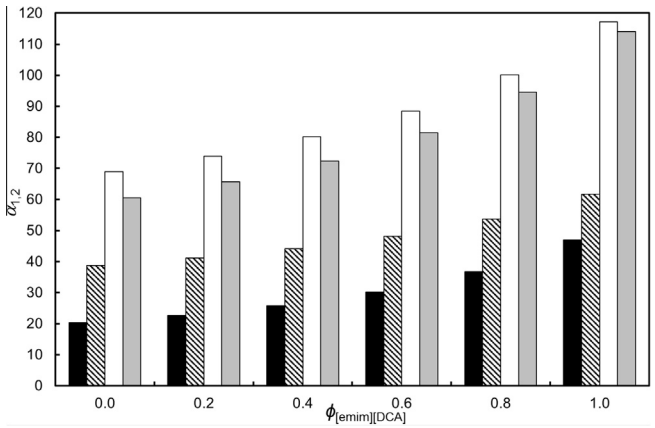

FIGURE 4. Influence of the aromatic in the relative volatility ($\alpha_{1,2}$) of *n*-heptane (1) from aromatic (2) at T = 323.2 K in *n*-heptane (1) + aromatic (2) + [4empy][Tf_2N] (3) + [emim][DCA] (4): black for benzene; lined for toluene; white for *p*-xylene; light gray for ethylbenzene.

TABLE 5
VLE of *n*-heptane (1) + toluene (2) + [emim][DCA] (3) at several temperatures (T). IL liquid mole fraction (x_3), IL-free mole fraction of *n*-heptane in the liquid phase (x'_1), *n*-heptane vapor mole fraction (y_1), total pressure (P), and alkane/aromatic relative volatility ($\alpha_{1,2}$).

x_3	x'_1	y_1	P/kPa	$\alpha_{1,2}$	Ref.
		T/K = 323.2			
0.9857	0.0233	0.5949	2.2	61.6	This work
0.9863	0.0234	0.5918	1.7	60.6	[35]
		T/K = 343.2			
0.9863	0.0196	0.4330	3.3	38.2	This work
0.9862	0.0196	0.4549	2.6	42.0	[35]
		T/K = 363.2			
0.9848	0.0206	0.3287	5.0	22.9	This work
0.9854	0.0212	0.3510	4.3	25.1	[35]

$$\ln x, y_{i,pred} = \sum_{j=3}^{4} f_j \cdot \ln x, y_{i,j}, \quad (4)$$

where x, $y_{i,pred}$ is the liquid or vapor hydrocarbon mole fraction predicted in the mixture of ILs, j denotes the pure ILs, f_j is the volume fraction in the mixtures of ILs, and x, $y_{i,j}$ is the liquid or vapor hydrocarbon mole fraction in the pure ILs. As can be seen in figures 1 and 2, the predicted and the experimental aliphatic relative volatilities from aromatics are in agreement, with a highest relative deviation of 4.8%.

3.5. Effect of IL impurities on the VLE

As cited in the experimental section, the [emim][DCA] IL used in this work was from a different lot than that employed previously in the {*n*-heptane + toluene + [emim][DCA]} VLE determinations at T = (323.2, 343.2, and 363.2) K [35]. As can be seen in table 5, differences were found, mainly in vapor composition and pressure.

As a result of the low uncertainty calculated from independent experiments in both works, the differences in the VLE seem to be mainly caused by the impurities in [emim][DCA]. In the experiments from table 5, the mole fraction of the hydrocarbons in feed was lower than 0.01, fact that increases the importance of the impurities in the IL.

4. Conclusions

The measurement of the VLE for (*n*-hexane, *n*-heptane, *n*-octane, cyclohexane, or 2,3-dimethylpentane) + toluene + {[4empy][Tf_2N] + [emim][DCA]} and *n*-heptane + (benzene, *p*-xylene, or ethylbenzene) + {[4empy][Tf_2N] + [emim][DCA]} systems were carried out at T = (323.2, 343.2, and 363.2) K temperatures and over the whole range of IL mixture compositions.

A high relative volatility of aliphatics from aromatics in all systems has been observed. An increase in temperature has provoked a decrease in the aliphatic relative volatility from aromatics, whereas the higher the fraction of [emim][DCA], the higher the relative volatility of aliphatics from aromatics. In addition to this, the {[4empy][Tf_2N] + [emim][DCA]} IL mixture flipped the order of volatilities in favor of the aliphatics in the {*n*-octane + toluene} and {*n*-heptane + benzene} systems. Finally, the Yalkowsky–Roseman mixing rule has accurately predicted the aliphatic relative volatilities from aromatic as function of the IL mixture composition.

Funding sources

Authors are grateful to the Ministerio de Economía y Competitividad (MINECO) of Spain and the Comunidad de Madrid for financial support of Projects CTQ2014-53655-R and S2013/MAE-2800, respectively. Pablo Navarro also thanks MINECO for awarding him an FPI grant (Reference BES-2012-052312). Marcos Larriba thanks Ministerio de Educación, Cultura y Deporte of Spain for awarding him an FPU grant (Reference AP2010-0318). Emilio J. González also thanks MINECO for awarding him a Juan de la Cierva Contract (Reference JCI-2012-12005).

References

[1] M. Matsumoto, K. Mochiduki, K. Fukunishi, K. Kondo, Sep. Purif. Technol. 40 (2004) 97–101.
[2] I. Domínguez, E.J. González, J. Palomar, A. Domínguez, J. Chem. Thermodyn. 77 (2014) 222–229.
[3] L.I.N. Tomé, V.R. Catambas, A.R.R. Teles, M.G. Freire, I.M. Marrucho, J.A.P. Coutinho, Sep. Purif. Technol. 72 (2010) 167–173.
[4] M. Larriba, P. Navarro, J. García, F. Rodríguez, Ind. Eng. Chem. Res. 52 (2013) 2714–2720.
[5] M. Larriba, P. Navarro, J. García, F. Rodríguez, J. Chem. Thermodyn. 79 (2013) 266–271.
[6] G.W. Meindersma, A.B. de Haan, Sci. China Chem. 55 (2012) 1488–1499.
[7] G.W. Meindersma, A.B. de Haan, Chem. Eng. Res. Des. 86 (2008) 745–752.
[8] G.W. Meindersma, A.J.G. Podt, A.B. de Haan, Fuel Process. Technol. 87 (2005) 59–70.
[9] G.W. Meindersma, A.R. Hansmeier, A.B. de Haan, Ind. Eng. Chem. Res. 49 (2010) 7530–7540.
[10] U. Domanska, A. Pobudkowska, M. Królikowski, Fluid Phase Equilib. 259 (2007) 173–179.
[11] M. Królikowski, K. Walczak, U. Domanska, J. Chem. Thermodyn. 65 (2013) 168–173.
[12] A.F.M. Claudio, M.G. Freire, C.S.R. Freire, A.J.D. Silvestre, J.A.P. Coutinho, Sep. Purif. Technol. 75 (2010) 39–47.
[13] F.S. Oliveira, J.M.M. Araujo, R. Ferreira, L.P.N. Rebelo, I.M. Marrucho, Sep. Purif. Technol. 85 (2012) 137–146.
[14] E. Alvarez-Guerra, A. Irabien, Sep. Purif. Technol. 98 (2012) 432–440.
[15] S. Corderí, E.J. González, N. Calvar, A. Domínguez, J. Chem. Thermodyn. 53 (2013) 60–66.
[16] M. Larriba, P. Navarro, J. García, F. Rodríguez, Fluid Phase Equilib. 364 (2013) 48–54.
[17] M. Larriba, P. Navarro, J. García, F. Rodríguez, Sep. Purif. Technol. 120 (2013) 392–401.
[18] M. Larriba, P. Navarro, E.J. González, J. García, F. Rodríguez, Sep. Purif. Technol. 144 (2015) 54–62.
[19] M. Larriba, P. Navarro, J. García, F. Rodríguez, Fluid Phase Equilib. 380 (2014) 1–10.
[20] S. Potdar, R. Anantharaj, T. Banerjee, J. Chem. Eng. Data 57 (2012) 1026–1035.
[21] P. Navarro, M. Larriba, J. García, F. Rodríguez, J. Chem. Thermodyn. 76 (2014) 152–160.
[22] P. Navarro, M. Larriba, J. García, F. Rodríguez, Thermochim. Acta 588 (2014) 22–27.
[23] M. Larriba, P. Navarro, J. García, F. Rodríguez, J. Chem. Thermodyn. 82 (2015) 58–75.
[24] M. Larriba, S. García, P. Navarro, J. García, F. Rodríguez, J. Chem. Eng. Data 58 (2013) 1496–1504.
[25] A. Stoppa, R. Buchner, G. Hefter, J. Mol. Liq. 153 (2010) 46–51.
[26] P. Navia, J. Troncoso, L. Romaní, J. Solution Chem. 37 (2008) 677–688.
[27] M.B. Oliveira, M. Domínguez-Pérez, M.G. Freire, F. Llovell, O. Cabeza, J.A. Lopes-da-Silva, L.F. Vega, J.A.P. Coutinho, J. Phys. Chem. B 116 (2012) 12133–12141.

[28] S. Aparicio, M. Atilhan, J. Phys. Chem. B 116 (2012) 8251–8258.
[29] H. Niedermeyer, J.P. Hallet, I.J. Villar-Garcia, P.A. Hunt, T. Welton, Chem. Soc. Rev. 41 (2012) 7780–7802.
[30] M. Brussel, M. Brehm, A.S. Pensado, F. Malberg, M. Ramzan, A. Stark, B. Kirchner, Phys. Chem. Chem. Phys. 14 (2012) 13204–13215.
[31] G. Annat, M. Forsyth, D.R. MacFarlane, J. Phys. Chem. B 116 (2012) 8251–8258.
[32] G. Chatel, J.F.B. Pereira, V. Debbeti, H. Wang, R. Rogers, Green Chem. 16 (2014) 2051–2083.
[33] S.H. Yalkowsky, T.J. Roseman, Chapter 3: Solubilization of drugs by cosolvents, in: Techniques of Solubilization of Drugs, Dekker, New York, 1981.
[34] M.T.G. Jongmans, B. Schuur, A.B. de Haan, Ind. Eng. Chem. Res. 50 (2011) 10800–10810.
[35] P. Navarro, M. Larriba, J. García, E.J. González, F. Rodríguez, Fluid Phase Equilib. 387 (2015) 209–216.
[36] E.J. González, P. Navarro, M. Larriba, J. García, F. Rodríguez, J. Chem. Thermodyn. 91 (2015) 156–164.
[37] K.R. Seddon, A. Stark, M.J. Torres, Pure Appl. Chem. 72 (2000) 2275–2287.
[38] Aspen Plus Version 7.1, Database, Aspen Technology, 2004.
[39] M.T.G. Jongmans, A. Londoño, S.B. Mamilla, H.J. Pragt, K.T.J. Aaldering, G. Bargeman, M.R. Nieuwhof, A. ten Kate, P. Verwer, A.A. Kiss, C.J.G. van Strien, B. Schuur, A.B. de Haan, Sep. Purif. Technol. 98 (2012) 206–215.
[40] M. Larriba, P. Navarro, J. García, F. Rodríguez, J. Chem. Eng. Data 59 (2014) 1692–1699.
[41] A. Li, Ind. Eng. Chem. Res. 40 (2001) 5029–5035.

JCT 15-610

Fluid Phase Equilibria 417 (2016) 41–49

Contents lists available at ScienceDirect

Fluid Phase Equilibria

journal homepage: www.elsevier.com/locate/fluid

Vapor-liquid equilibria for *n*-heptane + (benzene, toluene, *p*-xylene, or ethylbenzene) + {[4empy][Tf_2N] (0.3) + [emim][DCA] (0.7)} binary ionic liquid mixture

Pablo Navarro, Marcos Larriba, Julián García*, Francisco Rodríguez

Department of Chemical Engineering, Complutense University of Madrid, E–28040 Madrid, Spain

ARTICLE INFO

Article history:
Received 12 January 2016
Received in revised form
7 February 2016
Accepted 11 February 2016
Available online 15 February 2016

Keywords:
Mixed ionic liquids
Aromatic/aliphatic separation
Vapor–liquid equilibria
Headspace gas chromatography

ABSTRACT

Ionic liquids (ILs) have been extensively used as solvents in the liquid–liquid extraction of aromatics from aromatic/aliphatic mixtures. However, scarce studies have been done in order to experimentally evaluate the recovery of the hydrocarbons from the IL in extract-type streams. In this work, we have determined the vapor–liquid equilibria (VLE) for *n*-heptane + (benzene, toluene, *p*-xylene, or ethylbenzene) + {1-ethyl-4-methylpyridinium bis(trifluoromethylsulfonyl)imide ([4empy][Tf_2N]) (0.3) + 1-ethyl-3-methylimidazolium dicyanamide ([emim][DCA]) (0.7)}. This IL mixture was selected as a result of its high extractive performance. The VLE have been measured using a headspace – gas chromatography (HS-GC) technique at several temperatures (323.2 K, 343.2 K, and 363.2 K) and over the whole composition range in the miscibility region of the systems. The Non-Random Two Liquids (NRTL) model has been applied to fit the VLE data. The *n*-heptane/aromatic relative volatilities have been calculated to assess the recovery of *n*-heptane from the four aromatics of the aromatic fraction and the IL-mixture. Results show that the IL mixture induces a high selective *n*-heptane/aromatic separation over the whole range of compositions in all systems and at all temperatures set in this work.

1. Introduction

The use of alternative solvents instead of organic compounds is an interesting challenge for the research community, linking technological and environmental purposes. Room temperature ionic liquids (ILs) are compounds that combine the advantages of the handling of the liquids and the good performance of the salts in modifying the thermodynamic behavior [1,2]. As a consequence, a high number of studies have been carried out focusing on the use of ILs as solvents [3–15].

The aromatic extraction from aromatic/aliphatic mixtures is one of the most prolific uses of ILs as solvents due to the high extractive properties shown by ILs [3,5]. Lastly, the use of binary mixtures of ionic liquids has led to achieve IL-based solvents with high aromatic/aliphatic selectivities, high aromatic distribution ratios, adequate densities, and low viscosities [10]. The {[4empy][Tf_2N] + [emim][DCA]} binary IL mixture with [emim][DCA] mole fraction of 0.7 shows higher aromatic/aliphatic selectivities and aromatic distribution ratios than those of sulfolane, being comparable their densities and viscosities [9,10]. In addition to this, its maximum operation temperature (MOT), 413 K, assures a high thermal range of application at industrial scale [16].

However, the studies focused in the recovery of the hydrocarbons from the IL-based solvent are scarce nowadays to establish the feasibility of the aromatic extraction using ILs. For that reason in our last work we have studied the recovery of the hydrocarbons in several extract-type streams with the {[4empy][Tf_2N] + [emim][DCA]} mixture as a function of IL mixture composition. The best aliphatic/aromatic relative volatilities were found at the highest mole fraction of [emim][DCA] [14]. Hence, the {[4empy][Tf_2N] (0.3) + [emim][DCA] (0.7)} IL mixture seems to be a potential solvent to extract aromatics taking into account extractive and physical properties, thermal stability, and the recovery of hydrocarbons.

Here the VLE for *n*-heptane + (benzene, toluene, *p*-xylene, or ethylbenzene) + {[4empy][Tf_2N] (0.3) + [emim][DCA] (0.7)} have been determined over the whole composition range and at 323.2 K, 343.2 K, and 363.2 K by using a headspace – gas chromatography (HS-GC) technique [17–19]. Although the best aliphatic/aromatic relative volatilities were achieved using pure [emim][DCA], the

* Corresponding author.
E-mail address: jgarcia@quim.ucm.es (J. García).

http://dx.doi.org/10.1016/j.fluid.2016.02.018
0378-3812/

Table 1
Specifications of chemicals.

Chemical	Source	Purity/% wt	Analysis method
[emim][DCA]	Iolitec GmbH	98	NMR[a], IC[b]
[4empy][Tf_2N]	Iolitec GmbH	99	NMR[a], IC[b]
n-heptane	Sigma–Aldrich	99.7	GC[c]
toluene	Sigma–Aldrich	99.5	GC[c]
benzene	Sigma–Aldrich	99.5	GC[c]
p-xylene	Sigma–Aldrich	99.0	GC[c]
ethylbenzene	Sigma–Aldrich	99.8	GC[c]

[a] Nuclear Magnetic Resonance.
[b] Ion Chromatography.
[c] Gas Chromatography.

recovery of the aliphatics from aromatics over the whole range of composition and also modeling the VLE data to the Non-Random Two Liquids (NRTL) model [20].

2. Experimental

2.1. Chemicals

[emim][DCA] and [4empy][Tf_2N] were purchased from Iolitec GmbH. They were used here without further purifications, with the mass fraction purities listed in Table 1. The water and halide contents for [emim][DCA] were less than 937 ppm and 2%, respectively, whereas in the case of [4empy][Tf_2N] were below than 89 ppm and 0.1%, respectively. In order to maintain their identity, ILs were kept in their original vessels under a dry atmosphere into a moisture-controlled desiccator and were manipulated under a dry and inert atmosphere of nitrogen into a glove box. The structure of both ILs is presented in Fig. 1. The densities for both ILs were determined by an Anton Paar DMA-5000 at 293.2 K in order to compare their values with those just published as can be found in Table 2. The [emim][DCA] shows a density that is agreement with those reported by Freire et al., França et al., Seki et al., and Larriba et al. [21–24], whereas the [4empy][Tf_2N] has a density also in agreement with that published by Liu et al. [25]. Moreover, all hydrocarbons tested here were acquired from Sigma–Aldrich with purities higher than 99.5 wt. % as can be also seen in Table 1.

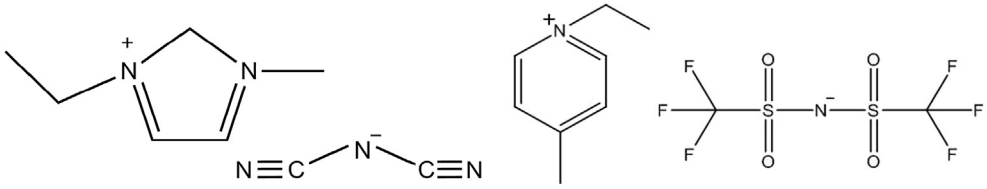

Fig. 1. Structure of the ILs. [emim][DCA] (*left*) and [4empy][Tf_2N] (*right*).

Table 2
Density[a] (g cm^{-3}) for the ionic liquids at 293.2 K: experimental and literature data.

Ionic liquid	Experimental	Literature
[emim][DCA]	1.1049	1.1074 [21], 1.1075 [22], 1.1046 [23], 1.1046 [24]
[4empy][Tf_2N]	1.4899	1.4961 [25]

[a] Standard uncertainty (u) are u(ρ) = 0.0001 and u(T) = 0.001 K.

Table 3
NRTL parameters[a] from the adjustments of VLE data for pseudobinary and pseudoternary systems with {[4empy][Tf_2N] (0.3) + [emim][DCA] (0.7)} IL mixture.

i − j	Δg_{ij}/J mol^{-1}	Δg_{ji}/J mol^{-1}	Δx	ΔP/kPa
n-heptane (1) + {[4empy][Tf_2N] + [emim][DCA]} (2)				
1–2	7120.6	332.28	0.002	0.01
toluene (1) + {[4empy][Tf_2N] + [emim][DCA]} (2)				
1–2	5525.3	−25,042	0.006	0.02
benzene (1) + {[4empy][Tf_2N] + [emim][DCA]} (2)				
1–2	3297.9	−21,534	0.005	0.05
p-xylene (1) + {[4empy][Tf_2N] + [emim][DCA]} (2)				
1–2	9394.3	−27,543	0.003	0.03
ethylbenzene (1) + {[4empy][Tf_2N] + [emim][DCA]} (2)				
1–2	7419.1	−20,792	0.003	0.02
n-heptane (1) + toluene (2) + {[4empy][Tf_2N] + [emim][DCA]} (3)				
1–2	158.64	4084.4	0.006	0.07
1–3	1764.4	13,844		
2–3	1843.2	−1909.3		
n-heptane (1) + benzene (2) + {[4empy][Tf_2N] + [emim][DCA]} (3)				
1–2	159.93	4100.9	0.005	0.08
1–3	4215.9	13,890		
2–3	4302.0	−1910.6		
n-heptane (1) + *p*-xylene (2) + {[4empy][Tf_2N] + [emim][DCA]} (3)				
1–2	840.62	5828.8	0.004	0.23
1–3	3336.4	15,920		
2–3	3468.6	−711.83		
n-heptane (1) + ethylbenzene (2) + {[4empy][Tf_2N] + [emim][DCA]} (3)				
1–2	831.38	5908.1	0.004	0.40
1–3	5898.9	15,997		
2–3	6029.9	−721.99		

[a] α_{12}, α_{13}, and α_{23} were set in 0.3 for all systems.

most adequate composition of the mixture taking into account the extraction and recovery processes is {[4empy][Tf_2N] (0.3) + [emim][DCA] (0.7)}. This work is aimed in confirming the selective

2.2. VLE procedure and analysis

The isothermal VLE data was obtained using the HS-GC technique, recently applied to determine VLE for mixtures containing an aliphatic, an aromatic, and an IL. The details of the method were widely described in our previous work [15]; hence, here we only comment the essential information to understand the background of the technique.

The equipment used was an Agilent Headspace 7697 A injector coupled to an Agilent GC 7890 A, the latter equipped with a flame ionization detector. The feed mixtures were prepared by mass using a Mettler Toledo XS205 balance with a precision of $\pm 10^{-5}$ g. The sample vials were filled with a controlled volume of 1.0 mL, being the headspace volume 19.0 mL. As commented before, the equilibrium temperatures were 323.2 K, 343.2 K, and 363.2 K, whereas an equilibration time of 2 h and a 100 rpm agitation were also needed to reach the equilibrium.

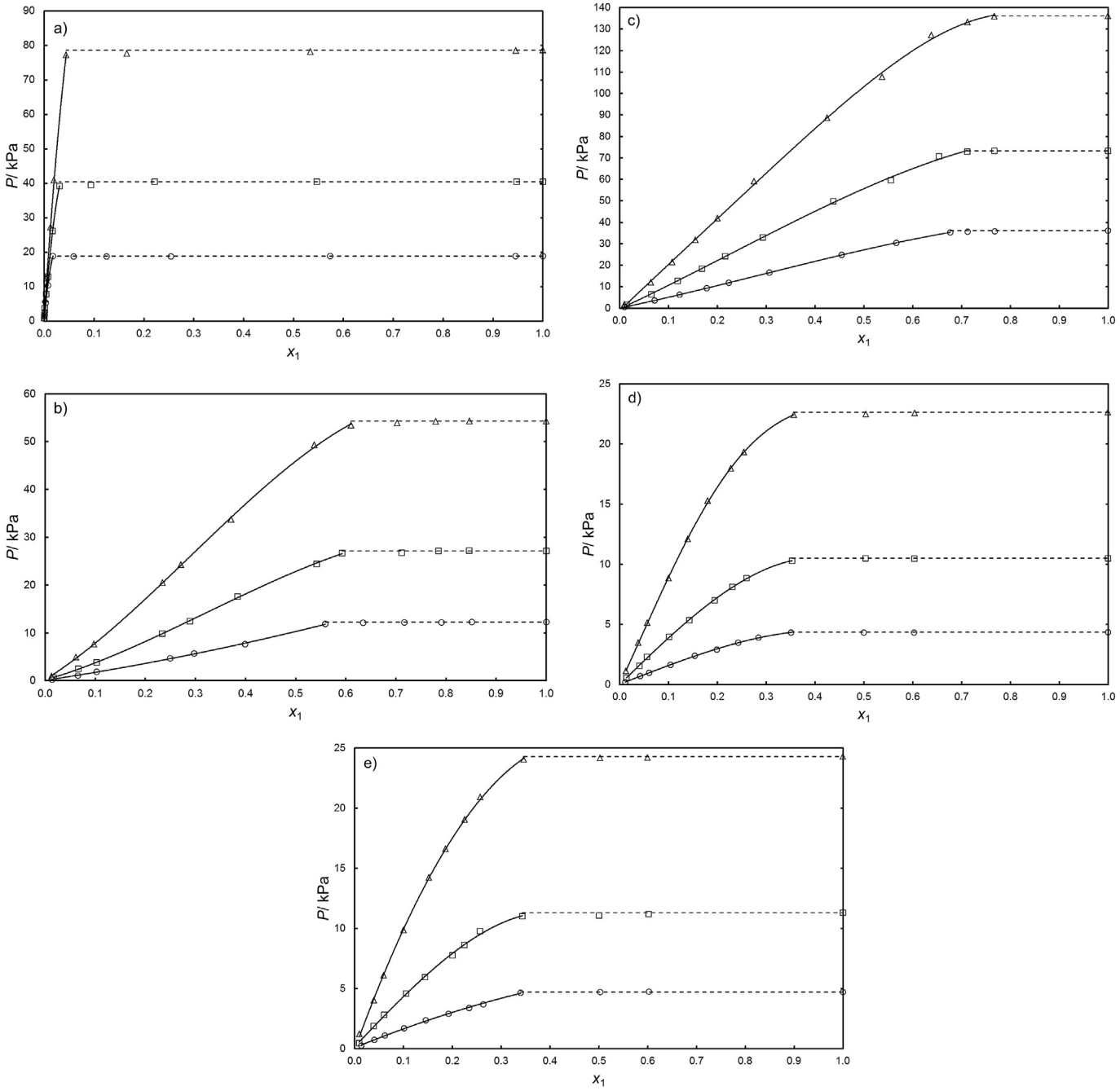

Fig. 2. VLE data for pseudobinary systems hydrocarbon (1) + {[4empy][Tf_2N] + [emim][DCA]} (2) at several temperatures: ○, T = 323.2 K; □, T = 343.2 K; Δ, T = 363.2 K. Solid lines denote the NRTL adjustment and dashed lines refer to constant pressure equal to pure component pressure from Ref. 26. a) *n*-heptane; b) toluene; c) benzene; d) *p*-xylene; e) ethylbenzene.

The partial pressures (P_i) developed by the hydrocarbons in the pseudobinary and pseudoternary mixtures with {[4empy][Tf_2N] (0.3) + [emim][DCA] (0.7)} binary IL mixture were calculated using the relationship between the peak areas developed by the hydrocarbons with the IL mixture (A_i) and the peak areas developed by each hydrocarbon alone in the same conditions (A_i^0) [17]:

$$P_i = \frac{P_i^0 \cdot A_i}{A_i^0} \quad (1)$$

where P_i^0 refers to the vapor pressure of each pure hydrocarbon from literature [26].

The vapor phase compositions were directly determined by the GC analysis. In the case of quaternary systems, the response factor method was used to correct the compositions. Finally, the liquid phase compositions (x_i) were calculated correcting the feed compositions (z_i) with the hydrocarbon amount that goes to the vapor phase:

$$x_i = \frac{z_i \cdot F - (P_i \cdot V_G / R \cdot T)}{\sum_{i=1}^{3} (z_i \cdot F - (P_i \cdot V_G / R \cdot T))} \quad (2)$$

where F denotes the molar amount of the feed, V_G is the headspace

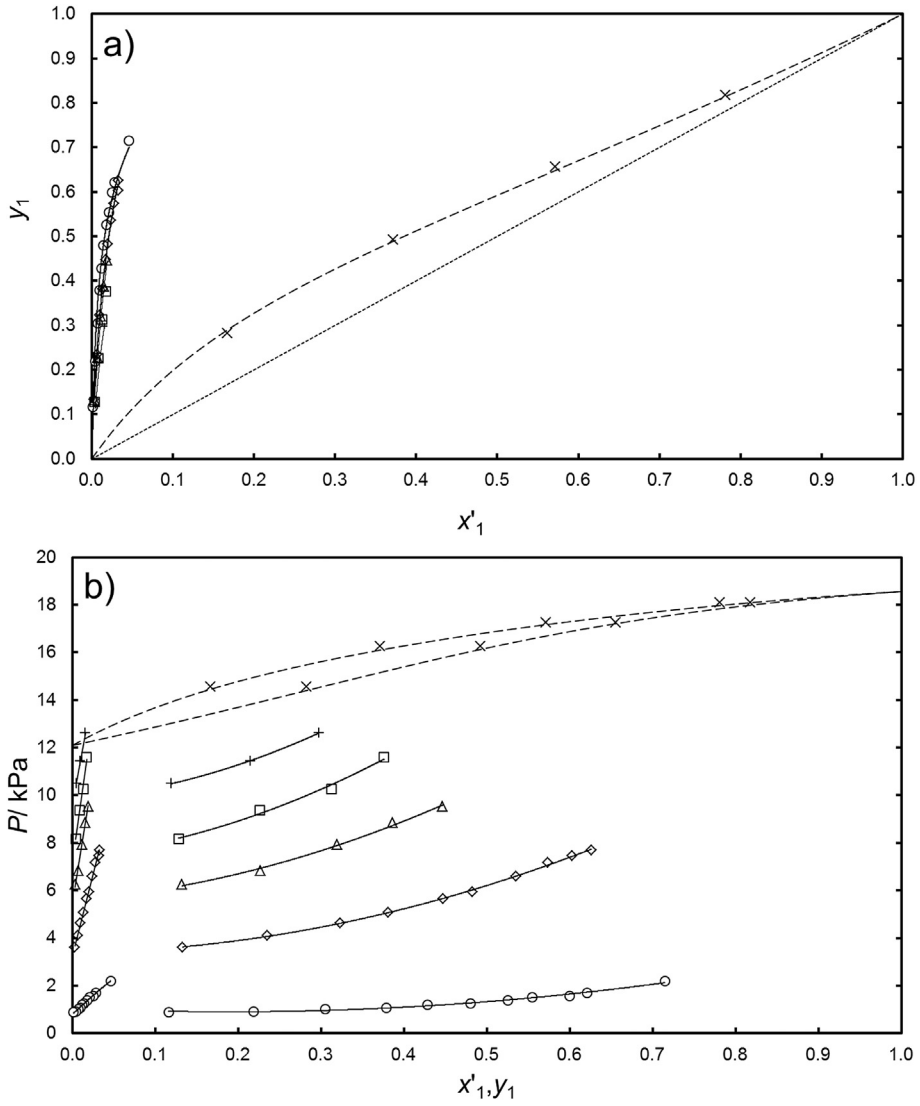

Fig. 3. VLE data for ternary system *n*-heptane (1) + toluene (2) + {[4empy][Tf_2N] + [emim][DCA]} (3) at T = 323.2 K *x′*-*y* diagram (a) and *x′*,*y*-*P* diagram (b). ILs mole fraction (x_3): ○, $x_3 \cong 0.97$; ◊, $x_3 \cong 0.87$; Δ, $x_3 \cong 0.76$; □, $x_3 \cong 0.66$; +, $x_3 \cong 0.55$; x, binary system of {*n*-heptane (1) + toluene (2)} from Ref. 15. Solid lines denote the NRTL adjustment and dashed lines refer to VLE data from Aspen Plus Simulator Software Database at 323.2 K for the binary system of *n*-heptane (1) + toluene (2) from Ref. [27].

volume of the vial, and *R* is the ideal gas law constant.

3. Results and discussion

The VLE were measured for all systems at 323.2 K, 343.2 K, and 363.2 K over the whole range of composition. The *x*-*P* data obtained for the hydrocarbon + {[4empy][Tf_2N] (0.3) + [emim][DCA] (0.7)} systems are displayed in Tables S1 and S2 in the Supplementary Information, whereas the *x*,*y*-*P* data corresponded to *n*-heptane + (toluene, benzene, *p*-xylene, or ethylbenzene) + {[4empy][Tf_2N] (0.3) + [emim][DCA] (0.7)} are listed in Tables S3 to S6 in the Supplementary Information, based on solvent-free compositions (*x′*). Finally, the *x*,*y*-*P* data for *n*-heptane + (benzene, *p*-xylene, or ethylbenzene) systems are collected in Table S7 (Supplementary Information) in order to validate the suitability of the method for these systems and to be used as benchmark. The VLE data for the *n*-heptane + toluene mixture were just published in our previous work concerning the VLE for *n*-heptane + toluene + [emim][DCA] [15].

The relative volatilities (α_{12}) of *n*-heptane (1) from aromatics (2) were calculated to evaluate the IL mixture effect on the hydrocarbon separation as:

$$\alpha_{12} = \frac{K_1}{K_2} = \frac{y_1/x_1}{y_2/x_2} \tag{3}$$

where *K* is the *K*-value for each hydrocarbon. The values of α_{12} are listed in Tables S3 to S7 in the Supplementary Information.

The VLE data of all systems including the IL mixture were modeled using Non-Random Two Liquids (NRTL) thermodynamic model [20]. The low deviations between the experimental VLE data and those calculated by NRTL in previous works dealing with hydrocarbons and ILs suggested the use of this thermodynamic model [15]. The objective function (*OF*) used in the NRTL model was defined as follows:

$$OF = \frac{a \cdot \sum_{i=1}^{I} \left| x_{i,calc} - x_{i,exptl} \right| + \sum_{i=1}^{I} \left| P_{i,calc} - P_{i,exptl} \right|}{N} \tag{4}$$

where *a*, which was fixed to 300, denotes the weighting coefficient of mole fraction deviations to balance the difference of magnitude

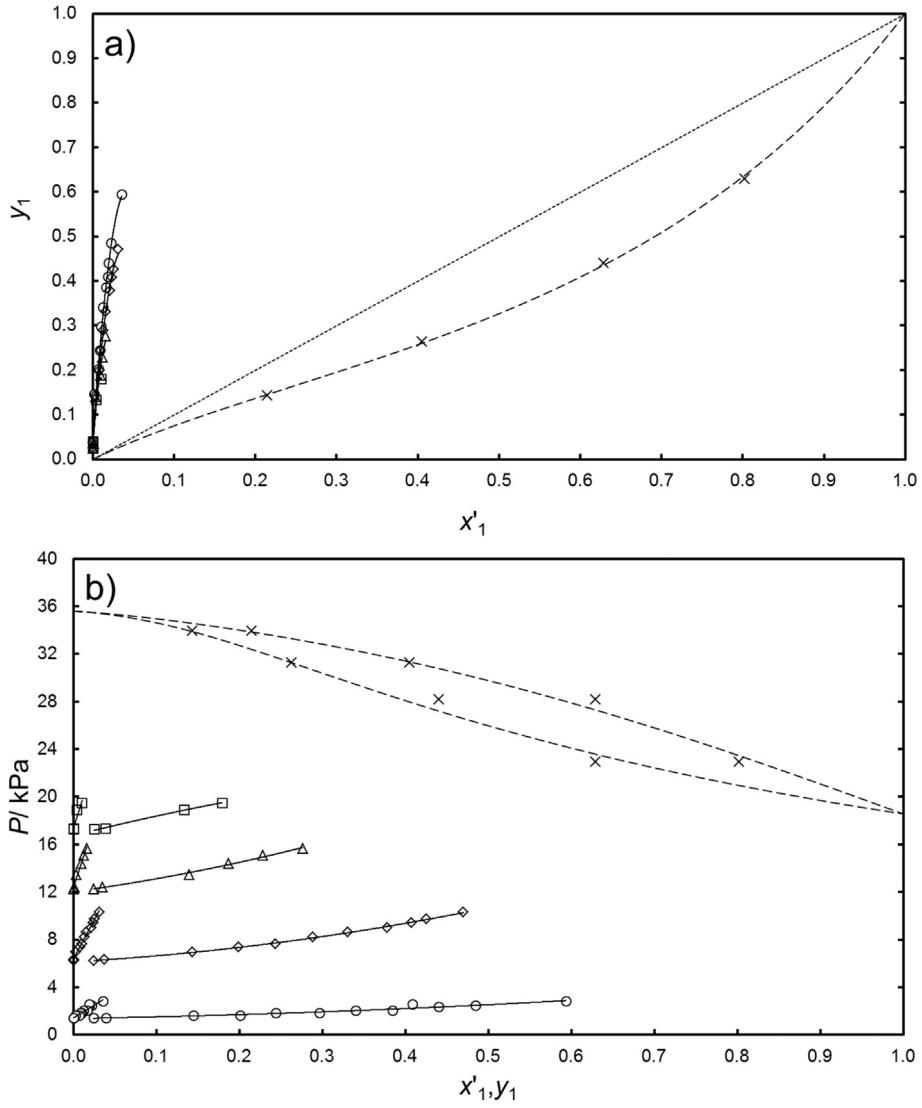

Fig. 4. VLE data for ternary system *n*-heptane (1) + benzene (2) + {[4empy][Tf_2N] + [emim][DCA]} (3) at T = 323.2 K *x′*-*y* diagram (a) and *x′*,*y*-*P* diagram (b). ILs mole fraction (x_3): ○, $x_3 \cong 0.98$; ◊, $x_3 \cong 0.90$; Δ, $x_3 \cong 0.80$; □, $x_3 \cong 0.73$; x, binary system of *n*-heptane (1) + benzene (2). Solid lines denote the NRTL adjustment and dashed lines refer to VLE data from Aspen Plus Simulator Software Database at 323.2 K for the binary system of *n*-heptane (1) + benzene (2) from Ref. 27.

between *x* and P_i and *N* is the number of VLE points. The Solver tool of Microsoft Excel spreadsheet software was employed to adjust all systems.

The parameters obtained from all adjustments are included in Table 2, jointly with the deviations of the liquid mole fractions, Δ*x*, and the equilibrium pressures, Δ*P*, determined as follows:

$$\Delta x = \frac{\sum_{i=1}^{I} \left| x_{i,calc} - x_{i,exptl} \right|}{N} \quad (5)$$

$$\Delta P = \frac{\sum_{i=1}^{I} \left| P_{i,calc} - P_{i,exptl} \right|}{N} \quad (6)$$

The goodness of the NRTL adjustments can be seen through the low liquid mole fraction and pressure deviations collected in Table 3 or by a graphical comparison between the experimental values and the adjustments to NRTL in Figs. 2 to 6 and S1 to S8 in the Supporting Information.

3.1. Hydrocarbon + {[4empy][Tf_2N] (0.3) + [emim][DCA] (0.7)} systems

The VLE data of (*n*-heptane, toluene, benzene, *p*-xylene, or ethylbenzene) + {[4empy][Tf_2N] (0.3) + [emim][DCA] (0.7)} as a function of temperature are shown in Fig. 2. As can be seen, the pressure increases as the mole fraction of the hydrocarbons does until the pressure is equal to those of the pure hydrocarbons. This zone in which the pressure is a function of the mole fraction corresponds to the VLE. The other composition gap with a constant value for the pressure represents a vapor–liquid–liquid equilibrium (VLLE) region, in which x_1 represent the overall liquid mole fraction. Thus, the composition at which the two zones converge is the maximum hydrocarbon solubility in the IL mixture. As a result, the compositions for the hydrocarbon in the two liquid phases in the VLLE experiments are their solubility in the IL mixture for the IL-rich phase and that regarding to pure hydrocarbon. The maximum solubilities of the hydrocarbons as a function of temperature are collected in Table S2 according to the experimental VLE data obtained in this work.

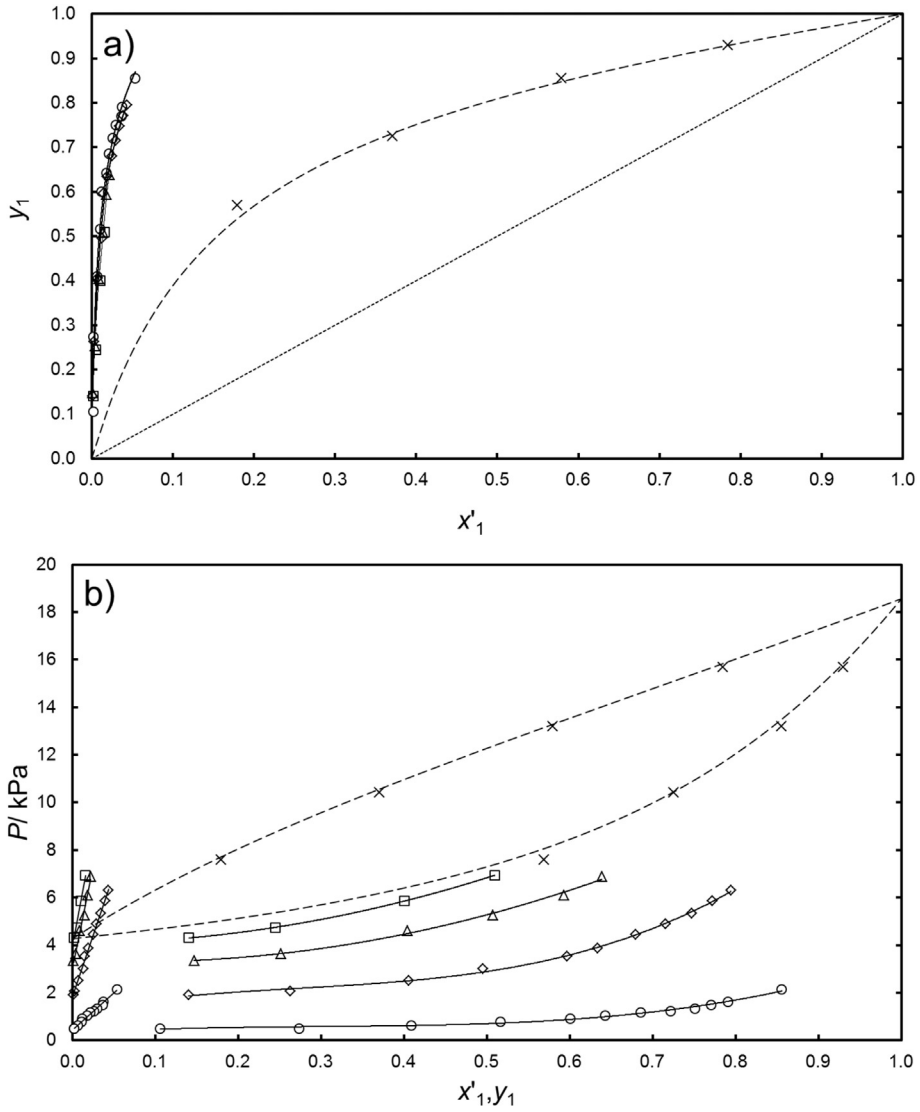

Fig. 5. VLE data for pseudoternary system *n*-heptane (1) + *p*-xylene (2) + {[4empy][Tf_2N] + [emim][DCA]} (3) at T = 323.2 K *x′*-*y* diagram (a) and *x′*,*y*-*P* diagram (b). ILs mole fraction (x_3): ○, $x_3 \cong 0.98$; ◊, $x_3 \cong 0.90$; Δ, $x_3 \cong 0.81$; □, $x_3 \cong 0.73$; x, binary system of {*n*-heptane (1) + *p*-xylene (2)}. Solid lines denote the NRTL adjustment and dashed lines refer to VLE data from Aspen Plus Simulator Software Database at 323.2 K for the binary system of *n*-heptane (1) + *p*-xylene (2) from Ref. 27.

As expected, the range of compositions of the VLE was higher for the aromatics than for the *n*-heptane because of the stronger interaction between the aromatics and ILs and, thus, their higher miscibility in the IL mixture. The temperature hardly affected the hydrocarbon solubility in the IL mixture in the range from 323.2 K to 363.2 K.

Focusing only on the aromatic + {[4empy][Tf_2N] (0.3) + [emim][DCA] (0.7)} systems, the benzene composition gap in the VLE region was quite higher than that of toluene, whereas the lowest gaps were for the *p*-xylene and ethylbenzene. Therefore, low values of molecular weight for the aromatic imply high solubility of the aromatic in the IL mixture. This trend was in agreement with our previous work about the liquid–liquid equilibrium in aromatic + {[4empy][Tf_2N] (0.3) + [emim][DCA] (0.7)} systems at 313.2 K [10].

3.2. *n*-Heptane + aromatic + {[4empy][Tf_2N] (0.3) + [emim][DCA] (0.7)} systems

The VLE data obtained for the pseudoternary mixtures of *n*-heptane + aromatic + {[4empy][Tf_2N] (0.3) + [emim][DCA] (0.7)} are graphically presented in Figs. 3 to 6 at the equilibrium temperature of 323.2 K and as a function of the IL mole fraction in the liquid phase. The VLE data for the same pseudoternary mixtures at 343.2 K and 363.2 K are graphically shown in Figs. S1 to S8 in the Supporting Information.

The VLE data for the same systems without the IL mixture are also shown in Figs. 3 to 6 and in Figs. S1 to S8 in the Supporting Information in order to be used as benchmark. As can be seen, the experimental values for the *n*-heptane + aromatic systems are in agreement with those taken from the literature, validating the HS-GC technique for all the systems included in this work.

The *x′*-*y* diagrams (a) from Figs 3 to 6 and S1 to S8 in the Supporting Information show that the vapor mole fraction of *n*-heptane in equilibrium is considerably higher for the *n*-heptane + aromatic + {[4empy][Tf_2N] (0.3) + [emim][DCA] (0.7)} systems than for the *n*-heptane + aromatic systems. This fact can be also seen in the *x′*,*y*-*P* diagrams (b) from the same figures, where the equilibrium lines of the vapor and liquid moves away one from the other as the IL mole fraction increases.

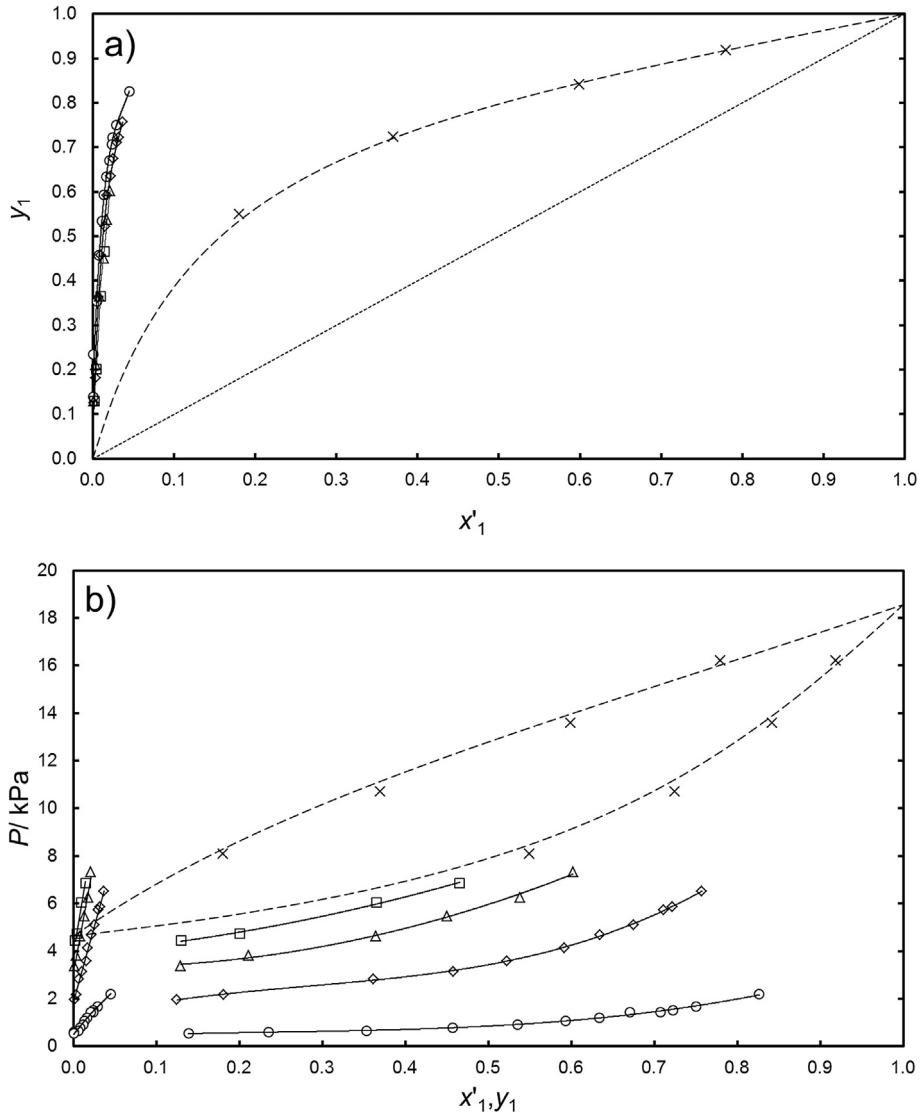

Fig. 6. VLE data for pseudoternary system *n*-heptane (1) + ethylbenzene (2) + {[4empy][Tf_2N] + [emim][DCA]} (3) at T = 323.2 K *x′-y* diagram (a) and *x′,y-P* diagram (b). ILs mole fraction (x_3): ○, $x_3 \cong 0.98$; ◊, $x_3 \cong 0.91$; Δ, $x_3 \cong 0.81$; □, $x_3 \cong 0.73$; x, binary system of {*n*-heptane (1) + ethylbenzene (2)}. Solid lines denote the NRTL adjustment and dashed lines refer to VLE data from Aspen Plus Simulator Software Database at 323.2 K for the binary system of *n*-heptane (1) + ethylbenzene (2) from Ref. 27.

The VLE data comparison of *n*-heptane + benzene system with and without the IL mixture deserves to be highlighted as a result of the flipping phenomenon observed with {[4empy][Tf_2N] + [emim][DCA]}. As can be noticed in Fig. 4 at 323.2 K and in Figs. S3 to S4 at the temperatures of 343.2 K and 363.2 K, the vapor pressure of benzene is higher than that of *n*-heptane in the *n*-heptane + benzene binary system. However, in the *n*-heptane + benzene + {[4empy][Tf_2N] + [emim][DCA]} system, the more volatile compound is the *n*-heptane. Hence, the order of volatilities drastically changed in favor to the *n*-heptane as a result of the effect of {[4empy][Tf_2N] + [emim][DCA]} in the equilibrium.

Taking into account the VLE data obtained in this work, it is possible to claim that the separation of *n*-heptane from the four aromatics in extract-type compositions is completely dependent on the molecular weight of the aromatic. The more selective *n*-heptane/aromatic separation was observed in the case of the highest aromatic molecular weight (*p*-xylene, ethylbenzene). In order to facilitate this comparison, the *n*-heptane/aromatic relative volatilities from all pseudoternary systems included in this work are graphically represented in Fig. 7. As observed, an increase in the aromatic molecular weight implies an increase in the *n*-heptane/aromatic relative volatility.

The temperature influence in the VLE is also discussed from Fig. 7 because its effect can be easily appreciated from the *n*-heptane/aromatic relative volatility. As can be seen, an increase in the temperature value causes a decrease in the *n*-heptane/aromatic relative volatility values in all systems.

4. Conclusions

In this work, the VLE for *n*-heptane + (toluene, benzene, *p*-xylene, or ethylbenzene) + {[4empy][Tf_2N] (0.3) + [emim][DCA] (0.7)} pseudoternary systems have been determined at 323.2 K, 343.2 K, and 363.2 K over the whole range of compositions into the miscible region. In addition, the VLE of all pure hydrocarbons in the IL mixture has been studied over the whole range of compositions and at the selected temperatures. All VLE data obtained have been successfully fitted to the NRTL model.

The main advance of this work has been the high *n*-heptane/aromatic relative volatility values obtained in the VLE

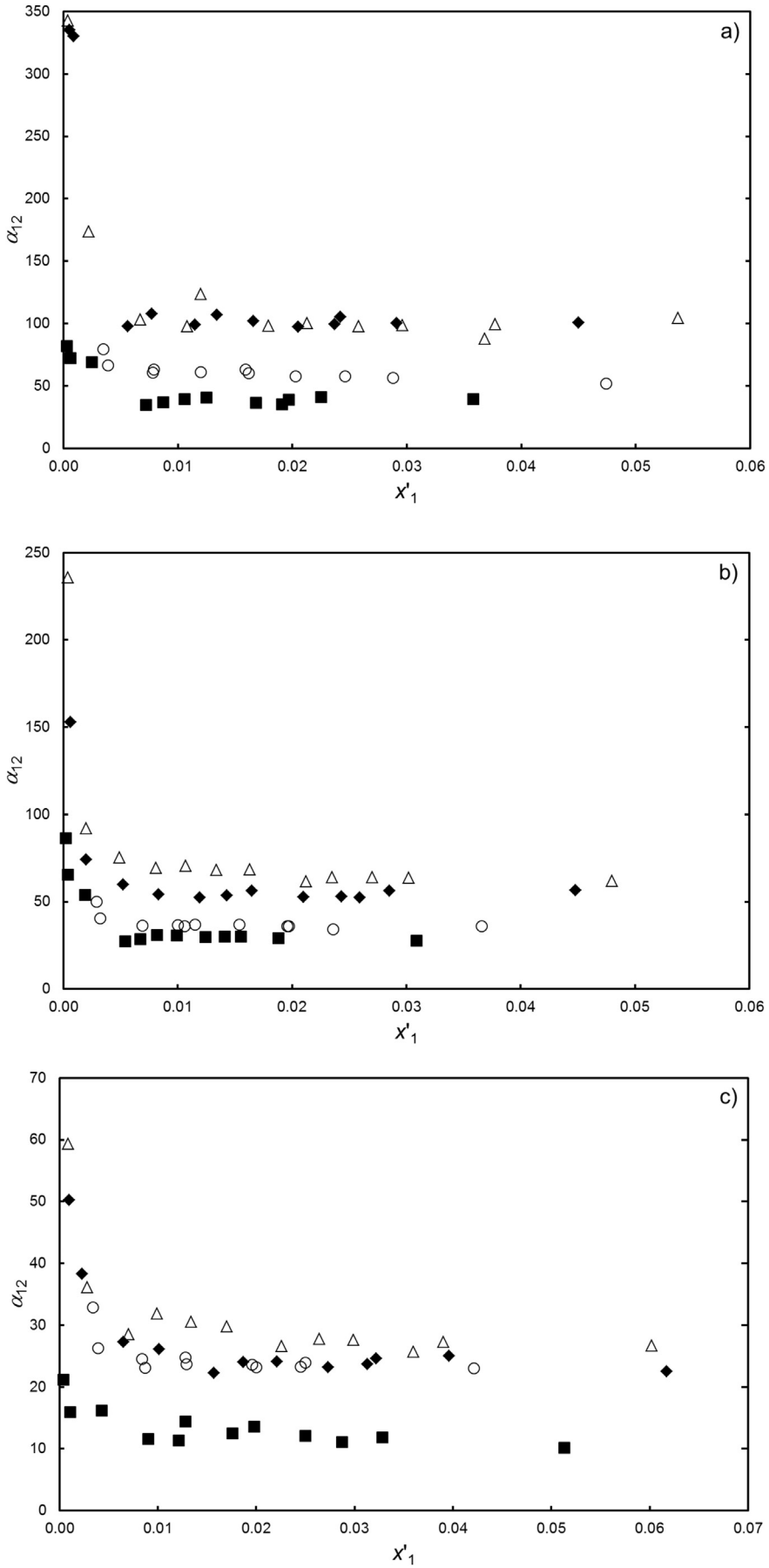

Fig. 7. Comparison of the *n*-heptane relative volatility from aromatics (α_{12}) in the presence of {[4empy][Tf_2N] (0.3) + [emim][DCA] (0.7)} at $x_3 \cong 0.98$: a) 323.2 K; b) 343.2 K; c) 363.2 K. ○, toluene; ■, benzene; △, *p*-xylene; ◆, ethylbenzene.

determinations carried out. The *n*-heptane relative volatility from benzene and toluene has been up to 30 and 50 times higher in the pseudoternary system than in the corresponding binary systems, respectively. The maximum increase in the *n*-heptane/aromatic relative volatility for the *p*-xylene and ethylbenzene cases has been about 15 times. The lowest temperature, 323.2 K, has let to achieve the highest *n*-heptane/aromatic relative volatilities values.

Finally, it is possible to claim that the {[4empy][Tf_2N] (0.3) + [emim][DCA] (0.7)} mixture show an efficient behavior in the *n*-heptane selective recovery from the aromatics in extract-type models.

Acknowledgments

Authors are grateful to the Ministerio de Economía y Competitividad (MINECO) of Spain and the Comunidad de Madrid for financial support of Projects CTQ2014-53655-R and S2013/MAE-2800, respectively. Pablo Navarro also thanks MINECO for awarding him an FPI grant (Reference BES-2012-052312).

Appendix A. Supplementary data

Supplementary data related to this article can be found at http://dx.doi.org/10.1016/j.fluid.2016.02.018.

References

[1] R.D. Rogers, K.R. Seddon, Science 302 (2003) 792–793.
[2] N.V. Plechkova, K.R. Seddon, Chem. Soc. Rev. 37 (2008) 123–150.
[3] F. Onink, C. Drumm, G.W. Meindersma, H.-J. Bart, A.B. de Haan, Chem. Eng. J. 160 (2010) 511–521.
[4] N. Calvar, I. Domínguez, E. Gómez, A. Domínguez, Chem. Eng. J. 175 (2011) 213–221.
[5] G.W. Meindersma, A.J.G. Podt, A.B. de Haan, Fluid Phase Equilib. 247 (2006) 158–168.
[6] A.E. Andreatta, A. Arce, E. Rodil, A. Soto, Fluid Phase Equilib. 287 (2010) 84–94.
[7] E. Alvarez-Guerra, S.P.M. Ventura, J.A.P. Coutinho, A. Irabien, Fluid Phase Equilib. 371 (2014) 67–74.
[8] A.V. Orchillés, J.P. Miguel, V. González-Alfaro, E. Vercher, J. Chem. Eng. Data 57 (2012) 394–399.
[9] M. Larriba, P. Navarro, J. García, F. Rodríguez, Fluid Phase Equilib. 380 (2014) 1–10.
[10] M. Larriba, P. Navarro, J. García, F. Rodríguez, Sep. Purif. Technol. 120 (2013) 392–401.
[11] B. Mokhtarani, J. Gmehling, J. Chem. Thermodyn. 42 (2010) 1036–1038.
[12] B. Mokhtarani, L. Valialahi, K.T. Heidar, H.R. Mortaheb, A. Sharifi, M. Mirzaei, J. Chem. Thermodyn. 51 (2012) 77–81.
[13] L. Zhang, J. Han, D. Deng, J. Ji, Fluid Phase Equilib. 255 (2007) 179–185.
[14] P. Navarro, M. Larriba, J. García, E.J. González, F. Rodríguez, J. Chem. Thermodyn. (2016), http://dx.doi.org/10.1016/j.jct.2015.12.033.
[15] P. Navarro, M. Larriba, J. García, E.J. González, F. Rodríguez, Fluid Phase Equilib. 387 (2015) 209–216.
[16] P. Navarro, M. Larriba, J. García, F. Rodríguez, J. Chem. Thermodyn. 76 (2014) 152–160.
[17] B. Kolb, L.S. Ettre, Static Headspace-Gas Chromatography: Theory and Practice, Wiley-VCH, New York, 1997.
[18] P. Luis, C. Wouters, N. Sweygers, C. Creemers, B. Van der Bruggen, J. Chem. Thermodyn. 49 (2012) 128–136.
[19] Z. Jiqin, C. Jian, L. Chengyue, F. Weiyang, Fluid Phase Equilib. 247 (2006) 102–106.
[20] H. Renon, J.M. Prausnitz, AlChE J. 14 (1968) 135–144.
[21] M.G. Freire, A.R.R. Teles, M.A.A. Rocha, B. Schroder, C.M.S.S. Neves, P.J. Carvalho, D.V. Evtuguin, L.M.N.B.F. Santos, J.A.P. Coutinho, J. Chem. Eng. Data 56 (2011) 4813–4822.
[22] J.M.P. França, F. Reis, S.I.C. Vieira, M.J.V. Lourenco, F.J.V. Santos, C.A. Nieto de Castro, A.A.H. Padua, J. Chem. Thermodyn. 79 (2014) 248–257.
[23] S. Seki, S. Tsuzuki, K. Hayamizu, Y. Umebayashi, N. Serizawa, K. Takei, H. Miyashiro, J. Chem. Eng. Data 57 (2012) 2211–2216.
[24] M. Larriba, P. Navarro, J. Garcia, F. Rodriguez, Fluid Phase Equilib. 364 (2014) 48–54.
[25] Q.-S. Liu, P.-P. Li, U. Welz-Biermann, X.-X. Liu, J. Chen, J. Chem. Eng. Data 57 (2012) 2999–3004.
[26] R.H. Perry, D.W. Green, J.O. Maloney, Perry's Chemical Engineers' Handbook, McGraw-Hill, 1999.
[27] Aspen Plus Version 7.1, Database, Aspen Technology, 2004.

Journal of chemical & engineering data

Article

pubs.acs.org/jced

Vapor−Liquid Equilibria for (*n*-Hexane, *n*-Octane, Cyclohexane, or 2,3-Dimethylpentane) + Toluene + {[4empy][Tf_2N] (0.3) + [emim][DCA] (0.7)} Mixed Ionic Liquids

Pablo Navarro, Marcos Larriba, Julián García,* and Francisco Rodríguez

Department of Chemical Engineering, Complutense University of Madrid, E−28040 Madrid, Spain

Supporting Information

ABSTRACT: Recently, the study about the use of ionic liquids (ILs) in the aromatic extraction is focused in the selective separation of the hydrocarbons and the solvent in order to propose a whole alternative process involving ILs. As a consequence, the vapor−liquid equilibria (VLE) for the hydrocarbons + ILs systems are required. In this work the VLE for several alkane + toluene systems in the presence of the 1-ethyl-4-methylpyridinium bis(trifluoromethylsulfonyl)-imide ([4empy][Tf_2N]) (0.3) + 1-ethyl-3-methylimidazolium dicyanamide ([emim][DCA]) (0.7) binary IL mixture were determined. In addition to extend the experimental VLE information, this work is aimed at the alkane structure evaluation: linear alkanes (*n*-hexane and *n*-octane), cyclic alkanes (cyclohexane), and branched-chain alkanes (2,3-dimethylpentane) have been used. All systems have been studied at 323.2, 343.2, and 363.2 K over the whole range of composition within the miscibility region. The NRTL thermodynamic model was used to adjust the VLE for all systems. The high values of alkane/toluene relative volatilities found suggest the alkane selective separation from the reference aromatic hydrocarbon, toluene.

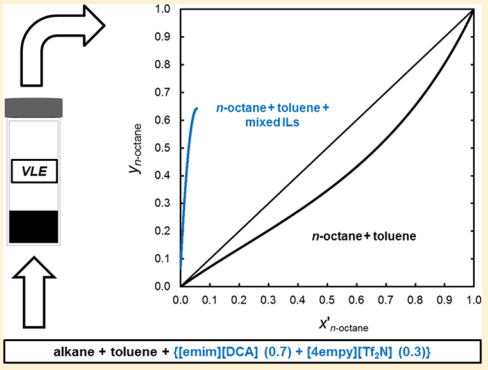

1. INTRODUCTION

Ionic liquids (ILs) are liquid salts at temperatures lower than 373 K. In addition to their liquid state, their negligible vapor pressure is the main advantage that become ILs as potential alternatives to organic solvents in separation processes.[1,2]

The good performance of ILs as solvents in extraction processes has been demonstrated so far.[3−7] The aromatic extraction is one of the topics in which ILs have been widely investigated as a result of the good extraction performance associated with these new solvents. However, analyzing the large number of studies, it is difficult to find pure ILs that simultaneously show good extractive and physical properties in comparison to a currently used solvent, such as sulfolane.[8−14]

Therefore, the use of binary mixtures of ILs has been proposed to improve the IL-based solvents, combining the goodness of two complementary ILs.[15,16] This way, our recent works concerning the use of the {[4empy][Tf_2N] (0.3) + [emim][DCA] (0.7)} IL mixture as solvent in the aromatic extraction has demonstrated that this IL mixture shows higher extractive properties than those of sulfolane and adequate densities and viscosities.[15,16] In addition to this, the maximum operation temperature (MOT) for the IL mixture was estimated to be 413 K.

Although the good extraction performance and the adequate properties of the {[4empy][Tf_2N] (0.3) + [emim][DCA] (0.7)} IL mixture, the recovery of the hydrocarbons from the extract stream should be studied to assay the feasibility of the alternative process. For that reason, the vapor−liquid equilibria (VLE) data for alkane + aromatic + {[4empy][Tf_2N] + [emim][DCA]} systems should be known.

Until now the alkane selective recovery from aromatics was observed at 0.2, 0.4, 0.6, and 0.8 mole fraction of [4empy][Tf_2N]

Table 1. Specifications of Chemicals

chemical	source	final mass fraction purity	purification method	analysis method
[emim][DCA]	Iolitec GmbH	0.98	none	NMR,[a] IC[b]
[4empy][Tf_2N]	Iolitec GmbH	0.99	none	NMR,[a] IC[b]
n-hexane	Sigma-Aldrich	0.995	molecular sieves	GC[c]
n-octane	Sigma-Aldrich	0.990	molecular sieves	GC[c]
cyclohexane	Sigma-Aldrich	0.995	molecular sieves	GC[c]
2,3-dimethylpentane	Sigma-Aldrich	0.990	molecular sieves	GC[c]
toluene	Sigma-Aldrich	0.995	molecular sieves	GC[c]

[a]Nuclear magnetic resonance. [b]Ion chromatography. [c]Gas chromatography.

Received: February 9, 2016
Accepted: May 28, 2016

DOI: 10.1021/acs.jced.6b00116
J. Chem. Eng. Data XXXX, XXX, XXX−XXX

Table 2. NRTL Parameters[a] from the Adjustment of Pseudobinary and Pseudoternary VLE with {[4empy][Tf_2N] (0.3) + [emim][DCA] (0.7)}

$i - j$	Δg_{ij}/J·mol^{-1}	Δg_{ji}/J·mol^{-1}	Δx	ΔP/ kPa
n-Hexane (1) + {[4empy][Tf_2N] (2) + [emim][DCA] (3)}				
1 − (2 + 3)	7187.5	454.14	0.002	0.01
n-Octane (1) + {[4empy][Tf_2N] (2) + [emim][DCA] (3)}				
1 − (2 + 3)	7599.0	634.81	0.002	0.05
cyclohexane (1) + {[4empy][Tf_2N] (2) + [emim][DCA] (3)}				
1 − (2 + 3)	6376.8	−2965.2	0.003	0.03
2,3-Dimethylpentane (1) + {[4empy][Tf_2N] (2) + [emim][DCA] (3)}				
1 − (2 + 3)	3802.1	7059.3	0.001	0.01
n-Hexane (1) + Toluene (2) + {[4empy][Tf_2N] (3) + [emim][DCA] (4)}				
1 − 2	−898.48	4786.8	0.005	0.08
1 − (3 + 4)	−1371.9	11 963		
2 − (3 + 4)	−1370.5	−2886.3		
n-Octane (1) + Toluene (2) + {[4empy][Tf_2N] (3) + [emim][DCA] (4)}				
1 − 2	−895.88	4831.3	0.006	0.05
1 − (3 + 4)	3843.5	12 085		
2 − (3 + 4)	3885.9	−2890.6		
Cyclohexane (1) + Toluene (2) + {[4empy][Tf_2N] (3) + [emim][DCA] (4)}				
1 − 2	−1207.7	2685.7	0.005	0.04
1 − (3 + 4)	−355.59	11 684		
2 − (3 + 4)	−647.70	−2622.8		
2,3-Dimethylpentane (1) + Toluene (2) + {[4empy][Tf_2N] (3) + [emim][DCA] (4)}				
1 − 2	−1206.2	2722.7	0.004	0.04
1 − (3 + 4)	224.99	11 711		
2 − (3 + 4)	143.50	−2629.3		

[a] $\alpha_{1(2+3)}$, α_{12}, $\alpha_{1(3+4)}$, and $\alpha_{2(3+4)}$ were set in 0.3 for all systems

in the IL mixture for benchmark compositions for the *n*-heptane + (benzene, toluene, *p*-xylene, or ethylbenzene) + {[4empy][Tf_2N] + [emim][DCA]} systems and in the (*n*-hexane, *n*-octane, cyclohexane, or 2,3-dimethylpentane) + toluene + {[4empy][Tf_2N] + [emim][DCA]} mixtures.[17,18]

However, the BTEX sources have a variable concentration of aromatic and nonaromatic hydrocarbons and it is important to know in detail the hydrocarbon structure influence in the aromatic/aliphatic separations. In our last work, the aromatic structure effect was exhaustively evaluated in the VLE data of the *n*-heptane + aromatic + {[4empy][Tf_2N] (0.3) + [emim][DCA] (0.7)} systems over the whole range of compositions in the VLE region.[19]

Here, the VLE data for *n*-hexane, *n*-octane, cyclohexane, or 2,3-dimethylpentane + toluene + {[4empy][Tf_2N] (0.3) + [emim][DCA] (0.7)} systems were determined to fully discuss the influence of the alkane structure in the equilibrium. The VLE data were determined using a novel headspace−gas chromatography (HS-GC) technique recently employed in VLE measurements involving hydrocarbons and ILs.[20] In the last few years, the use of this technique has been highly extended by its high reproducibility.[21−23]

The analysis of the alkane influence in the VLE for alkane + toluene + {[4empy][Tf_2N] (0.3) + [emim][DCA] (0.7)} systems was focused in three cases: the chain length in linear alkanes (*n*-hexane, *n*-heptane, *n*-octane), the cyclic or linear structure for alkanes with the same number of carbon atoms (*n*-hexane, cyclohexane), and the branched or linear chain also for alkanes with the same number of carbon atoms (*n*-heptane,

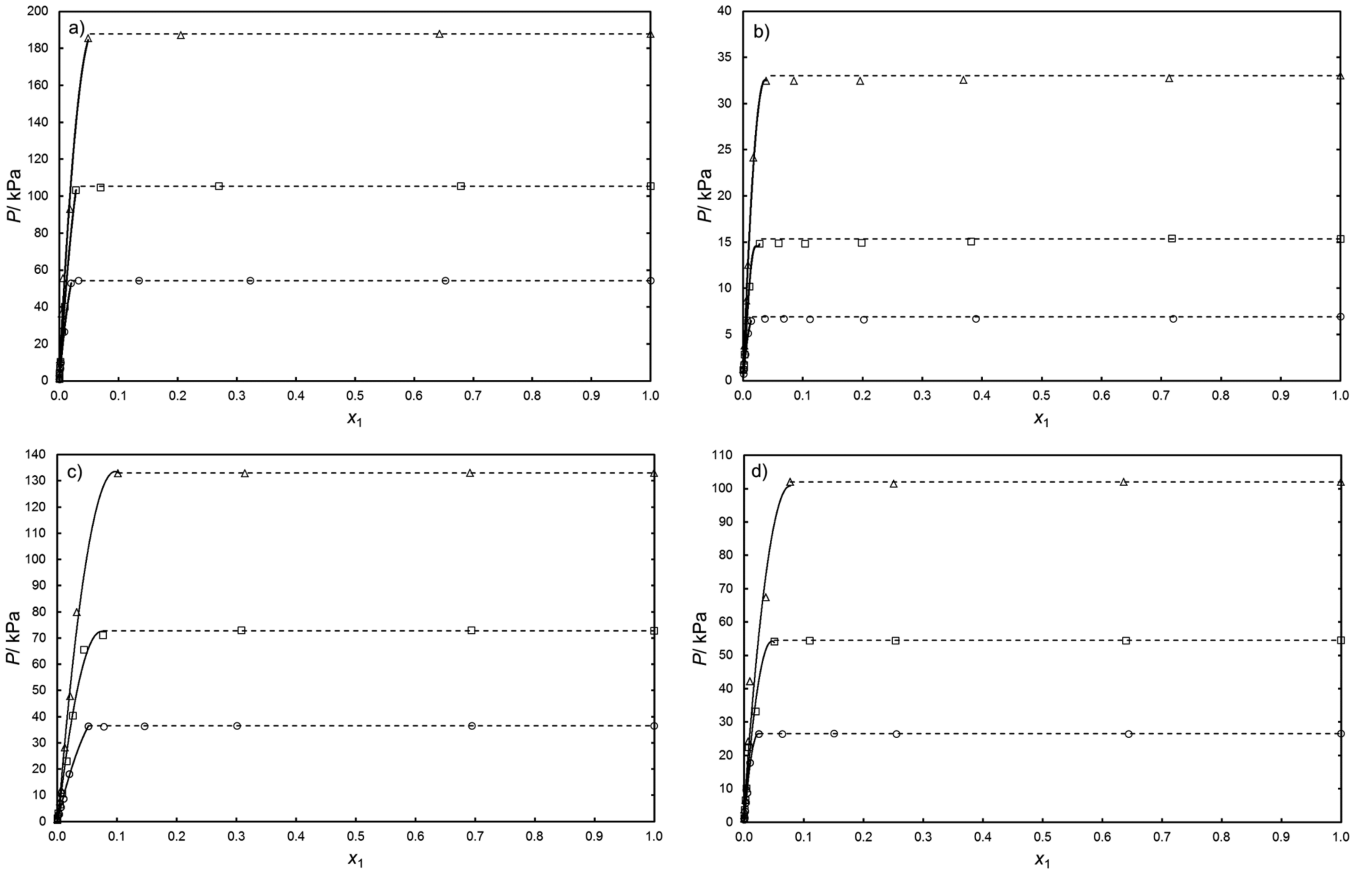

Figure 1. VLE data for binary system alkane (1) + {[4empy][Tf_2N] (2) + [emim][DCA] (3)} with a [emim][DCA] mole fraction in the IL mixture of 0.7 at several temperatures for (a) *n*-hexane, (b) *n*-octane, (c) cyclohexane, and (d) 2,3-dimethylpentane: ○, T = 323.2 K; □, T = 343.2 K; △, T = 363.2 K; solid lines denote the NRTL adjustment; dashed lines refer to constant pressure equal to the vapor pressure of the pure alkane.

DOI: 10.1021/acs.jced.6b00116
J. Chem. Eng. Data XXXX, XXX, XXX−XXX

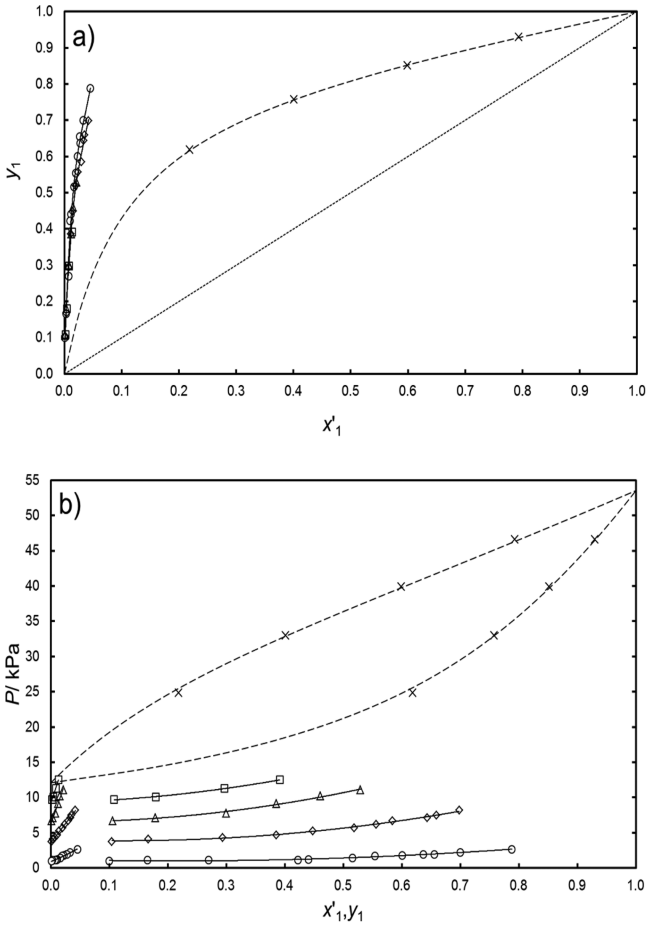

Figure 2. VLE data for ternary system *n*-hexane (1) + toluene (2) + {[4empy][Tf_2N] (3) + [emim][DCA] (4)} at T = 323.2 K. (a) $x'-y$ diagram and (b) $x',y-P$ diagram. ILs mole fraction (x_{3+4}): ○, x_{3+4} = 0.98; ◇, x_{3+4} = 0.90; △, x_{3+4} = 0.80; □, x_{3+4} = 0.70; ×, binary system of {*n*-hexane (1) + toluene (2)}. Solid lines denote the NRTL adjustment and dashed lines refer to VLE data from Aspen Plus Simulator Software Database at 323.2 K for the binary system of *n*-hexane (1) + toluene (2) from ref 27.

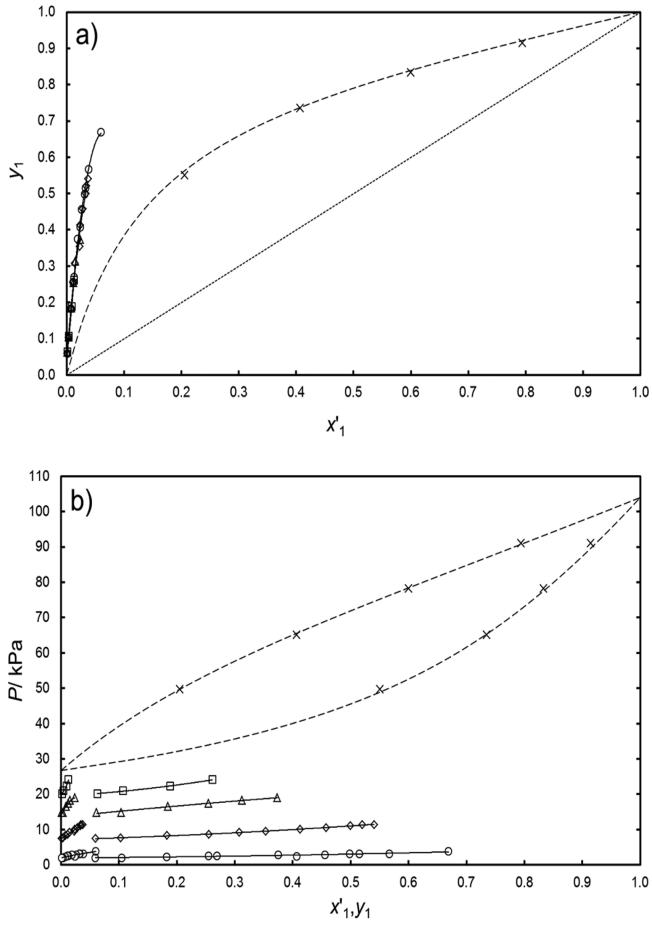

Figure 3. VLE data for ternary system *n*-hexane (1) + toluene (2) + {[4empy][Tf_2N] (3) + [emim][DCA] (4)} at T = 343.2 K. (a) $x'-y$ diagram and (b) $x',y-P$ diagram. ILs mole fraction (x_{3+4}): ○, x_{3+4} = 0.98; ◇, x_{3+4} = 0.90; △, x_{3+4} = 0.80; □, x_{3+4} = 0.71; ×, binary system of {*n*-hexane (1) + toluene (2)}. Solid lines denote the NRTL adjustment and dashed lines refer to VLE data from Aspen Plus Simulator Software Database at 343.2 K for the binary system of *n*-hexane (1) + toluene (2) from ref 27.

2,3-dimethylpentane). In addition to this, the VLE data for the alkane + toluene binary mixtures without the IL mixture were measured to be used as benchmark and to validate the experimental method in these particular hydrocarbon binary systems. The VLE data for *n*-hexane, *n*-octane, cyclohexane, or 2,3-dimethylpentane + {[4empy][Tf_2N] (0.3) + [emim][DCA] (0.7)} systems were also determined to compare the different interactions alkane-IL. Finally, the non-random two liquids (NRTL) thermodynamic model was employed to fit the VLE data.

2. EXPERIMENTAL SECTION

2.1. Chemicals. [emim][DCA] and [4empy][Tf_2N] were purchased from Iolitec GmbH and were employed as received without further purifications. The purities of the ILs were listed in Table 1. The water and halide concentration in the [emim][DCA] were analyzed by the manufacturer being less than 1790 ppm and 2%, respectively, whereas in the case of [4empy][Tf_2N] were less than 42 ppm for the water and 100 ppm for the halides. In order to keep the purities of the ILs, they were maintained in their original vessels into a desiccator filled with silica gel and were handed under a dry atmosphere of nitrogen into a closed glovebox. Moreover, all hydrocarbons were acquired from Sigma-Aldrich with mass fraction purities higher than 99 wt % as can be also find in Table 1.

2.2. VLE Procedure and Analysis. The VLE was measured employing an HS-GC technique. This method was widely described in our previous work;[20] thus, here, we included the equipment used and the essential information to understand the experimental determinations. The equipment were an Agilent Headspace 7697 A injector coupled to an Agilent GC 7890 A, the latter equipped with a flame ionization detector.

The feed mixtures were gravimetrically prepared with a Mettler Toledo XS205 balance that assays a precision of $\pm 10^{-5}$ g. The VLE was reached in vials of 20.0 mL filled with a controlled volume of sample of 1.0 mL. In addition to the selection of the equilibrium temperatures, which were 323.2, 343.2, and 363.2 K, also an equilibration time of 2 h and an agitation of 100 rpm were required to ensure the VLE in the vial.

The partial pressures (P_i) associated with each hydrocarbon in the vapor phase were determined by employing the

DOI: 10.1021/acs.jced.6b00116
J. Chem. Eng. Data XXXX, XXX, XXX−XXX

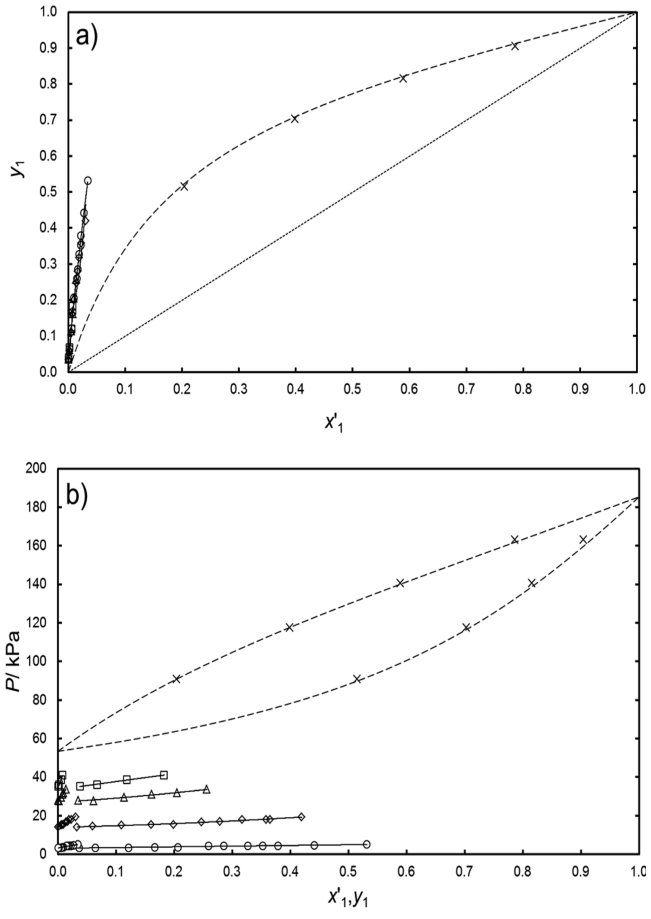

Figure 4. VLE data for ternary system *n*-hexane (1) + toluene (2) + {[4empy][Tf_2N] (3) + [emim][DCA] (4)} at T = 363.2 K. (a) x'−y diagram and (b) x',y−P diagram. ILs mole fraction (x_{3+4}): ○, x_{3+4} = 0.98; ◇, x_{3+4} = 0.91; △, x_{3+4} = 0.81; □, x_{3+4} = 0.73; ×, binary system of {*n*-hexane (1) + toluene (2)}. Solid lines denote the NRTL adjustment and dashed lines refer to VLE data from Aspen Plus Simulator Software Database at 363.2 K for the binary system of *n*-hexane (1) + toluene (2) from ref 27.

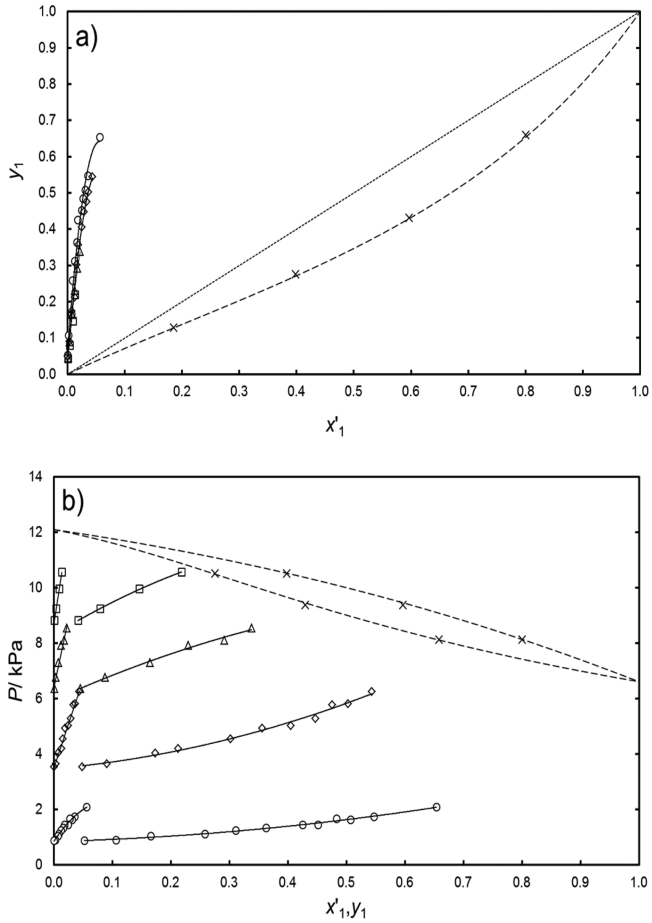

Figure 5. VLE data for ternary system *n*-octane (1) + toluene (2) + {[4empy][Tf_2N] (3) + [emim][DCA] (4)} at T = 323.2 K. (a) x'−y diagram and (b) x',y−P diagram. ILs mole fraction (x_{3+4}): ○, x_{3+4} = 0.97; ◇, x_{3+4} = 0.89; △, x_{3+4} = 0.79; □, x_{3+4} = 0.71; ×, binary system of {*n*-octane (1) + toluene (2)}. Solid lines denote the NRTL adjustment and dashed lines refer to VLE data from Aspen Plus Simulator Software Database at 323.2 K for the binary system of *n*-octane (1) + toluene (2) from ref 27.

relationship between the peak areas of each hydrocarbons in the VLE (A_i) and the peak areas related to each hydrocarbon alone in the same conditions (A_i^0); we also needed the vapor pressure of each hydrocarbon (P_i^0) at the same temperature[21,24]

$$P_i = \frac{P_i^0 \cdot A_i}{A_i^0} \tag{1}$$

It is important to highlight that the repeatability of peak areas was lower than 1% for all hydrocarbons. The vapor phase compositions were obtained by the GC analysis and using the response factor method. Finally, the liquid compositions (x_i) were calculated correcting the feed compositions (z_i) of each hydrocarbon with the amount of each hydrocarbon that goes to the vapor phase

$$x_i = \frac{z_i \cdot F - (P_i \cdot V_G / R \cdot T)}{\sum_{i=1}^{3} (z_i \cdot F - (P_i \cdot V_G / R \cdot T))} \tag{2}$$

where F is the molar amount of the overall feed, V_G denotes the headspace volume of the vial (19.0 mL), and R refers to the ideal gas law constant.

3. RESULTS AND DISCUSSION

The VLE for (*n*-hexane, *n*-octane, cyclohexane, or 2,3-dimethylpentane) + {[4empy][Tf_2N] (0.3) + [emim][DCA] (0.7)}, (*n*-hexane, *n*-octane, cyclohexane, or 2,3-dimethylpentane) + toluene + {[4empy][Tf_2N] (0.3) + [emim][DCA] (0.7)}, and (*n*-hexane, *n*-octane, cyclohexane, or 2,3-dimethylpentane) + toluene systems were determined as a function of temperature and over the whole composition range

The hydrocarbon binary mixtures were determined to validate the experimental method, whereas the NRTL model was selected to correlate the new VLE data with the mixture of ILs. This was aimed in the good correlation between the experimental VLE data and those calculated by using NRTL in similar systems from previous works.[19,20,25,26] The adjustment was done minimizing the next objective function (OF)

$$\mathrm{OF} = \frac{a \cdot \sum_{i=1}^{I} |x_{i,\mathrm{calc}} - x_{i,\mathrm{exptl}}| + \sum_{i=1}^{I} |P_{i,\mathrm{calc}} - P_{i,\mathrm{exptl}}|}{N} \tag{3}$$

where a is the weighting coefficient of liquid mole fraction deviations to balance their difference of magnitude with partial pressures and N refers to the number of VLE points.

DOI: 10.1021/acs.jced.6b00116
J. Chem. Eng. Data XXXX, XXX, XXX−XXX

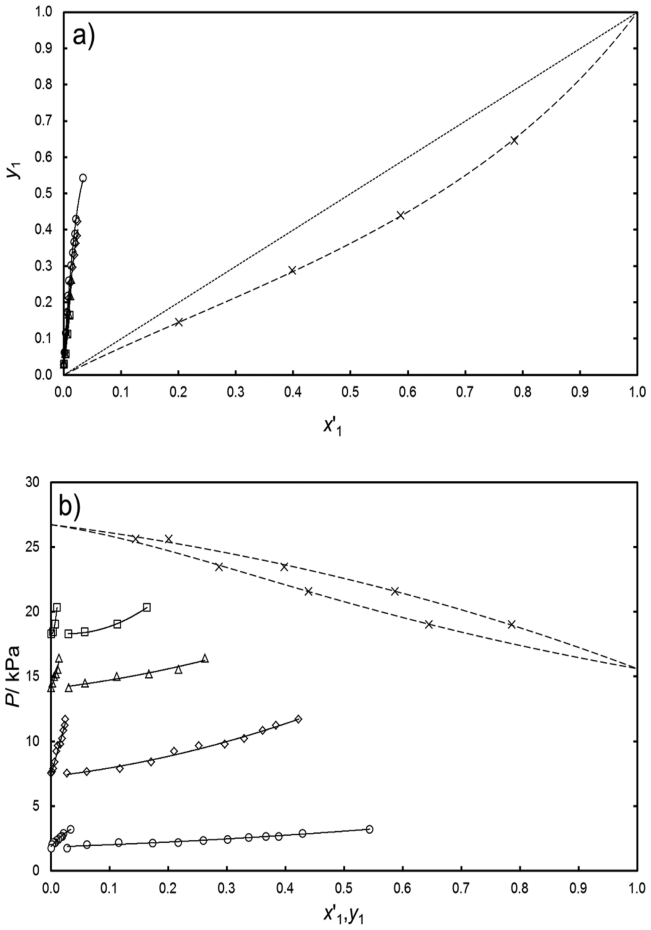

Figure 6. VLE data for ternary system *n*-octane (1) + toluene (2) + {[4empy][Tf_2N] (3) + [emim][DCA] (4)} at T = 343.2 K. (a) $x'-y$ diagram and (b) $x',y-P$ diagram. ILs mole fraction (x_{3+4}): ○, x_{3+4} = 0.97; ◇, x_{3+4} = 0.89; △, x_{3+4} = 0.79; □, x_{3+4} = 0.70; ×, binary system of {*n*-octane (1) + toluene (2)}. Solid lines denote the NRTL adjustment and dashed lines refer to VLE data from Aspen Plus Simulator Software Database at 343.2 K for the binary system of *n*-octane (1) + toluene (2) from ref 27.

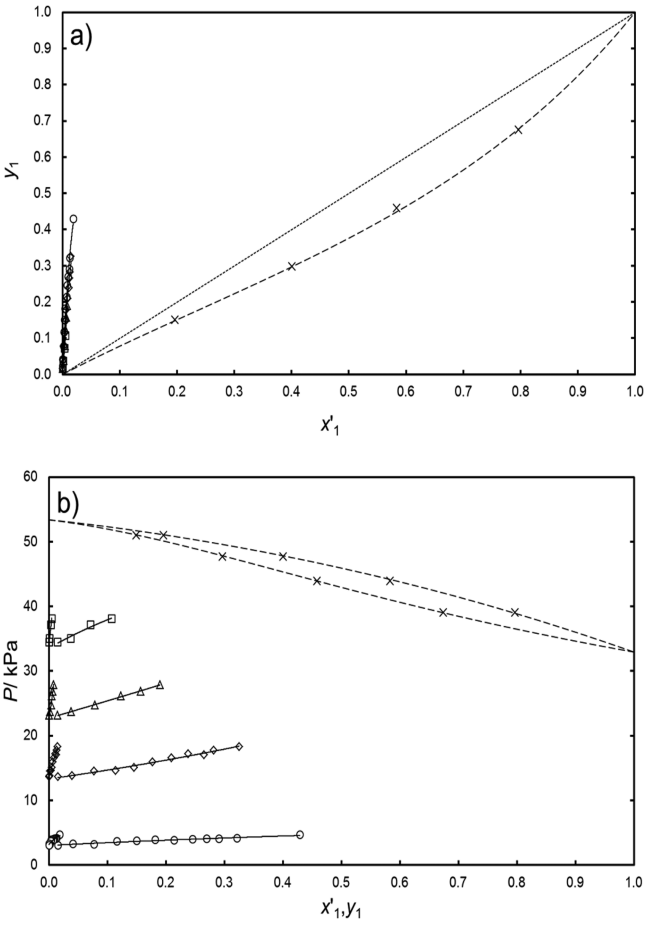

Figure 7. VLE data for ternary system *n*-octane (1) + toluene (2) + {[4empy][Tf_2N] (3) + [emim][DCA] (4)} at T = 363.2 K. (a) $x'-y$ diagram and (b) $x',y-P$ diagram. ILs mole fraction (x_{3+4}): ○, x_{3+4} = 0.98; ◇, x_{3+4} = 0.90; △, x_{3+4} = 0.80; □, x_{3+4} = 0.74; ×, binary system of {*n*-octane (1) + toluene (2)}. Solid lines denote the NRTL adjustment and dashed lines refer to VLE data from Aspen Plus Simulator Software Database at 363.2 K for the binary system of *n*-octane (1) + toluene (2) from ref 27.

The a value was fixed in 300 based on the standard uncertainties of pressure and liquid mole fractions. The Solver tool of Microsoft Excel spreadsheet software runs the algorithm. The NRTL parameters obtained from the fit are displayed in Table 2, with the mean deviations of the liquid mole fractions, Δx, and the equilibrium pressures, ΔP, calculated as

$$\Delta x = \frac{\sum_{i=1}^{I} |x_{i,\mathrm{calc}} - x_{i,\mathrm{exptl}}|}{N} \quad (4)$$

$$\Delta P = \frac{\sum_{i=1}^{I} |P_{i,\mathrm{calc}} - P_{i,\mathrm{exptl}}|}{N} \quad (5)$$

As can be seen in Table 2, the low mean deviations of the liquid mole fractions and pressures confirmed the reliability of NRTL to correlate the VLE for systems containing hydrocarbons and ILs.

3.1. VLE for Alkane + {[4empy][Tf_2N] (0.3) + [emim][DCA] (0.7)}. The $x-P$ data obtained for the systems (*n*-hexane, *n*-octane, cyclohexane, or 2,3-dimethylpentane) + {[4empy][Tf_2N] (0.3) + [emim][DCA] (0.7)} systems are collected in Table S1 in the Supporting Information and are shown in Figure 1 as a function of temperature and liquid mole fraction of the alkane. At all temperatures, there are two delimitate zones: the VLE zone between the minimum mole fraction of the alkane and the maximum solubility of the alkane in the IL mixture; and the vapor−liquid−liquid equilibria (VLLE) at mole fraction of the alkane higher than its maximum solubility in the IL mixture. The former is characterized by a vapor pressure directly dependent on the mole fraction of the alkane, whereas the VLLE region is defined by a constant vapor pressure equal to the pure alkane.

The order of the alkane solubility in the {[4empy][Tf_2N] (0.3) + [emim][DCA] (0.7)} mixture was cyclohexane >2,3-dimethylpentane > *n*-hexane > *n*-octane, completely in agreement with our previous study of liquid−liquid equilibria involving the same alkanes and the same solvent at 313.2 K.[16]

Comparing these results with those previous gathered in the VLE measurement for the (*n*-heptane, toluene, benzene, *p*-xylene, or ethylbenzene) + {[4empy][Tf_2N] (0.3) + [emim][DCA] (0.7)} systems, the alkane solubility order including *n*-heptane was cyclohexane >2,3-dimethylpentane > *n*-hexane >

DOI: 10.1021/acs.jced.6b00116
J. Chem. Eng. Data XXXX, XXX, XXX−XXX

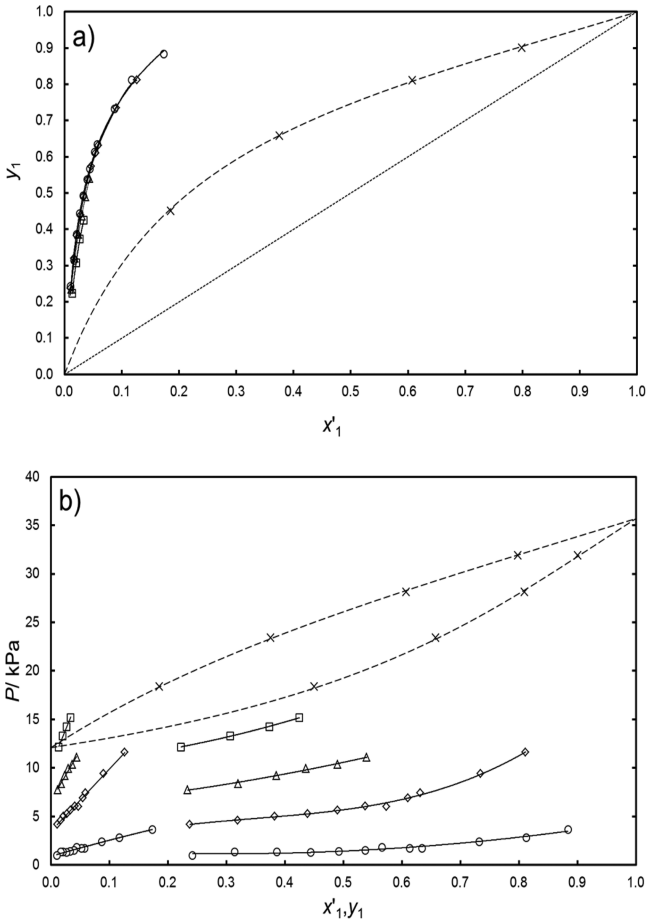

Figure 8. VLE data for ternary system cyclohexane (1) + toluene (2) + {[4empy][Tf_2N] (3) + [emim][DCA] (4)} at T = 323.2 K. (a) x'−y diagram and (b) x',y−P diagram. ILs mole fraction (x_{3+4}): ○, x_{3+4} = 0.97; ◇, x_{3+4} = 0.89; △, x_{3+4} = 0.78; □, x_{3+4} = 0.62; ×, binary system of {cyclohexane (1) + toluene (2)}. Solid lines denote the NRTL adjustment and dashed lines refer to VLE data from Aspen Plus Simulator Software Database at 323.2 K for the binary system of cyclohexane (1) + toluene (2) from ref 27.

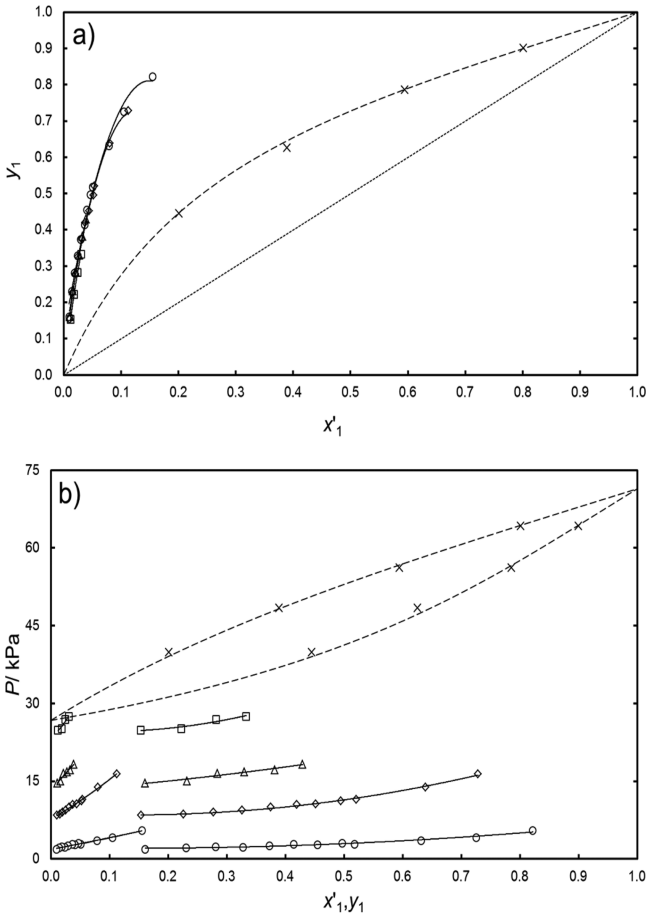

Figure 9. VLE data for ternary system cyclohexane (1) + toluene (2) + {[4empy][Tf_2N] (3) + [emim][DCA] (4)} at T = 343.2 K. (a) x'−y diagram and (b) x',y−P diagram. ILs mole fraction (x_{3+4}): ○, x_{3+4} = 0.97; ◇, x_{3+4} = 0.89; △, x_{3+4} = 0.79; □, x_{3+4} = 0.64; ×, binary system of {cyclohexane (1) + toluene (2)}. Solid lines denote the NRTL adjustment and dashed lines refer to VLE data from Aspen Plus Simulator Software Database at 343.2 K for the binary system of cyclohexane (1) + toluene (2) from ref 27.

n-heptane > *n*-octane, whereas all alkane solubilities are far from those for the aromatics.[19] In addition to this, an increase in temperature seems to slightly increase the alkane solubilities in the IL mixture, as was just found previously.[20]

The analysis of the main chain length of the alkanes can explain these results partially. As expected, *n*-octane (eight carbon atoms) was lower soluble than *n*-hexane (six carbon atoms) in the IL mixture, whereas the 2,3-dimethylpentane was more soluble than both *n*-alkanes as a result of a five carbon atoms main chain. The case of cyclohexane, which was the more soluble alkane in this work, can be explained by their cyclic nature, similar structure to the imidazolium and pyridinium rings of the ILs forming the {[4empy][Tf_2N] (0.3) + [emim][DCA] (0.7)} binary IL mixture.

3.2. VLE for Alkane + Toluene + {[4empy][Tf_2N] (0.3) + [emim][DCA] (0.7)}. The x,y−P data achieved in the (*n*-hexane, *n*-octane, cyclohexane, or 2,3-dimethylpentane) + toluene + {[4empy][Tf_2N] (0.3) + [emim][DCA] (0.7)} systems are displayed in Tables S2 to S5 in the Supporting Information, based on solvent-free basis compositions (x'). In addition, the experimental VLE data of the (*n*-hexane, *n*-octane, cyclohexane, or 2,3-dimethylpentane) + toluene systems are listed in Table S6 in the Supporting Information.

The VLE data are graphically represented in Figures 2 to 13 at the three temperatures evaluated in this work, using both x'−y and x',y−P diagrams. The experimental VLE data for the same hydrocarbon systems without the IL mixture, alkane + toluene, and the corresponding VLE data from the database of Aspen Plus are also shown to be used as benchmark and to validate the VLE technique.[27] Both collections of VLE for alkane + toluene systems are clearly in agreement.

The x'−y diagrams (a) from Figures 2 to 13 show that the vapor mole fraction of the alkane in equilibrium is quite higher for the alkane + toluene + {[4empy][Tf_2N] (0.3) + [emim]-[DCA] (0.7)} systems than for the same systems without the IL mixture. This fact can be also seen in the x',y−P diagrams (b) from the same figures, where the equilibrium lines of the vapor and liquid moves away one from the other as the IL mole fraction increases. This increase in the selective evaporation of the alkane is completely relevant for all systems, but the comparison between the VLE for *n*-octane + toluene + {[4empy][Tf_2N] (0.3) + [emim][DCA] (0.7)} system and the VLE for the *n*-octane + toluene system deserves to be highlighted.

As seen in Figures 5 to 7, the *n*-octane has a lower vapor pressure than that of toluene, and thus, toluene preferably

DOI: 10.1021/acs.jced.6b00116
J. Chem. Eng. Data XXXX, XXX, XXX−XXX

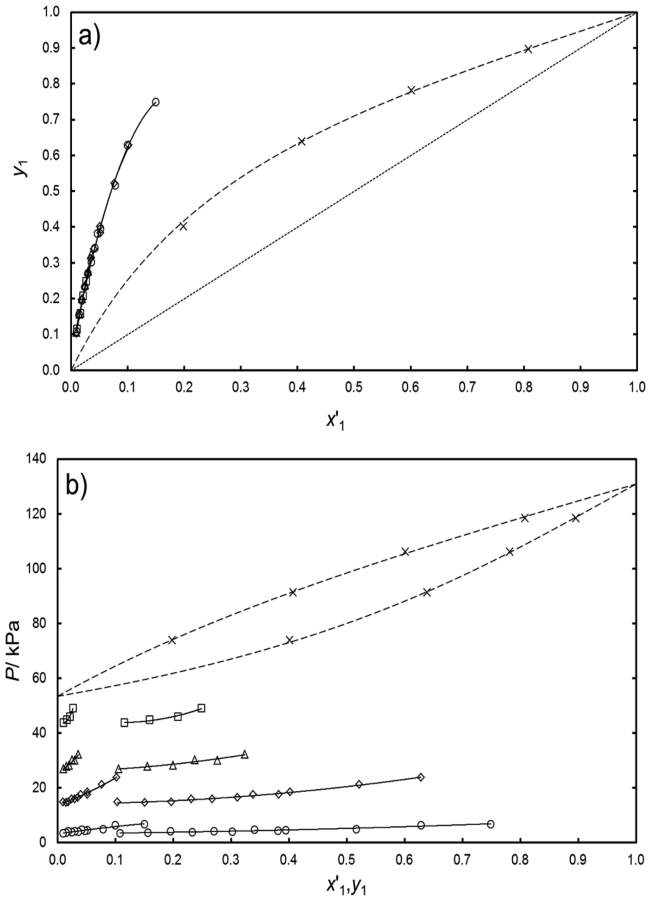

Figure 10. VLE data for ternary system cyclohexane (1) + toluene (2) + {[4empy][Tf_2N] (3) + [emim][DCA] (4)} at T = 363.2 K. (a) x'−y diagram and (b) x',y−P diagram. ILs mole fraction (x_{3+4}): ○, x_{3+4} = 0.97; ◇, x_{3+4} = 0.90; △, x_{3+4} = 0.80; □, x_{3+4} = 0.66; ×, binary system of {cyclohexane (1) + toluene (2)}. Solid lines denote the NRTL adjustment and dashed lines refer to VLE data from Aspen Plus Simulator Software Database at 363.2 K for the binary system of cyclohexane (1) + toluene (2) from ref 27.

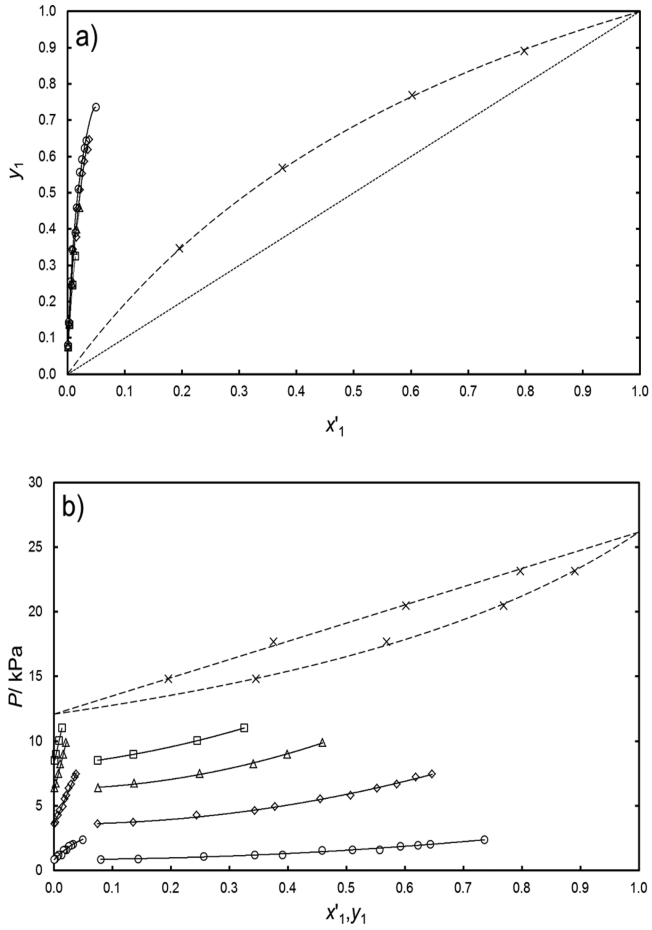

Figure 11. VLE data for ternary system 2,3-dimethylpentane (1) + toluene (2) + {[4empy][Tf_2N] (3) + [emim][DCA] (4)} at T = 323.2 K. (a) x'−y diagram and (b) x',y−P diagram. ILs mole fraction (x_{3+4}): ○, x_{3+4} = 0.97; ◇, x_{3+4} = 0.89; △, x_{3+4} = 0.79; □, x_{3+4} = 0.71; ×, binary system of {2,3-dimethylpentane (1) + toluene (2)}. Solid lines denote the NRTL adjustment and dashed lines refer to VLE data from Aspen Plus Simulator Software Database at 323.2 K for the binary system of 2,3-dimethylpentane (1) + toluene (2) from ref 27.

goes to the vapor phase in the *n*-octane + toluene system. However, the *n*-octane has a considerably higher concentration than toluene in the VLE for *n*-octane + toluene + {[4empy][Tf_2N] (0.3) + [emim][DCA] (0.7)} system, drastically changing the volatility order of both hydrocarbons.

The relative volatilities (α_{12}) of alkane (1) from toluene (2) were calculated to correctly compare the effect of the {[4empy][Tf_2N] (0.3) + [emim][DCA] (0.7)} in the hydrocarbons separation as follows:

$$\alpha_{12} = \frac{y_1/x_1}{y_2/x_2} \tag{6}$$

where y are the vapor mole fraction of the hydrocarbons. The calculated values of α_{12} are collected along with the experimental VLE in Tables S2 to S6 in the Supporting Information.

The alkane/toluene relative volatilities are graphically shown in Figure 14 for the (*n*-hexane, *n*-heptane, *n*-octane, cyclohexane, or 2,3-dimethylpentane) + toluene + {[4empy][Tf_2N] (0.3) + [emim][DCA] (0.7)} systems. As can be seen at all temperatures used in this work, the next alkane/toluene relative volatility order as a function of the alkane structure was found: *n*-hexane >2,3-dimethylpentane > *n*-heptane > *n*-octane > cyclohexane.

In linear alkanes, the alkyl chain length increase highly reduces the alkane/toluene relative volatility, especially at 323.2 K. Although *n*-hexane is the most soluble in the {[4empy][Tf_2N] (0.3) + [emim][DCA] (0.7)} mixture, its higher volatile character had a dominant effect in its vapor−liquid separation from toluene.

The change of a linear alkane of seven carbon atoms by a branched-chain alkane with the same number of carbon atoms (2,3-dimethylpentane) means a little increase in the alkane/ relative volatility. This is because a shorter main chain increases the volatile character of an alkane, and this effect is more important in alkane + aromatic + {[4empy][Tf_2N] (0.3) + [emim][DCA] (0.7)} systems than the higher solubility of shorter alkanes in the IL mixture, as explained above.

Finally, the cyclic structure instead of a linear structure was analyzed in the VLE data for (cyclohexane or *n*-hexane) + toluene + {[4empy][Tf_2N] (0.3) + [emim][DCA] (0.7)} systems. As a result of the lower vapor pressure of cyclohexane and its higher solubility in the IL mixture than the *n*-hexane values, the *n*-hexane/toluene relative volatilities were quite higher than the cyclohexane/toluene ones.

DOI: 10.1021/acs.jced.6b00116
J. Chem. Eng. Data XXXX, XXX, XXX−XXX

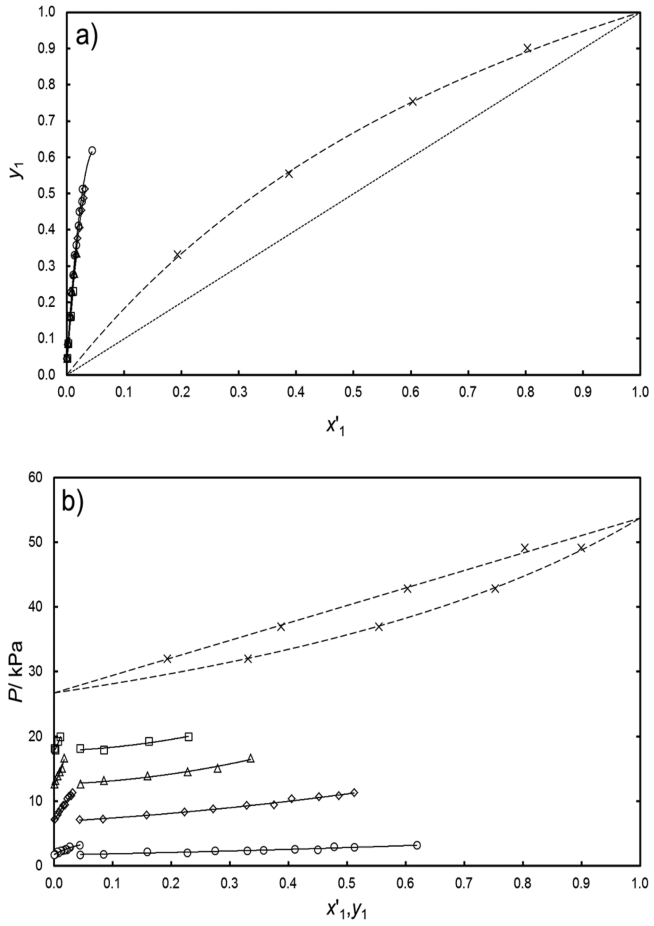

Figure 12. VLE data for ternary system 2,3-dimethylpentane (1) + toluene (2) + {[4empy][Tf_2N] (3) + [emim][DCA] (4)} at T = 343.2 K. (a) x'−y diagram and (b) x',y−P diagram. ILs mole fraction (x_{3+4}): ○, x_{3+4} = 0.97; ◇, x_{3+4} = 0.90; △, x_{3+4} = 0.80; □, x_{3+4} = 0.71; ×, binary system of {2,3-dimethylpentane (1) + toluene (2)}. Solid lines denote the NRTL adjustment and dashed lines refer to VLE data from Aspen Plus Simulator Software Database at 343.2 K for the binary system of 2,3-dimethylpentane (1) + toluene (2) from ref 27.

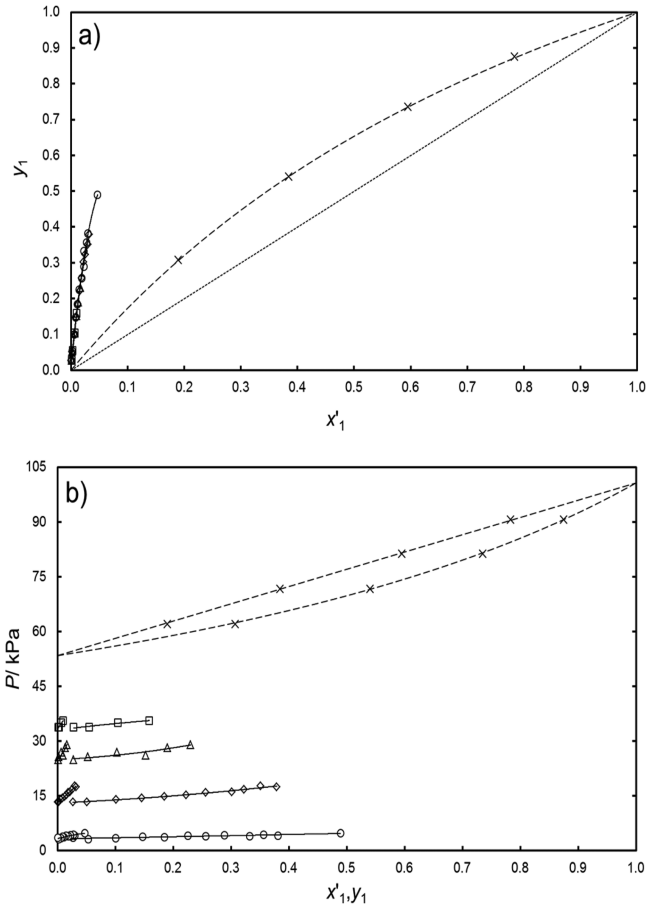

Figure 13. VLE data for ternary system 2,3-dimethylpentane (1) + toluene (2) + {[4empy][Tf_2N] (3) + [emim][DCA] (4)} at T = 363.2 K. (a) x'−y diagram and (b) x',y−P diagram. ILs mole fraction (x_{3+4}): ○, x_{3+4} = 0.97; ◇, x_{3+4} = 0.90; △, x_{3+4} = 0.80; □, x_{3+4} = 0.72; ×, binary system of {2,3-dimethylpentane (1) + toluene (2)}. Solid lines denote the NRTL adjustment and dashed lines refer to VLE data from Aspen Plus Simulator Software Database at 363.2 K for the binary system of 2,3-dimethylpentane (1) + toluene (2) from ref 27.

Comparing these trends with the extract compositions obtained in the aromatics separation from gasoline models using {[4empy][Tf_2N] (0.3) + [emim][DCA] (0.7)} binary mixture as solvent, several remarks can be given.[28] These extract streams are formed only by the three linear alkanes analyzed, benzene, toluene, and *p*-xylene for pyrolysis gasoline and also by ethylbenzene in the case of reformer gasoline. This work has provided the selectivity of the *n*-alkane recovery from toluene, which is the aromatic compound that could better represent the BTEX fraction.

Thus, it seems that the alkanes that form the extract would be selectively recovered from this stream, increasing the BTEX fraction purity achieved in the aromatic extraction step using the {[4empy][Tf_2N] (0.3) + [emim][DCA] (0.7)} binary mixture as solvent.

4. CONCLUSIONS

In this work the VLE for (*n*-hexane, *n*-octane, cyclohexane, or 2,3-dimethylpentane) + toluene + {[4empy][Tf_2N] (0.3) + [emim][DCA] (0.7)} systems have been determined at 323.2, 343.2, and 363.2 K and over the whole range of compositions. In order to improve the knowledge about the interaction between alkanes and the IL mixture, the VLE for all alkane + {[4empy][Tf_2N] (0.3) + [emim][DCA] (0.7)} systems also have been determined at the same temperatures and over the whole composition range. To complete the study, the VLE for all alkane + toluene binary systems have been measured to validate the experimental method and to be used as benchmark.

The main advance of this work has been the high increase in the alkane relative volatility from toluene in the alkane + toluene + {[4empy][Tf_2N] (0.3) + [emim][DCA] (0.7)} systems, being the highest values obtained at 323.2 K and with the higher mass fraction of the IL mixture. Short linear alkanes, branched-chain alkanes instead of linear alkanes with the same number of carbon atoms, and linear alkanes instead of cyclic alkanes with the same number of carbon atoms are the best scenarios observed in the selective separation of alkanes from toluene. In addition to this, the NRTL model has correctly adjusted the VLE data for all systems analyzed.

The high values achieved in the alkane/toluene relative volatility have demonstrated that the aromatics obtained by liquid−liquid extraction using ILs as solvents can be purified by selectively removing the alkanes.

DOI: 10.1021/acs.jced.6b00116
J. Chem. Eng. Data XXXX, XXX, XXX−XXX

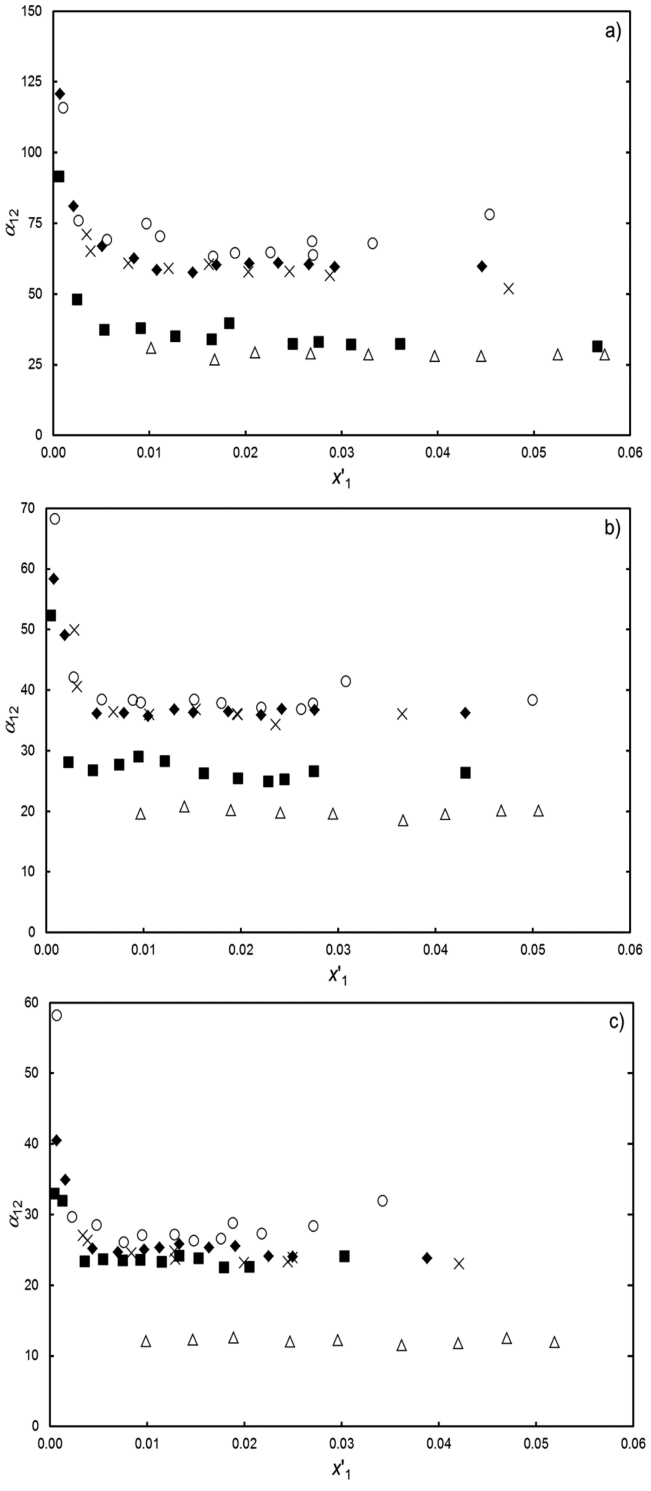

Figure 14. Comparison of the alkane relative volatility from toluene (a_{12}) in the alkane (1) + toluene (2) + {[4empy][Tf_2N] (3) + [emim][DCA] (4)} with a mole fraction of [emim][DCA] of 0.7 in the IL mixture at x_{3+4} = 0.98 at (a) 323.2 K, (b) 343.2 K, and (c) 363.2 K: ○, *n*-hexane; ×, *n*-heptane; ■, *n*-octane; △, cyclohexane; ◆, 2,3-dimethylpentane.

■ ASSOCIATED CONTENT

Supporting Information

The Supporting Information is available free of charge on the ACS Publications website at DOI: 10.1021/acs.jced.6b00116.

Data tables for the graphs above. (PDF)

■ AUTHOR INFORMATION

Corresponding Author

*E-mail: jgarcia@quim.ucm.es. Tel.: +34 91 394 51 19. Fax: +34 91 394 42 43.

Notes

The authors declare no competing financial interest.

Funding

Authors are grateful to the Ministerio de Economía y Competitividad (MINECO) of Spain and the Comunidad de Madrid for financial support of Projects CTQ2014-53655-R and S2013/MAE-2800, respectively. P.N. also thanks MINECO for awarding him an FPI grant (Reference BES-2012-052312).

■ REFERENCES

(1) Rogers, R. D.; Seddon, K. R. Ionic Liquids–Solvents of the Future? *Science* **2003**, *302*, 792−793.

(2) Plechkova, N. V.; Seddon, K. R. Applications of Ionic Liquids in the Chemical Industry. *Chem. Soc. Rev.* **2008**, *37*, 123−150.

(3) Gutiérrez, J. P.; Meindersma, G. W.; de Haan, A. B. COSMO-RS-Based Ionic-Liquid Selection for Extractive Distillation Processes. *Ind. Eng. Chem. Res.* **2012**, *51*, 11518−11529.

(4) Ferreira, A. R.; Freire, M. G.; Ribeiro, J. C.; Lopes, F. M.; Crespo, J. G.; Coutinho, J. A. P. Overview of the Liquid−Liquid Equilibria of Ternary Systems Composed of Ionic Liquid and Aromatic and Aliphatic Hydrocarbons, and Their Modeling by COSMO-RS. *Ind. Eng. Chem. Res.* **2012**, *51*, 3483−3507.

(5) Revelli, A. L.; Mutelet, F.; Jaubert, J. N. Extraction of Benzene or Thiophene from n-Heptane using Ionic Liquids. NMR and Thermodynamic Study. *J. Phys. Chem. B* **2010**, *114*, 4600−4608.

(6) Marciniak, A.; Krolikowski, M. Ternary (Liquid + liquid) Equilibria of {Trifluorotris(perfluoroethyl)phosphate based Ionic Liquids + Thiophene + Heptane}. *J. Chem. Thermodyn.* **2012**, *49*, 154−158.

(7) Aparicio, S.; Atilhan, M. Nanoscopic Vision on Fuel Dearomatization Using Ionic Liquids: The Case of Piperazine-Based Fluids. *Energy Fuels* **2013**, *27*, 2515−2527.

(8) Meindersma, G. W.; de Haan, A. B. Conceptual process design for aromatic/aliphatic separation with ionic liquids. *Chem. Eng. Res. Des.* **2008**, *86*, 745−752.

(9) Meindersma, G. W.; de Haan, A. B. Cyano-containing ionic liquids for the extraction of aromatic hydrocarbons from an aromatic/aliphatic mixture. *Sci. China: Chem.* **2012**, *55*, 1488−1499.

(10) Meindersma, G. W.; Podt, A. J. G.; de Haan, A. B. Selection of Ionic Liquids for the Extraction of Aromatic Hydrocarbons from Aromatic/aliphatic Mixtures. *Fuel Process. Technol.* **2005**, *87*, 59−70.

(11) Meindersma, G. W.; Hansmeier, A. R.; de Haan, A. B. Ionic liquids for aromatics extraction. Present status and future outlook. *Ind. Eng. Chem. Res.* **2010**, *49*, 7530−7540.

(12) Corderí, S.; Gómez, E.; Calvar, N.; Domínguez, A. Measurement and Correlation of Liquid-Liquid Equilibria for Ternary and Quaternary Systems of Heptane, Cyclohexane, Toluene, and [EMim][OAc] at 298.15 K. *Ind. Eng. Chem. Res.* **2014**, *53*, 9471−9477.

(13) Hansmeier, A. R.; Minoves Ruiz, M.; Meindersma, G. W.; de Haan, A. B. Liquid − liquid Equilibria for the Three Ternary Systems (3-Methyl-N-butylpyridinium Dicyanamide + Toluene + Heptane), (1-Butyl-3-Methylimidazolium Dicyanamide + Toluene + Heptane), and (1-Butyl-3-Methylimidazolium Thiocyanate + Toluene + Heptane) at T = (313.15 and 348.15) K and p = 0.1 MPa. *J. Chem. Eng. Data* **2010**, *55*, 708−713.

(14) Aparicio, S.; Atilhan, M.; Karadas, F. Thermophysical Properties of Pure Ionic Liquids: Review of Present Situation. *Ind. Eng. Chem. Res.* **2010**, *49*, 9580−9595.

(15) Larriba, M.; Navarro, P.; García, J.; Rodríguez, F. Separation of Toluene from *n*-Heptane, 2,3-Dimethylpentane, and Cyclohexane using Binary Mixtures of [4empy][Tf_2N] and [emim][DCA] Ionic Liquids as Extraction Solvents. *Sep. Purif. Technol.* **2013**, *120*, 392−401.

DOI: 10.1021/acs.jced.6b00116
J. Chem. Eng. Data XXXX, XXX, XXX−XXX

(16) Larriba, M.; Navarro, P.; García, J.; Rodríguez, F. Liquid-liquid Extraction of Toluene from *n*-Alkanes using {[4empy][Tf_2N] + [emim][DCA]} Ionic Liquid Mixtures. *J. Chem. Eng. Data* **2014**, *59*, 1692−1699.
(17) Navarro, P.; Larriba, M.; García, J.; Rodríguez, F. Thermal stability, specific heats, and surface tensions of {[emim][DCA] + [4empy][Tf_2N]} ionic liquid mixtures. *J. Chem. Thermodyn.* **2014**, *76*, 152−160.
(18) Navarro, P.; Larriba, M.; González, E. J.; García, J.; Rodríguez, F. Selective recovery of aliphatics from aromatics in the presence of the {[4empy][Tf_2N] + [emim][DCA]} ionic liquid mixture. *J. Chem. Thermodyn.* **2016**, *96*, 134−142.
(19) Navarro, P.; Larriba, M.; García, J.; Rodríguez, F. Vapor-liquid equilibria for *n*-heptane + (benzene, toluene, *p*-xylene, or ethylbenzene) + {[4empy][Tf_2N] (0.3) + [emim][DCA] (0.7)} binary ionic liquid mixture. *Fluid Phase Equilib.* **2016**, *417*, 41−49.
(20) Navarro, P.; Larriba, M.; García, J.; González, E. J.; Rodríguez, F. Vapor-liquid equilibria of {*n*-heptane + toluene + [emim][DCA]} system using headspace gas chromatography. *Fluid Phase Equilib.* **2015**, *387*, 209−216.
(21) Kolb, B.; Ettre, L. S. *Static Headspace-Gas Chromatography: Theory and Practice*; Wiley-VCH: New York, 1997.
(22) Jiqin, Z.; Jian, C.; Chengyue, L.; Weiyang, F. Study on the separation of 1-hexene and trans-3-hexene using ionic liquids. *Fluid Phase Equilib.* **2006**, *247*, 102−106.
(23) Luis, P.; Wouters, C.; Sweygers, N.; Creemers, C.; Van der Bruggen, B. The potential of head-space gas chromatography for VLE measurements. *J. Chem. Thermodyn.* **2012**, *49*, 128−136.
(24) Perry, R. H.; Green, D. W.; Maloney, J. O. *Perry's Chemical Engineers' Handbook*; McGraw-Hill: New York, 1999.
(25) Andreatta, A. E.; Arce, A.; Rodil, E.; Soto, A. Physical properties and phase equilibria of the system isopropyl acetate + isopropanol + 1-octyl-3-methyl-imidazolium bis(trifluoromethylsulfonyl)imide. *Fluid Phase Equilib.* **2010**, *287*, 84−94.
(26) Zhang, L.; Han, J.; Deng, D.; Ji, J. Selection of ionic liquids as entrainers for separation of water + 2-propanol. *Fluid Phase Equilib.* **2007**, *255*, 179−185.
(27) *Aspen Plus Version 7.1*; Aspen Technology: Bedford, MA, 2004.
(28) Larriba, M.; Navarro, P.; García, J.; Rodríguez, F. Liquid−Liquid Extraction of BTEX from Reformer Gasoline Using Binary Mixtures of [4empy][Tf_2N] and [emim][DCA] Ionic Liquids. *Energy Fuels* **2014**, *28*, 6666−6676.

DOI: 10.1021/acs.jced.6b00116
J. Chem. Eng. Data XXXX, XXX, XXX−XXX

energy&fuels

Article

pubs.acs.org/EF

Design of the Hydrocarbon Recovery Section from the Extract Stream of the Aromatic Separation from Reformer and Pyrolysis Gasolines Using a Binary Mixture of [4empy][Tf_2N] + [emim][DCA] Ionic Liquids

Pablo Navarro, Marcos Larriba, Julián García,* and Francisco Rodríguez

Department of Chemical Engineering, Complutense University of Madrid, E−28040 Madrid, Spain

Supporting Information

ABSTRACT: Reformer and pyrolysis gasolines are the main benzene, toluene, ethylbenzene, and xylenes (BTEX) sources. In our previous works, the aromatic extraction from reformer and pyrolysis gasoline models formed by three *n*-alkanes, benzene, toluene, and xylenes were studied using a binary mixture of ionic liquids (ILs). The results showed that the {[4empy][Tf_2N] + [emim][DCA]} IL mixture with [4empy][Tf_2N] mole fraction of 0.3 required a comparable countercurrent extraction column to that of the Sulfolane process, and extracted BTEX had quite a higher purity using the IL mixture in the three gasoline models analyzed. Here, we have studied the hydrocarbon recovery from the extract stream obtained in these works. For that purpose, the vapor−liquid equilibria (VLE) data involving the extracted hydrocarbons and the IL mixed solvent have been determined by the headspace−gas chromatography (HS−GC) technique for several temperatures. Afterward, the simulation of two new process configurations based on adiabatic flash distillation units was carried out using a new algorithm developed in the framework of this study, useful for further flash distillation cases with a high concentration of IL or non-volatile character compounds. The commercial purity obtained in the aromatic product stream (99.9 wt %) has demonstrated the technical feasibility of the aromatic extraction process using ILs as solvents, including the hydrocarbon recovery section.

1. INTRODUCTION

Nearly 75% of the benzene, toluene, ethylbenzene, and xylenes (BTEX) production in the U.S.A. is obtained by liquid−liquid extraction from reformer gasoline, whereas Europe and Japan mainly extract aromatics from pyrolysis gasolines.[1] The most employed liquid−liquid extraction technology is the Sulfolane process, licensed by UOP.[1−3] The Sulfolane process achieves high extraction yields of BTEX as a result of the high extraction capacity associated with its solvent, sulfolane; however, the separation section used in the recovery of the hydrocarbons works at high temperatures, even up to the boiling point of sulfolane (560 K), and required several distillation columns among other separation equipment as a washed extraction to recover the solvent from the raffinate stream or an extractive stripper to selectively remove the aliphatics from the extract stream.

Ionic liquids (ILs) have been exhaustively studied in extraction processes, especially in dearomatization and desulfuration of fuels. The good extractive and physical properties associated with ILs in these two processes have been demonstrated thus far.[4−18] Our last works based on the liquid−liquid extraction of BTEX from reformer and pyrolysis gasoline models have demonstrated that an IL-based solvent with good extractive and physical properties achieves similar extraction yields and higher BTEX purity in the extract stream than those of sulfolane, needing similar equilibrium steps.[19,20]

However, the recovery of the extracted hydrocarbons from the IL-based solvent has not been already studied in a multicomponent system, avoiding correctly comparing the real impact that ILs have in the aromatic extraction processes. Several authors have claimed that the hydrocarbon recovery will be technically solved as a result of the negligible vapor pressure associated with ILs and their high thermal stability.[21,22] However, the absence of vapor−liquid equilibria (VLE) data referring to multicomponent extract-type streams has not led to experimentally show this claim, and the thermal stability of ILs has been considerably overestimated in the last few years.[23]

In a recent review on this topic, Canales and Brennecke claimed that the use of cyano- and bis(trifluoromethylsulfonyl)-imide-based ILs seems to be the best election, whereas the recovery section for the extract stream needs to be studied.[24] Nowadays, only the vapor−liquid selective separation of aliphatics from aromatics in the presence of ILs has been partially demonstrated by our research group in experimental determinations for simplified models formed by an aliphatic, an aromatic, and the {[4empy][Tf_2N] (0.3) + [emim][DCA] (0.7)} IL mixture.[25]

Because of that, in this work, the VLE for the multicomponent extract stream obtained in the aromatic extraction from reformer and pyrolysis gasoline models using the {[4empy][Tf_2N] (0.3) + [emim][DCA] (0.7)} IL mixture have been determined at several temperatures to deeply understand the behavior in a more representative model. A headspace−gas chromatography (HS−GC) technique has been used to reproduce the VLE, as previously performed in our previous works for simplified systems involving hydrocarbons and ILs.[26−28] The temperatures were selected up to the

Received: November 18, 2016
Published: December 15, 2016

DOI: 10.1021/acs.energyfuels.6b03068
Energy Fuels 2017, 31, 1035−1043

maximum operation temperature (MOT) estimated for the {[4empy][Tf_2N] (0.3) + [emim][DCA] (0.7)} IL mixture from thermogravimetric analysis (TGA) (413 K) to assay no thermal decomposition for 8000 h.[23]

After that, the adiabatic flash distillation units needed for separating the aliphatics, the aromatics, and the IL mixture have been simulated, developing a new algorithm based on the experimental K values of the hydrocarbons in the conditions regarding the extract stream in the presence of the IL mixture. This new route of calculus will be useful to easily converge flash distillation designs for such mixtures mainly composed by ILs or non-volatile character compounds. The hydrocarbon recovery section was conceptually designed planning two new configurations (A and B), formed by two and three adiabatic flash distillation units, respectively, as a result of the high aliphatic/aromatic relative volatility and the non-volatile character of ILs.

The aromatic product stream was obtained with a purity of 99.9 wt % for all gasolines evaluated, demonstrating the technical feasibility of selectively separating the aromatics from the extract stream and, thus, the technical feasibility of the aromatic extraction process from gasolines using ILs as solvents.

2. EXPERIMENTAL SECTION

2.1. Chemicals. The [emim][DCA] and [4empy][Tf_2N] ILs were purchased from Iolitec GmbH with mass fraction purities of 0.98 and 0.99, respectively. They were used as received without further purifications. The water content was 937 and 89 ppm, respectively, for [emim][DCA] and [4empy][Tf_2N], with the halide content being below 200 ppm for [emim][DCA] and below 100 ppm for [4empy][Tf_2N]. ILs were kept in a desiccator with silica gel and handled in an inert atmosphere of nitrogen in a glove to avoid water absorption. The aliphatic and aromatic hydrocarbons were acquired from Sigma-Aldrich with mass fraction purities higher than 0.99. All chemical specifications are listed in Table 1.

Table 1. Specifications of Chemicals

name	source	purity	analysis
n-hexane	Sigma-Aldrich	0.995	GC[a]
n-heptane	Sigma-Aldrich	0.997	GC[a]
n-octane	Sigma-Aldrich	0.990	GC[a]
benzene	Sigma-Aldrich	0.995	GC[a]
toluene	Sigma-Aldrich	0.995	GC[a]
p-xylene	Sigma-Aldrich	0.990	GC[a]
ethylbenzene	Sigma-Aldrich	0.998	GC[a]
[emim][DCA]	Iolitec GmbH	0.98	NMR[b] and IC[c]
[4empy][Tf_2N]	Iolitec GmbH	0.99	NMR[b] and IC[c]

[a]GC = gas chromatography. [b]NMR = nuclear magnetic resonance. [c]IC = ion chromatography.

2.2. Procedure and Analysis. VLE was determined using an isothermal technique with an Agilent Headspace 7697A injector coupled to an Agilent gas chromatograph 7890A. A detailed description of the method and the equipment can be found in our previous work.[26]

The IL binary mixture and the multicomponent feeds were prepared by mass with a Mettler Toledo XS205 balance, which assays a precision of 1×10^{-5} g. The feed of the VLE experiments was prepared adding first the IL mixture and then the hydrocarbon mixture just before hermetically closing the vial. The compositions of the extract stream are collected in Table 2.

After the equilibrium was reached at the selected temperature for 2 h, the vapor phase was analyzed by GC, obtaining the vapor compositions. Then, the composition of the liquid phase was recalculated as follows:

$$x_i = \frac{z_i F - (P_i V_G/RT)}{\sum_{i=1}^{N} (z_i F - (P_i V_G/RT))} \quad (1)$$

where x_i is the mole fraction of the component i in the liquid phase, z_i is the mole fraction of the component i in the feed, F denotes the molar amount of the feed, V_G refers to the vapor volume of the vial, N is the number of the components, and P_i is the partial pressure of the component i calculated as follows:

$$P_i = \frac{A_i}{A_i^0} P_i^0 \quad (2)$$

where A_i are the peak areas of the hydrocarbons, whereas P_i^0 and A_i^0 are the vapor pressures and peak areas of the pure hydrocarbons in the same conditions as those used to reach the equilibrium, respectively.

2.3. Adiabatic Flash Distillation Simulation. First of all, an analysis of the degrees of freedom for a flash distillation unit is performed. As seen in Table 3, the number of independent equations that can be planned to simulate a flash distillation unit are $2C + 6$. In these independent equations, there are $3C + 10$ variables; therefore, the degrees of freedom for a distillation flash unit are $C + 4$.

P_V and T_V are known from the VLE; fixing the feed flow, $C - 1$ compositions, and the pressure in the feed, $(C + 3)$ variables are defined needing an additional fixed variable. With selection of adiabatic flash distillation units ($Q = 0$), which are less expensive than isothermal units,[29] the system is completely defined.

The new algorithm developed to solve the simulation of the adiabatic flash distillation units as a function of the temperature and pressure can be seen in Figure 1. The algorithm starts with the supposition of the individual flows in the vapor phase based on the experimental results. Taking into account an experimental pressure and temperature scenario, the flows in the vapor phase are known; after that, the pressure value is modified from the experimental value to a contiguous value and the individual flows in the vapor phase for all hydrocarbons quickly converge to the solution following the next steps.

When the K values are calculated at T_V and P_V, it is possible to determine the mole fractions in the liquid phase. Taking into account that the liquid mole fractions of the hydrocarbons are quite low as well as their variations within the range of temperatures, it is suitable to consider K values independent of composition.[29] On the other hand, the liquid mole fractions are also calculated by mass balance using the feed flow and the feed compositions. The objective function of the algorithm is the difference between the liquid mole fractions calculated from the chemical equilibrium and those also calculated from mass balance. Varying the individual flows in the vapor phase, the convergence was achieved for several P_V–T_V scenarios. As a result of the low total vapor flow and the low mole fraction of the hydrocarbons in the liquid phase, this strategy permits easy solving of the vapor–liquid separation. After that, the enthalpy balance is solved and the feed temperature is calculated to completely define the system and check if this temperature is below 413 K, the MOT estimated for the IL mixture.[23] The specific heat for each stream and the vaporization heat were calculated using those with regard to the pure compounds at the corresponding temperature taken from the literature.[23,30]

3. RESULTS AND DISCUSSION

3.1. Experimental Vapor–Liquid Separation and Aliphatic/Aromatic Relative Volatility. The VLE for *n*-hexane + *n*-heptane + *n*-octane + benzene + toluene + *p*-xylene + ethylbenzene + {[4empy][Tf_2N] (0.3) + [emim][DCA] (0.7)} systems were measured between 303.2 and 363.2 K. The VLE data are listed in Tables S1–S3 of the Supporting Information as a function of the temperature for the three

DOI: 10.1021/acs.energyfuels.6b03068
Energy Fuels 2017, 31, 1035–1043

Table 2. Compositions of the Extract Stream from the Aromatic Extraction from Reformer and Pyrolysis Gasolines,[19,20] in wt %, and Abbreviations of the Compounds Used in the Work

compound	abbreviation	reformer gasoline	pyrolysis gasoline	
			mild cracking	severe cracking
n-hexane	hexa	0.09	0.10	0.07
n-heptane	hepta	0.08	0.10	0.07
n-octane	octa	0.07	0.06	0.05
benzene	benz	0.90	3.98	5.96
toluene	tol	4.32	3.19	3.40
p-xylene	*p*-xyl	3.81	2.02	2.24
ethylbenzene	etbenz	0.72		
[4empy][Tf_2N] + [emim][DCA]	ILs	90.02	90.55	88.21

Table 3. Independent Equations To Simulate a Flash Distillation Unit with *C* Components

name	formula		number of equations
thermal equilibrium	$T_L = T_V$	(A)	1
mechanical equilibrium	$P_L = P_V$	(B)	1
chemical equilibrium	$y_i = K_i x_i$	(C)	C
component mass balances	$Fz_i = Lx_i + Vy_i$	(D)	$C - 1$
total mass balance	$F = L + V$	(E)	1
compositions in feed	$\sum z_i = 1$	(F)	1
compositions in liquid phase	$\sum x_i = 1$	(G)	1
compositions in vapor phase	$\sum y_i = 1$	(H)	1
enthalpy balance	$FH_F + Q = LH_L + VH_V$	(I)	1
total			$2C + 6$

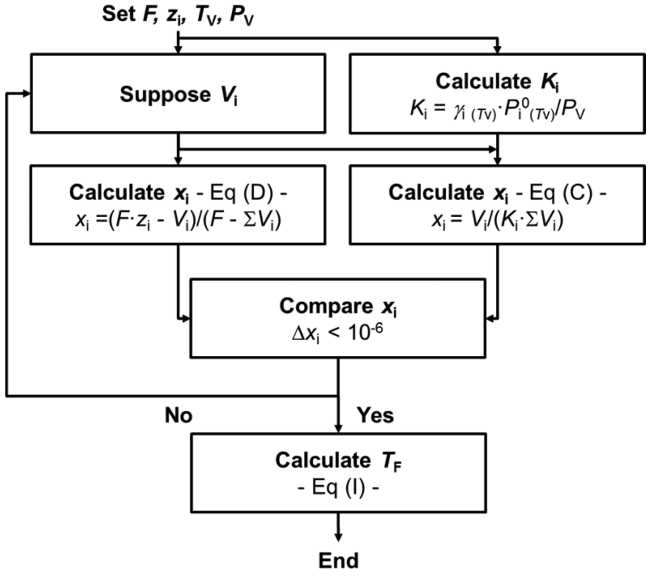

Figure 1. Algorithm used to simulate the adiabatic flash distillation units in this work.

cases: reformer and pyrolysis gasolines from mild and severe cracking.

To analyze the separation of aliphatics (aliph) from aromatics (arom), the overall aliphatic/aromatic relative volatility was calculated as follows:

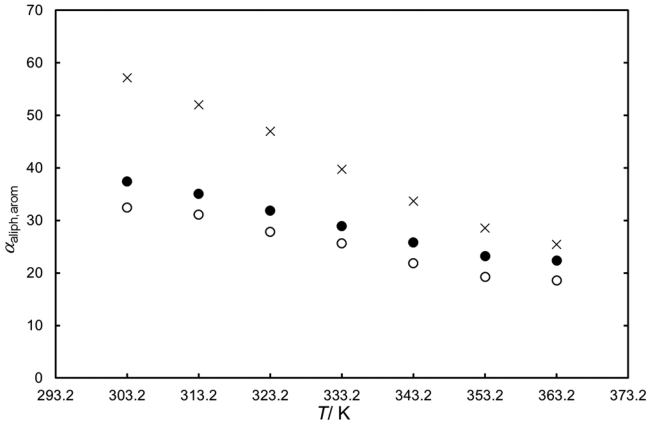

Figure 2. Relative volatility of aliphatics from aromatics as a function of the temperature. Cases of reformer gasoline (×) and pyrolysis gasolines from mild (●) and severe (○) cracking.

$$\alpha_{\text{aliph,arom}} = \frac{K_{\text{aliph}}}{K_{\text{arom}}} = \left[\frac{(y_{\text{hexa}} + y_{\text{hepta}} + y_{\text{octa}})}{(x_{\text{hexa}} + x_{\text{hepta}} + x_{\text{octa}})}\right] \left[\frac{(y_{\text{benz}} + y_{\text{tol}} + y_{p\text{-xyl}} + y_{\text{etbenz}})}{(x_{\text{benz}} + x_{\text{tol}} + x_{p\text{-xyl}} + x_{\text{etbenz}})}\right]^{-1} \quad (3)$$

where *K* values are the *K* values for the aliphatics or aromatics, *y* values denote the molar vapor compositions, and *x* values refer to the molar liquid compositions.

The aliphatic/aromatic relative volatilities were also collected in Tables S1–S3 of the Supporting Information. The values with regard to the feed equal to the extract compositions are graphically shown in Figure 2.

As seen, the high aliphatic/aromatic relative volatilities showed in the VLE involving three aliphatic hydrocarbons (*n*-hexane, *n*-heptane, and *n*-octane) and the BTEX or benzene, toluene, and xylenes (BTX) fraction in the cases of reformer or pyrolysis gasolines, respectively, have confirmed those values observed in simplified aliphatic + aromatic + {[4empy][Tf_2N] (0.3) + [emim][DCA] (0.7)} pseudo-ternary systems.[24] The IL induces a concentration increase of aliphatics in the vapor phase by its interaction with the aromatics. The temperature influence was quite linear, and an increase in this variable implies a reduction in the aliphatic/aromatic relative volatilities, a fact also found previously.[24]

With focus on the aromatic source, the extract stream from the reformer gasoline model showed higher aliphatic/aromatic relative volatilities than those for the pyrolysis gasoline cases. This is explained by the lower concentration of benzene, which

DOI: 10.1021/acs.energyfuels.6b03068
Energy Fuels 2017, 31, 1035−1043

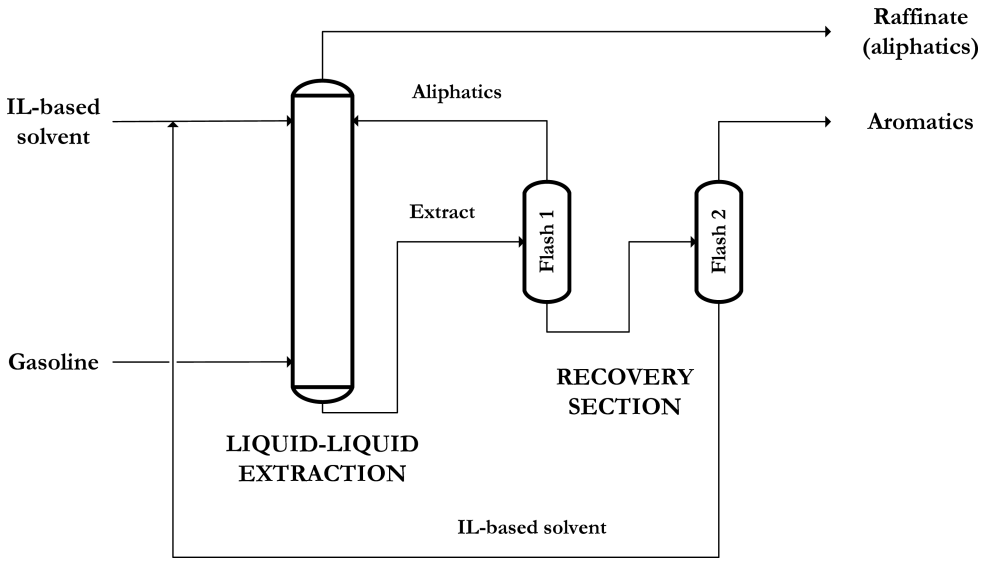

Figure 3. Aromatic extraction process conceptual design: configuration A.

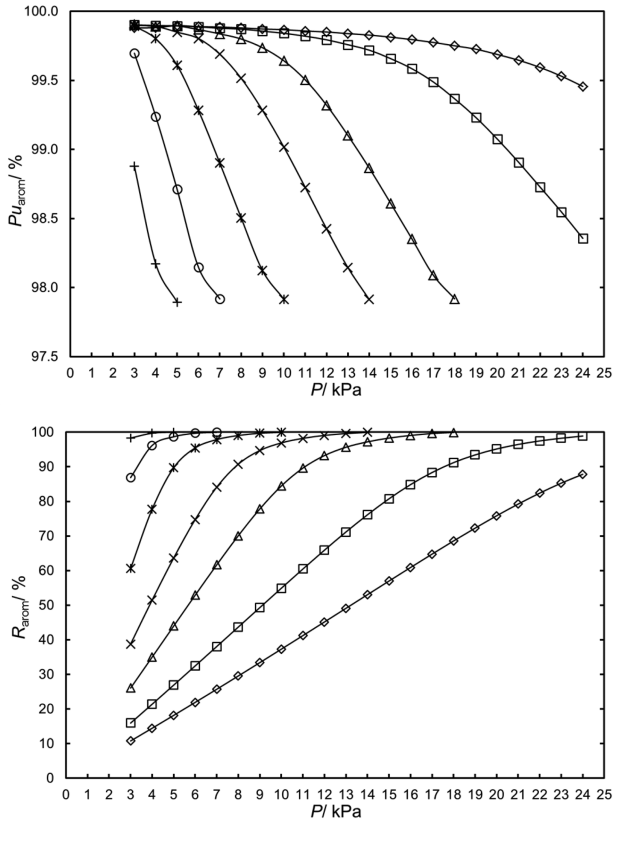

Figure 4. Aromatic purity (Pu_{arom}) and aromatic recovery (R_{arom}) as a function of the temperature and pressure for flash 1 in the reformer gasoline case: (+) T = 303.2 K, (○) T = 313.2 K, (∗) T = 323.2 K, (×) T = 333.2 K, (△) T = 343.2 K, (□) T = 353.2 K, and (◇) T = 363.2 K. Solid lines are used to guide the eyes.

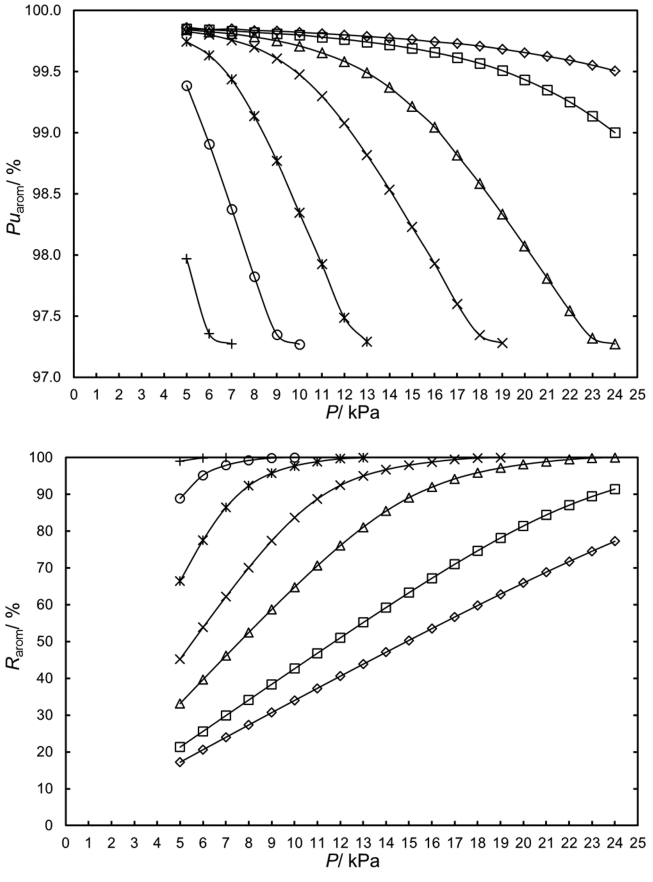

Figure 5. Aromatic purity (Pu_{arom}) and aromatic recovery (R_{arom}) as a function of the temperature and pressure for flash 1 in the pyrolysis gasoline case from mild cracking: (+) T = 303.2 K, (○) T = 313.2 K, (∗) T = 323.2 K, (×) T = 333.2 K, (△) T = 343.2 K, (□) T = 353.2 K, and (◇) T = 363.2 K. Solid lines are used to guide the eyes.

is the most volatile aromatic, in reformer gasolines. In comparison of both pyrolysis gasoline models, the same relationship is found with the benzene content.

3.2. Hydrocarbon Recovery Section Conceptual Design: Configuration A. The vapor and liquid compositions for several scenarios in the temperature and pressure ranges of 303.2−363.2 K and 5−24 kPa have been determined for the three extract streams reported in Table 2 following the algorithm described above. As a result of the high aliphatic/aromatic relative volatilities obtained, we have planned configuration A as the first approach to the conceptual design

DOI: 10.1021/acs.energyfuels.6b03068
Energy Fuels 2017, 31, 1035−1043

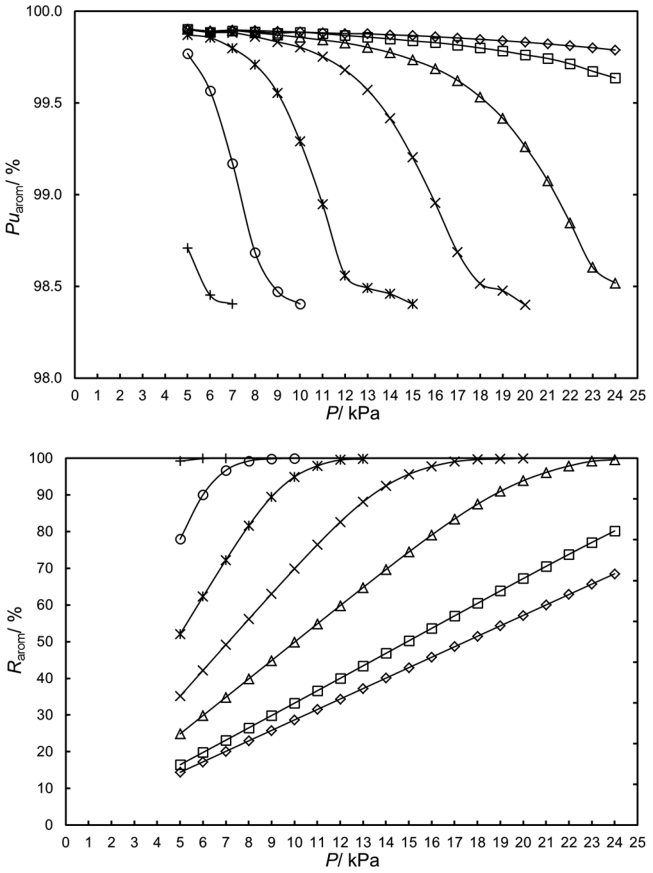

Figure 6. Aromatic purity (Pu_{arom}) and aromatic recovery (R_{arom}) as a function of the temperature and pressure for flash 1 in the pyrolysis gasoline case from severe cracking: (+) T = 303.2 K, (○) T = 313.2 K, (∗) T = 323.2 K, (×) T = 333.2 K, (△) T = 343.2 K, (□) T = 353.2 K, and (◇) T = 363.2 K. Solid lines are used to guide the eyes.

of the hydrocarbon recovery section. A simplified scheme is shown in Figure 3. The first flash distillation unit is destined to remove the aliphatic hydrocarbons to achieve a free-solvent purity for the aromatics of 99.9 wt % that is the purity achieved at the bottom of the extractive stripper for the Sulfolane process,[2] whereas the second flash distillation is destined to perform the aromatic hydrocarbon/IL-based solvent separation.

To properly select the most suitable temperature−pressure scenario, the aromatic purities (Pu_{arom}) and recoveries (R_{arom}) were calculated from the simulations as follows:

$$Pu_{arom} = (m_{benz} + m_{tol} + m_{p\text{-}xyl} + m_{etbenz})_{stream} / (m_{hexa} + m_{hepta} + m_{octa} + m_{benz} + m_{tol} + m_{p\text{-}xyl} + m_{etbenz})_{stream} \quad (4)$$

$$R_{arom} = \frac{(m_{benz} + m_{tol} + m_{p\text{-}xyl} + m_{etbenz})_{stream}}{(m_{benz} + m_{tol} + m_{p\text{-}xyl} + m_{etbenz})_{feed}} \quad (5)$$

where m refers to the mass of each hydrocarbon in each corresponding stream (liquid or vapor) that was calculated in the simulations. The global recoveries of aromatics and their purities in the liquid stream are graphically shown in Figures 4−6 as a function of both the temperature and pressure.

As expected, the recovery of aromatics in the liquid stream decreases with an increment in the temperature and a decrease in the pressure value, showing the opposite effect for the aromatic purities in the same stream. Accordingly, to obtain aromatics with commercial purity, i.e., 99.9 wt %, the first flash distillation unit should work at least at 353.2 K and 5 kPa. However, the recovery of aromatics in the liquid stream would be lower than 30% for the three gasoline models. The high investment fixed costs associated with the recycling streams at these conditions have concluded to plan the recovery of aliphatics in two adiabatic flash distillation units at milder conditions to work with higher values of aliphatic/aromatic relative volatilities and a third flash to perform the aromatic/IL-based solvent separation.

3.3. Hydrocarbon Recovery Section Conceptual Design: Configuration B. The second conceptual design for the recovery section (configuration B) is shown in Figure 7. The whole recovery section is formed by three flash distillation

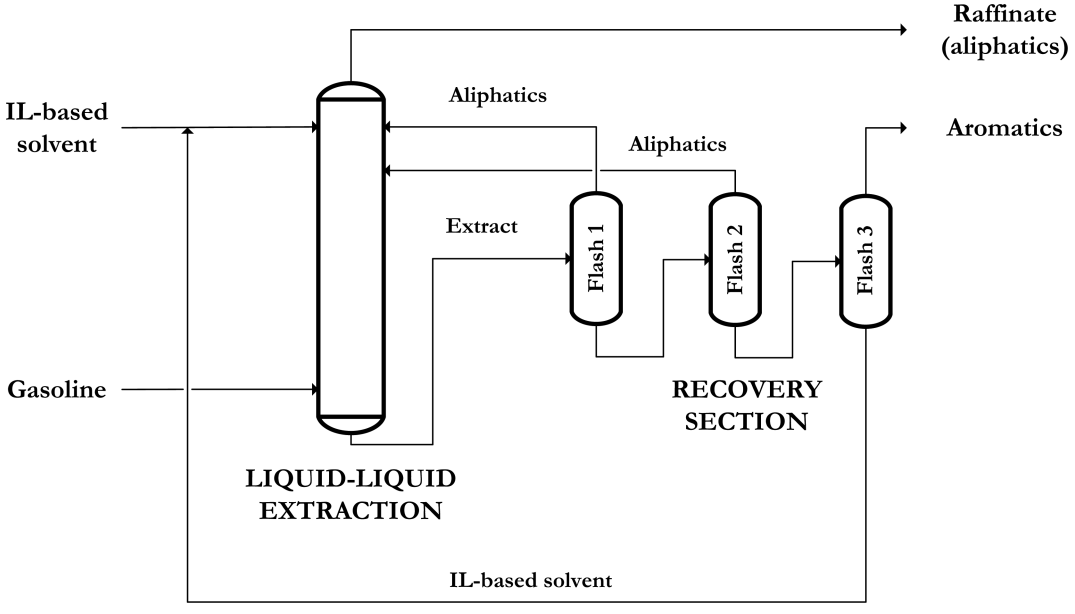

Figure 7. Aromatic extraction process conceptual design: configuration B.

DOI: 10.1021/acs.energyfuels.6b03068
Energy Fuels 2017, 31, 1035−1043

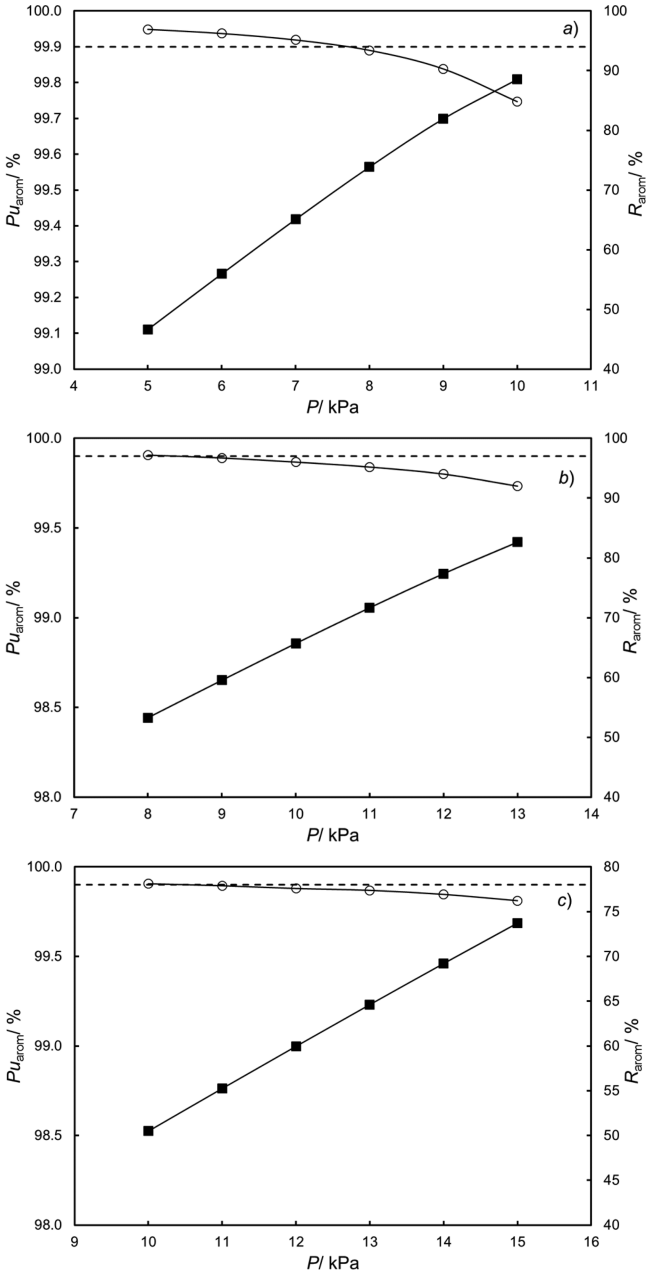

Figure 8. Aromatic purity (Pu_{arom}, ○) and aromatic recovery (R_{arom}, ■) for flash 2 (configuration B) at 343.2 K as a function of the pressure. Reformer gasoline (a) and pyrolysis gasolines from mild (b) and severe (c) cracking. The dashed line denotes the aromatic purity at the bottom of the Sulfolane stripper,[2] and solid lines are used to guide the eyes.

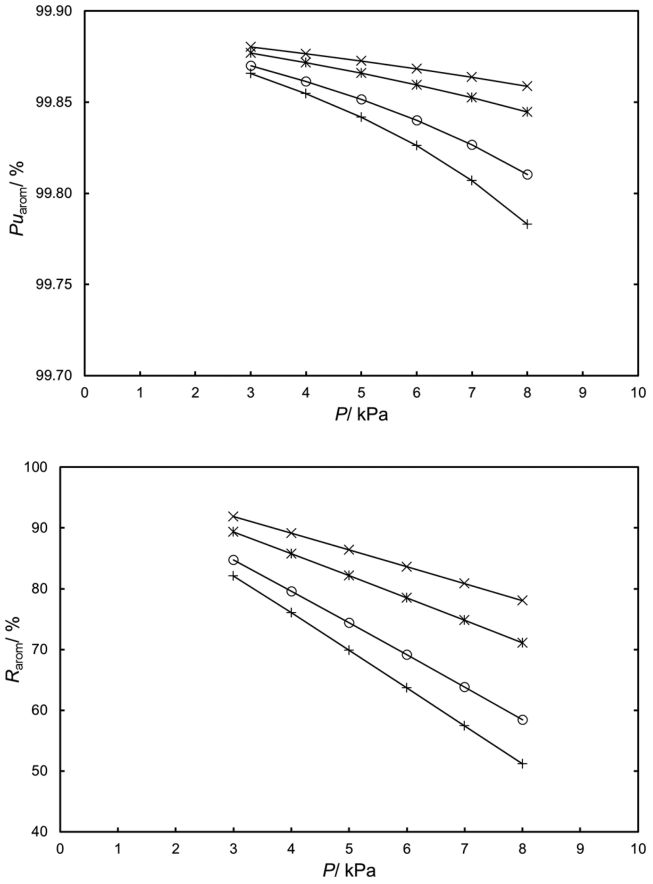

Figure 9. Aromatic purity (Pu_{arom}) and aromatic recovery (R_{arom}) as a function of the temperature and pressure for flash 3 in the case of reformer gasoline: (+) T = 363.2 K, (○) T = 373.2 K, (∗) T = 383.2 K, and (×) T = 393.2 K.

units: flash 1 and flash 2 units with the purpose of removing the aliphatics and flash 3 to remove the aromatics from the solvent with a commercial purity of 99.9 wt %.

The operation temperature for the first flash distillation unit was selected to 333.2 K for the three gasoline models, and an operation pressures of 10, 13, and 15 kPa were chosen as a result of the intermediate removal of aliphatics in the vapor stream (56, 60, and 53%) and the high recovery of aromatics in the liquid stream (97, 95, and 96%) for the reformer gasoline and the pyrolysis gasoline from mild and severe cracking, respectively. Taking into account that the aliphatic removal is planned in two steps, it is necessary to recover a little more than the 50% of the aliphatics in the first flash distillation unit.

The simulation for the second flash distillation unit required new VLE experiments considering the composition of the liquid stream obtained in the first flash distillation unit. These VLE data for flash 2 are summarized in Tables S1−S3 of the Supporting Information. The temperature election for flash 2, 343.2 K, is based on the drastic decrease observed in the aromatic recovery in the liquid stream at higher temperatures.

As cited previously, an aromatic purity of 99.9 wt % should be obtained in the liquid stream of flash 2, whereas it is important to maximize the recovery of aromatics in this stream. To justify the selection of the operation pressure for flash 2, the purity of aromatics and the recovery of aromatics in the liquid stream are graphically shown in Figure 8 as a function of the operation pressure for the three sources evaluated.

As seen, pressures of 8, 11, and 14 kPa for the reformer gasoline and pyrolysis gasoline from mild and severe cracking cases, respectively, led to the achievement of a commitment election. The purities of aromatics with these operation pressures were almost 99.9 wt %, whereas the recovery of aromatics was around 70%, recycling a much lower flow of aromatics to the extractor in configuration B in comparison to configuration A, i.e., 30%.

The third flash distillation unit is aimed in the BTEX recovery from the IL mixture. Although the concentration of aliphatics is very low, their influence in the aromatic recovery was considered in the new VLE determinations associated with

DOI: 10.1021/acs.energyfuels.6b03068
Energy Fuels 2017, 31, 1035−1043

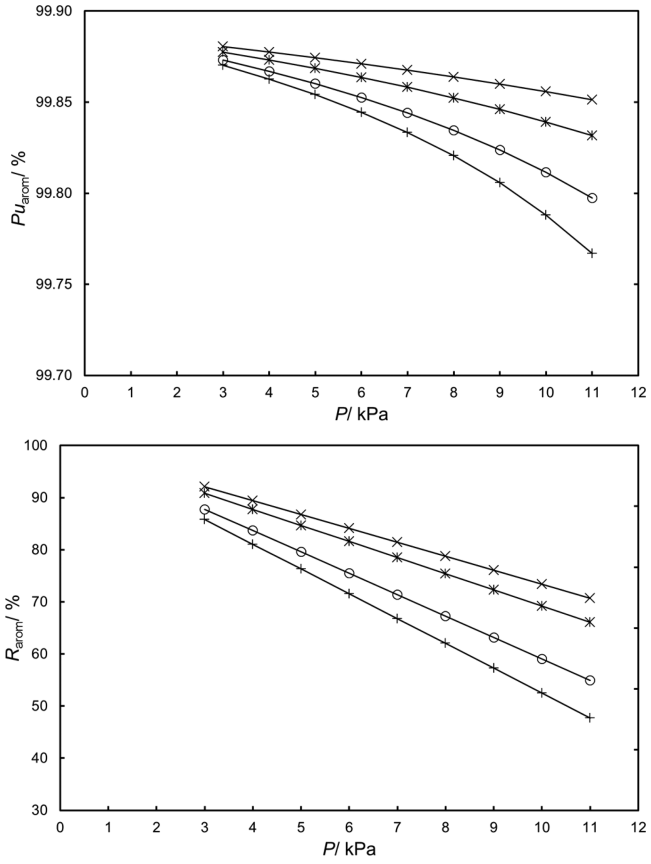

Figure 10. Aromatic purity (Pu_{arom}) and aromatic recovery (R_{arom}) as a function of the temperature and pressure for flash 3 in the case of pyrolysis gasoline from mild cracking: (+) T = 363.2 K, (○) T = 373.2 K, (∗) T = 383.2 K, and (×) T = 393.2 K.

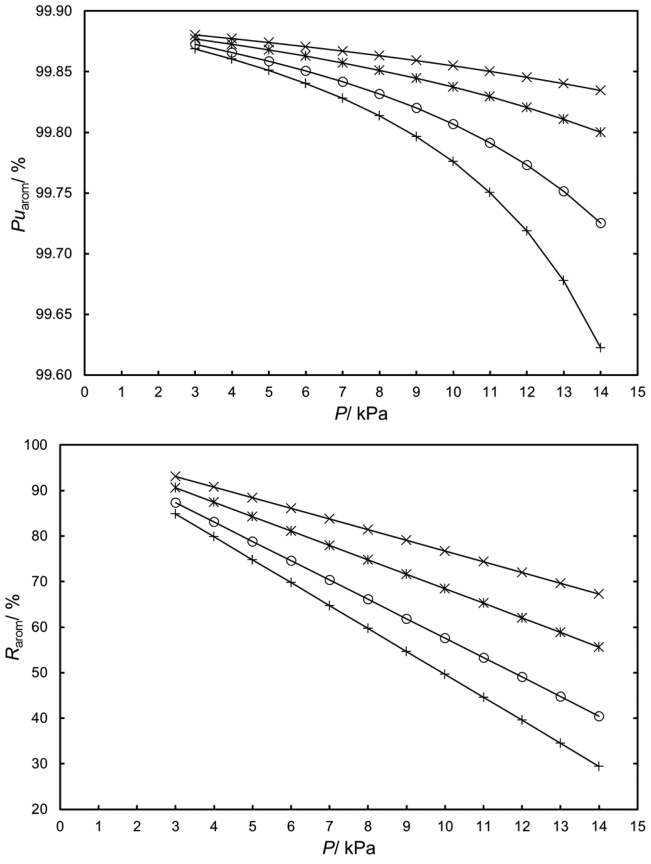

Figure 11. Aromatic purity (Pu_{arom}) and aromatic recovery (R_{arom}) as a function of the temperature and pressure for flash 3 in the case of pyrolysis gasoline from severe cracking: (+) T = 363.2 K, (○) T = 373.2 K, (∗) T = 383.2 K, and (×) T = 393.2 K.

the liquid stream obtained from flash 2, as shown in Tables S1–S3 of the Supporting Information.

In addition to this, the equilibrium temperature range was 363.2–393.2 K to achieve high aromatic recoveries in the vapor phase and avoid thermal decomposition of the IL mixture because the MOT is 413 K.[23] On the other hand, the vacuum was evaluated up to 3 kPa, looking for the same performance. Lower values of pressure were not considered because the vacuum conditions in the oil industry processes are rarely below this value.[31,32]

To properly select temperature and pressure in the aromatic/solvent separation, the recovery of aromatics in the vapor phase and the aromatic purity in the vapor phase were calculated and they are shown in Figures 9–11.

As expected, the best scenario for the third flash distillation unit is a temperature of 393.2 K and a pressure of 3 kPa for all gasoline models. As seen, the aromatics were recovered with a purity of 99.9 wt %, whereas the IL mixture in the liquid phase was obtained with a purity of 99.4 wt %.

3.4. Global Overview of the Aromatic Separation Process from Reformer and Pyrolysis Gasolines Using the {[4empy][Tf_2N] (0.3) + [emim][DCA] (0.7)} Binary IL Mixture. The aromatic extraction process including both extraction and recovery sections has been simulated and is graphically exhibited in Figure S1 of the Supporting Information, and flow, composition, temperature, pressure, and enthalpy for all streams are collected in Tables S4–S6 of the Supporting Information. The extraction column was simulated with a solvent/feed ratio of 5.0 at 303.2 K, needing 24 equilibrium steps for reformer and pyrolysis from mild cracking gasolines and 14 equilibrium steps for pyrolysis gasoline from severe cracking to achieve the next individual extraction yields of 99.9, 99.0, and 97.0% for benzene, toluene, and xylenes, respectively.[2,19,20] In addition to this, configuration B was selected to simulate the recovery of hydrocarbons obtaining the aromatics with a mass purity higher than 99.9%, whereas the IL-based solvent was recovered with a mass purity higher than 99.4%.

As expected, the process proposed works at milder temperatures in both extraction and recovery sections in comparison to the Sulfolane process. Therefore, the heating costs would be lower for the IL-based process; however, the vacuum costs associated with the alternative process with ILs would be quite higher. In addition, the recovery section for the IL-based process would be formed by three flash distillation units instead of the three distillation columns needed in the Sulfolane process as a result of the non-volatile character associated with ILs. Although investment and operative costs should be properly evaluated in further studies, it is possible to claim that the aromatic extraction process is technically feasible, including the recovery section of the extracted hydrocarbons.

4. CONCLUSION

In this work, the recovery section for the hydrocarbons in an aromatic extraction process from reformer and pyrolysis gasolines using the {[4empy][Tf_2N] (0.3) + [emim][DCA]

DOI: 10.1021/acs.energyfuels.6b03068
Energy Fuels 2017, 31, 1035–1043

(0.7)} IL mixture has been studied. The vapor−liquid separation between all hydrocarbons and the IL mixture forming the extract streams has been studied at several temperatures using a HS−GC technique.

This is the first work including the whole conceptual design of the aromatic liquid−liquid extraction process based on only experimental determinations. Two configurations based on adiabatic flash distillation units have been evaluated. The best hydrocarbon recovery section would be formed by three adiabatic flash distillation units that would work at moderate temperatures and vacuum conditions. The final purity of the aromatics was higher than 99.9 wt %, whereas the IL-based solvent was recovered with a purity over 99.4 wt %.

■ ASSOCIATED CONTENT

Supporting Information

The Supporting Information is available free of charge on the ACS Publications website at DOI: 10.1021/acs.energyfuels.6b03068.

VLE for each flash distillation unit in the case of reformer gasoline (Table S1), VLE for each flash distillation unit in the case of pyrolysis gasoline from mild cracking (Table S2), VLE for each flash distillation unit in the case of pyrolysis gasoline from severe cracking (Table S3), stream conditions and compositions in the case of reformer gasoline for configuration B (Table S4), stream conditions and compositions in the case of pyrolysis gasoline from mild cracking for configuration B (Table S5), stream conditions and compositions for the case of pyrolysis gasoline from severe cracking for configuration B (Table S6), and process scheme for the aromatic extraction from reformer and pyrolysis gasolines using the {[4empy][Tf_2N] (0.3) + [emim][DCA] (0.7)} IL mixture as the solvent (configuration B) (Figure S1) (PDF)

■ AUTHOR INFORMATION

Corresponding Author

*Telephone: +34-91-394-51-19. Fax: +34-91-394-42-43. E-mail: jgarcia@quim.ucm.es.

Notes

The authors declare no competing financial interest.

■ ACKNOWLEDGMENTS

Authors are grateful to the Ministerio de Economía y Competitividad (MINECO) of Spain and the Comunidad de Madrid for financial support of Projects CTQ2014-53655-R and S2013/MAE-2800, respectively. Pablo Navarro also thanks MINECO for awarding him a FPI grant (Reference BES-2012-052312).

■ REFERENCES

(1) Franck, H. G.; Staldelhofer, J. W. *Industrial Aromatic Chemistry*; Springer-Verlag: Berlin, Germany, 1988.

(2) Gary, J.; Handwerk, G.; Kaiser, M. *Petroleum Refining Technology and Economics*, 5th ed.; CRC Press: Boca Raton, FL, 2007.

(3) Meyers, R. A. *Handbook of Petroleum Refining Processes*, 3rd ed.; McGraw-Hill: New York, 2004.

(4) Aparicio, S.; Atilhan, M. Nanoscopic Vision on Fuel Dearomatization Using Ionic Liquids: The Case of Piperazine-Based Fluids. *Energy Fuels* **2013**, *27*, 2515−2527.

(5) Aparicio, S.; Atilhan, M.; Karadas, F. Thermophysical properties of pure ionic liquids: Review of present situation. *Ind. Eng. Chem. Res.* **2010**, *49*, 9580−9595.

(6) Meindersma, G. W.; Podt, A. J. G.; de Haan, A. B. Selection of Ionic Liquids for the Extraction of Aromatic Hydrocarbons from Aromatic/aliphatic Mixtures. *Fuel Process. Technol.* **2005**, *87*, 59−70.

(7) Fang, W.; Shao, D.; Lu, X.; Guo, Y.; Xu, L. Extraction of Aromatics from Hydrocarbon Fuels Using N-Alkyl Piperazinium-Based Ionic Liquids. *Energy Fuels* **2012**, *26*, 2154−2160.

(8) Ko, N. H.; Lee, J. S.; Huh, E. S.; Lee, H.; Jung, K. W.; Kim, H. S.; Cheong, M. Extractive Desulfurization Using Fe-Containing Ionic Liquids. *Energy Fuels* **2008**, *22*, 1687−1690.

(9) Domańska, U.; Wlazlo, M. Effect of the Cation and Anion of the Ionic Liquid on Desulfurization of Model Fuels. *Fuel* **2014**, *134*, 114−125.

(10) Domańska, U.; Walczak, K.; Królikowski, M. Extraction Desulfurization Process of Fuels with Ionic Liquids. *J. Chem. Thermodyn.* **2014**, *77*, 40−45.

(11) Zhang, J.; Huang, C.; Chen, B.; Ren, P.; Lei, Z. Extraction of Aromatic Hydrocarbons from Aromatic/Aliphatic Mixtures Using Chloroaluminate Room-Temperature Ionic Liquids. *Energy Fuels* **2007**, *21*, 1724−1730.

(12) Huang, C.; Chen, B.; Zhang, J.; Liu, Z.; Li, Y. Desulfurization of Gasoline by Extraction with New Ionic Liquids. *Energy Fuels* **2004**, *18*, 1862−1864.

(13) Li, Z.; Li, C.; Chi, Y.; Wang, A.; Zhang, Z.; Li, H.; Liu, Q.; Welz-Biermann, U. Extraction Process of Dibenzothiophene with New Distillable Amine-Based Protic Ionic Liquids. *Energy Fuels* **2012**, *26*, 3723−3727.

(14) Lu, X.; Yue, L.; Hu, M.; Cao, Q.; Xu, L.; Guo, Y.; Hu, S.; Fang, W. Piperazinium-Based Ionic Liquids with Lactate Anion for Extractive Desulfurization of Fuels. *Energy Fuels* **2014**, *28*, 1774−1780.

(15) Gao, H.; Li, Y.; Wu, Y.; Luo, M.; Li, Q.; Xing, J.; Liu, H. Extractive Desulfurization of Fuel Using 3-Methylpyridinium-Based Ionic Liquids. *Energy Fuels* **2009**, *23*, 2690−2694.

(16) Wang, Q.; Lei, L.; Zhu, J.; Yang, B.; Li, Z. Deep Desulfurization of Fuels by Extraction with 4-Dimethylaminopyridinium-Based Ionic Liquids. *Energy Fuels* **2013**, *27*, 4617−4623.

(17) Zawadzki, M.; Niedzicki, L.; Wieczorek, W. I.; Domańska, U. Estimation of Extraction Properties of New Imidazolide Anion Based Ionic Liquids on the Basis of Activity Coefficient at Infinite Dilution Measurements. *Sep. Purif. Technol.* **2013**, *118*, 242−254.

(18) Domańska, U.; Walczak, K.; Zawadzki, M. Separation of Sulfur Compounds from Alkanes with 1-Alkylcyanopyridinium-based Ionic Liquids. *J. Chem. Thermodyn.* **2014**, *69*, 27−35.

(19) Larriba, M.; Navarro, P.; García, J.; Rodríguez, F. Liquid−Liquid Extraction of BTEX from Reformer Gasoline Using Binary Mixtures of [4empy][Tf_2N] and [emim][DCA] Ionic Liquids. *Energy Fuels* **2014**, *28*, 6666−6676.

(20) Larriba, M.; Navarro, P.; González, E. J.; García, J.; Rodríguez, F. Dearomatization of Pyrolysis Gasolines from Mild and Severe Cracking by Liquid−liquid Extraction Using a Binary Mixture of [4empy][Tf_2N] and [emim][DCA] Ionic Liquids. *Fuel Process. Technol.* **2015**, *137*, 269−281.

(21) Anjan, S. T. Ionic Liquid for Aromatic Extraction: Are They Ready? *Chem. Eng. Prog.* **2006**, *102*, 30−39.

(22) Meindersma, G. W.; de Haan, A. B. Conceptual Process Design for Aromatic/aliphatic Separation with Ionic Liquids. *Chem. Eng. Res. Des.* **2008**, *86*, 745−752.

(23) Navarro, P.; Larriba, M.; García, J.; Rodríguez, F. Thermal Stability, Specific Heats, and Surface Tensions of ([emim][DCA] + [4empy][Tf_2N]) Ionic Liquid Mixtures. *J. Chem. Thermodyn.* **2014**, *76*, 152−160.

(24) Canales, R. I.; Brennecke, J. F. Comparison of Ionic Liquids to Conventional Organic Solvents for Extraction of Aromatics from Aliphatics. *J. Chem. Eng. Data* **2016**, *61*, 1685−1699.

(25) Navarro, P.; Larriba, M.; García, J.; González, E. J.; Rodríguez, F. Selective Recovery of Aliphatics from Aromatics in the Presence of the

DOI: 10.1021/acs.energyfuels.6b03068
Energy Fuels 2017, 31, 1035−1043

{[4empy][Tf_2N] + [emim][DCA]} Ionic Liquid Mixture. *J. Chem. Thermodyn.* **2016**, *96*, 134−142.
(26) Navarro, P.; Larriba, M.; García, J.; González, E. J.; Rodríguez, F. Vapor-liquid Equilibria of {*n*-Heptane + Toluene + [emim][DCA]} System Using Headspace Gas Chromatography. *Fluid Phase Equilib.* **2015**, *387*, 209−216.
(27) Navarro, P.; Larriba, M.; García, J.; Rodríguez, F. Vapor−Liquid Equilibria for (*n*-Hexane, *n*-Octane, Cyclohexane, or 2,3-Dimethylpentane) + Toluene + {[4empy][Tf_2N] (0.3) + [emim][DCA] (0.7)} Mixed Ionic Liquids. *J. Chem. Eng. Data* **2016**, *61*, 2440−2449.
(28) Navarro, P.; Larriba, M.; García, J.; Rodríguez, F. Vapor-liquid Equilibria for *n*-Heptane + (Benzene, Toluene, *p*-Xylene, or Ethylbenzene) + {[4empy][Tf_2N] (0.3) + [emim][DCA] (0.7)} Binary Ionic Liquid Mixture. *Fluid Phase Equilib.* **2016**, *417*, 41−49.
(29) Henley, E. J.; Seader, J. D. *Equilibrium-Stage Separation Operations in Chemical Engineering*; John Wiley and Sons: New York, 1981.
(30) Perry, R. H.; Green, D. W.; Maloney, J. O. *Perry's Chemical Engineers' Handbook*; McGraw-Hill: New York, 1999.
(31) Fahim, M.; Al-Sahhaf, T.; Elkilani, A. *Fundamentals of Petroleum Refining*; Elsevier: Amsterdam, Netherlands, 2010.
(32) Ferro, V. R.; Ruiz, E.; de Riva, J.; Palomar, J. Introducing Process Simulation in Ionic Liquids Design/Selection for Separation Processes Based on Operational and Economic Criteria through the Example of Their Regeneration. *Sep. Purif. Technol.* **2012**, *97*, 195−204.

DOI: 10.1021/acs.energyfuels.6b03068
Energy Fuels 2017, 31, 1035−1043

Separation and Purification Technology 180 (2017) 149–156

Contents lists available at ScienceDirect

Separation and Purification Technology

journal homepage: www.elsevier.com/locate/seppur

Design of the recovery section of the extracted aromatics in the separation of BTEX from naphtha feed to ethylene crackers using [4empy][Tf_2N] and [emim][DCA] mixed ionic liquids as solvent

Pablo Navarro, Marcos Larriba, Julián García *, Francisco Rodríguez

Department of Chemical Engineering, Complutense University of Madrid, E–28040 Madrid, Spain

ARTICLE INFO

Article history:
Received 28 November 2016
Received in revised form 24 February 2017
Accepted 27 February 2017
Available online 28 February 2017

Keywords:
Mixed ionic liquids
Aromatic/aliphatic separation
Vapor-liquid separation
Naphtha

ABSTRACT

Aromatic hydrocarbons are mainly obtained from reformer and pyrolysis gasolines by liquid-liquid extraction. In these streams, the content of aromatics is between 40 wt.% and 70 wt.%. However, several streams as the naphtha feed to ethylene crackers, in which the aromatics are between 10 wt.% and 25 wt.%, have not available technology to obtain a commercial stream of BTEX. In our previous contribution, the BTEX removing from a naphtha model with the minimum aromatic content, 10 wt.%, was studied using ionic liquids (ILs) as solvents. The high aromatic purity in the extract stream and the good extraction yields obtained suggested liquid-liquid extraction using ILs as a good technological election. To confirm this, in this work the vapor-liquid separation of all hydrocarbons from the solvent in the extract stream have been determined at several temperatures by using a headspace – gas chromatography (HS-GC) technique. After that, the operating conditions were simulated to maximize the purity and recovery of the aromatics. The proposed recovery section to selectively separate the aromatics from the extract stream consists in three flash distillation units that operate at low temperatures and high vacuum conditions, achieving an aromatic-rich stream with a purity of 98.5 wt.%.

1. Introduction

Reformer and pyrolysis gasolines are the main sources of aromatic compounds [1]. In these streams, the aromatic fraction is from 40 wt.% to 70 wt.%, being the liquid-liquid extraction with organic solvents such as sulfolane the most employed dearomatization process [1–3]. At higher aromatic contents, from 65 wt.% to 90 wt.%, the extractive distillation is commonly used [1]. However, at lower aromatic concentrations, below 20 wt.%, there are not available technologies to recover aromatics [4–7].

The naphtha feed to ethylene crackers has an aromatic content that can vary between 10 wt.% and 25 wt.%. This aromatic fraction does not convert to olefins in the naphtha cracking and both investment fixed and operating costs associated to the aromatics should be eliminated [7]. Thus, the dearomatization of this stream before the cracking would imply lower costs and also it would let to increase the benefits by selling the obtained aromatics.

The liquid-liquid extraction using ILs has been deeply studied to fulfill several separation problems of interest from the industrial point of view, achieving high extractive performance especially in terms of selectivity [8–14]. However, scarce studies can be found dealing with the recovery of the extracted substances, fact that could limit these technologies. This has been advised by Canales and Brennecke in their recent review on the liquid-liquid extraction for the particular case of the aromatics separation from aliphatics [15].

In our previous work, a binary mixture of ionic liquids was used to simultaneously extract the aromatics (benzene, toluene, ethylbenzene, and *p*-xylene) from a naphtha feed to ethylene crackers model in which several representative alkanes were included (*n*-hexane, *n*-heptane, and *n*-octane), being the aromatic content of 10 wt.% [7]. The {[4empy][Tf_2N] (0.3) + [emim][DCA] (0.7)} IL mixture was selected because of its good extractive and physical properties [16]. The results indicated that this IL-based solvent can selectively extract aromatics; in fact, the aromatic purity in the extract stream was 85 wt.% for the IL mixture, whereas only a 65 wt.% was achieved using sulfolane, the most employed organic solvent in aromatic extraction processes at industrial scale [7]. Although the high purity obtained from a stream with only a 10 wt.% of aromatics, this value must be increased to obtain an aromatic stream with commercial interest. Here is the point in which the recovery of the aromatics from the extract stream plays an important role. However, the vapor-liquid equilibria (VLE) data

* Corresponding author.
E-mail address: jgarcia@quim.ucm.es (J. García).

http://dx.doi.org/10.1016/j.seppur.2017.02.052
1383-5866/

that would let to propose the equipment and the conditions to achieve a higher aromatic purity was not available for extract-type streams involving ILs.

Therefore, in this work we have determined first the VLE for the extract stream obtained in the extraction of aromatics from a naphtha feed to ethylene crackers model using the {[4empy][Tf_2N] (0.3) + [emim][DCA] (0.7)} as solvent, evaluating several temperatures in order to analyze its influence in the recovery of hydrocarbons. After that, we have planned two new configurations (A and B) to conceptually design the hydrocarbon recovery section. As a result of the high IL mixture content in the extract stream, flash distillation units have been considered as a result of the difference of volatility [17], first in the aliphatics/aromatics separation and then in the aromatics/IL-based solvent separation. There are other options as an extractive stripper. However, using a reboiler working at high temperatures or working with a stripping agent drastically reduce aliphatic/aromatic relative volatilities and, thus, the purity of the aromatics at the end of the recovery process not seem to be advantageous solutions. In addition to this, the use of a series of flashes leads to finely select the most suitable temperature-pressure scenario for each required equilibrium step in the aromatic purification.

Additionally to this, we have developed a new algorithm to simulate flash distillation units that quickly converges although a non-volatile substance has a high concentration, fact that implies low mole fractions of the volatile compounds in the liquid stream and very low vapor flow in comparison with the liquid one.

2. Experimental

2.1. Chemicals

The [emim][DCA] and [4empy][Tf_2N] ILs were acquired from Iolitec GmbH with purities of 0.98 and 0.99, respectively, in mass basis. [emim][DCA] had a content of water of 937 ppm and the halides were below 200 ppm, whereas [4empy][Tf_2N] had 89 ppm and 100 ppm, respectively, in water and halide impurities. They were not purified after their reception. ILs were kept in a desiccator with silica gel and handled under an inert atmosphere of dry nitrogen in a glove box to avoid water content modification. The aliphatic and aromatic hydrocarbons were supplied by Sigma-Aldrich with mass fraction purities higher than 0.99. The specifications for the ILs and the hydrocarbons are listed in Table 1.

2.2. Vapor-liquid separation procedure and analysis

The VLE was reproduced with an Agilent headspace (HS) 7697A injector and was measured with an Agilent gas chromatograph 7890A. A detailed description of the method and the equipment can be found in our previous studies [17–20].

Table 1
Specification of chemicals.

Name	Source	Purity	Analysis
n-hexane	Sigma–Aldrich	0.995	GC[a]
n-heptane	Sigma–Aldrich	0.997	GC[a]
n-octane	Sigma–Aldrich	0.990	GC[a]
benzene	Sigma–Aldrich	0.995	GC[a]
toluene	Sigma–Aldrich	0.995	GC[a]
p-xylene	Sigma–Aldrich	0.990	GC[a]
ethylbenzene	Sigma–Aldrich	0.998	GC[a]
[emim][DCA]	Iolitec GmbH	0.98	NMR[b], IC[c]
[4empy][Tf_2N]	Iolitec GmbH	0.99	NMR[b], IC[c]

[a] Gas Chromatography.
[b] Nuclear Magnetic Resonance.
[c] Ion Chromatography.

Both the IL mixture and the multicomponent hydrocarbon fraction were gravimetrically prepared with a Mettler Toledo XS205 balance with a precision of $1 \cdot 10^{-5}$ g. The global feed of the VLE experiments was prepared adding first the IL mixture and then the hydrocarbon fraction, just before hermetically closing the vial. The composition of the extract stream is listed in Table 2.

Once the equilibrium was reached, the vapor phase was directly analyzed by gas chromatography, obtaining the compositions for this phase. Using mass balance and the ideal gas law, in addition to knowing the vapor compositions, the mole fractions (x_i) for the liquid phase were recalculated as follows:

$$x_i = \frac{z_i \cdot F - (P_i \cdot V_G / R \cdot T)}{\sum_{i=1}^{8} (z_i \cdot F - (P_i \cdot V_G / R \cdot T))} \quad (1)$$

where z_i is the mole fraction of the component i in the feed, F denotes the molar amount of the feed, V_G is the vapor volume in the vial, and P_i is the partial pressure of the component i calculated as follows:

$$P_i = \frac{A_i}{A_i^0} P_i^0 \quad (2)$$

where A_i are the peak areas of the hydrocarbons, whereas P_i^0 and A_i^0 are the vapor pressures and the peak areas of the pure hydrocarbons in the same experimental conditions, respectively.

2.3. Adiabatic flash distillation simulation

An analysis of the degrees of freedom is presented for a flash distillation unit in Table S1 in the Supplementary Material. There are 2C + 6 independent equations and 3C + 10 variables; thus, the degrees of freedom are C + 4.

As a consequence of knowing the VLE as a function of temperature and pressure, P_V and T_V are initially fixed. The flow, C − 1 compositions, and the pressure in the feed (C + 1) are also set. Finally, Q = 0 because adiabatic flash distillation units, which are less expensive than isothermal ones [17,21–23], are selected. In summary, (C + 4) variables are known that is in agreement with the degrees of freedom of the system.

The new algorithm proposed in this work is graphically presented in Fig. 1. Because of the low values of the total vapor flow and mole fraction of the hydrocarbons in the liquid phase, the algorithm starts with the estimation of the individual flows in the vapor phase (V_i), based on the experimental results obtained. This means starting with T_V and the corresponding P_V at which the VLE was achieved, fact that allows using the experimental vapor flows for each hydrocarbon. At the same time, the *K*-values were calculated as a function of T_V and using the activity coefficients experimentally obtained at the same temperature. In this simulation the hydrocarbon *K*-values are considered independent on the liquid mole fractions since in the conditions of the extract streams the liquid compositions are quite low as well as their variations within the range of temperatures. In order to evidence the approximation

Table 2
Extract stream compositions of the aromatic extraction from a naphtha feed to ethylene crackers model from Ref. [7] and the abbreviations of the compounds

Compound	Abbreviation	Composition/wt.%
n-hexane	hexa	0.13
n-heptane	hepta	0.12
n-octane	octa	0.07
benzene	benz	0.35
toluene	tol	0.58
p-xylene	*p*-xyl	0.33
ethylbenzene	etbenz	0.53
[4empy][Tf_2N] + [emim][DCA]	ILs	97.89

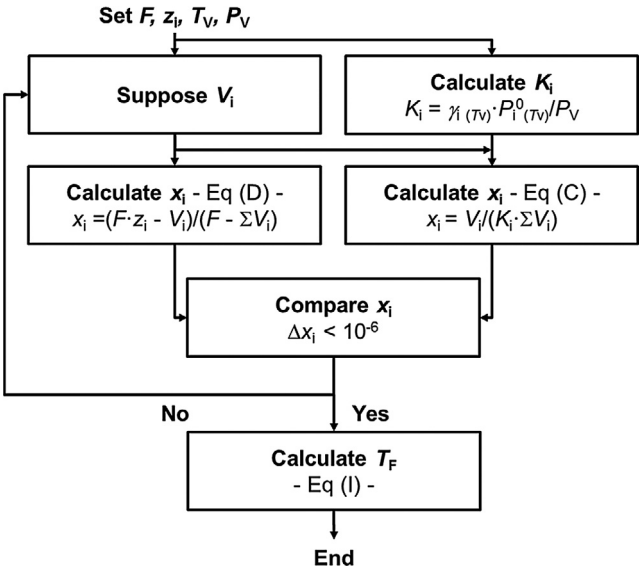

Fig. 1. Algorithm used to simulate the adiabatic flash distillation unit in this work.

done, activity coefficients are shown against temperature in Fig. 2 to graphically demonstrate that although the feed composition changed between the three series analyzed for each hydrocarbons, temperature seems to be the only variable that affects to activity coefficients.

Knowing V_i and K_i for all hydrocarbons, it is possible to determine the mole fractions in the liquid phase by two routes of calculation, by using Eqs. C and D from Table 3. The objective function of the algorithm is the difference between the liquid mole fractions calculated from the chemical equilibrium (Eq. C) and those also calculated from mass balance (Eq. D). Once the system has converged, other values of pressure are evaluated for each experimental T_V to completely define both temperature and pressure influences in the flash distillation simulations. Recoveries and purities calculated from the simulations have uncertainties lower than 1.3%. These uncertainties were calculated taking into account pressure and vapor and liquid composition uncertainties.

Finally, the feed temperature is calculated to completely define each T_V-P_V simulation by enthalpy balance. First the enthalpy (h) was calculated for feed, vapor, and liquid streams as indicated as follows:

$$h_{stream} = \sum_{i=0}^{I} m_i C_{P,i}(T_{stream}) + \sum_{i=0}^{I} m_i \lambda_i \quad (3)$$

where C_P refers to specific heats as function of temperature, m denotes mass flows, and λ is the latent heat of vaporization only used for the vapor phase also as function of temperature. The specific heats and the latent heats of vaporization for all hydrocarbons were taken from literature [22] and specific heats regarding the IL mixture were taken from our previous work [24]. In addition to characterize the process, the enthalpy balance is also aimed to check that the feed temperature is below 413 K, the maximum operation temperature (MOT) estimated for the IL mixture [24]. Once the enthalpy was calculated for the liquid and the vapor streams, the unique unknown variable is the feed temperature that is solved by the next balance:

$$h_{feed} - h_{liquid} - h_{vapor} = Q = 0 \quad (4)$$

This whole strategy was also designed to ensure the maximum use of experimental VLE in each equilibrium step simulated in this work. For that reason, the VLE was determined for the feed stream of each flash distillation unit at all temperatures and the algorithm was used only to evaluate the working pressure influence in the separations because this cannot be experimentally evaluated.

3. Results and discussion

3.1. Vapor-liquid separation: aliphatics/aromatics relative volatilities

The VLE for the n-hexane + n-heptane + n-octane + benzene + toluene + p-xylene + ethylbenzene + {[4empy][Tf_2N] (0.3) + [emim][DCA] (0.7)} system were measured between 303.2 K and 393.2 K. The vapor and liquid compositions for all compounds involved in the VLE are listed in Table S2 in the Supplementary Material as function of temperature. The overall aliphatics/aromatics relative volatilities were calculated from the VLE data to quantify the separation of aliphatics from aromatics in terms of selectivity. This parameter was determined for all VLE experiments as follows:

$$\alpha_{aliph,arom} = \frac{K_{aliph}}{K_{arom}} = \left[\frac{(y_{hexa} + y_{hepta} + y_{octa})}{(x_{hexa} + x_{hepta} + x_{octa})}\right]\left[\frac{(y_{benz} + y_{tol} + y_{p-xyl} + y_{etbenz})}{(x_{benz} + x_{tol} + x_{p-xyl} + x_{etbenz})}\right]^{-1} \quad (5)$$

where K denote the K-values for the aliphatic (aliph) or aromatic (arom) hydrocarbon groups, y denote the molar vapor compositions, and x refer to the molar liquid compositions. The calculated aliphatics/aromatics relative volatilities are listed in Table 4 along with the VLE experimental data and graphically represented in Fig. 3.

The high values for the aliphatics/aromatics relative volatility, especially at low temperatures, have confirmed the previous results observed in the separation of an aliphatic from an aromatic in pure or mixed ILs [20]. Therefore, adiabatic flash distillation units are planned to increase the aromatic purity by selectively removing the aliphatics.

3.2. Hydrocarbon recovery section conceptual design formed by two flash distillation units: Configuration A

The first approach in this conceptual design is named *Configuration A* (Fig. 4). This is formed by two flash distillation units. Flash 1 is aimed in selectively removing the aliphatics from the extract stream to increment the aromatic purity and Flash 2 is destined to perform the aromatics/IL-based solvent separation.

The vapor and liquid streams for several T_V-P_V scenarios in the ranges of (303.2–363.2) K and (3–9) kPa have been simulated to evaluate the aliphatic removing from the extract stream in Flash 1. The lowest pressure considered in this work was 3 kPa, supported by related studies involving ILs and the common vacuum range in hydrocarbon separation processes at industrial scale [23,25].

The aromatic purities (Pu_{arom}) and recoveries (R_{arom}) were calculated from the simulations as:

$$Pu_{arom} = \frac{(m_{benz} + m_{tol} + m_{p-xyl} + m_{etbenz})_{stream}}{(m_{hexa} + m_{hepta} + m_{octa} + m_{benz} + m_{tol} + m_{p-xyl} + m_{etbenz})_{stream}} \quad (6)$$

$$R_{arom} = \frac{(m_{benz} + m_{tol} + m_{p-xyl} + m_{etbenz})_{stream}}{(m_{benz} + m_{tol} + m_{p-xyl} + m_{etbenz})_{feed}} \quad (7)$$

where m refers to the mass of each hydrocarbon in the corresponding stream (vapor or liquid). The aromatic purities and recoveries in the liquid stream are graphically shown in Fig. 5 as a function of temperature and pressure.

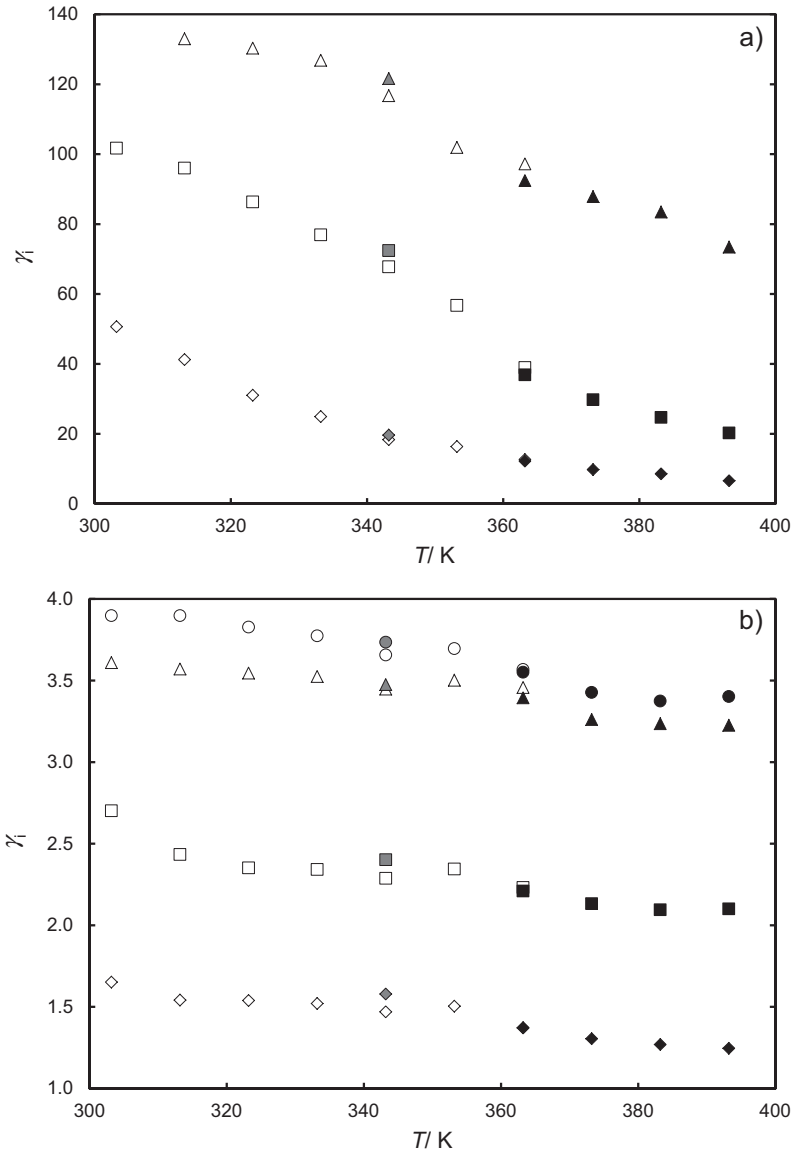

Fig. 2. Activity coefficients against temperature for the three VLE collections studied in this work: empty series denote feed composition to Flash 1 (extract stream), grey series denote feed composition to Flash 2, and black series represent feed composition to Flash 3. (a) *n*-hexane (◇), *n*-heptane (□), *n*-octane (△); b) benzene (◇), toluene (□), *p*-xylene (○), ethylbenzene (△).

To maximize the aromatic purity in the liquid stream, it is necessary to work at 363.2 K and very low pressures (3 kPa). However, these conditions also mean a very low aromatic recovery in the liquid stream. Therefore, it is not possible to achieve both high aromatic purities and aromatic recoveries in the liquid stream using *Configuration A*. The aromatic purification would achieve a maximum value of purity of 98 wt.%, but the aromatics recovered in the liquid stream (45%) are so low, fact that would drastically reduce the flow of aromatics at the end of the process.

Because of that, we have not followed studying *Configuration A* since this process scheme is not suitable to selectively recover aromatics from the extract stream and the simulation for Flash 2 would not reveal any interesting result herein.

3.3. Hydrocarbon recovery section conceptual design formed by three flash distillation units: Configuration B

As a result of the high recycled aromatics in *Configuration A*, the aliphatic removing from the extract stream has been reconfigured. This is aimed in working at milder conditions to increase the aliphatic/aromatic relative volatility in the separations and, then, minimize the aromatic content in the recycling streams.

Configuration B is shown in Fig. 6. As can be seen, two flash distillation units are aimed in selectively removing the aliphatics (Flash 1 and Flash 2) and Flash 3 is focused in performing the aromatics/solvent separation.

The operation temperature for Flash 1 was selected to 333.2 K, whereas the operation pressure was set in 5 kPa. These values led to achieve an important increase in the aromatic purity in the liquid stream, whereas also permit recovering the 90% of the aromatics.

The simulation for Flash 2 was also done following the aforementioned algorithm. As a result of the change in feed, new VLE data was required and these values are listed in Table S2 in the Supplementary Material. The operation temperature for Flash 2 was set in 343.2 K in order to assure the total aliphatic removing, whereas the pressure influence was studied from (3 to 5) kPa. As shown in Fig. 7, a minimum value of 3 kPa was needed to increase the aromatic purity up to 98.5 wt.%, recovering the 82% of the aromatics, reducing the aromatic recycled to the half. The values

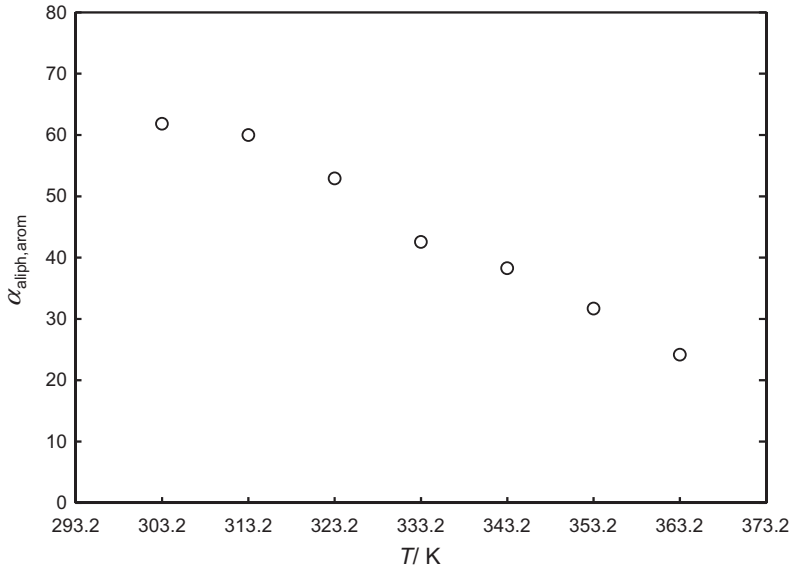

Fig. 3. Experimental relative volatility of aliphatics from aromatics as a function of temperature obtained from the experimental VLE data regarding the extract stream fed to Flash 1 in both Configuration A and B.

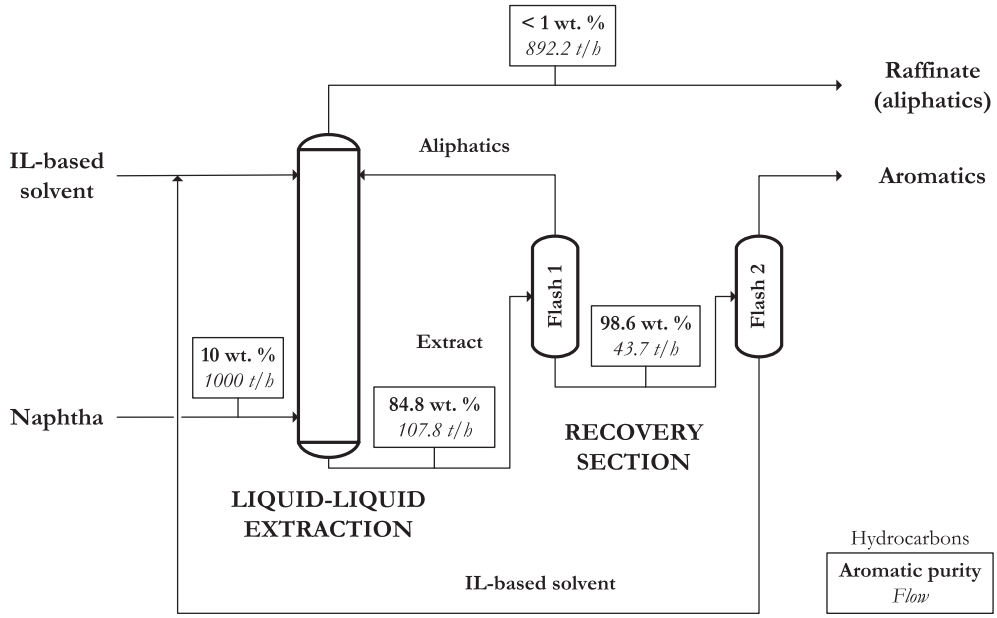

Fig. 4. Conceptual design for the dearomatization of the naphtha feed to ethylene crackers using ILs. Configuration A: liquid-liquid extraction section and recovery section formed by two flash distillation units.

obtained, as expected, have highly improved those obtained in the liquid stream of Flash 1 in *Configuration A* (purity of 98 wt.% and recovery of 45%).

Finally, Flash 3 was simulated to separate the aromatics from the IL binary mixture. For that purpose, new experimental VLE data was needed. These data are collected in Table S2 in the Supplementary Material. The operation pressure was fixed in 3 kPa (maximum vacuum considered in this work) and the temperature was studied from 363.2 K to 393.2 K. Higher temperatures were not considered as a result of the aforementioned MOT of the solvent, 413.2 K, to ensure no thermal decomposition for 8000 h [24]. In order to adequately select the temperature, the Pu_{arom} and R_{arom} in the vapor phase were calculated and they are graphically shown in Fig. 8. As expected, the recovery of aromatics and their purity were higher at the maximum temperature, 393.2 K, selecting this value as working condition in Flash 3. This is related to the almost full recovery of aliphatics at all conditions, which means that higher temperatures permit to increase the flow of aromatics in the vapor stream increasing both their purity and their recovery.

In order to experimentally evaluate the regeneration ability of the ILs, we have experimentally checked that it is possible to fully recover the hydrocarbons that form the naphtha feed to ethylene crackers from the IL mixture at lower temperatures than 413.2 K as no peak areas referring to the hydrocarbons were found in the GC analysis of the recovered ILs in that case.

3.4. Global overview

The complete aromatic extraction process is schematically shown in Fig. S1, whereas the conditions and compositions of all

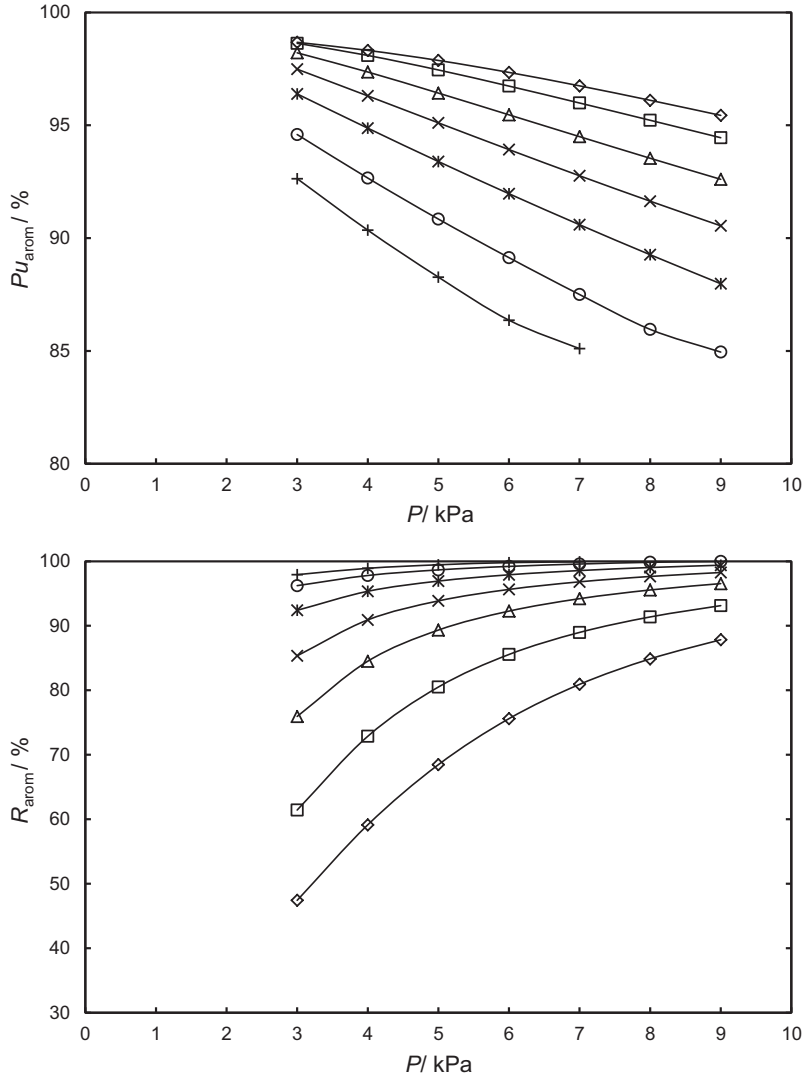

Fig. 5. Aromatic purity (Pu_{arom}) and aromatic recovery (R_{arom}) in the liquid stream as a function of temperature and pressure from the simulations for Flash 1 regarding Configurations A and B. +, T = 303.2 K; ○, T = 313.2 K; *, T = 323.2 K; ×, T = 333.2 K; △, T = 343.2 K; □, T = 353.2 K; ◇, T = 363.2 K. Solid lines are used to guide the eyes.

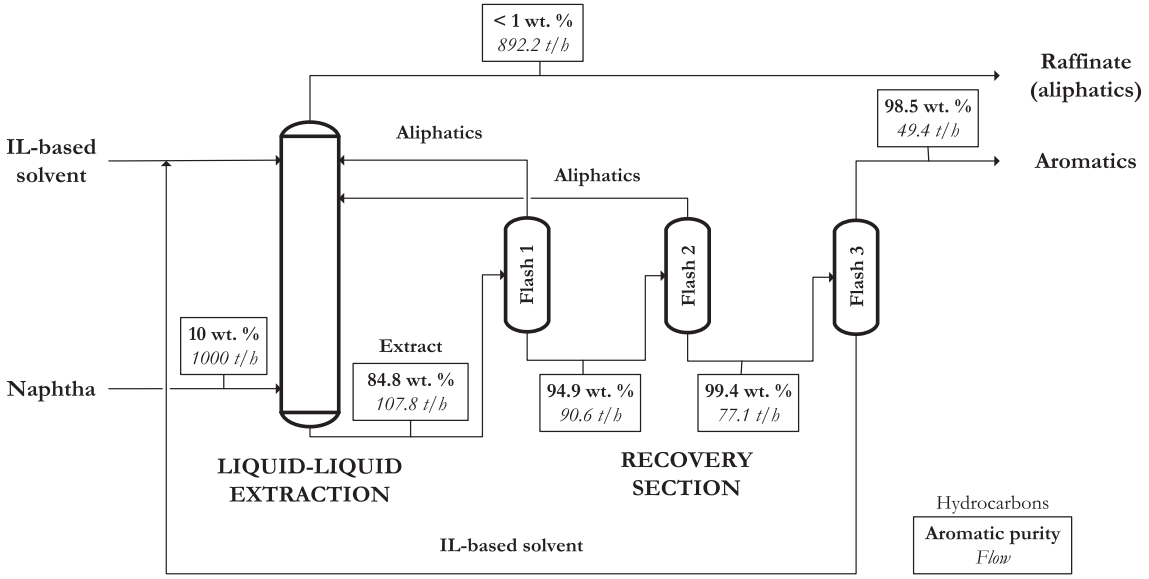

Fig. 6. Conceptual design for the dearomatization of the naphtha feed to ethylene crackers using ILs. Configuration B: liquid-liquid extraction section and recovery section formed by three flash distillation units.

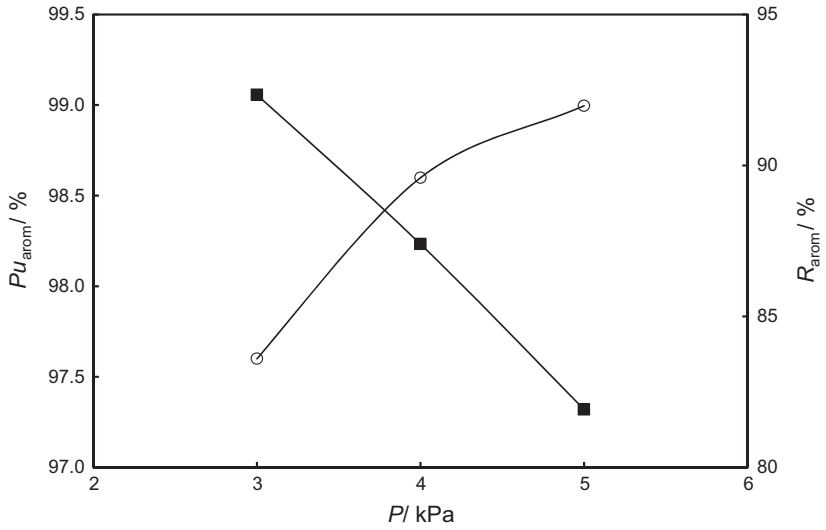

Fig. 7. Aromatic purity (Pu_{arom}, ■) and aromatic recovery (R_{arom}, ○) in the liquid stream at 343.2 K as a function of pressure from the simulations for Flash 2 regarding Configuration B. Solid lines are used to guide the eyes.

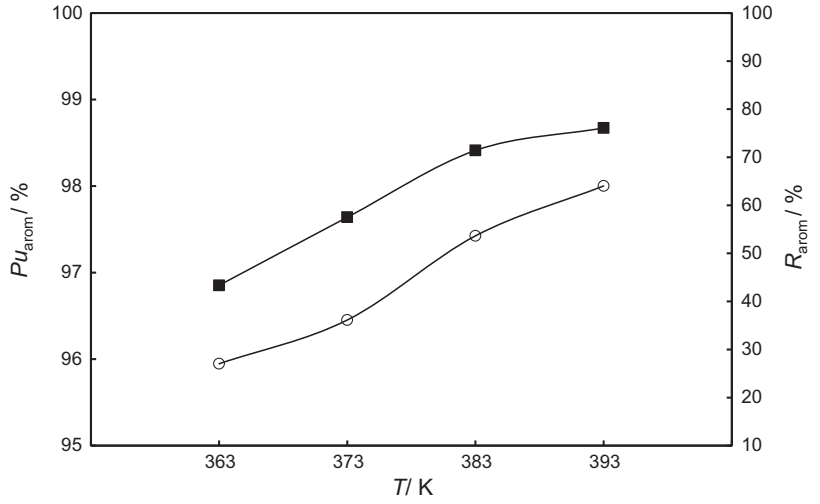

Fig. 8. Aromatic purity (Pu_{arom}, ■) and aromatic recovery (R_{arom}, ○) in the vapor stream as a function of temperature at 3 kPa from the simulations for Flash 3 regarding Configuration B.

streams are reported in Table S3 in the Supplementary Material to give the whole information regarding the simulation of *Configuration B*. In our previous work, the extraction column was previously simulated with a solvent to feed ratio of 5.0 and a temperature of 303.2 K, needing 18 equilibrium steps to achieve quite similar extraction yields as those achieved in the Sulfolane process: 99.9% and 99.0%, for benzene and toluene, respectively [2]. In this work, the recovery of the hydrocarbons was studied, obtaining an aromatic-rich stream with a mass fraction purity of 98.5 wt.%. In addition to this, in the liquid stream from Flash 3 the purity of the IL mixture was 99.4 wt.%.

Previous conceptual designs for the recovery section using ILs proposed by de Riva et al. have been formed by only one flash distillation unit or a combination of an stripping with N_2 and a flash distillation unit [26]. Using an IL with similar extractive properties ([4bmpy][BF_4]) and a quite similar composition of the naphtha model, their best aromatic purity was lower than 85 wt.% in comparison with the 98.5 wt.% obtained using *Configuration B*.

The absence of technology at industrial scale to separate aromatics from streams with low content of aromatics as the naphtha feed to the ethylene crackers are reasons to claim that it seems that the liquid-liquid extraction using {[4empy][Tf_2N] (0.3) + [emim][DCA] (0.7)} and the hydrocarbon recovery section *named Configuration B* are a first step towards a feasible technology.

4. Conclusions

In this work, the recovery of hydrocarbons has been studied for the extract stream obtained in the dearomatization of a naphtha feed to ethylene crackers model using the {[4empy][Tf_2N] (0.3) + [emim][DCA] (0.7)} IL mixture as solvent.

Firstly, the VLE involving all hydrocarbons and the IL mixture have been determined at several temperatures, achieving quite high aliphatics/aromatics relative volatility values in the temperature range of (303.2–363.2) K. These values have led to selectively separate the extracted hydrocarbons to obtain a high purity stream of aromatics.

Secondly, the simulation of two different configurations of the recovery section formed by flash distillation units has been carried

out, based on the experimental VLE data and developing a new algorithm to solve flash distillation units for cases in which a non-volatile compound is presented at high concentration. Configuration B, which has shown the best separation results, was formed by three distillation units that work at moderate temperatures and vacuum conditions. The former two flashes are destined to selectively remove the aliphatics and the latter to separate the aromatics from the IL-based solvent. The aromatic-rich stream had a purity of 98.5 wt.% considering a naphtha model with the lowest aromatic content (10 wt.%), whereas the IL mixture is obtained with a purity of 99.4 wt.% working at temperatures that assay no thermal decomposition of the IL mixture.

Acknowledgements

Authors are grateful to the Ministerio de Economía y Competitividad (MINECO) of Spain and the Comunidad de Madrid for financial support of Projects CTQ2011-23533-R and S2013/MAE-2800, respectively. Pablo Navarro also thanks MINECO for awarding him an FPI grant (Reference BES-2012-052312).

Appendix A. Supplementary material

Supplementary data associated with this article can be found, in the online version, at http://dx.doi.org/10.1016/j.seppur.2017.02.052.

References

[1] H.G. Franck, J.W. Staldelhofer, Industrial Aromatic Chemistry, Springer-Verlag, Berlin, 1988.
[2] J. Gary, G. Handwerk, M. Kaiser, Petroleum Refining Technology and Economics, fifth ed., CRC Press, Boca Raton, FL, 2007.
[3] R.A. Meyers, Handbook of Petroleum Refining Processes, third ed., McGraw-Hill, New York, 2004.
[4] G.W. Meindersma, A.J.G. Podt, A.B. de Haan, Selection of ionic liquids for the extraction of aromatic hydrocarbons from aromatic/aliphatic mixtures, Fuel Process. Technol. 87 (2005) 59–70.
[5] G.W. Meindersma, A.B. de Haan, Conceptual process design for aromatic/aliphatic separation with ionic liquids, Chem. Eng. Res. Des. 86 (2008) 745–752.
[6] G.W. Meindersma, A.B. de Haan, Cyano-containing ionic liquids for the extraction of aromatic hydrocarbons from an aromatic/aliphatic mixture, Sci. China Chem. 55 (2012) 1488–1499.
[7] M. Larriba, P. Navarro, E.J. González, J. García, F. Rodríguez, Separation of BTEX from a naphtha feed to ethylene crackers using a binary mixture of [4empy][Tf_2N] and [emim][DCA] ionic liquids, Sep. Purif. Technol. 144 (2015) 54–62.
[8] M. Matsumoto, K. Mochiduki, K. Fukunishi, K. Kondo, Extraction of organic acids using imidazolium-based ionic liquids and their toxicity to *Lactobacillus rhamnosus*, Sep. Purif. Technol. 40 (2004) 97–101.
[9] A.B. Pereiro, A. Rodríguez, Azeotrope-breaking using [BMIM][$MeSO_4$] ionic liquid in an extraction column, Sep. Purif. Technol. 62 (2008) 733–738.
[10] L.I.N. Tomé, V.R. Catambas, A.R.R. Teles, M.G. Freire, I.M. Marrucho, J.A.P. Coutinho, Tryptophan extraction using hydrophobic ionic liquids, Sep. Purif. Technol. 72 (2010) 167–173.
[11] A.F.M. Claudio, M.G. Freire, C.S.R. Freire, A.J.D. Silvestre, J.A.P. Coutinho, Extraction of vanillin using ionic-liquid-based aqueous two-phase systems, Sep. Purif. Technol. 75 (2010) 39–47.
[12] F.S. Oliveira, J.M.M. Araujo, R. Ferreira, L.P.N. Rebelo, I.M. Marrucho, Extraction of L-lactic, L-malic, and succinic acids using phosphonium-based ionic liquids, Sep. Purif. Technol. 85 (2012) 137–146.
[13] E. Alvarez-Guerra, A. Irabien, Extraction of lactoferrin with hydrophobic ionic liquids, Sep. Purif. Technol. 98 (2012) 432–440.
[14] M. Zawadzki, L. Niedzicki, W. Wieczorek, U. Domanska, Estimation of extraction properties of new imidazolide anion based ionic liquids on the basis of activity coefficient at infinite dilution measurements, Sep. Purif. Technol. 118 (2013) 242–254.
[15] R.I. Canales, J.F. Brennecke, Comparison of ionic liquids to conventional organic solvents for extraction of aromatics from aliphatics, J. Chem. Eng. Data 61 (2016) 1685–1699.
[16] M. Larriba, P. Navarro, J. García, F. Rodríguez, Separation of toluene from n-heptane, 2,3–dimethylpentane, and cyclohexane using binary mixtures of [4empy][Tf_2N] and [emim][DCA] ionic liquids as extraction solvents, Sep. Purif. Technol. 120 (2013) 392–401.
[17] E.J. Henley, J.D. Seader, Equilibrium-Stage Separation Operations in Chemical Engineering, John Wiley and Sons, New York, 1981.
[18] P. Navarro, M. Larriba, J. García, E.J. González, F. Rodríguez, Vapor-liquid equilibria of n-heptane + toluene + [emim][DCA] system using headspace gas chromatography, Fluid Phase Equilib. 387 (2015) 209–216.
[19] P. Navarro, M. Larriba, J. García, F. Rodríguez, Vapor-liquid equilibria for n-heptane + (benzene, toluene, p-xylene, or ethylbenzene) + [4empy][Tf2N] (0.3) + [emim][DCA] (0.7) binary ionic liquid mixture, Fluid Phase Equilib. 417 (2016) 41–49.
[20] P. Navarro, M. Larriba, E.J. González, J. García, F. Rodríguez, Selective recovery of aliphatics from aromatics in the presence of the [4empy][Tf2N] + [emim][DCA] ionic liquid mixture, J. Chem. Thermodyn. 96 (2016) 134–142.
[21] C.R. Branan, Chemical Engineering Practical Solutions, second ed., McGraw-Hill, New York, 2008.
[22] R.H. Perry, D.W. Green, J.O. Maloney, Perry's Chemical Engineers' Handbook, McGraw-Hill, New York, 1999.
[23] M. Fahim, T. Al-Sahhaf, A. Elkilani, Fundamentals of Petroleum Refining, Elsevier, Amsterdam, 2010.
[24] P. Navarro, M. Larriba, J. García, F. Rodríguez, Thermal stability, specific heats, and surface tensions of ([emim][DCA] + [4empy][Tf_2N]) ionic liquid mixtures, J. Chem. Thermodyn. 76 (2014) 152–160.
[25] V.R. Ferro, E. Ruiz, J. de Riva, J. Palomar, Introducing process simulation in ionic liquids design/selection for separation processes based on operational and economic criteria through the example of their regeneration, Sep. Purif. Technol. 97 (2012) 195–204.
[26] J. de Riva, V.R. Ferro, D. Moreno, I. Díaz, J. Palomar, Aspen Plus supported conceptual design of the aromatic–aliphatic separation from low aromatic content naphtha using 4-methyl-N-butylpyridinium tetrafluoroborate ionic liquid, Fuel Process. Technol. 146 (2016) 29–38.